PROBLEMS OF FLUID FLOW IN A DEFORMABLE RESERVOIR

A Dissertation

by

ILDAR DIYASHEV

Submitted to the Office of Graduate Studies of
Texas A&M University
in partial fulfillment of the requirements for the degree of

DOCTOR OF PHILOSOPHY

December 2005

Major Subject: Petroleum Engineering

PROBLEMS OF FLUID FLOW IN A DEFORMABLE RESERVOIR

A Dissertation

by

ILDAR DIYASHEV

Submitted to the Office of Graduate Studies of
Texas A&M University
in partial fulfillment of the requirements for the degree of

DOCTOR OF PHILOSOPHY

Approved by:

Chair of Committee,	Stephen A. Holditch
Committee Members,	James E. Russell
	Peter Valkó
	Brann Johnson
Head of Department,	Stephen A. Holditch

December 2005

Major Subject: Petroleum Engineering

ABSTRACT

Problems of Fluid Flow in a Deformable Reservoir. (December 2005)

Ildar Diyashev, Diploma, Kazan State University;

Candidate of Science, Kazan State University;

M. Eng., Texas A&M University

Chair of Advisory Committee: Dr. Stephen A. Holditch

This research is focused on development and enhancement of the model of fluid flow in a formation with stress-dependent permeability. Several typical axi-symmetrical problems of fluid flow in a multi-layered reservoir with account for wellbore storage and skin have been solved numerically. The permeability was assumed to be a function of the vertical deformation of the reservoir. This deformation is the result of changing stress-strain state in the elastic system, comprised of the reservoir itself and the surrounding rock mass. The change in the stress-strain state of the system is induced by pressure change in the layers of the reservoir.

Numerical results qualitatively agree with observed field behavior. Such behavior includes (1) deviation of an inflow performance curve from the straight-line relationship at pressures above bubble-point pressure, (2) time- and rate-dependence of well-testing derivative, (3) asymmetry of processes of production and of injection, and (4) inconsistent results between drawdown and buildup, or injection and falloff tests.

Based on the results, a procedure to estimate the parameters of the suggested permeability model is proposed.

ACKNOWLEDGMENTS

I would like to express my gratitude to the members of my committee – I was able to learn a lot from them when taking their classes and from many discussions. I'm especially grateful to Dr. Stephen A. Holditch, as his constant encouragement and support have made it possible for this work to go through.

Many thanks are due to Professors Eduard Skvortsov and Alexander Kosterin of Kazan State University. This research was originated under their guidance and supervision.

My parents and my brother have been very supportive throughout the years. Their love and understanding cannot be overestimated.

TABLE OF CONTENTS

Page

Page

LIST OF FIGURES

Page

Page

Page

Page

Page

Page

Page

Page

LIST OF TABLES

Page

1 INTRODUCTION

1.1 Complications of well test analysis in stress-dependent formations

The analysis of pressure transient data obtained during a conventional single-well test can provide estimates of in-situ permeability, near-wellbore damage or stimulation, and average reservoir pressure. The interpretation is normally based on reservoir, well, and fluid models that best approximate the principal features of fluid flow in porous media. In many cases, the existing fluid-flow models satisfactorily describe the well pressures measured during the test. However, there are situations when the observed pressure data do not "fit" predictions from any of the existing fluid-flow models, but rather exhibit distinctively different trends. For example, an inflow performance curve may deviate from the linear Darcy behavior to a much greater degree than can be explained by the multi-phase flow effects alone. Another example would be that the derivative curve on a diagnostic plot may behave as if the permeability-thickness product (kh) were not constant, suggesting the value of kh either increases or decreases with time as the test continues. Such trends in the pressure data can be attributed to a number of causes. One factor that can lead to inconsistencies would be when both the rock and fluid properties are stress dependent.

It is well known from numerous laboratory experiments on cores that rock properties, such as permeability and porosity, measured under various loading conditions, change as the effective stress in a specimen changes. While the relative change of porosity is, generally, fairly small (within several percent), the relative change of permeability may be as large as one or two orders of magnitude. These effects can be more pronounced for naturally fractured reservoirs, where the ability of the rock to transmit fluid is determined by a network

---

This dissertation follows the style of *Journal of Petroleum Technology*.

of cracks and fractures. Reduction of pore pressure under constant load may lead to closure of cracks and fissures with a resulting decrease in permeability.

Field experiments also indicate that permeability in most rocks depends upon the effective stress. Oil production above the bubble-point pressure, or gas production above the dew-point pressure, if conducted without pressure support, will cause reservoir pressure to decrease, which will increase the effective stress in the formation. When the effective stress increases, the permeability of the formation will decrease. This decrease in permeability, coupled with multiphase flow, once the pressure drops below the bubble point or dew point, can cause substantial decreases in well productivity in stress-sensitive formations. Derivative analysis of pressure transient tests in such wells suggests that the permeability-thickness product changes with time. Another feature, characteristic of the stress-dependent permeability, is the observed asymmetry of pressure response for drawdown and buildup tests (or injection and falloff tests). Field data also show that there is a degree of interaction of the pressures in individual layers, which may be tens or hundreds of feet apart. The latter indicates that we need to account for the stress changes not only in the reservoir, but also in the surrounding rocks when we are analyzing pressure data in stress-sensitive formations.

Though it is obvious that permeability of any reservoir rock is affected to a greater or lesser degree by the change in effective stress, it can be fairly difficult to recognize the stress-dependent behavior in real data, as many other factors tend to offset such behavior. For example, an increase in the pressure drawdown may lead to closure of the cracks and fractures in the vicinity of a well, which results in decreased near-wellbore permeability and, therefore, a decreased production rate. At the same time, some layers may require such increased drawdown to initiate any production, either due to the non-Newtonian behavior of

the reservoir oil, or because of the smaller magnitude of permeability, or both. Other factors, such as multi-phase flow effects and non-Darcy flow will tend to mask the characteristics of stress-dependent permeability, as many pressure/rate-dependent factors quantitatively work in the same direction of the production rate decrease. Therefore, it can be difficult to recognize and quantify the effect of reduced permeability caused by increased effective stress.

Nevertheless, it is possible to identify and describe the stress-dependent permeability from pressure transient tests on water injection wells, or by observing long-term data from permanent downhole pressure gauges in oil or gas producing wells. However, the tests must be properly designed and analyzed using the best data if one is to quantify the effects of stress-dependent permeability in layered reservoirs.

1.2 Mechanics of stress-dependent permeability

The physics of stress-dependent permeability is based on the deformation of porous rock under changing effective stress. Increasing the effective stress on rock leads to reduction in the size of pores and pore throats which is a consequence of deformation of the matrix. This process can be described with a set of equations that relate changes in effective stress and porosity. Modern geomechanical simulators incorporate such equations to calculate changes in porosity induced by changes in pore pressure and effective stress. One then must assume that changes in porosity cause changes in permeability.

The existing understanding of stress-dependent permeability is based largely on experimental data. In the laboratory, a rock sample is saturated with a fluid, such as water or nitrogen, then the sample is placed in a sleeve so that an overburden stress can be applied to the outside of the sample and the pore pressure inside the rock sample can be set to simulate

the reservoir pressure. The single-phase fluid (water or gas) is flowed through the sample to measure permeability. By reducing the pressure of the fluid flowing through the rock sample, one can measure how the rock permeability changes as the effective stress increases. In most cases, we can establish the relationship between the changes in porosity with changes in permeability as the effective stress increases. The functional form of such relationships varies from a simple power-law dependence of permeability with porosity, such as Kozeny-Carman's formula, to fairly complicated expressions, which may additionally account for the mechanical constants of the rock, grain size, or other properties, such as surface area. There is no single formula that adequately describes every formation, due to obvious wide variation of lithology, mechanical properties, and pore size distribution of those rocks.

Since it is obvious from the literature that rocks deform under changing effective stress, and the deformation causes changes in values of porosity and permeability, we will not discuss the details concerning the mechanics of the process in this research. Moreover, we will assume that vertical deformation of a reservoir is representative of any of the reasons for permeability decrease – pore and pore throat size reduction, repacking of the matrix, closure of cracks and fissures, etc. Instead of having to describe various mechanical processes, which are impossible to measure under in-situ conditions and, therefore, to verify, we will consider the integral effect of changing effective stress on the two readily available characteristics of a well – flow rate and wellbore pressure. In our work, based on the experimental observations, the permeability is assumed to be a simple exponential function of the vertical deformation only, i.e. $k = k_0 \exp(-\beta\varepsilon)$. Here k_0 and k are the values of permeability at initial and current reservoir pressure, ε is the relative vertical deformation, and coefficient β characterizes the sensitivity of permeability to deformation. Relative

vertical deformation is, of course, a function of the effective stress. This approach captures the essence of the stress-dependent behavior of permeability, which allows us to investigate the response of a reservoir to a wide range of producing conditions and is simple enough to allow for identification of the parameters of flow from well test data.

1.3 Research approach

To resolve the differences between theoretical predictions of flow rate vs. pressure in a well test, we need to account for physical factors, such as rock deformation. It is known that the weight of the overburden is compensated in the reservoir by stresses in the rock matrix and by the fluid pressure in the pore space. Change in pore pressure will alter the stress-strain state in the reservoir and in the surrounding rocks. The respective deformation induces changes in the structure of the pore space and permeability. Thus, permeability implicitly depends on fluid pressure via deformation, which can help explain non-linear behavior of flow rate vs. pressure that is sometimes observed in field data.

The odd behavior of some well test data can be, to some extent, explained by spatially varying stress state in the reservoir. Such non-uniformity results from two factors. The first factor is due to drilling. Whenever a shale layer is present above and near a producing oil or gas reservoir, drilling allows the shale to be squeezed into the well, which causes relaxation of both the shale layer and the reservoir rock layers near the shale and near the wellbore. Reduced overburden pressure in the zone of relaxation is compensated by the "arch" effect of the overlaying layers. The reservoir beyond the "relaxed" zone remains in an undisturbed condition. The second factor contributing to deformational non-uniformity is associated with fluid pressure redistribution caused by oilfield operations, such as the production of oil and/or gas.

It should be noted that the importance of the described deformational effects depends upon the magnitude of the deformations. Consider, for example, a simple one-dimensional case of an elastic deformation. According to the hypothesis of constant total stress, the magnitude of strain is equal to the ratio of change of pore pressure to Young's modulus, which in practice is about 0.0001. This means that for a 10 m thick reservoir, the change in thickness will be only 1 mm. Nevertheless, such a tiny change can significantly impact the flow characteristics, especially if the permeability depends on the elements of the structure that are sensitive enough to deform. In naturally fractured formations such elements are the natural fractures.

Let us consider a uniform horizontal layer with a system of vertical fractures[1]. The reservoir is characterized by substantial anisotropy of mechanical properties. Young's modulus in the vertical direction is essentially the same as the formation matrix. However, Young's modulus in the horizontal direction can be much less than the value in the vertical direction if there are a lot of vertical natural fractures. The vertical natural fractures substantially reduce the effective horizontal stiffness when such fractures are open and conductive. If the fractures are mineral filled or sealed, the stiffness in the horizontal direction will not be reduced as much as when the fractures are open. Assuming that the overburden pressure is constant, the weight of the overburden, Γ, is compensated by the stress σ_z in the porous matrix and by the fluid pressure in the pore space as follows:

$$\Gamma = \phi_1 p_1 + (1-\phi_1)\phi_2 p_2 - (1-\phi_1)(1-\phi_2)\sigma_z$$

subscripts *1* and *2* denote, respectively, fractures and blocks; *z* is vertical coordinate. (Here and henceforth we use engineering, rather than geosciences sign convention for stresses, i.e.

compression is negative and tension is positive. We denote overburden pressure, P_{ob}, as Γ to indicate this accepted sign convention.)

Since ϕ_1<<1, the above expression can be written as

$$\Gamma = -\sigma_z^e + p_2 \qquad (1.1)$$

where $\sigma_z^e = (1-\phi_2)(\sigma_z + p_2)$ is the effective stress in blocks. A small change of pressure, δp, causes a small change of the stress state in the reservoir and in the surrounding formations. According to the hypothesis of constant overburden pressure and from Eq. 1.1, it follows that $\delta\sigma_z^e = \delta p_2$. For the considered conditions the blocks between parallel fractures experience only simple tension (compression), and the respective principal components of strain, ε, are

$$\varepsilon_z = \frac{\delta p_2}{E} \qquad \varepsilon_x = \varepsilon_y = -\nu\frac{\delta p_2}{E}$$

where E is Young's modulus and ν is Poisson's ratio.

For this case of linear isotropic behavior of the blocks, the values ε_x and ε_y determine the change in the width of the fractures. Compared to the thickness of the overlaying formations, the reservoir is of negligible thickness and can be reasonably assumed to deform mainly vertically, so that the sum of the lateral dimension of a block, a, and fracture width, w, can be considered virtually constant: $\delta a + \delta w = 0$. Hence

$$\delta w = -\delta a = -a\varepsilon_x = -\nu a\frac{p_2 - p_2^0}{E}$$

The pressure of fracture closure p^* is determined from the condition $\delta w = -w^0$ (superscript *0* denotes initial state, prior to applied δp), therefore

$$p^* = p_2^0 - \frac{E}{w}\frac{w^0}{a}$$

Since p^* should be greater than 0, then if $w^0 / a > \nu p_2^0 / E$ the fracture will not close at all.

Let us estimate the change of fracture permeability due to change of fluid pressure in blocks, p_2. For E=10^4 MPa, ν=0.2, and assuming that a fracture transmissibility is proportional to w^3, a 0.2 m long, 1 μm wide fracture ($a / w^0 = 2 * 10^{-4}$) will change its permeability by a factor of 8 (δw=0.5w) due to a 1 MPa (145 psi) change in pressure.

A more complicated analysis and similar estimates are available for inclined fractures[1]. The estimates illustrate the expected more significant permeability change, which is the greater the closer is the fracture orientation to horizontal.

Even though the above discussion refers to naturally fractured formations, the discussion may also be useful for cases when the formation is not naturally fractured. Indeed, disturbances introduced when drilling a well (including a zone of relaxation around a wellbore) will result in creation of microcracks and fissures in a near wellbore zone. Hydraulic fracturing, when performed, can as well be responsible for creating such microcracks around the fracture. Production or injection will also alter the conditions in the near wellbore zone to some extent, depending on the degree of formation consolidation. It is understood that sand production is sometimes caused by an increase in drawdown pressure which increases the effective stress causing formation failure near the wellbore.

1.4 Objectives and results

The main objective of this research is to investigate the effects of stress-dependent permeability upon transient production/injection behavior of a well. The understanding of

such impact is required in many applications, including reservoir simulation and pressure transient testing. In this research, we build upon a known solution of the coupled problem of elastic deformation and fluid flow in porous media.

Following approach, presented in[2,1], the problem of elasticity theory is formulated for an elastic semi-space, which includes the reservoir and the overburden. The solution of the problem results in an operator relationship between the vertical deformation of the reservoir and the pressure distribution in the reservoir. Fluid production or injection alters the stress-strain state in the reservoir and in the overburden, which causes elastic vertical deformation in both the reservoir and the surrounding layers. This, in turn, affects the fluid flow, as the permeability is assumed to be a function of the strain.

In this work, we solve several axisymmetrical problems of fluid flow with typical boundary conditions: constant well rate or wellbore pressure, and with closed or constant pressure outer boundary. The reservoir may consist of an arbitrary number of layers. We investigate the effect of layers' elastic constants on the flow, as well as how the pressure and deformation fields in layers interact with each other.

A computer program was developed that allows for calculating non-linear problems for flow of a single-phase compressible fluid in a multi-layered circular reservoir with cross-flow between layers. The problems were solved with conventional inner and outer boundary conditions that account for wellbore storage and skin for cases of both production and injection.

2 PREVIOUS WORK

As the petroleum industry moves towards producing oil and gas from increasingly challenging reservoirs, such as low-permeability, naturally fractured or high-pressure, high temperature reservoirs, the problem of understanding and adequately describing such reservoirs also increases. One of the tools used to obtain information about a reservoir is pressure transient testing. Unfortunately, in many cases the recorded pressures can not be matched using any of the existing models. The reasons for such discrepancies are fairly well understood qualitatively and may include, among others, pressure-dependent fluid properties, rate-dependent non-Darcy flow effects, and stress-dependence of formation properties. If quantitative descriptions of the first two factors do not commonly represent a difficulty, a comprehensive description of the third factor is, and, probably always will, remain a problem. There are several reasons why stress-dependent reservoir properties are not widely used in pressure transient analysis solutions. The principal reasons include inability to directly measure the properties under in-situ conditions and limited applicability of laboratory results because of inherent problems with measurements on cores and lithology variations and heterogeneities of the reservoir rocks. Also, many analysts do not recognize the need to take stress-dependent reservoir properties into account during the analysis of the data.

Based on the laboratory results, permeability is the rock property that may undergo significant changes during production. Other properties, such as porosity and rock compressibility, change comparatively less. Efforts of many researchers have been focused on the mechanisms of permeability reduction and incorporation of such mechanisms into flow problems.

Raghavan et al.[3] defined a pseudo-pressure function, which includes variable reservoir properties, as well as pressure-dependent fluid properties. Raghavan illustrated applicability of his approach in transforming non-linear differential equations to diffusivity-type equations.

Based on the results of measurements on cores, Vairogs et al.[4] concluded that permeability is a complex function of effective stress. Effective stress is a function of pore pressure, which, in turn, is a function of permeability. The authors investigated rock stresses around a wellbore and developed a model of the effect. They concluded that rock heterogeneities, such as hairline natural fractures and shale streaks, accentuate the permeability reduction due to change of effective stress.

In subsequent work, Vairogs and Rhoades[5] applied the developed model to simulate drawdown and buildup tests. They applied methods of conventional analysis to simulated data and showed that the results from drawdown tests analyzed with conventional methods are not reliable when pressure dependent permeability exists, but buildup tests if conducted early in the life of the reservoir will give values of kh about 10 percent below true values. Skin factors from either test are not representative of the true condition around the wellbore.

Evers and Soeiinah[6] used an exponential form of dependence of permeability on effective stress and then related permeability and pressure based on the hypothesis of the constant overburden pressure. They showed how to recognize stress-sensitivity from a series of constant-rate drawdowns, if turbulence and viscosity changes are minimal.

Pedrosa[7] introduced the concept of permeability modulus – fractional change of permeability with unit change in pressure, which is equivalent to exponential variation of permeability with pressure. Permeability modulus of zero corresponds to the absence of

stress-sensitivity. This approach allowed the author to generate type curves in term of this parameter.

Celis et al.[8] applied the concept of permeability modulus to develop an analytical model for pressure transient analysis in stress-sensitive, naturally fractured formations. They showed that the variation of fracture properties with pressure can drastically change the estimates of parameters.

Buchsteiner et al.[9] investigated stress-induced permeability reduction in fissured reservoirs and developed a model to account for directional permeability variation. These same authors[10] developed an analysis procedure that allows one to measure stress-sensitive permeability of rocks and determine the permeability anisotropy.

Zhang and Ambastha[11] introduced a stepwise permeability modulus to better describe experimental data and suggested use of long duration pressure transient tests to infer a permeability vs. stress relationship.

When formulating their models, the authors of all of the above cited references considered the reservoir only. Permeability was assumed to be a function of the effective stress and the functional form was normally selected based on the laboratory data[12]. It was noted that the degree of the permeability reduction is different for homogeneous and fractured/fissured rock, so several authors developed models that allowed them to estimate permeability change vs. change of effective stress for various configurations of pore space – packing of spheres, or cracks, as well as crack orientation[13,14].

It also was noted that the properties of the over-, under-, and side-burden (rock mass that surrounds the reservoir) should be also taken into account when examining problems on a field-wide scale[15, 16]. Since most of the solved problems were on a limited scale, both in

time (duration of a drawdown or a buildup test) and in space (area drained by a well), the authors implicitly assumed that the surrounding rocks do not have a significant impact on the flow[17].

It is known, however, that substantial deviation of pressure from the initial pressure field in a reservoir is possible during field development. This deviation causes stress-strain state to change not only in the reservoir but also in the surrounding rocks. This, in turn, leads to alteration of the flow characteristics of a reservoir and production indicators of a well.

These and other effects concerned with the influence of the stress-strain state on the fluid flow were investigated in Former Soviet Union by Basniev, Ban, Gorbunov, Yentov, Zazovsky, Zotov, Maximov, Malakhova, Marmorshtein, Nikolayevsky, Ramazanov, and others. They suggested various models to account for interaction of fluid flow and deformation processes.

Yentov and Malakhova[2] discuss several such models and present the scheme according to which the reservoir within the rocks is modeled as a cut. The approach allowed the authors to investigate the stress-strain state in the rocks adjacent to the reservoir, including the well vicinity. Yentov, et. al.[18] obtained a qualitative estimate of the change in the well's productivity index (PI) following step pressure change in adjacent layer. Zazovskii[19] developed a way to account for shearing stresses in the vicinity of a well.

Nikolayevsky and Ramazanov[20] used the approach suggested by Yentov, et. al.[2], but instead of making assumptions, they calculated the pressure using transient flow equation. The same authors[21] expanded on their previous method[20] with account for wellbore radius, which allowed them to estimate the magnitude of the shearing stress on the casing.

Pressure and deformation fields induced by a constant rate well in a thick aquifer were investigated by Lewis, et. al.[22] using the finite element method. The processes in the aquifer and surrounding rocks are described using equations of consolidation, and the permeability is considered to be vanishingly small. The conclusion was that similar problems should be solved using a system of coupled consolidation equations.

It is known that formation permeability depends on the fluid pressure in the reservoir[23]. This dependence is a result of formation deformation caused by changes in the stress-strain state in the system "reservoir – surrounding rocks". The dependence of permeability on the deformation of the skeleton was explained by Lewis, et. al.[24]. Hence, the interaction of the stress-strain state with the pressure field in the reservoir should be taken into account.

Work of several researchers indicates that permeability of a core sample can be significantly affected by change in confining and pore pressure. This effect can be explained by repacking of the grains and by opening or closure of microcracks. The results show that deformation of low-permeability samples is mainly elastic. In Fig. 2-1 presented are results obtained by Gubanov[25]. These are permeability change of several core samples under constant confining pressure and changing pore pressure. Each data set has been fitted with a trend of the same color. It has been noted by many workers that the most permeability reduction occurs in low-permeability samples and the measured data can be satisfactorily fitted using exponential function.

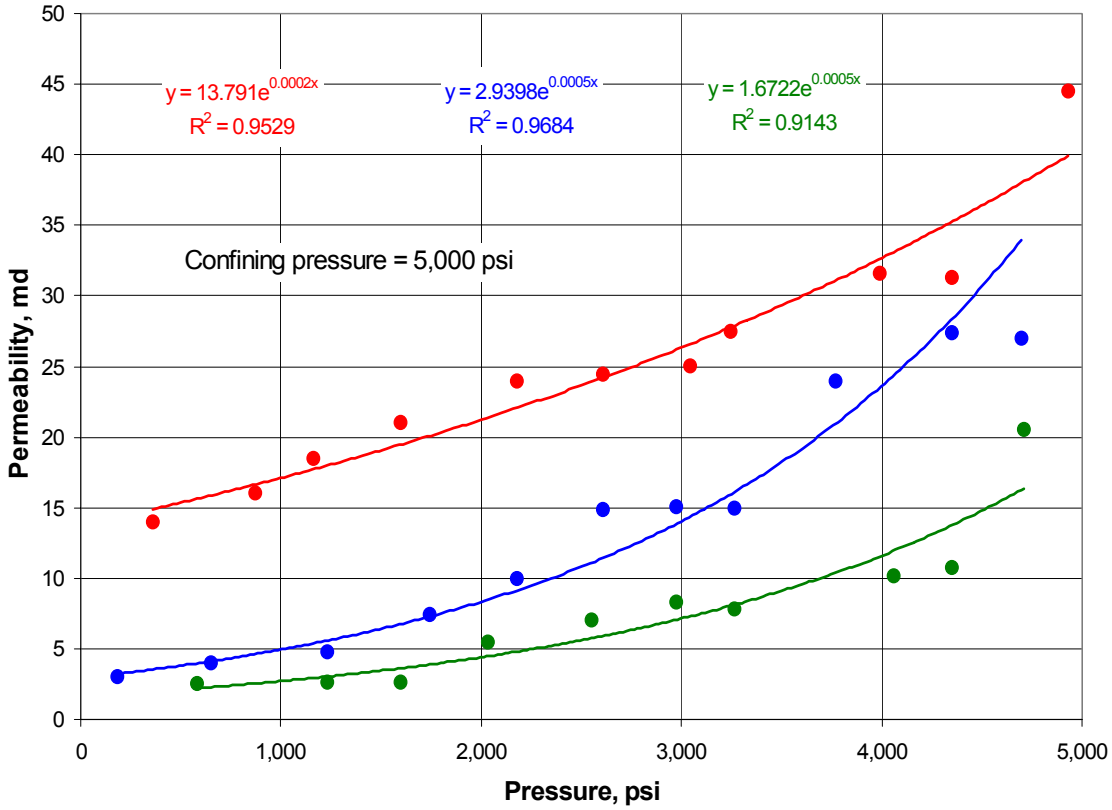

Figure 2-1. Variation of core permeability with pore pressure

Several authors[24,26] noted that in a number of injection tests increase in injection pressure lead to rapid non-linear increase of injectivity. This observation also is explained by the development or the opening of existing microcracks in the near-wellbore zone.

The effects of permeability reduction as a result of repacking are discussed by Chernikov et al.[27]. The experiments on specimens indicate that the permeability, when the specimen is affected by the stress caused by the drawdown increase, can reduce significantly – by tens of percent, and for some types of rock in the described conditions the permeability vanishes. These effects can take place within the drawdown ranges that are characteristic for actual field practice. This naturally leads to reduced production rates.

The deviation of an IPR from straight-line behavior can be explained, among other factors, by deformation effects such as closure of microcracks and repacking following the decline of the reservoir pressure. It also has been noted[28,29] that the observed non-linear behavior effects are not symmetric for production and injection.

Diyashev, et. al.[1] provide a discussion on permeability reduction in a formation with strong dependence of permeability on effective stress via deformation. The deformation is calculated using model of Yentov et. al.[2] and incorporating properties of the entire rock mass, i.e. the reservoir itself and the surrounding it rocks. The authors solved several axi-symmetric steady-state and transient problems with constant wellbore pressure and constant pressure outer boundary in a one- and two-layer reservoir and demonstrated the interaction of the deformational and pressure fields in adjacent layers. In the same reference and in the authors have considered linear flow and flow in presence of a circular zone around the wellbore, which may have different properties than the rest of the reservoir.

As follows from the above, it is interesting to evaluate the impact of deformation of the "reservoir – surrounding rocks" system on the pressure behavior and productive indicators of a well that operates in steady-state or transient regimes in a multilayer reservoir.

3 METHODOLOGY

In this section we present the formulation and solution of the elasticity theory problem, followed by the dimensionless equations and boundary conditions, which describe fluid flow in a reservoir with stress-dependent of permeability caused by deformation. We then discuss the additional dimensionless parameters, introduced by accounting for the deformation. Finally, we present the details of numerical solution of the problems of elasticity theory and fluid flow.

3.1 Formulation and solution of the elasticity theory problem

Consider a horizontal, porous, fluid-saturated reservoir of thickness h at depth H, penetrated with a well. We will use cylindrical coordinate system (r, z, φ), where z-axis coincides with the well axis (Fig. 3-1). The plane $z = H$ is perpendicular to the direction of the gravitational force and coincides with the surface. The plane $z = 0$ lies in the middle of the reservoir. The non-uniform pressure distribution in the reservoir is assumed to be axisymmetrical.

For the purpose of the subsequent analysis of fluid flow in an elastic reservoir, interacting with surrounding rocks, we will use the model that was suggested by Yentov and Malakhova[2]. According to this model, the reservoir is considered to be thin $(h << H)$, so that only its deformations in the vertical direction are important. It is assumed that the reservoir has no impact on the deformations of the surrounding rocks in the radial direction. Thus, uniform elastic semi-space bounded by plane $z = H$ with a cut at $z = 0 \pm 0$ corresponds to the reservoir system.

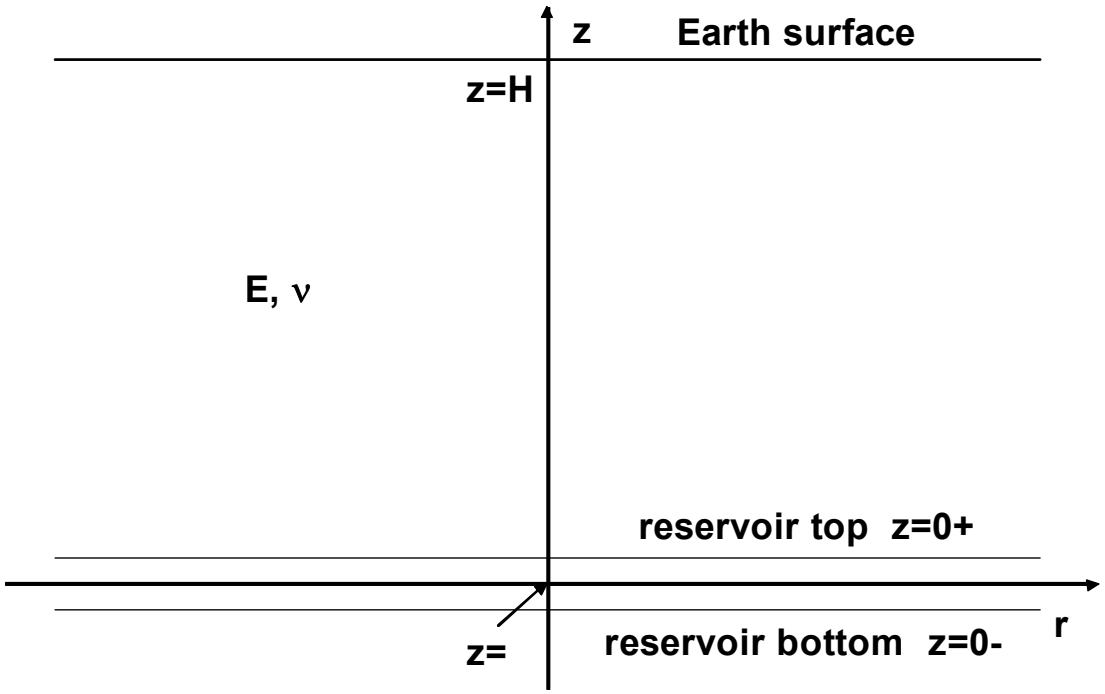

Figure 3-1. Scheme of the system

One could visualize a reservoir in this model as a set of tiny springs separating two elastic domains, which represent the surrounding rock mass (Fig. 3-2). Decrease of reservoir pressure near a well in such visualization is equivalent to compaction of the springs in the vicinity of a well. This compaction leads to deformation of over- and underburden. As the surrounding rocks have certain elastic properties, the deformation will not be local, i.e. limited only to the near-wellbore zone, where the pressure reduction has occurred. The springs further away from the well will also experience compaction, caused by the deformation of the surrounding media (Fig. 3-2b). At the same time, because of the assumption of a thin reservoir, it is reasonable to neglect stresses and strains in all but vertical direction, as illustrated in Fig. 3-3. Of course, when either of the model assumptions do not hold, i.e. the reservoir thickness or extent are comparable to its depth, one needs to properly account for all pertinent stresses and strains.

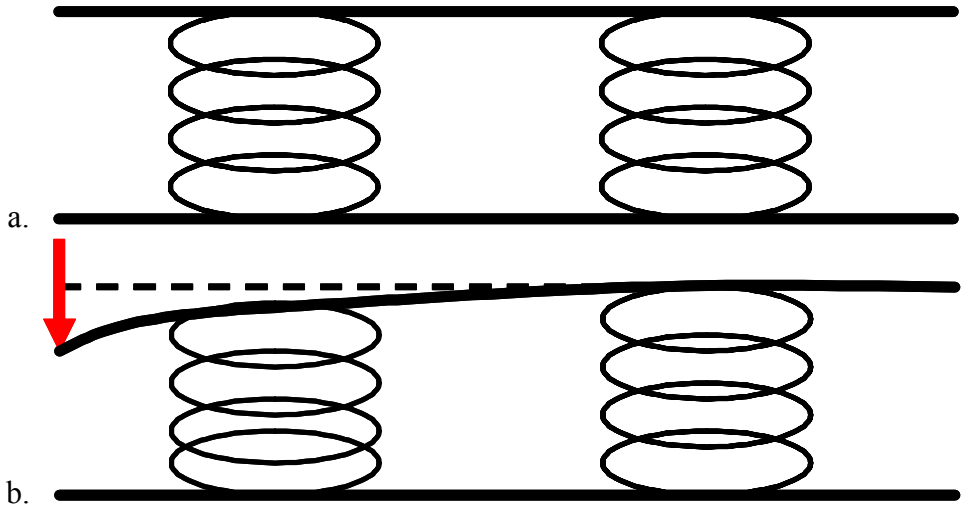

Figure 3-2. Visualization of the model

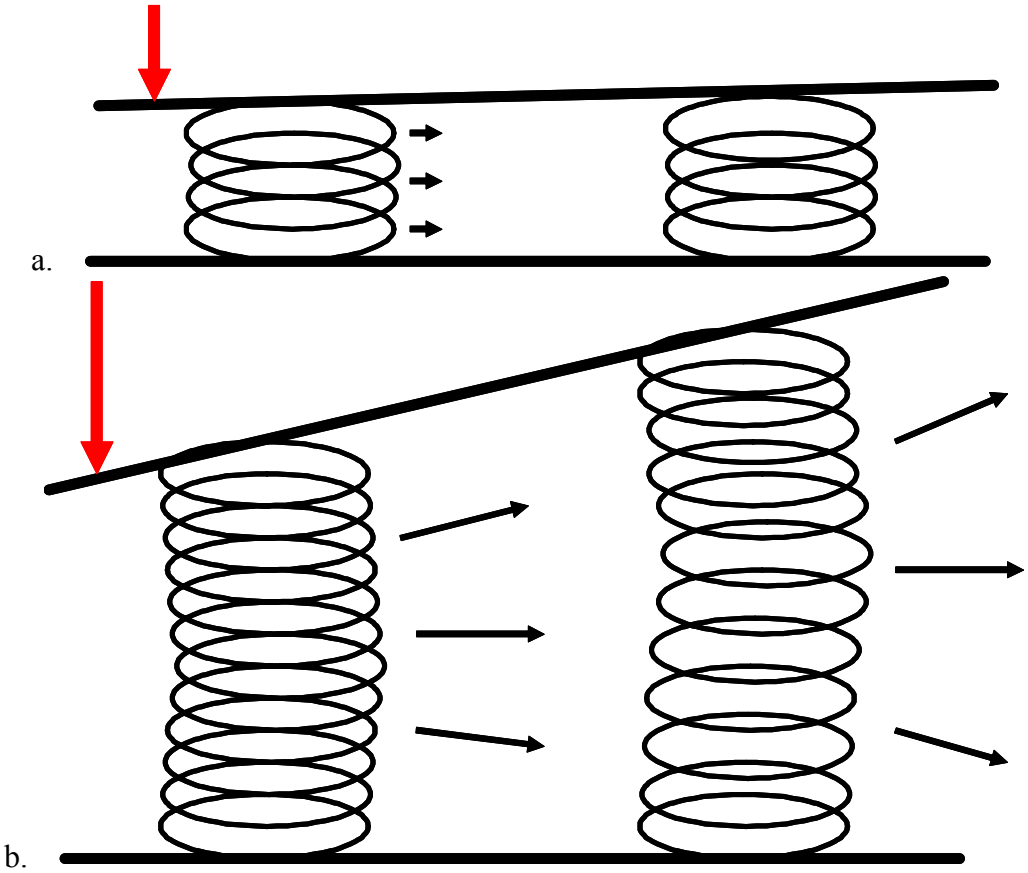

Figure 3-3. Schematic of radial stress in (a) thin, and (b) thick reservoir

Because of the assumed axial symmetry of the pressure distribution, the stress-strain state will also be axisymmetrical, so that the components of the stress tensor $\tau_{r\varphi} = \tau_{z\varphi} = 0$, and the component of the displacement vector $u_{\varphi} = 0$.

Further, we are not interested in finding the absolute values of pressure and displacement, but only the deviations from the values that correspond to a reservoir with constant pressure. In the derivations, which follow, we imply such deviations.

Elastic semi-space is characterized by Poisson's ratio, ν, and Young modulus, E. The displacement vector **u** satisfies the equation

$$grad\ \mathrm{div}\,\mathbf{u} - \frac{1-2\nu}{2(1-\nu)}\,\mathrm{rot}\,\mathrm{rot}\,\mathbf{u} = 0 \qquad (3.1)$$

with the boundary conditions

$$z = H: \qquad \sigma_z = \tau_{rz} = 0 \qquad (3.2)$$

$$z = 0: \qquad [\sigma_z] = [\tau_{rz}] = 0, \qquad [u_r] = 0 \qquad (3.3)$$

$$[u_z] = \frac{\sigma_z + \eta p(r)}{c} \qquad (3.4)$$

Here the square brackets denote the difference (jump) of a value on the top and bottom borders of the reservoir. σ_z and τ_{rz} are components of the stress tensor. u_r and u_z are components of the displacement vector **u**. The magnitude of η characterizes the degree that the reservoir pressure, $p(r)$, is transmitted to the reservoir top and bottom boundaries; it is close to unity[2]. The rigidity of the vertical deformation, c, can be expressed as $c = E/h$, where E is the Young modulus for the reservoir. A linear elastic constitutive law is used.

The elasticity theory problem Eqs. (3.1)-(3.4) is "external" in relation to the fluid flow in the reservoir and implicitly states the operator relationship of vertical deformations of the

reservoir with the pressure change in it. To obtain the operator explicitly, we need to have an analytical solution of the problem. Such a solution was obtained in[2] by using a stress function. Alternatively, we can use the Papkovich-Neiber representations of components of the stress-strain tensor and displacement vector for the axisymmetrical case via two harmonic functions Φ and φ[30]

$$\begin{aligned}
\sigma_z &= 2(1-\nu)\frac{\partial \Phi}{\partial z} - \frac{\partial^2 \varphi}{\partial z^2} - z\frac{\partial^2 \Phi}{\partial z^2} \\
\tau_{rz} &= \frac{\partial}{\partial r}\left[(1-2\nu)\Phi - \frac{\partial \varphi}{\partial z} - z\frac{\partial \Phi}{\partial z}\right] \\
u_z &= \frac{1+\nu}{E}\left[(3-4\nu)\Phi - \frac{\partial \varphi}{\partial z} - z\frac{\partial \Phi}{\partial z}\right] \\
u_r &= -\frac{1-\nu}{E}\left[\frac{\partial \varphi}{\partial z} + z\frac{\partial \Phi}{\partial z}\right]
\end{aligned} \tag{3.5}$$

We let layer $0 < z < H$ and semi-space $z < 0$ be, respectively, sub-domains 1 and 2. The functions Φ_j, φ_j, and p (here and henceforth j=1,2) can then be expressed as Hankel's integrals

$$0 < z < H: \qquad \Phi_1(r,z) = \int_0^\infty \left[A_1(\xi)e^{\xi z} + B_1(\xi)e^{-\xi z}\right] J_0(\xi r)\xi d\xi$$

$$\varphi_1(r,z) = \int_0^\infty \left[C_1(\xi)e^{\xi z} + D_1(\xi)e^{-\xi z}\right] J_0(\xi r)\xi d\xi$$

$$z < 0: \qquad \Phi_2(r,z) = \int_0^\infty A_2(\xi)e^{\xi z} J_0(\xi r)\xi d\xi$$

$$\varphi_2(r,z) = \int_0^\infty C_2(\xi)e^{\xi z} J_0(\xi r)\xi d\xi$$

$$p(r) = \int_0^\infty P(\xi) J_0(\xi r)\xi d\xi$$

Satisfying boundary conditions Eqs. (3.2)-(3.4) and accounting for Eq. (3.5), we find $A_j(x),\ B_1(x),\ C_j(x),\ D_1(x)$. The vertical stress on the borders of the cut $z=0$ is given by an integral

$$\sigma_z(r,0) = -\int_0^\infty \frac{H\xi^2[1-f(\xi)]P(\xi)J_0(r\xi)}{a_0 + H\xi - H\xi f(\xi)}d\xi \tag{3.6}$$

where $a_0 = 4(1-\nu^2)\frac{E_1 H}{Eh}$ and $f(\xi) = e^{-2H\xi}\left(1+2H\xi+2H^2\xi^2\right)$, which coincides with the results, obtained in[2]. Further development is the evaluation of the magnitude of $f(\xi)$ and neglecting the terms that include this small function. This is equivalent to setting H to infinity and, after changing the integration variable, the magnitude of $\sigma_z(r,0)$ does not depend on H. Therefore, if $\sigma_z(r,0)$ is needed as a function of H, the calculation should be performed using the full integral representation, Eq. (3.6).

Since we are interested in the characteristics of a well, we assume that the reservoir is located at a significant depth ($h/H << 1$), which allows for the above simplification. Simplifying, we obtain

$$[u_z(\rho,0)] = \frac{a}{c}\int_0^\infty \xi p(\xi) A(\xi,\rho)d\xi \tag{3.7}$$

where $\rho = r/r_w$, where r_w is a characteristic dimension, the wellbore radius

$$A(\xi,\rho) = \int_0^\infty \frac{yJ_0(\xi y)J_0(\rho y)}{y+a}dy \tag{3.8}$$

$$a = 4\eta(1-\nu^2)\frac{r_w E_1}{hE}$$

The internal integral (3.8) can be written as

$$A(\xi,\rho)=\int_0^\infty J_0(\xi y)J_0(\rho y)dy-a\int_0^\infty \frac{J_0(\xi y)J_0(\rho y)}{y+a}dy= \\ =I_1(\xi,\rho)-aI_2(\xi,\rho) \tag{3.9}$$

The integral I_1 can be written as[31]

$$I_1(\xi,\rho)=\begin{cases}(2/\pi\xi)K(\rho/\xi), & \rho<\xi \\ (2/\pi\rho)K(\xi/\rho), & \rho>\xi\end{cases} \tag{3.10}$$

where $K(x)$ is full elliptical integral. We can re-write integral I_2, which has an oscillating kernel in a form that allows for easy calculations. Let $\alpha=\rho/\xi<1$ and $b=a\xi$. Then

$$I_2(\alpha,b)=\int_0^\infty \frac{J_0(\alpha y)J_0(y)}{y+b}dy$$

Using the representation of a Bessel function of a complex argument u with Hankel functions of the third kind[31]

$$J_0(u)=\frac{1}{2}\left[H_0^{(1)}(u)+H_0^{(2)}(u)\right]$$

consider contour integral

$$I_{\Gamma_1}=\oint_{\Gamma_1}\frac{J_0(\alpha u)H_0^{(1)}(u)}{u+b}du$$

along a closed contour, which is comprised of the part (γ,M) of the real axis $\mathrm{Im}\,u=0$, quarter of circle (M,iM), part $(i,i\gamma)$ of the imaginary axis $\mathrm{Re}\,u=0$, and quarter of circle $(i\gamma,i)$ $(\gamma<<1,M>>1)$. It is known that $I_{\Gamma_1}=0$.

Also consider an integral, obtained by replacing $H_0^{(1)}$(u) with $H_0^{(2)}(u)$ in the integrand and taken along contour Γ_2, which is symmetric over real axis to Γ_1. When $M\to\infty$, the contributions to I_{Γ_1} and I_{Γ_2} of the quarter circles of infinitely large radii tend to zero. For

$\gamma \to 0$ the contributions of the quarter circles of infinitely small radii depend on the behavior of the integrands in the vicinity of zero. It is known that here $J_0(u) \to 1$ and functions $H_0^{(1)}, H_0^{(2)}$ have integrable logarithmic singularity. Therefore, the contributions of small quarter circles also tend to zero, and the integral I_2 is equal to the half-difference of the integrals taken along the real axis

$$I_2(\alpha, b) = \frac{1}{2} \lim_{\gamma \to 0} \left[-\int_{i\gamma}^{i\infty} \frac{J_0(\alpha u) H_0^{(1)}(u)}{u + b} du + \int_{-i\gamma}^{-i\infty} \frac{J_0(\alpha u) H_0^{(2)}(u)}{u + b} du \right]$$

Using the relations between Bessel functions of integer order and modified Bessel functions $I_0(x), K_0(x)$ [31]

$$J_0(\alpha u) = I_0(\alpha y), \qquad \mathrm{H}_0^{(1)}(u) = \frac{2}{\pi} K_0(y)$$

with account for equality $H_0^{(2)}(\bar{z}) = \overline{H_0^{(1)}(z)}$, obtain

$$I_2(\xi, \rho) = \frac{2a}{\pi} \int_0^{\infty} \frac{I_0(\rho y) K_0(\xi y)}{y^2 + a^2} dy, \qquad \rho < \xi \tag{3.11}$$

Similarly, we can show that

$$I_2(\xi, \rho) = \frac{2a}{\pi} \int_0^{\infty} \frac{I_0(\xi y) K_0(\rho y)}{y^2 + a^2} dy, \qquad \rho > \xi \tag{3.12}$$

And the expression $A(\xi, \rho)$ in Eq. (3.9) is written in the form, which does not contain oscillating functions

$$A(\xi, \rho) = \begin{cases} \dfrac{2}{\pi} \left[\dfrac{1}{\xi} K\left(\dfrac{\rho}{\xi} \right) - a^2 \displaystyle\int_0^{\infty} \frac{I_0(\rho z) K_0(\xi z)}{z^2 + a^2} dz \right], & \rho < \xi \\ \dfrac{2}{\pi} \left[\dfrac{1}{\rho} K\left(\dfrac{\xi}{\rho} \right) - a^2 \displaystyle\int_0^{\infty} \frac{I_0(\xi z) K_0(\rho z)}{z^2 + a^2} dz \right], & \rho > \xi \end{cases} \tag{3.13}$$

Formulas (3.7), (3.8), (3.13) allow for calculating of the jump $[u_z(\rho,0)]$ for given pressure distribution $p = p(\rho)$, which allows to proceed to analysis of fluid flow in an elastic reservoir, i.e. to formulation and solution of the respective "internal" problem.

We can note that condition (3.4) is physically the rheological equation of one-dimensional flow consolidation of a linearly elastic reservoir. Such interpretation allows for natural generalization to the case of a layered reservoir.

Let the reservoir be comprised of n layers with rigidities $c_j = E_j / h_j$, $j = 1,...n$ and E_j, h_j are Young's modulus and thickness of layer j. The jump of displacement of a layered reservoir is equal to the sum of the jumps of all layers

$$[u_z] = \sum_{j=1}^{n} [u_z^j], \qquad \text{where} \qquad [u_z^j] = \frac{\sigma_z + \eta p_j(r)}{c_j}$$

and the condition (3.4) is replaced by

$$[u_z] = \sum_{j=1}^{n} \frac{\sigma_z + \eta p_j(r)}{c_j} \tag{3.14}$$

Applying the solution procedure to problem (3.1)-(3.3), (3.14), we find

$$[u_z(\rho,0)] = a\int_0^\infty \xi A(\xi,\rho) \sum_{j=1}^{n} \frac{p_j(\xi)}{c_j} d\xi \tag{3.15}$$

where $A(\xi,\rho)$ is given by Eq. (3.13) and

$$a = \frac{4\eta r_w (1-\nu^2)}{E\sum_{j=1}^{n} (1/c_j)} \tag{3.16}$$

The formulas (3.14)-(3.16) allow for effective calculation of the jump $[u_z(\rho,0)]$, and, subsequently, of individual layers' displacements

$$\left[u_z^j\right] = \frac{\left[u_z\right] - \eta \sum_{k=1}^{n} \frac{p_k}{c_k}}{c_j \sum_{k=1}^{n} \frac{1}{c_k}} + \eta \frac{p_j}{c_j}$$

The obtained expressions allow one to proceed to the solution of the "internal" problem, which is analysis of flow in the reservoir. In simulating fluid flow in the elastic reservoir, we will assume that layer permeability is a function of its vertical deformation, and, for a multi-layer reservoir, dimensionless permeability $K_j = k_j / k_j^0 = K_j(\varepsilon_j)$, where $\varepsilon_j = \varepsilon_j(p_1,...,p_n) = \left[u_z^j\right]/h_j$, and k_j^0 are constants.

Further, using several simple models of fluid flow as examples and stating explicitly the functional form of permeability dependence on vertical deformation, we will consider the effect of accounting for interdependent flow and deformations processes on the production indicators of a well in a multi-layered reservoir.

We should again note that in the actual conditions of reservoir development, the reservoir deformations, ε, are not greater than 10^{-3}. Such small deformations do not usually significantly impact the reservoir permeability; however, in naturally fractured reservoirs, for which resistance to flow is determined by a network of fractures, such small deformations can cause changes in permeability by an order of magnitude or more. Similar response, according to laboratory measurements, can be expected in low-permeability un-fractured reservoirs. In this study we use a formal model of a uniform reservoir that strongly interacts with the surrounding rocks (allowing for large change of K with change of ε). Qualitatively, the model correctly describes actual behavior of a naturally fractured reservoir and other possible situations.

3.2 Transient fluid flow equations

For this problem, we consider radial, Darcy flow of a slightly compressible liquid of constant viscosity to a well located at the center of a circular drainage area. The reservoir is comprised of an arbitrary number of layers of uniform thicknesses with pressure-dependent permeabilities as given by solution of the "external" problem of the elasticity theory. A well is produced at constant total rate, or at constant flowing bottom hole pressure. Following Ehlig-Economides and Joseph[32], we introduce dimensionless variables (n is the number of layers)

$$r_D = \frac{r}{r_w} \qquad C_D = \frac{C}{2\pi(\phi h)_t c_t r_w^2}$$

$$(kh)_t = \sum_{j=1}^{n} (kh)_j \qquad (\phi h)_t = \sum_{j=1}^{n} (\phi h)_j$$

$$\kappa_j = \frac{(kh)_j}{(kh)_t} \qquad \omega_j = \frac{(\phi h)_j}{(\phi h)_t}$$

$$p_{jD} = \frac{2\pi(kh)_t}{q_t \mu} p_j \qquad t_D = \frac{(kh)_t}{(\phi h)_t \mu c_t r_w^2} t$$

$$q_{jD} = \frac{q_j}{q_t} = -\kappa_j K_j r_D \frac{\partial p_{jD}}{\partial r_D}$$

The pressure equation for an individual layer in dimensionless variables becomes

$$\frac{1}{r_D}\frac{\partial}{\partial r_D}\left[r_D K_j \frac{\partial p_{jD}}{\partial r_D} \right] = \frac{\omega_j}{\kappa_j}\frac{\partial p_{jD}}{\partial t_D}$$

Initial condition

$$p_{jD}(r_D, 0) = 0$$

Inner boundary condition is formulated using the following expressions

$$p_{wD} = \left(p_{jD} - s_j r_D K_j \frac{\partial p_{jD}}{\partial r_D} \right)_{r_D=1} \qquad 1 = \left(C_D \frac{dp_{wD}}{dt_D} - \sum_{j=1}^{n} \kappa_j K_j r_D \frac{\partial p_{jD}}{\partial r_D} \right)_{r_D=1}$$

The outer boundary condition is

$$\left(p_{jD}\right)_{r_D=r_{eD}} = 0 \qquad \text{or} \qquad \left(\frac{\partial p_{jD}}{\partial r_D} \right)_{r_D=r_{eD}} = 0$$

The problem is solved numerically for $K_j = K_j\left(\varepsilon_j\right) = \exp\left(-\beta_j \varepsilon_j\right)$, where

$$\varepsilon_j = \varepsilon_j\left(p_1,...,p_n\right) = \left[u_z^j\right]/h_j \qquad \text{and} \qquad \left[u_z^j\right] = \frac{\left[u_z\right] - \eta \sum_{k=1}^{n} \frac{p_k}{c_k}}{c_j \sum_{k=1}^{n} \frac{1}{c_k}} + \eta \frac{p_j}{c_j}$$

Additionally, we introduce $\gamma_j = \frac{E_j}{E}$. Then, the total deformation in dimensionless variables is

$$\left[u_z\right] = \frac{q_t \mu}{2\pi (kh)_t} \frac{a}{E} \int_0^{\infty} \left(\sum_{k=1}^{n} \frac{h_k}{\gamma_k} p_{kD} \right) y A(y, r_D) dy \qquad a = \frac{4\eta r_w (1-\nu^2)}{\sum_{k=1}^{n} \left(h_k/\gamma_k\right)}$$

The individual deformation of *j*-th layer is

$$\left[u_z^j\right] = \frac{q_t \mu}{2\pi (kh)_t} \frac{\eta}{E} \left(\frac{\frac{a}{\eta} \int_0^{\infty} \left(\sum_{k=1}^{n} \frac{h_k}{\gamma_k} p_{kD} \right) y A(y, r_D) dy - \sum_{k=1}^{n} \frac{h_k}{\gamma_k} p_{kD}}{\frac{\gamma_j}{h_j} \sum_{k=1}^{n} \frac{h_k}{\gamma_k}} + \frac{h_j}{\gamma_j} p_{jD} \right)$$

Denote $\alpha_j = \beta_j \frac{\eta}{E} \frac{q_t \mu}{2\pi (kh)_t}$, then

$$K_j\left(r_D\right) = \exp\left[-\alpha_j \left(\frac{\frac{a}{\eta} \int_0^{\infty} \left(\sum_{k=1}^{n} \frac{h_k}{\gamma_k} p_{kD} \right) y A(y, r_D) dy - \sum_{k=1}^{n} \frac{h_k}{\gamma_k} p_{kD}}{\gamma_j \sum_{k=1}^{n} \frac{h_k}{\gamma_k}} + \frac{p_{jD}}{\gamma_j} \right) \right]$$

We can further make use of the radial symmetry of the flow system to simplify the equations by performing the following coordinate transformation

$$x = \frac{\ln r_D}{\ln r_{eD}} \qquad r_D = r_{eD}^x \qquad dr_D = x r_{eD}^{x-1} dx$$

Then, since $1 \le r_D \le r_{eD}$, the new variable $0 \le x \le 1$ and the equation becomes

$$\frac{\partial}{\partial x}\left[K_j \frac{\partial p_{jD}}{\partial x} \right] = r_{eD}^{2x} \left(\ln r_{eD}\right)^2 \frac{\omega_j}{\kappa_j} \frac{\partial p_{jD}}{\partial t_D}$$

Using the new variable, the dimensionless wellbore pressure is

$$p_{wD} = \left(p_{jD} - \frac{s_j K_j}{\ln r_{eD}} \frac{\partial p_{jD}}{\partial x} \right)_{x=0}$$

And the rate boundary condition is

$$1 = \left(C_D \frac{dp_{wD}}{dt_D} - \frac{1}{\ln r_{eD}} \sum_{j=1}^{n} \kappa_j K_j \frac{\partial p_{jD}}{\partial x} \right)_{x=0}$$

The outer boundary condition is either constant flux (or no-flow), or constant pressure circular boundary.

3.3 Parameters of the problem

The problem depends on a set of parameters, which describe various rock and fluid properties, and the geometry of the system. Rock properties are normally determined as a result of core analysis or are derived from open hole well logs and well tests. Fluid properties can be obtained either from PVT analysis of a reservoir fluid sample or estimated using correlations. The geometry of the system can be inferred using data from logs, seismic, well tests, and the geologic understanding of the reservoir. Well-specific parameters are

measured (flow rate, flowing pressure), or estimated/calculated (wellbore storage, skin) from well test and production data.

In addition to conventional dimensionless variables used in well test analysis, our problem depends on the two additional dimensionless groups; which are a

$$a = \frac{4\eta r_w (1-\nu^2)}{\sum_{k=1}^{n} (h_k/\gamma_k)} = \frac{4\eta r_w (1-\nu^2)}{E\sum_{k=1}^{n} (h_k/E_k)} \tag{3.17}$$

that incorporates the elastic properties of rocks, and parameter α_j

$$\alpha_j = \beta_j \frac{\eta}{E} \frac{q_t \mu}{2\pi (kh)_t} \tag{3.18}$$

that characterizes the sensitivity of reservoir rock's permeability to deformation and also includes the Young's modulus of the overburden.

Consider parameter a. According to various estimates, Biot's parameter, η, can vary from 0.6 to 1, but is usually close to unity. Poisson's ratio, ν, for typical rocks is in the range from 0.15 to 0.25. γ, the ratio of Young's modulus of reservoir rock to that of the surrounding rock mass, may vary within two orders of magnitude, from 0.1 to 10, or more. The ratio of the wellbore radius to the reservoir thickness for all practical purposes is much less than 0.1.

The dimensionless α_j includes parameter β_j, which is the coefficient that characterizes the degree of permeability change with deformation. It follows from the experimental results of permeability change with changes in effective stress that greater permeability reduction with an increase of effective stress occurs in low-permeability rocks. This reduction can be as high as 90% of the initial value. High-permeability rocks also exhibit stress-dependent behavior, though on a much smaller scale.

At the same time, if flow in a reservoir is determined to a major degree by the presence of natural fractures or micro-cracks, the initially high rock permeability (due to micro-cracks) will suffer the most dramatic reduction. According to the estimates, actual relative deformation of a reservoir will not exceed 10^{-3}. To allow for large permeability variation, parameter β_j should be on the order of 10^3. The magnitude of α_j depends also on the Young's modulus of the overburden. Let in (3.18) $\alpha_j = 2$ for $E = 10^{10}\ Pa$. If other variables (total flow rate, total permeability-thickness product, and fluid viscosity) are kept the same, then for $E = 10^{11}\ Pa$, the same α=2 is equivalent to a 10-fold increase in β_j, which is the sensitivity to deformations. It is impossible to narrow down, with certainty, the range of β_j for a particular lithology, because its magnitude also will depend on the magnitude of pressure change in the reservoir, stress history, and many other factors such as shale content. We can, however, identify this parameter, β_j, on a case-by-case basis, as it will be shown later.

For typical values of the parameters and based on the results of laboratory measurements, α_j should be in the range from -3 to 3 (negative values correspond to injection). Within this range of sensitivity values, permeability varies from about 3-fold increase (injection) and to less than 10% retained of the initial value. Clearly, our estimate of the range of parameter α_j reflects only the available data, i.e. measurements on consolidated sandstone samples. For fractured/fissured rocks and/or in presence of shale streaks sensitivity of permeability to deformation may be significantly greater.

It also can be concluded from the experimental data[25], that the results can be adequately approximated with an exponential function, which served as justification for selecting permeability dependence in the form $K_j = K_j(\varepsilon_j) = \exp(-\beta_j \varepsilon_j)$.

3.4 Numerical solution

In solving the problem numerically, we proceed as follows. First, we calculate the vertical deformation of the entire reservoir. This establishes the relationship of vertical deformation with pressure change in the layers. The step is performed only once for the given set of geometric and elastic parameters. Second, we determine the deformation of individual layers. Third, we assign a functional dependence of layers' permeability on their deformation and calculate the flow characteristics – rate and pressure.

3.4.1 Calculation of deformations

Effective and accurate calculation of the vertical displacement is extremely important to solving this problem. Total deformation is of the following form,

$$U(r_D) = \frac{2\pi(kh)_t}{q_t \mu} E[u_z] = a \int_0^{\infty} \left(\sum_{k=1}^{n} \frac{h_k}{\gamma_k} p_{kD} \right) yA(y, r_D) dy$$

The integral from zero to infinity is a sum of these three parts

$$U(r_D) = a p_{wD} \left(\sum_{k=1}^{n} \frac{h_k}{\gamma_k} \right) \int_0^1 yA(y, r_D) dy + a \int_1^{r_{eD}} \left(\sum_{k=1}^{n} \frac{h_k}{\gamma_k} p_{kD} \right) yA(y, r_D) dy + 0$$

Or, when accounting for the log-transformation of the radial coordinate in the second integral,

$$U(r_D) = ap_{wD}\sum_{k=1}^{n}\frac{h_k}{\gamma_k}\int_0^1 yA(y,r_D)dy + a\int_0^1\left(\sum_{k=1}^{n}\frac{h_k}{\gamma_k}p_{kD}\right)yA(y,x)dy =$$

$$= ap_{wD}\sum_{k=1}^{n}\frac{h_k}{\gamma_k}J_1 + aJ_2$$

Consider, first, integral J_2 and its kernel

$$yA(y,x) = \begin{cases} \dfrac{2y}{\pi}\left[\dfrac{1}{y}K\left(\dfrac{x}{y}\right) - a^2\displaystyle\int_0^\infty \frac{I_0(xz)K_0(yz)}{z^2+a^2}dz\right], & x < y \\ \dfrac{2y}{\pi}\left[\dfrac{1}{x}K\left(\dfrac{y}{x}\right) - a^2\displaystyle\int_0^\infty \frac{I_0(yz)K_0(xy)}{z^2+a^2}dz\right], & x > y \end{cases}$$

In the integral $I_1 = a^2\displaystyle\int_0^\infty \frac{I_0(xz)K_0(yz)}{z^2+a^2}dz$ introduce $t = yz$; $z^2 = \dfrac{t^2}{y^2}$; $dz = \dfrac{dt}{y}$

$$I_1 = a^2\int_0^\infty \frac{I_0\left(\dfrac{x}{y}t\right)K_0(t)}{\dfrac{t^2}{y^2}+a^2}\frac{dt}{y} = ya^2\int_0^\infty \frac{I_0\left(\dfrac{x}{y}t\right)K_0(t)}{t^2+y^2a^2}dt$$

Similarly,

$$I_2 = a^2\int_0^\infty \frac{I_0\left(\dfrac{y}{x}t\right)K_0(t)}{\dfrac{t^2}{x^2}+a^2}\frac{dt}{x} = xa^2\int_0^\infty \frac{I_0\left(\dfrac{y}{x}t\right)K_0(t)}{t^2+x^2a^2}dt$$

And

$$yA(y,x) = \begin{cases} \dfrac{2}{\pi}\left[K\left(\dfrac{x}{y}\right) - y^2a^2\displaystyle\int_0^\infty \frac{I_0\left(\dfrac{x}{y}t\right)K_0(t)}{t^2+y^2a^2}dt\right], & x < y \\ \dfrac{2}{\pi}\left[\dfrac{y}{x}K\left(\dfrac{y}{x}\right) - xya^2\displaystyle\int_0^\infty \frac{I_0\left(\dfrac{y}{x}t\right)K_0(t)}{t^2+x^2a^2}dt\right], & x > y \end{cases} \qquad (3.19)$$

At $y = x$ there is an integrable logarithmic singularity in the full elliptic integral and, for example for $x = 0.5$, the plot of the kernel vs. y is shown in Fig. 3-4.

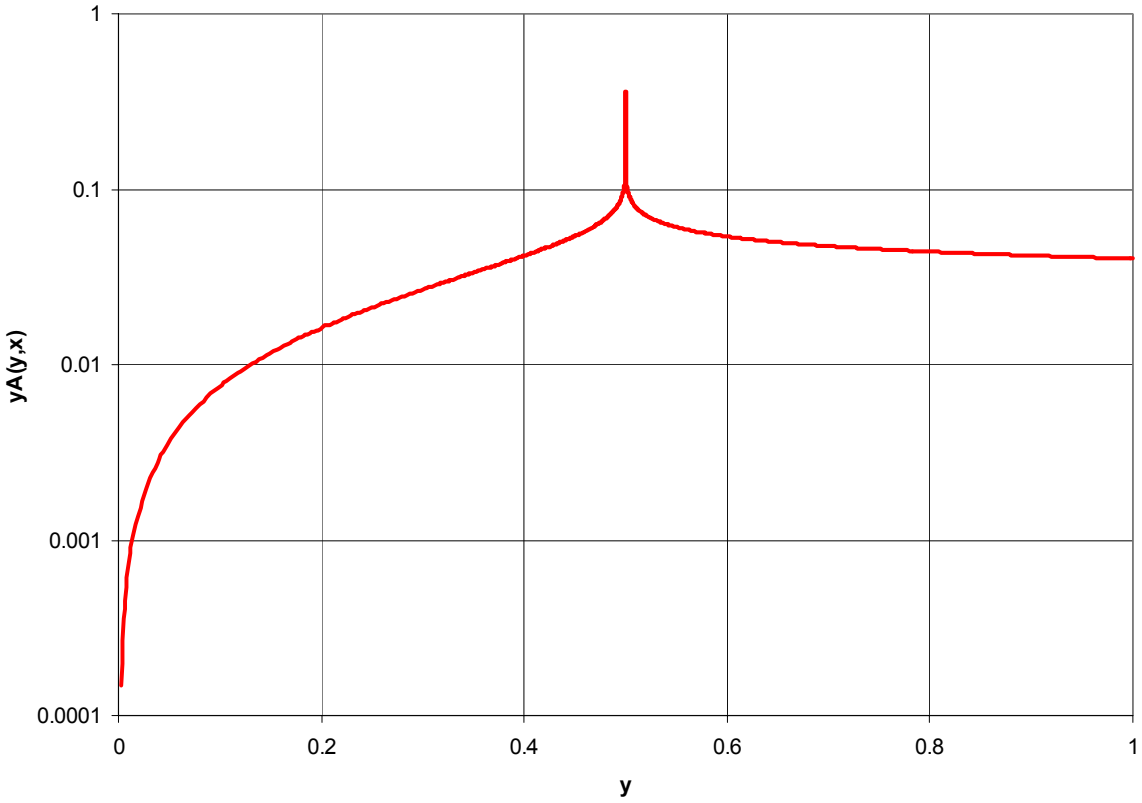

Figure 3-4. Kernel vs. integration parameter at x=0.5

To accurately account for the rapidly changing function in the vicinity of x, a non-uniform grid is introduced with spacing increasing away from x. Both the grid and the values of the kernel for each x are pre-computed and stored, which allows later for fast and accurate calculations of deformation. The internal integral with modified Bessel functions is calculated using the Romberg method.

The double integral

$$J_1 = \int_0^1 yA(y, r_D)dy = \frac{2}{\pi}\int_0^1 \left[\frac{y}{r_D} K\left(\frac{y}{r_D}\right) - r_D y a^2 \int_0^\infty \frac{I_0\left(\frac{y}{r_D}t\right)K_0(t)}{t^2 + r_D^2 a^2} dt \right] dy$$

is computed using Romberg integration twice and is also stored.

When calculating deformation for each value of *x,* the term $\sum_{k=1}^{n} \frac{h_k}{\gamma_k} p_{kD}$ is interpolated using cubic spline at the pre-computed grid points. Final integration is performed using the trapezoidal rule. On each stage of the computations extensive numerical testing has been performed to ensure acceptable accuracy.

3.4.2 Numerical solution of set of non-linear equations

The set of non-linear equations, obtained after putting flow equations for individual layers into finite-difference form, was solved numerically using the globally convergent Newton method. Detailed explanation of the method and the code can be found in Ref. 33. The finite-difference equations result in the following system

$$\mathbf{F}(\mathbf{p}) = 0$$

where **F** is vector-function, and **p** is vector of unknown pressures. On each Newton iteration we calculate the values of vector-function for new vector

$$\mathbf{p}_{new} = \mathbf{p}_{old} + \delta\mathbf{p}$$

where $\delta\mathbf{p} = -\mathbf{J}^{-1}\mathbf{F}$, $\mathbf{J}$ is the Jacobian matrix, and the step $\delta\mathbf{p}$ is accepted if it reduces on each iteration the norm $f = \frac{1}{2}\mathbf{F} \bullet \mathbf{F}$. The Jacobian is computed numerically.

3.4.3 Finite-difference scheme

The non-linear dimensionless pressure equation for an individual layer (omitting dimensionless subscript *D* and layer subscript *j* for brevity)

$$\frac{\partial}{\partial x}\left[K\frac{\partial p}{\partial x}\right] = r_{eD}^{2x}\left(\ln r_{eD}\right)^2 \frac{\omega}{\kappa}\frac{\partial p}{\partial t}$$

is put in finite-difference form in conventional way. The implicit pressure equation is

$$\frac{1}{\Delta x}\left(K_{i+1/2}^{n}\frac{p_{i+1}^{n+1}-p_i^{n+1}}{\Delta x} - K_{i-1/2}^{n}\frac{p_i^{n+1}-p_{i-1}^{n+1}}{\Delta x}\right) = r_{eD}^{2x_i}\left(\ln r_{eD}\right)^2 \frac{\omega}{\kappa}\frac{p_i^{n+1}-p_i^{n}}{\Delta t}$$

here $K_{i+1/2}^{n} = \dfrac{K_{i+1}^{n}+K_i^{n}}{2}$ and $i = 2,...N-1$. The non-linear coefficients are calculated on the previous time step, *n*. Denote $\lambda_i = r_{eD}^{2x_i}\left(\ln r_{eD}\right)^2 \dfrac{\omega}{\kappa}\dfrac{(\Delta x)^2}{\Delta t}$, then

$$K_{i+1/2}^{n}p_{i+1}^{n} - \left(K_{i+1/2}^{n}+K_{i-1/2}^{n}+\lambda_i\right)p_i^{n+1} + K_{i-1/2}^{n}p_{i-1}^{n+1} = -\lambda_i p_i^{n}$$

The explicit formulation is

$$K_{i+1/2}^{n}p_{i+1}^{n} - \left(K_{i+1/2}^{n}+K_{i-1/2}^{n}-\lambda_i\right)p_i^{n} + K_{i-1/2}^{n}p_{i-1}^{n} = \lambda_i p_i^{n+1}$$

We then use the weighted average of implicit and explicit formulations

$$\sigma K_{i+1/2}^{n}p_{i+1}^{n} - \sigma\left(K_{i+1/2}^{n}+K_{i-1/2}^{n}+\lambda_i\right)p_i^{n+1} + \sigma K_{i-1/2}^{n}p_{i-1}^{n+1} = -\sigma\lambda_i p_i^{n}$$

$$(1-\sigma)\lambda_i p_i^{n+1} = (1-\sigma)\left[K_{i+1/2}^{n}p_{i+1}^{n} - \left(K_{i+1/2}^{n}+K_{i-1/2}^{n}-\lambda_i\right)p_i^{n} + K_{i-1/2}^{n}p_{i-1}^{n}\right]$$

And the layer flow equation at the interior points is approximated with the second order in space and the first order in time (for $0.5 < \sigma \le 1$) by vector-function with components

$$F_i = \sigma K_{i+1/2}^{n}p_{i+1}^{n} - \left(\sigma K_{i+1/2}^{n}+\sigma K_{i-1/2}^{n}+\lambda_i\right)p_i^{n+1} + \sigma K_{i-1/2}^{n}p_{i-1}^{n+1} +$$
$$+\sigma\lambda_i p_i^{n} + (1-\sigma)\left[K_{i+1/2}^{n}p_{i+1}^{n} - \left(K_{i+1/2}^{n}+K_{i-1/2}^{n}-\lambda_i\right)p_i^{n} + K_{i-1/2}^{n}p_{i-1}^{n}\right]$$

In order to put the rate boundary condition into finite-difference form, we need to approximate pressure derivative at $x = 0$. Using Taylor series have

$$p(\Delta x) = p(0) + \Delta x \frac{\partial p(0)}{\partial x} + \frac{\Delta x^2}{2} \frac{\partial p^2(0)}{\partial x^2} + O\left(\Delta x^3\right)$$

$$\frac{\partial p(0)}{\partial x} = \frac{p(\Delta x) - p(0)}{\Delta x} - \frac{\Delta x}{2} \frac{\partial p^2(0)}{\partial x^2} + O\left(\Delta x^2\right)$$

Expression for the second pressure derivative at $x = 0$ follows from the pressure equation

$$\frac{\partial}{\partial x}\left[K \frac{\partial p}{\partial x} \right] = \frac{\partial K}{\partial x} \frac{\partial p}{\partial x} + K \frac{\partial^2 p}{\partial x^2} = r_{eD}^{2x} \left(\ln r_{eD}\right)^2 \frac{\omega}{\kappa} \frac{\partial p}{\partial t} = \left(\ln r_{eD}\right)^2 \frac{\omega}{\kappa} \frac{\partial p}{\partial t}$$

$$\frac{\partial p}{\partial x}\left(1 - \frac{\Delta x}{2} \frac{\partial K}{K \partial x} \right) = \frac{p(h) - p(0)}{\Delta x} - \left(\ln r_{eD}\right)^2 \frac{\Delta x \omega}{2K\kappa} \frac{\partial p}{\partial t}$$

$$\frac{\partial p}{\partial x} = \frac{1}{1 - \frac{\Delta x}{2} \frac{\partial \ln K}{\partial x}} \left[\frac{p(h) - p(0)}{\Delta x} - \left(\ln r_{eD}\right)^2 \frac{\Delta x \omega}{2K\kappa} \frac{\partial p}{\partial t} \right]$$

Since $p(0) = p_1$, $p(\Delta x) = p_2$, etc., obtain

$$\left. \frac{\partial p}{\partial x} \right|_{x=0} = \frac{2K_1^n}{2 - \ln K_2^n + \ln K_1^n} \left[\frac{p_2^{n+1} - p_1^{n+1}}{\Delta x} - \left(\ln r_{eD}\right)^2 \frac{\Delta x \omega}{2K_1^n \kappa} \frac{p_1^{n+1} - p_1^n}{\Delta t} \right]$$

Denote

$$T_0 = \frac{2K_1^n}{2 - \ln K_2^n + \ln K_1^n}; \qquad T_1 = \frac{\kappa}{\ln r_{eD}} \frac{T_0}{\Delta x}; \qquad T_2 = \frac{\Delta x}{\Delta t} \frac{\omega \ln r_{eD}}{2K_1^n} T_0$$

Implicit and explicit rate formulations are, respectively,

$$q_{im} = \frac{\kappa K_1^n}{\ln r_{eD}} \frac{\partial p}{\partial x}\bigg|_{x=0} =$$
$$= -T_1 p_1^{n+1} + T_1 p_2^{n+1} - T_2 p_1^{n+1} + T_2 p_1^n = -(T_1 + T_2) p_1^{n+1} + T_1 p_2^{n+1} + T_2 p_1^n$$

$$q_{ex} = \frac{\kappa K_1^n}{\ln r_{eD}} \frac{\partial p}{\partial x}\bigg|_{x=0} =$$
$$= -T_1 p_1^n + T_1 p_2^n - T_2 p_1^{n+1} + T_2 p_1^n = -T_2 p_1^{n+1} - (T_1 - T_2) p_1^n + T_1 p_2^n$$

Recall that dimensionless wellbore pressure for layer *j* is written as

$$p_{wD} = \left(p_{jD} - \frac{s_j}{\kappa_j} \frac{\kappa_j K_j}{\ln r_{eD}} \frac{\partial p_{jD}}{\partial x} \right)_{x=0}$$

and individual layer rate boundary condition includes rates from all *m* layers

$$1 = \left(C_D \frac{dp_{wD}}{dt_D} - \sum_{j=1}^{m} \frac{\kappa_j K_j}{\ln r_{eD}} \frac{\partial p_{jD}}{\partial x} \right)_{x=0}$$

Then, for example, the component of the vector-function, which corresponds to the inner boundary of the first layer is

$$F_{inner}^{layer1} = \frac{C_D}{\Delta t} \left(p_{wD} - p_1^{n+1} + \frac{s_1}{\kappa_1} \left[\sigma q_{im} + (1-\sigma) q_{ex} \right] \right) +$$
$$+ \sigma q_{im} + (1-\sigma) q_{ex} + \sum_{\substack{remaining \\ layers}} \left[\sigma q_{im} + (1-\sigma) q_{ex} \right] + 1$$

If we specify constant wellbore pressure, p_{wD}, the boundary condition is

$$F_{inner}^{layer1} = \sigma p_1^{n+1} + (1-\sigma) p_1^n - \frac{s_1}{\kappa_1} \left[\sigma q_{im} + (1-\sigma) q_{ex} \right] - p_{wD}$$

Similar expressions are written for the other layers.

Possible cross flow between layers is described by a term that includes pressure difference in adjacent layers and cross flow coefficient. For example, for layers 1 and 2 this term is simply $X\left(p_{1,i}^{n+1} - p_{2,i}^{n+1}\right)$, where X is the dimensionless cross flow coefficient.

On each time step we first calculate values of the vector-function with the non-linear coefficients, taken from the previous time step. Then, we calculate the Jacobian using forward difference[33], and determine the descent direction for the norm of the vector-function. We then move along this direction with steps designed to reduce the norm and to bring the vector-function closer to zero. Once acceptable convergence on the norm has been achieved, we calculate the non-linear coefficients and continue with the next Newton iteration, until the values of the vector-function are sufficiently close to zero. We then proceed to the next time step.

3.4.4 Code implementation

In coding of the algorithm, we have applied certain ideas of the object-oriented programming (OOP). The benefits of the object-oriented approach are well-known and discussions of the philosophy behind the OOP can be found elsewhere. Though Visual Basic for Applications (supplied with Microsoft Excel) does not yet have full support for OOP, it was possible to structure the code in such a way that it allows for easy analysis and subsequent modifications. A brief explanation of the code implementation follows (code itself is supplied in the Appendix).

On the initialization stage, we input static parameters of the reservoir (number of layers, extent, temperature, etc.), of layers (porosity, permeability, thickness, skin, etc), of the well (wellbore radius, wellbore storage coefficient), and fluid data. We also specify the

boundary conditions and numerical parameters of the problem (time step, etc.), as well as read-in the values of the kernel, pre-calculated using Eq. (3.19).

Following input of the data, the code creates a number of objects. The first collection of objects is a collection of points. Each point object carries the point-specific grid and values of the kernel at the grid points. The reservoir object includes the collection of points and additionally methods (subroutines and functions) that calculate for given pressure distributions in layers the term $\sum_{k=1}^{n} \frac{h_k}{\gamma_k} p_{kD}$ and total vertical deformation.

Once total deformation has been calculated, its values are passed to layers. The layers are separate objects with different properties (Young's modulus, thickness, porosity, etc.), but with identical methods to calculate the permeability and fluid non-linear terms. The layer objects are generated using the same template and are assigned respective different values of properties. The non-linear terms, once determined for all layers, allow us to calculate the values of the vector-function, which is also an object. The next two objects perform Newton iterations and iterative solution of a sparse matrix (in non-OOP terms, these modules have subroutines and functions to run these calculations). Along with these principal objects we also generate separate objects, which perform check on the convergence criteria and output.

The result of such an approach is a clearly structured code. On each step of the numerical solution, we are dealing with objects that carry their respective properties and methods. If there is a need to add a property or a method (a subroutine) to a collection of objects, all we have to do is to add the required property to the template. All objects subsequently generated using this template will automatically include the desired features.

3.4.5 Numerical testing

Calculations were performed on a spatial grid with uniform step size and with a time step multiplier. To select these parameters, the finite-difference scheme was tested against Van Everdingen and Hurst constant terminal rate solution in an infinite reservoir. The relative difference between the two solutions was calculated for various combinations of step sizes with $C_D = 100$ and no sensitivity of reservoir permeability to deformation ($\alpha = 0$).

The testing was performed for 20-, 50-, and 100-point spatial grids and with 1.01, 1.1, 1.2, 1.5 time step multiplier. Since the results have shown that a 20-point grid with time step multiplier of 1.2 (12 steps per log cycle) provides acceptable accuracy (less than 0.1% error in the practical time range) within reasonable calculation times, these grid parameters have been used. The value of the weighting parameter, σ, in the finite-difference scheme is 0.7.

In the Fig. 3-5, the blue curves are the calculated pressure change and the derivative, respectively, and the red curve is the relative difference with Van Everdingen and Hurst terminal rate solution.

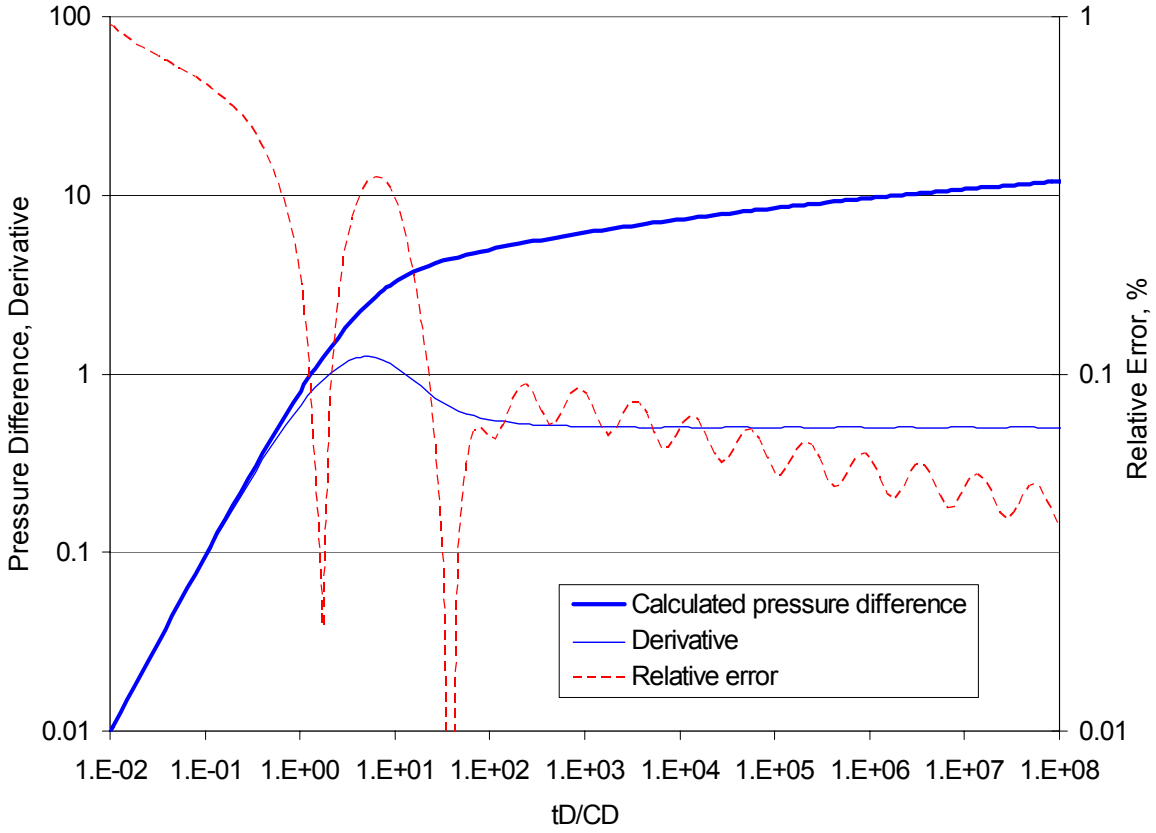

Figure 3-5. Comparison with Van Everdingen and Hurst terminal rate solution

4 SINGLE LAYER CASE

In this chapter we present the results of calculations for a single-layer case. This case is the least complicated and its consideration allows to arrive to certain conclusions, which are helpful in understanding of multi-layer cases. In the first section, we show how the flow principal characteristics – pressure, deformation, and permeability – vary vs. distance and time. Second, we consider several typical transient problems, present the type curves and their sensitivity on the geometric and elastic parameters. And, finally, we consider the steady-state problems and examine the IPRs.

4.1 Sensitivity to elastic and geometrical parameters of the problem

In this section, we investigate the dependence of flow on the elastic and geometric parameters has been investigated. Since the magnitude of permeability change depends also on the direction of flow, we consider separately cases of production and injection.

To develop an understanding of how the magnitude of deformation depends on the elastic and geometric parameters of the problem, we first consider the following example. Let a well be produced at constant flow rate in a circular reservoir with a constant pressure outer boundary located at $r_{eD} = 10{,}000$. For this case, the permeability is not stress-dependent, i.e. $\alpha = 0$ and $k = 10\ md$. The other parameters are as follows: $\gamma = E_1 / E = 1$ and Young's modulus of the surrounding rocks $E = 10^{10}\ Pa$; $r_w / h = 10^{-2}$ and $h = 10\ m$; Poisson's ratio $\nu = 0.2$, coefficient $\eta = 1$. With these parameters $a = 0.0384$. Pressures vs. distance at several moments in time are presented in Fig 4-1. The pressure distribution curves are approximately one log-cycle apart in time and red curve corresponds to $t_D / C_D \approx 1000$.

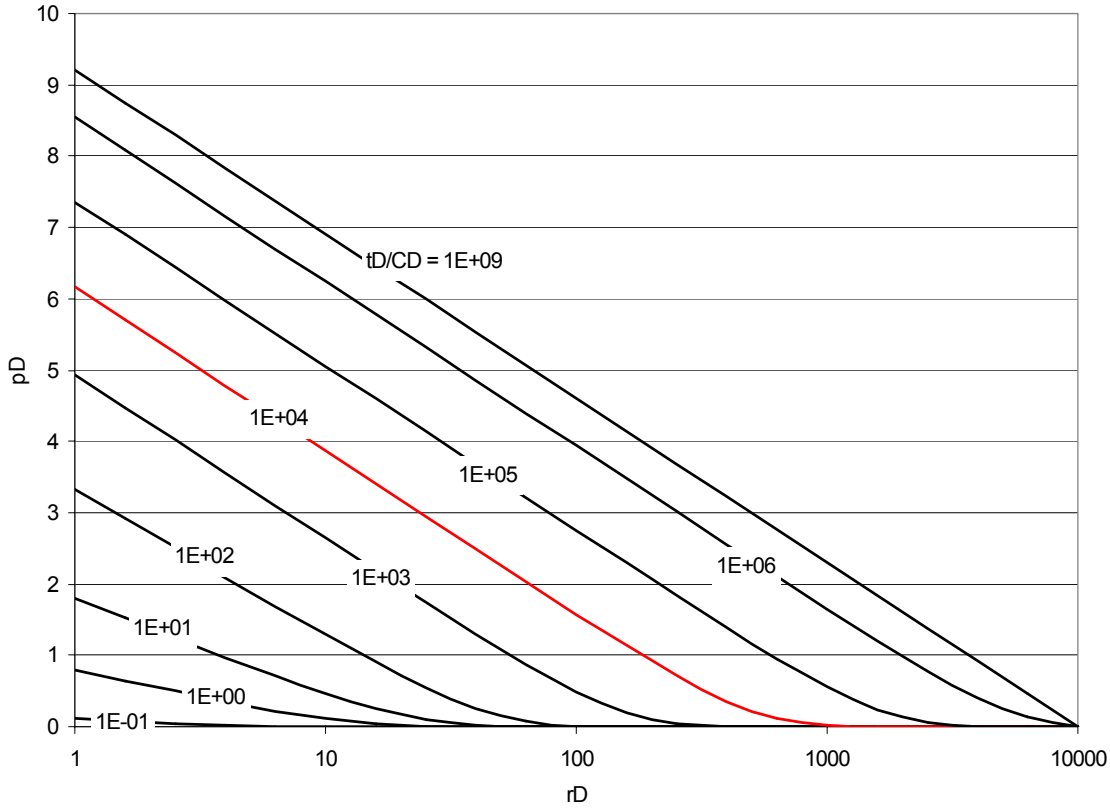

Figure 4-1. Pressure vs. distance at several times. Linear case – no permeability stress dependency

Pressure distributions in time follow an expected pattern. As the duration of the drawdown increases, more of the formation contributes to flow. When pressure finally reaches the constant pressure outer boundary, we observe steady-state flow.

Distributions of deformation at the same moments in time are given in Fig. 4-2. We can see that even though the pressure has not yet reached the boundary, the entire reservoir already "feels" the effect of the reduced pressure closer to the wellbore (red curve in Fig 4-2 corresponds to $t_D/C_D \approx 10{,}000$). If we assume that permeability is stress-dependent, flow everywhere in the formation will be very quickly affected by the redistribution, caused by well operation, of the stress-strain state in the reservoir and the surrounding rock mass.

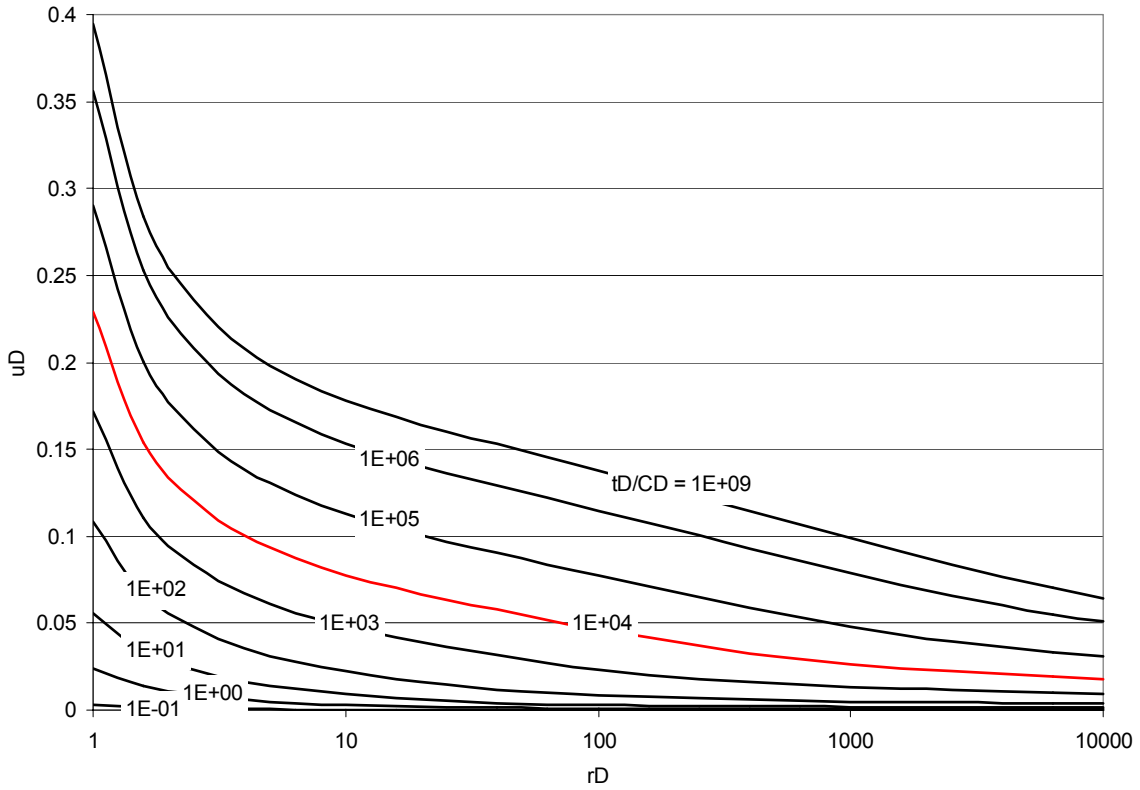

Figure 4-2. Deformation vs. distance at several times. Linear case – no permeability stress dependency

It can also be seen that the largest deformation occurs in the vicinity of the wellbore within a distance of about 10 wellbore radii. The mechanical integrity of this zone can be altered fairly significantly by drilling and/or well operation, i.e. it is most prone to fissuring/fracturing. If we assume that permeability is stress-dependent, then most of permeability impairment will occur in the near-wellbore zone.

Let us now consider how the magnitude of the reservoir deformation near the well depends on the elastic parameters of the problem. Presented in Fig. 4-3 is the steady-state normalized deformation at $r_D = 1$ for $E = 10^{10}\ Pa$, $\alpha = 0$, and different values of γ (blue curve). The deformations are normalized by the value, which corresponds to $\gamma = 1$. As one would expect, for the same stiffness of the surrounding rocks, a more pliable or "softer"

reservoir ($\gamma < 1$) deforms to a greater degree. At the same time, the deformations, which are the vertical displacements of the interface reservoir-embedding strata, are limited to some magnitude, which is defined by both of the Young's moduli. Stiffer reservoir rocks ($\gamma > 1$) deform to a lesser degree. We can conclude that for a softer reservoir its deformation is defined by the properties of the surrounding rocks and the magnitude of deformation does not change significantly for $\gamma < 1$, whereas deformation of a stiffer reservoir depends strongly on its Young's modulus and not so much on the elastic properties of the surrounding strata.

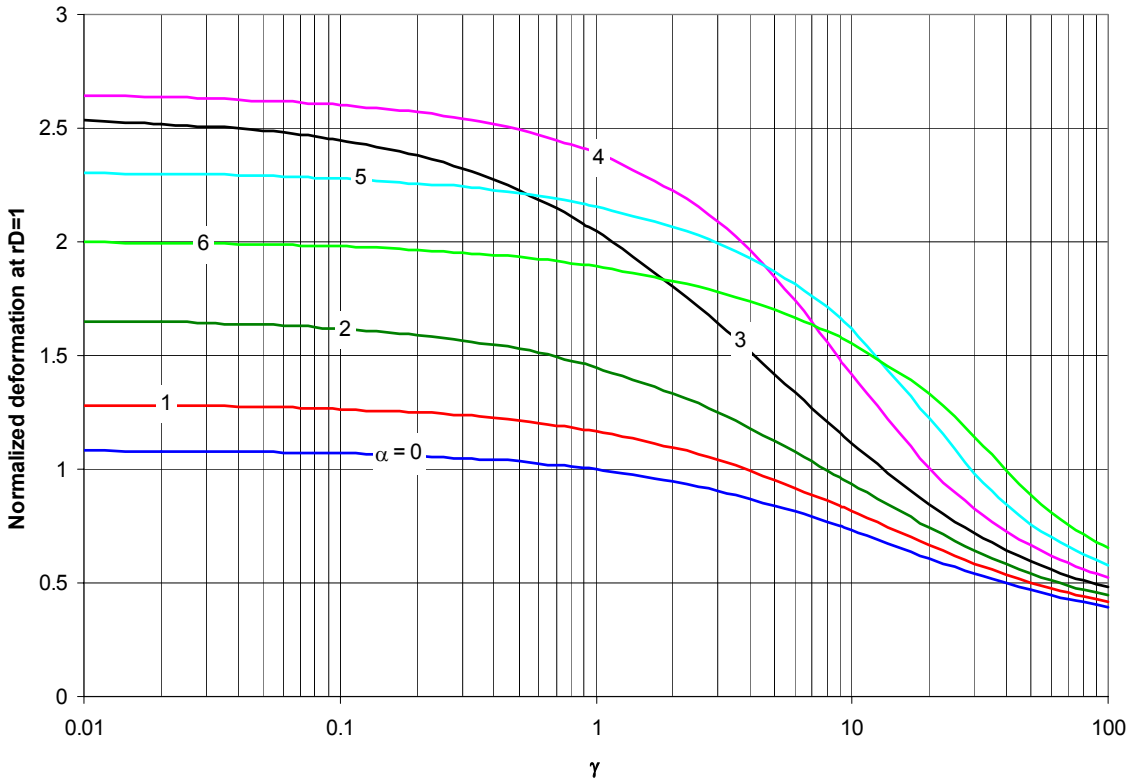

Figure 4-3. Steady-state near-well deformation as function of reservoir Young's modulus for various values of parameter α

If formation permeability is stress-dependent, then the magnitude of deformation changes, which reflects the impaired conditions of the flow. Red, green, black, pink, light blue, and light green curves in Fig. 4-3 correspond to normalized as before deformation at

$r_D = 1$ for $\alpha = 1,\ 2,\ 3,\ 4,\ 5,$ and 6, respectively. It can be seen that for $\alpha < 4$ as the sensitivity of permeability to deformation increases, so does the deformation itself. This is a result of an increased pressure drop in the formation in order to offset the decreased permeability, since the well is produced at constant flow rate. Increased pressure drop leads to increase of effective stress in the reservoir. The corresponding normalized steady-state wellbore pressure and permeability curves are given in Figs. 4-4 and 4-5. Though the curves for $\alpha > 4$ show less deformation, but coupled with the increased sensitivity of permeability to deformation, permeability is further decreased and for these values of α the steady-state retained permeability is below 10 percent in a wide range of γ.

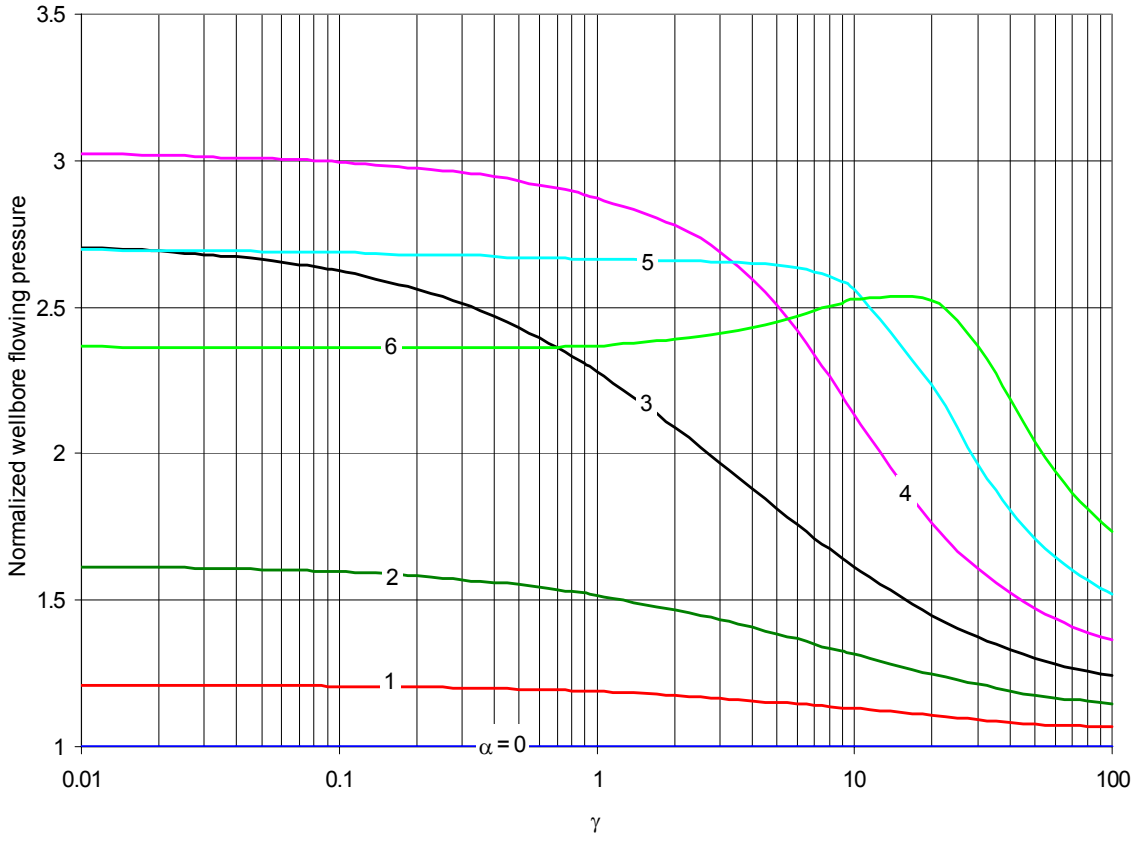

Figure 4-4. Steady-state wellbore pressure as function of reservoir Young's modulus for various values of parameter α

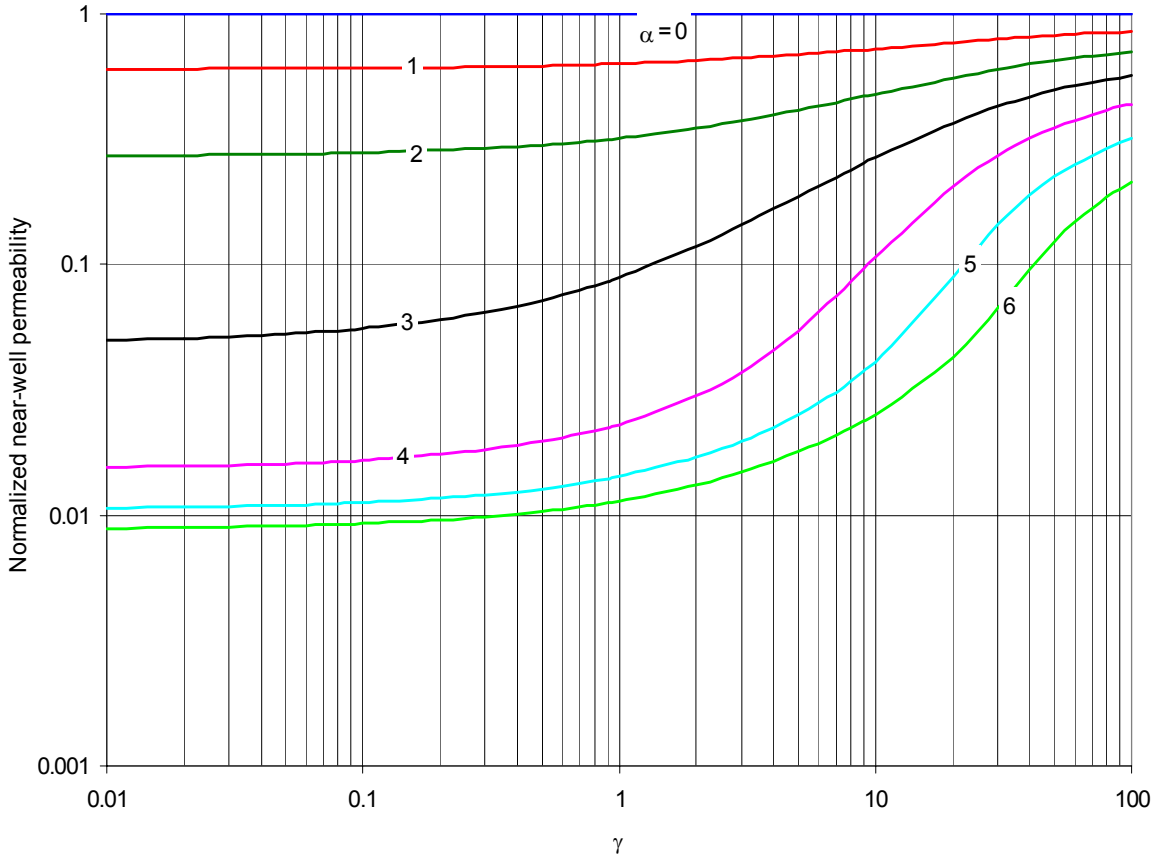

Figure 4-5. Steady-state near-well permeability as function of reservoir Young's modulus for various values of parameter α

Let us now consider sensitivity of deformation to Young's modulus of the surrounding rocks. The blue curve in Fig. 4-6 corresponds to normalized deformation at $r_D = 1$ for fixed $E_1 = 10^{10}\ Pa$ and $\alpha = 0$. Stiffer surrounding rocks ($\gamma < 1$) do not deform as easily and, respectively, allow for comparatively lesser deformation of the reservoir. A stiffer reservoir ($\gamma > 1$) is less affected by the properties of the surrounding rocks and deforms accordingly to its Young's modulus. It can be concluded that properties of both the reservoir rock and the surrounding strata have a significant impact on the magnitude of deformations.

Though in reality the variation of the elastic moduli is not that wide, it still should be properly accounted for, especially if permeability is stress-dependent. Consider the red curve in Fig. 4-6. Here we plot similarly normalized deformation at $r_D = 1$ vs. γ but now with account for permeability dependence on deformation. The values of the variables in parameter α are such that $\alpha = 1$ (red curve) for $\gamma = 1$. Since α is inversely proportional to E, then for other variables, including β – sensitivity of reservoir permeability to deformation, kept constant, it follows that α is equal to 100 for $E = 10^8$ Pa, and α is equal to 0.01 for $E = 10^{12}$ Pa, etc. Green, black, and pink curves correspond to $\alpha = 2$, 3, 4. It can be seen that for large γ (and large α) the deformation is small, as it is limited by the properties of the reservoir. For small γ the stiffer surrounding rocks deform to a lesser degree and limit the deformation of the reservoir. The equivalent α is also small, the reservoir deforms as if there were little or no permeability stress-dependence, and blue, red, and green curves almost coincide. On each curve there is a point of maximum, the location of which is determined by the combination of deformation and sensitivity effects.

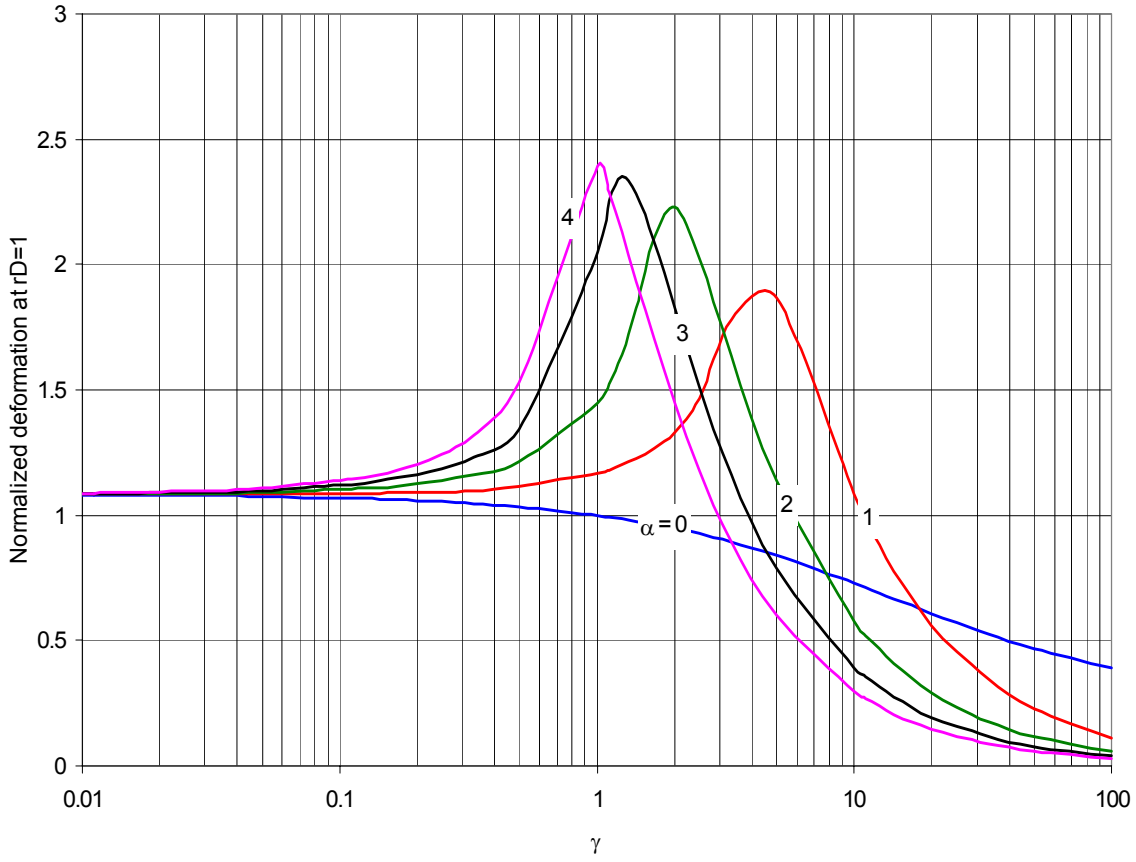

Figure 4-6. Steady-state near-well deformation as function of Young's modulus of surrounding rocks for various values of parameter α

Let us now consider also negative values of α, which correspond to injection. In Fig. 4-7 we present the product $\alpha[u_z]$ vs. γ for constant $E = 10^{10}\ Pa$. This product combines the elastic properties and sensitivity to deformation and is responsible for the degree of permeability impairment or improvement. Red, green, and black curves correspond to $|\alpha| = 2,\ 4,\ 6$, respectively. The blue line is for $\alpha[u_z] = 0$ and corresponds to the linear case, dashed lines correspond to injection. The respective dimensionless permeability curves, $k/k_0 = \exp(-\alpha[u_z])$, are presented in Fig. 4-8. Here the blue line also corresponds to linear case, i.e. with constant permeability.

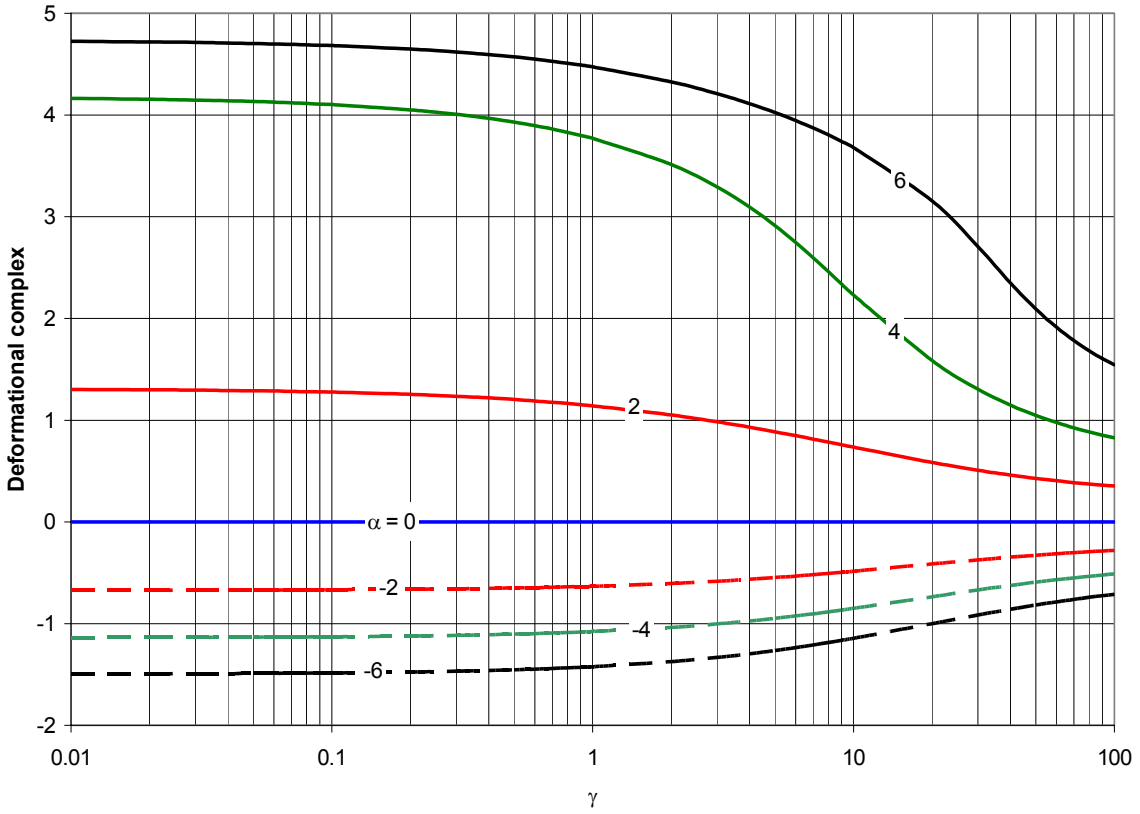

Figure 4-7. Steady-state complex $\alpha[u_z]$ as function of Young's modulus of the surrounding rocks for various values of parameter α

We can see that deviation from the linear case of deformation with account for permeability stress-dependence is greater for the case of production (positive $\alpha[u_z]$). Respectively, permeability reduction is much more significant in this case. For large γ (greater Young's modulus of the reservoir than that of the surrounding rocks) both deformation and permeability change to a lesser degree than in a case of a softer reservoir.

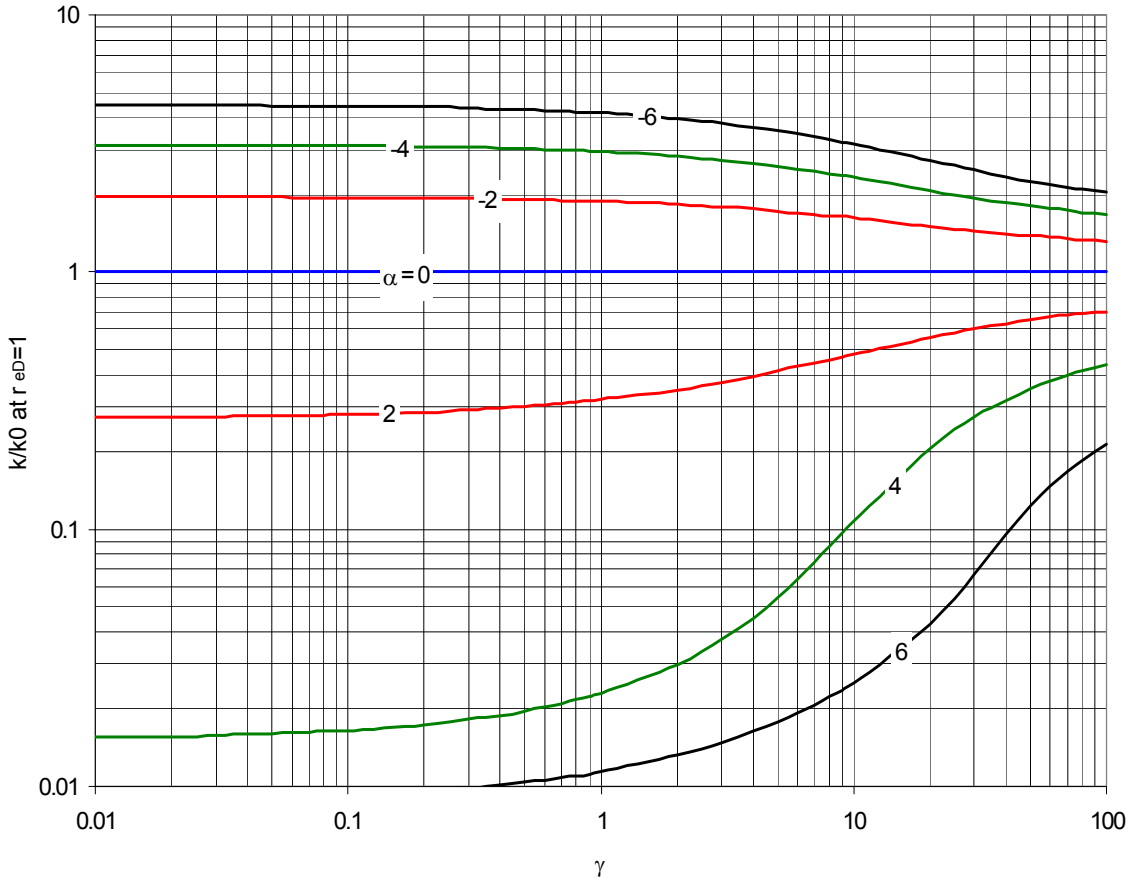

Figure 4-8. Steady-state near-wellbore permeability as function of Young's modulus of the surrounding rocks for various values of parameter α

In Fig. 4-9, we present the product $\alpha[u_z]$ vs. γ for constant $E_1 = 10^{10}\ Pa$ for cases of production and injection. Here again, as in Fig. 4-6, parameter α changes as γ changes, variation of γ is due to varying Young's modulus of the surrounding rocks, E, and for each value of E we calculate a value of α, which is equivalent to the value at $\gamma = 1$. Red, green, black, and pink curves correspond, respectively, to $|\alpha| = 1, 2, 3, 4$.

It can be seen that deformation of a soft reservoir ($\gamma << 1$) are limited by the elasticity of the surrounding rocks – all curves, inflation and compaction, converge to the linear case (blue line). The degree of compaction of a stiff reservoir ($\gamma >> 1, \alpha[u_z] > 0$) is limited by the

elasticity of the reservoir itself – all curves converge to the same value. Inflation of a stiff reservoir leads to non-linear increase of its deformation.

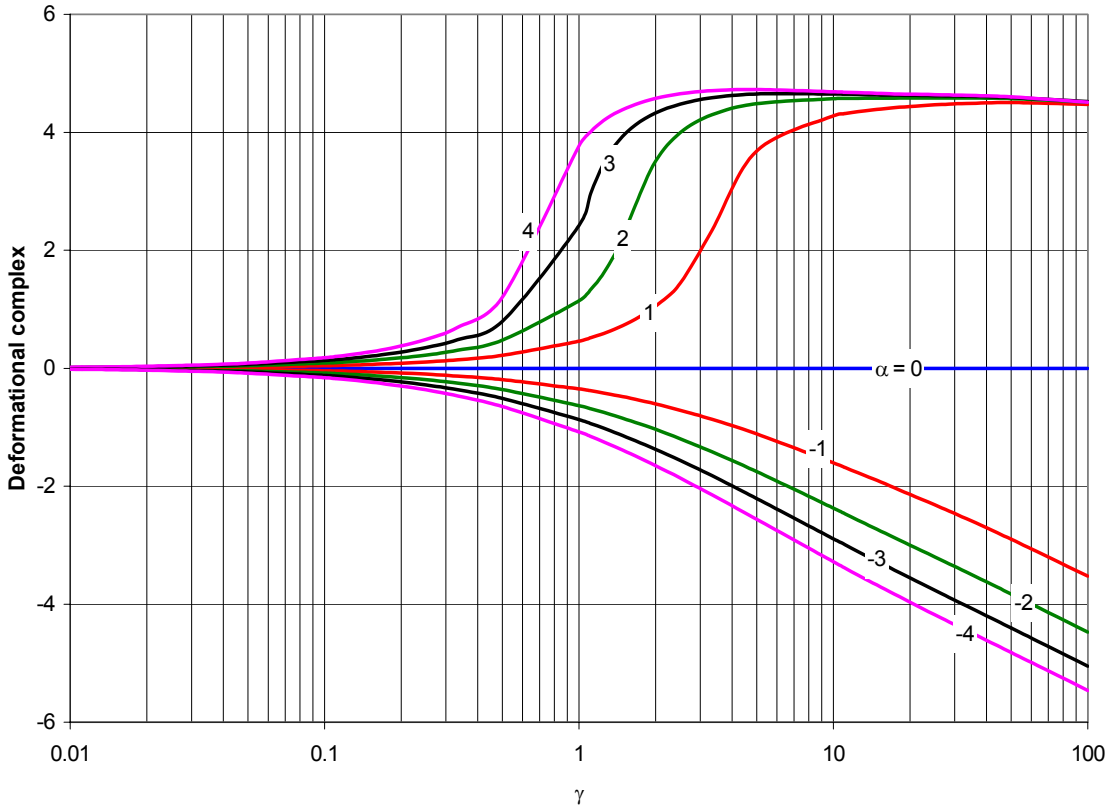

Figure 4-9. Steady-state near-well complex $\alpha[u_z]$ as function of Young's modulus of the surrounding rocks for various values of parameter α

The results above were obtained using some typical values for Young's moduli. Curves in Fig. 4-10 is the product $\alpha[u_z]$ at $r_D = 1$ vs. γ, calculated for $E_1 = 10^9\ Pa$ (blue curve), $E_1 = 10^{10}\ Pa$ (red curve), and $E_1 = 10^{11}\ Pa$ (green curve). We can see that the magnitude of deformation depends both on the rigidity of the surrounding rocks and the reservoir stiffness. For example, at $\gamma = 0.01$ deformation of a stiffer reservoir (green curve) is much smaller than deformation of a more pliable reservoir (blue curve). The magnitude of deformation in either case is fairly small as the stiffer surrounding rocks limit the

deformation. As γ increases and the rigidity of the reservoir becomes comparable to the rigidity of the surrounding rocks, so does the deformation. After reaching a certain value of γ, the magnitude of deformation does not change significantly. This characteristic value of γ depends on the rigidity of the reservoir. As γ increases, for a weak reservoir (blue curve) the deformation slightly decreases, which indicates less influence of the surrounding rocks.

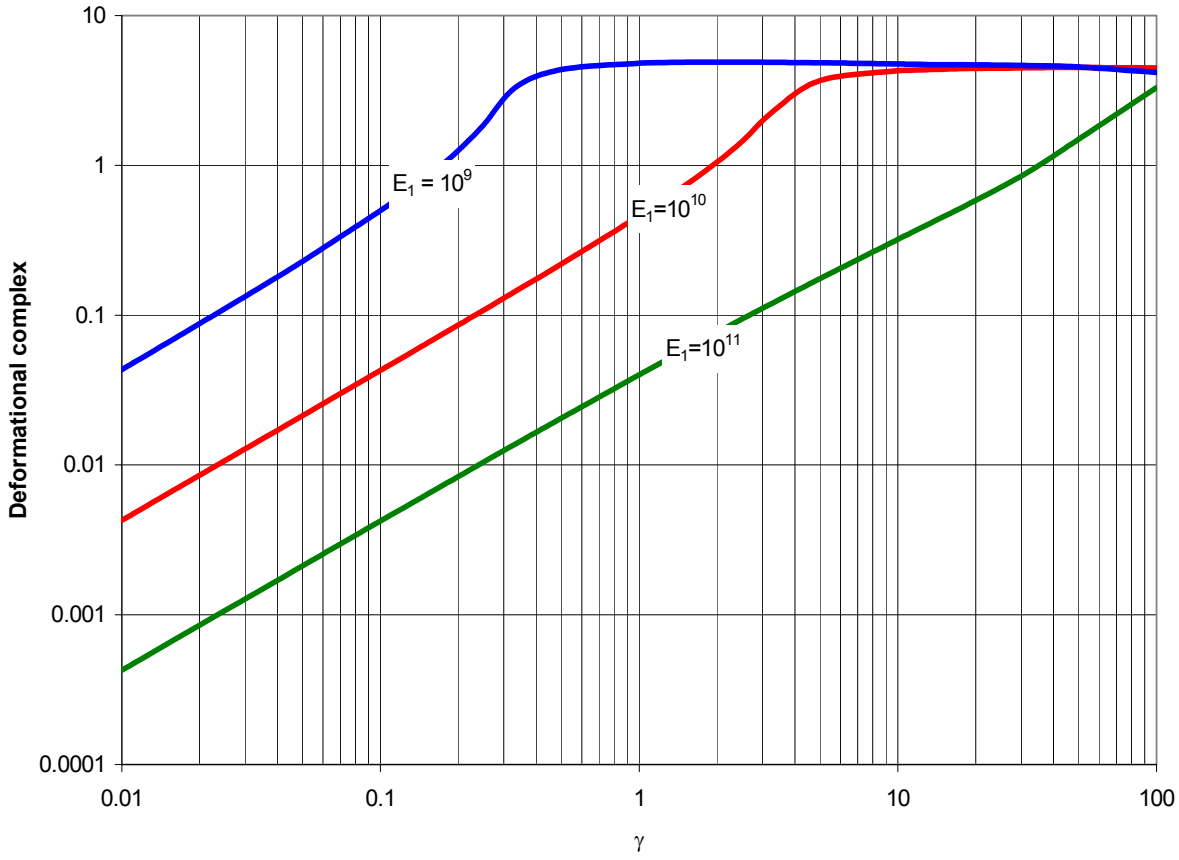

Figure 4-10. Steady-state near-well complex α[u]z as function of Young's modulus of the surrounding rocks for various values of reservoir Young's modulus

The principal geometric parameter that affects the deformation is the reservoir thickness. Presented in Fig. 4-11 dimensionless permeability curves for $|\alpha| = 1$ and 2 (red and green curves) vs. normalized by the previously used value of reservoir thickness

($h = 10\ m$). The blue straight line represents linear case. We can see that a thin reservoir exhibits significant deviation of permeability from the straight line $k/k_0 = 1$, more so in case of injection. As the reservoir thickness increases, its relative deformation, $\varepsilon = [u_z]/h$, decreases, which results in less permeability deviation from the linear case. For very thick reservoirs ($r_w/h > 0.001$) the deformation is small.

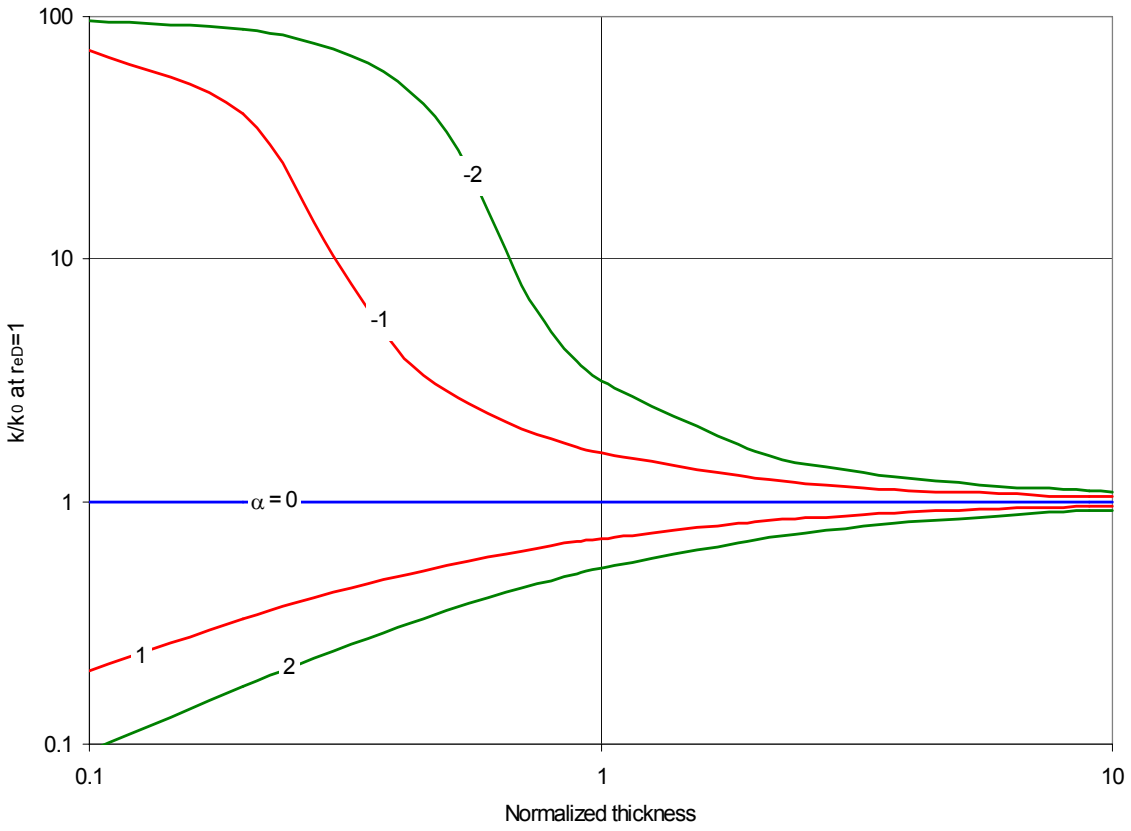

Figure 4-11. Steady-state near-wellbore permeability as function of reservoir thickness for various values of parameter α

Another geometric parameter that impacts the flow is the radius of the drainage area. Presented in Fig. 4-12 are the dimensionless permeability curves for α=-2, -1, 0, 1, 2 (red, green, blue, black, and purple curves, respectively) vs. drainage radius, normalized by 1,000

m. It can be seen that the size of the drainage area, compared to other parameters, has only a minor effect for a given magnitude of sensitivity of permeability to deformation.

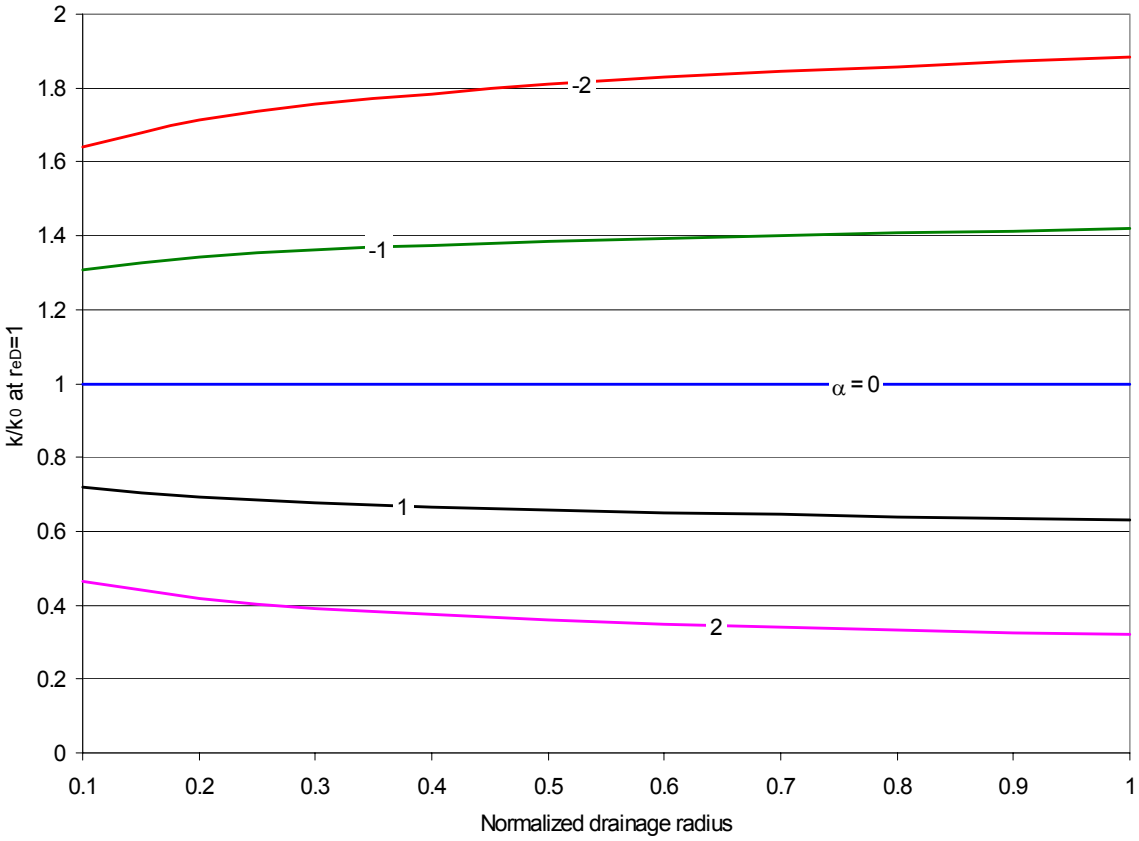

Figure 4-12. Steady-state near-wellbore permeability as function of drainage radius for various values of parameter α

4.2 Typical drawdown problems

In this section we present the drawdown type curves generated from our model, and examine how the elastic and geometric parameters affect the shape of the pressure/rate and derivative curves. We solve numerically several fluid flow problems with stress-dependent permeability with conventional inner and boundary conditions.

4.2.1 Constant rate drawdown, infinite reservoir

First, let us introduce the drawdown base case and list the values of the principal parameters. Calculations for the base case were performed with $a = 0.0384$, $\alpha = 2$, $\gamma = E_1/E = 1$, $E = 10^{10}\ Pa$, $r_w/h = 0.001$, $h = 10\ m$, $C_D = 100$, $s = 0$. The reservoir is considered to be infinite, which is modeled by setting constant pressure outer boundary at $10^5\ m$. Comparison of the base case with the linear case (no account for deformation) is presented in Fig. 4-13.

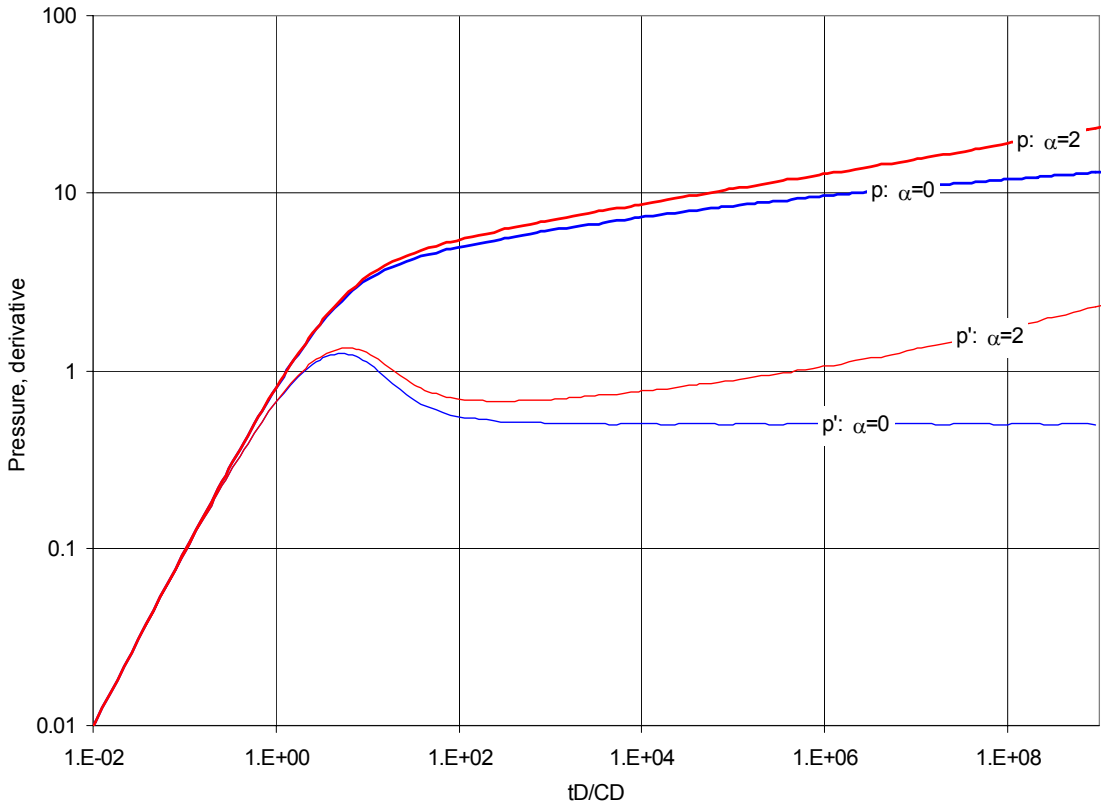

Figure 4-13. Drawdown type curves for linear (α=0) and base (α=2) case

Linear (blue) and base (red) case dimensionless pressure difference (thick lines) and well-testing derivative (thin lines of same color) are plotted vs. dimensionless time. Let us consider the red curves. The pressure difference is greater than in the linear case because

permeability is stress-dependent and decreases in response to fluid withdrawal and reduction of pressure within an expanding zone around the well. The derivative simply reflects this increase of pressure difference and behaves as if the permeability-thickness product, kh, were decreasing with time, or equivalently, if skin were increasing with time. One might also interpret such behavior of the derivative as a closed boundary located fairly close to the well. The possibility of such incorrect interpretation is greater when the duration of the test is short.

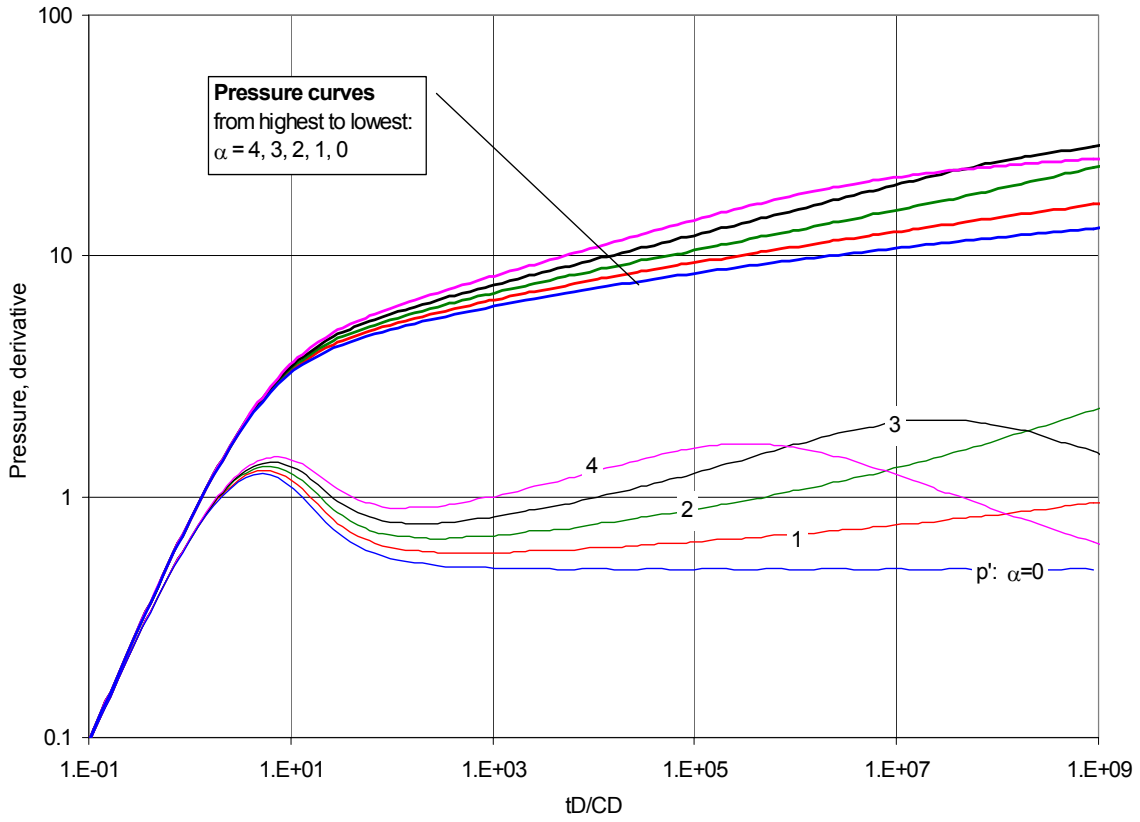

Figure 4-14. Drawdown type curves for various values of α

Fig. 4-14 presents the pressure and derivative curves for different values of permeability sensitivity to deformation. For blue, red, green, and black pairs of curves $\alpha = 1, 2, 3,$ and 4, respectively. The greater is α, the greater is the deviation from the linear

case (plotted as filled and empty dots). We can see that for α=3 and 4 the derivative first increases, reaches a maximum, and then decreases. It appears as if *kh* were initially decreasing and then began to increase. To understand such behavior, consider Fig. 4-15, where we plot pressure vs. distance at several moments in time for α=1 and 4. Respective permeability distributions are given in Fig. 4-16. The blue curves are for $t_D/C_D \approx 1$, consecutive curves correspond to later times and are approximately two log-cycles in time apart, the last curve is for $t_D/C_D \approx 10^9$

As the pressure transient travels into the formation, the redistribution of the stress-strain state in the entire system causes reduction of permeability everywhere in the reservoir. Since the largest pressure drop occurs within about 5 wellbore radii around the well, this zone suffers the most permeability reduction. Greater sensitivity to deformation leads to a more rapid decrease in permeability. In turn, this zone around the wellbore determines to a large degree the flow into the wellbore. Once the permeability near the wellbore has been significantly reduced, continuing reduction of permeability in the reservoir further away from the well has less significant impact on the flow into the wellbore. The created near the well "deformational choke" is the principal factor that governs subsequent behavior of the well pressure and rate. Once the "choke" is in place, it impedes further decrease of well pressure (increase of drawdown). Well pressure still continues to decrease, but a slower rate, which is reflected by the derivative.

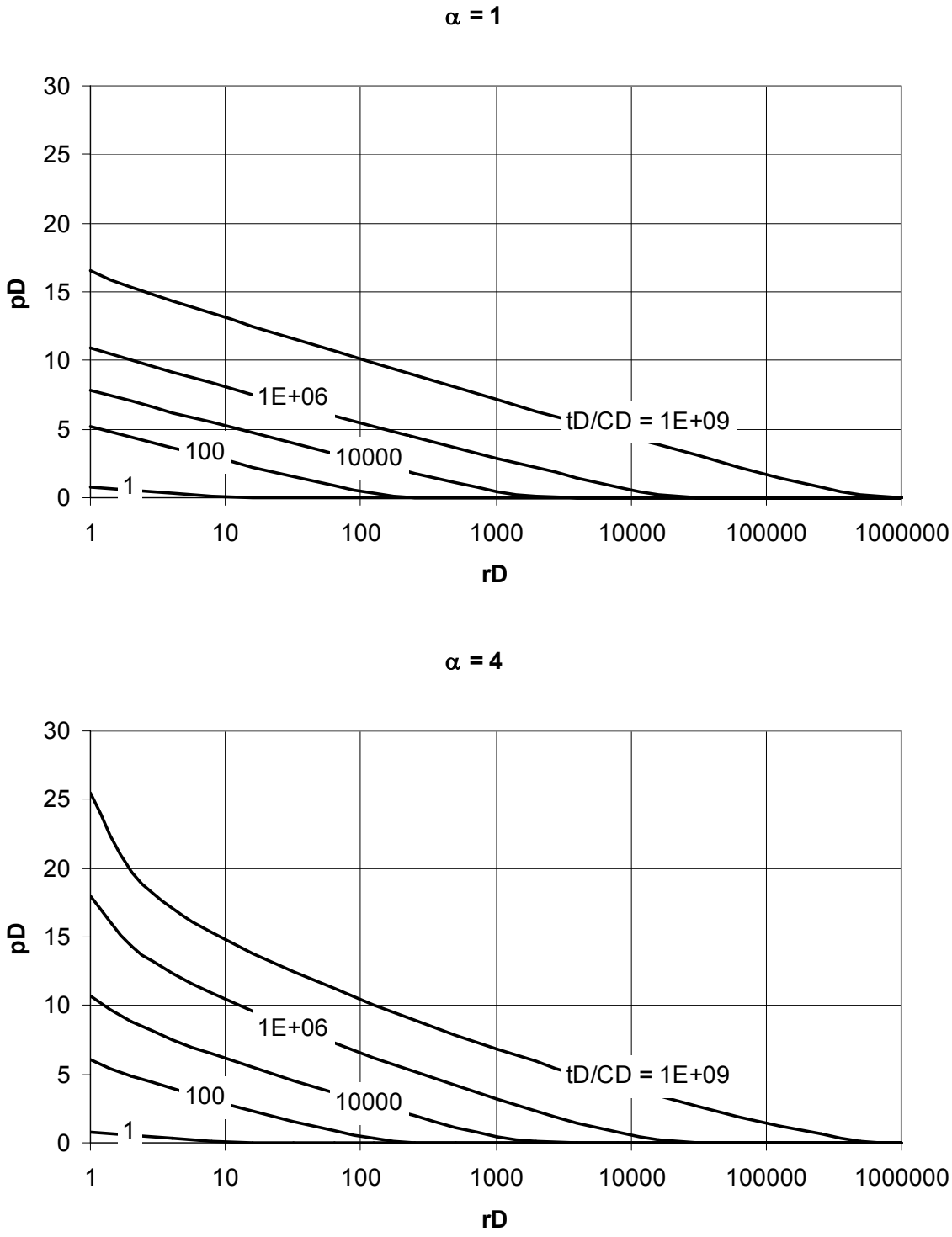

Figure 4-15. Pressure vs. distance for several times

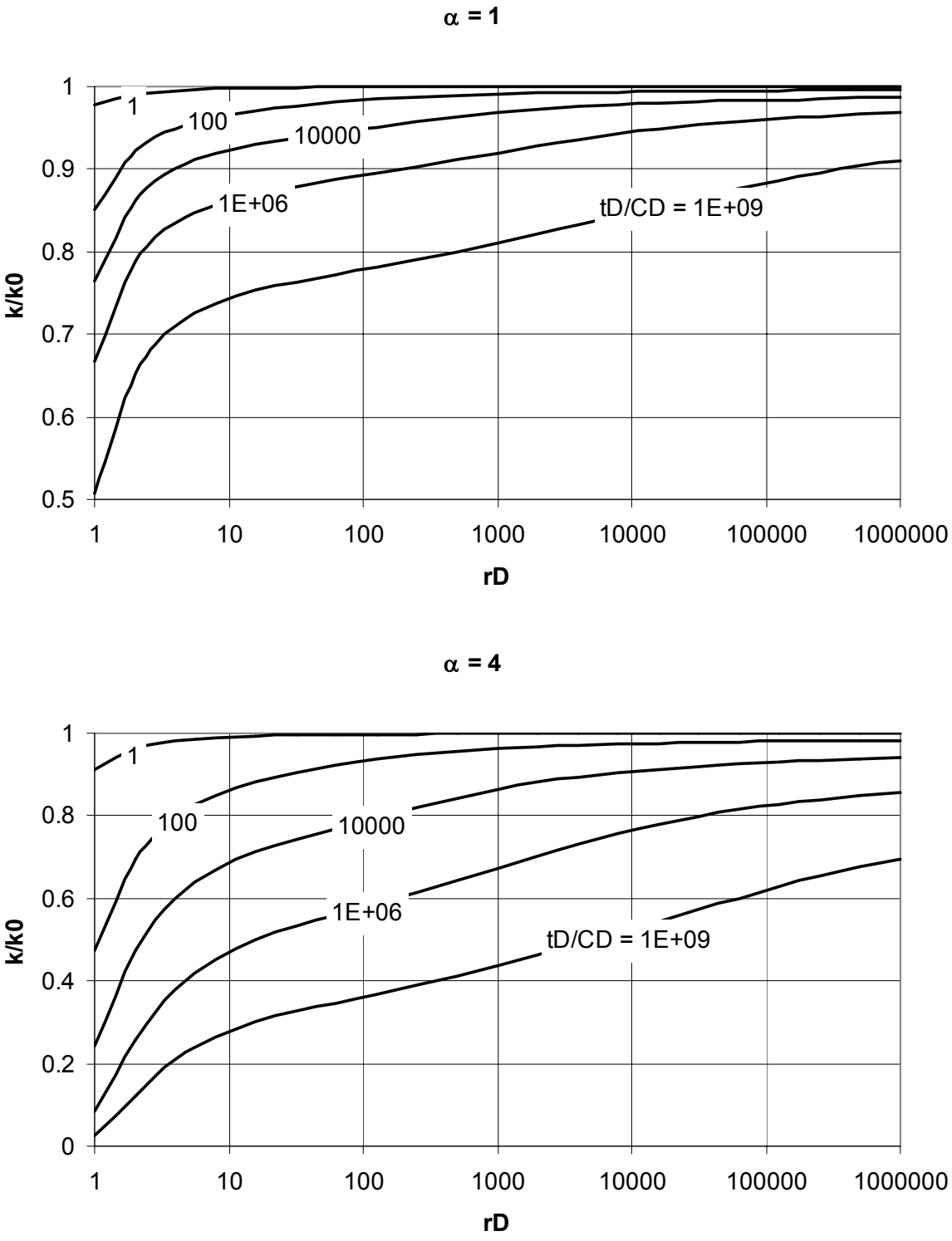

Figure 4-16. Permeability vs. distance for several times

In Fig. 4-17, we present the dimensionless permeability at $r_D = 1$ vs. time for the values of α=1, 2, 3, 4, and 10. Let us consider the blue and red curves (α=1 and 2, respectively). Following the end of wellbore storage distortion ($t_D/C_D \approx 100$), the permeability declines approximately linearly with the logarithm of time. The green and black curves (α=3 and 4) also exhibit a linear decline after the end of wellbore storage. There is, however, another period of linear decline at a slower rate, which appears at later times. If we draw straight lines through both of these time periods (dashed lines), they intersect at a time when derivative changes its character (see also Fig. 4-14 – curve α=4).

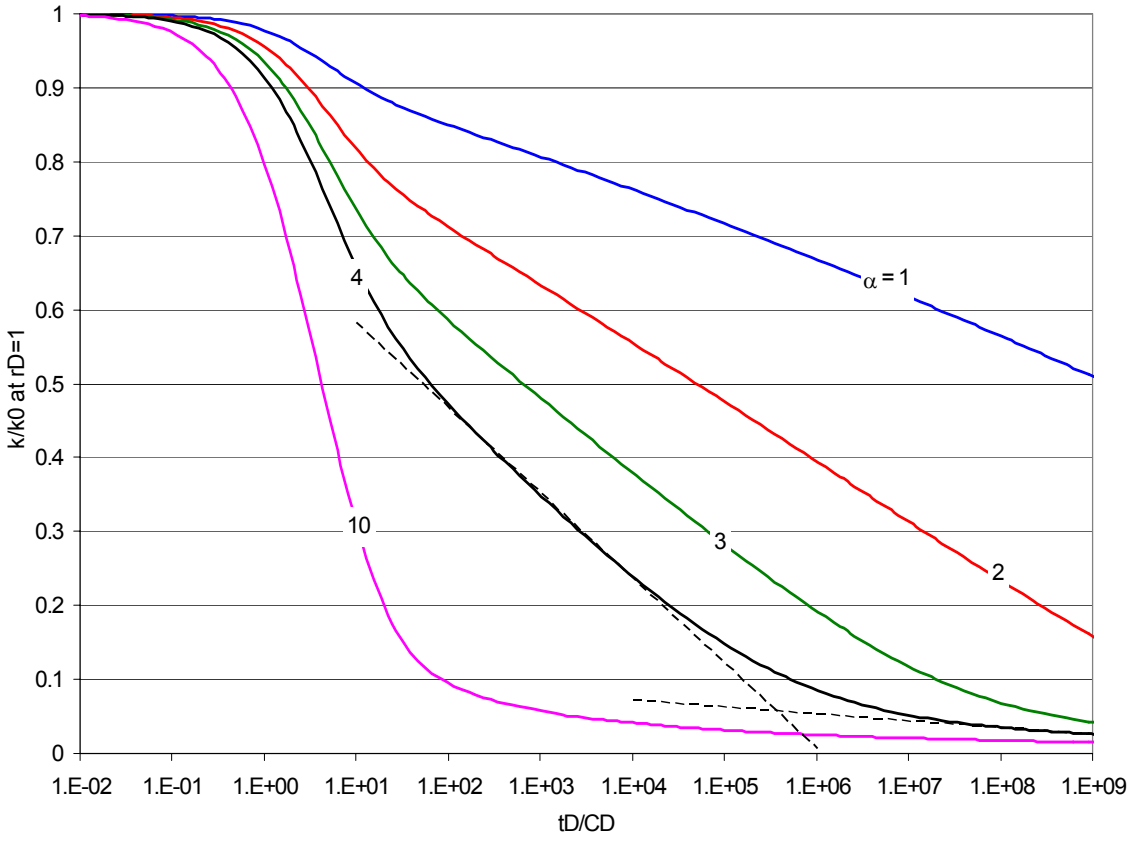

Figure 4-17. Near-well permeability vs. time for various values of α

If the sensitivity of permeability to deformation is substantial, then the permeability at the well drops very quickly, and after that initial rapid decline, the permeability decreases at

a much slower rate (see pink curve for α=10). Everywhere else in the reservoir, permeability continues to decline, which shows up as the increasing separation of the pressure and the derivative curves. The increasing separation can be interpreted either as increasing kh, or as increasing impedance to flow (skin), which in this case is a better explanation.

As explained previously, the elastic properties of the reservoir and surrounding rocks are of principal importance as these properties determine the magnitude of the reservoir deformation. The effect of the described above near-wellbore deformational "choke" is more pronounced when the surrounding rocks are more pliable (or less stiff) than the formation, i.e. the deformation is not confined significantly by the rigidity of the embedding strata. Less stiff surrounding rocks also mean greater α.

Presented in Fig. 4-18 are type curves for constant Young's modulus of the reservoir, $E_1 = 10^{10}\ Pa$ and γ=100, 10, 1, 0.1, 0.01 (blue, red, green, black, and purple curves, respectively). We can see that for large γ=100 (blue curves) the reservoir quickly responds to the drawdown by developing the "choke" – obviously both permeability and pressure on the well drop very quickly (within the time of well unloading) and further production results in expansion of the zone of reduced permeability into the formation. Similar effects, though on a smaller scale, occur for γ=10 (red curves). Pressure for both pairs of curves rises fast initially and then at a much slower rate. Such behavior might be incorrectly interpreted as a no flow boundary very close to the well.

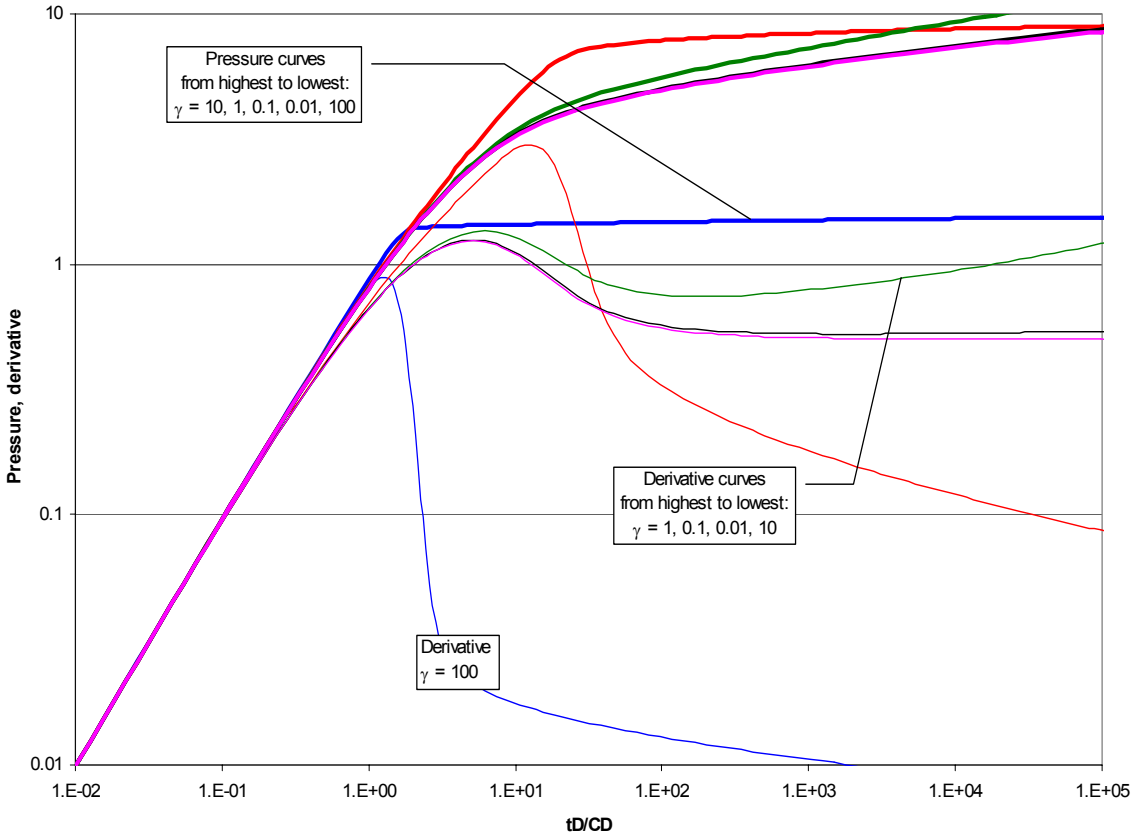

Figure 4-18. Drawdown type curves for various values of Young's modulus of the surrounding rocks

For γ=1 (green curves), the behavior of the derivative, when analyzed using conventional methods, might be interpreted as negative skin or constant pressure boundary close to the well. For a reservoir that is stiffer than the surrounding strata (γ=0.1 and 0.01 – black and purple pairs practically coincide) and with given sensitivity to deformation, the deviation of the type curves from the linear case with no account for deformation is practically undetectable.

Let us now consider sensitivity of the results to the Young's modulus of the reservoir. In Fig. 4-19, the type curves for γ=0.01 (red curves), and 100 (green curves) are presented. For the curves α=2 and Young's modulus of the surrounding rocks, E, is constant at

10^{10} *Pa*. The blue curves are linear case pressure and derivative, respectively. It follows from the graph that a softer reservoir (lower γ) will exhibit more deviation from the linear case.

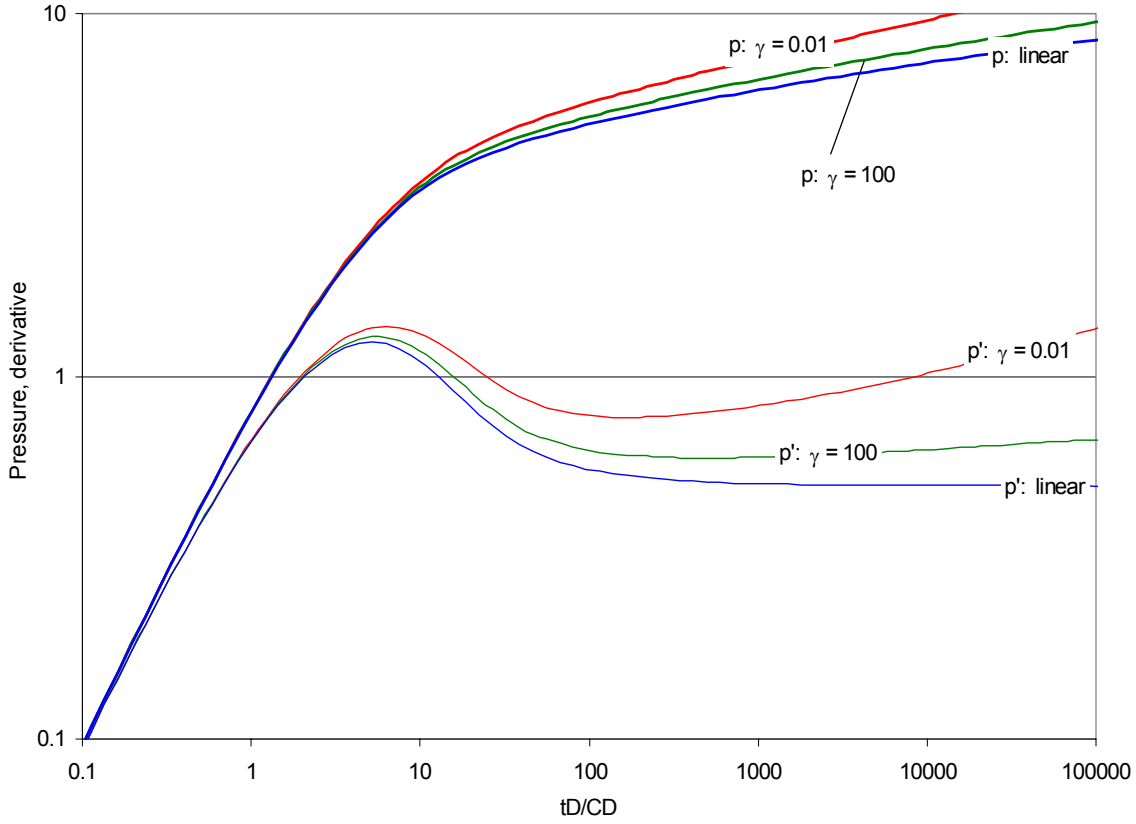

Figure 4-19. Drawdown type curves for various values of reservoir Young's modulus

4.2.2 Constant rate drawdown, constant pressure outer boundary

Let a well be produced at a constant flow rate from a circular reservoir with constant pressure on the outer boundary. In Fig. 4-20, the blue, red, green, and black pairs of curves, respectively, correspond to $r_{eD} = \infty$ (base case); 1,000; 5,000; and 10,000. All other parameters, except for r_{eD}, are same as in the base case.

We can see that prior to reaching the boundary, the differences among the pressure and derivative curves, which correspond to various r_{eD} are very small. The distance to the boundary, if the test is conducted long enough, can be estimated. More discernable results are presented later, when we describe pseudo- and steady-state flow and a drawdown followed by a buildup.

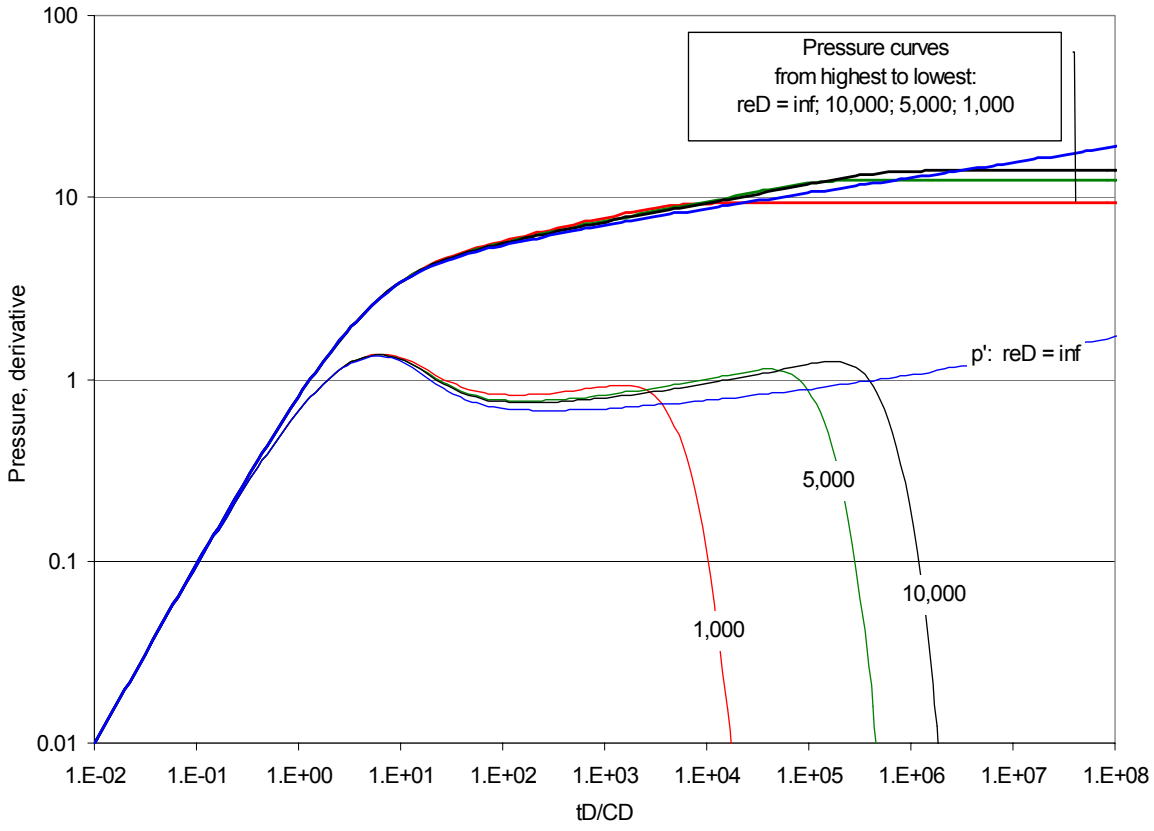

Figure 4-20. Drawdown type curves for various values of drainage radius and α=2

Sensitivity to parameter α for $r_{eD} = 10{,}000$ is presented in Fig. 4-21. For blue, red, green, and black pairs of curves α=1, 2, 3, and 4, respectively. As the value of α increases, the effects of deformation and permeability stress-dependence also increase. We can see that if using conventional analysis one could underestimate wellbore storage coefficient and calculate negative skin. It is also interesting to note that for large α=4, the boundary

apparently is being "felt" by the derivative somewhat earlier than for smaller values of α. This is not the effect of the boundary, this is the described above effect of the deformational "choke".

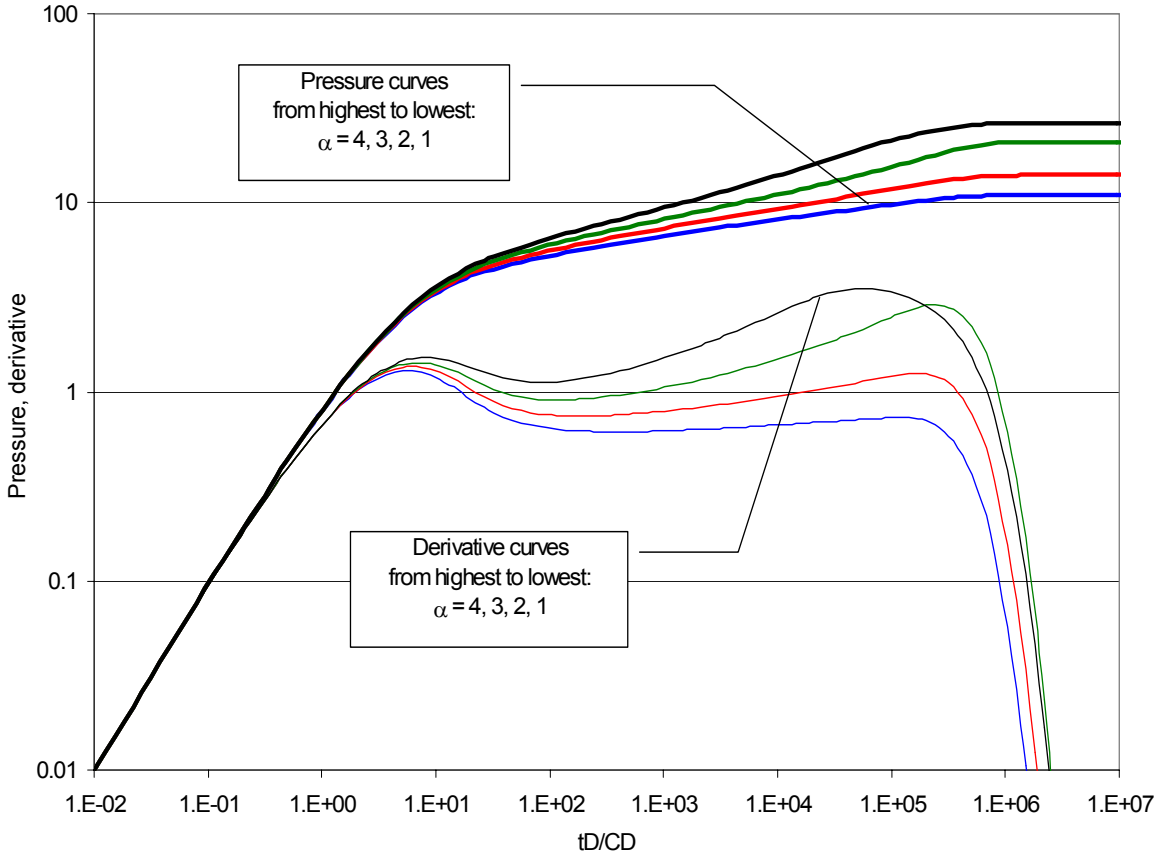

Figure 4-21. Drawdown type curves for various values of α and reD = 10,000

4.2.3 Constant rate drawdown, no-flow outer boundary

Let us now consider a case of a well put on production with constant rate and located at the center of a closed circular reservoir. The boundary is at $r_{eD} = 10{,}000$, all other parameters are the same as in the base case. Fig. 4-22 presents type curves for this case (red curves) along with the linear case (blue curves).

We can see that the behavior of the two sets of curves substantially differs from each other. Drawdown from a closed area in the linear case follows a familiar pattern – after the boundary has been reached the pseudo-steady flow takes place. The pressure declines at the same rate everywhere in the reservoir in order to maintain constant production. Both pressure and derivative follow a unit-slope straight line.

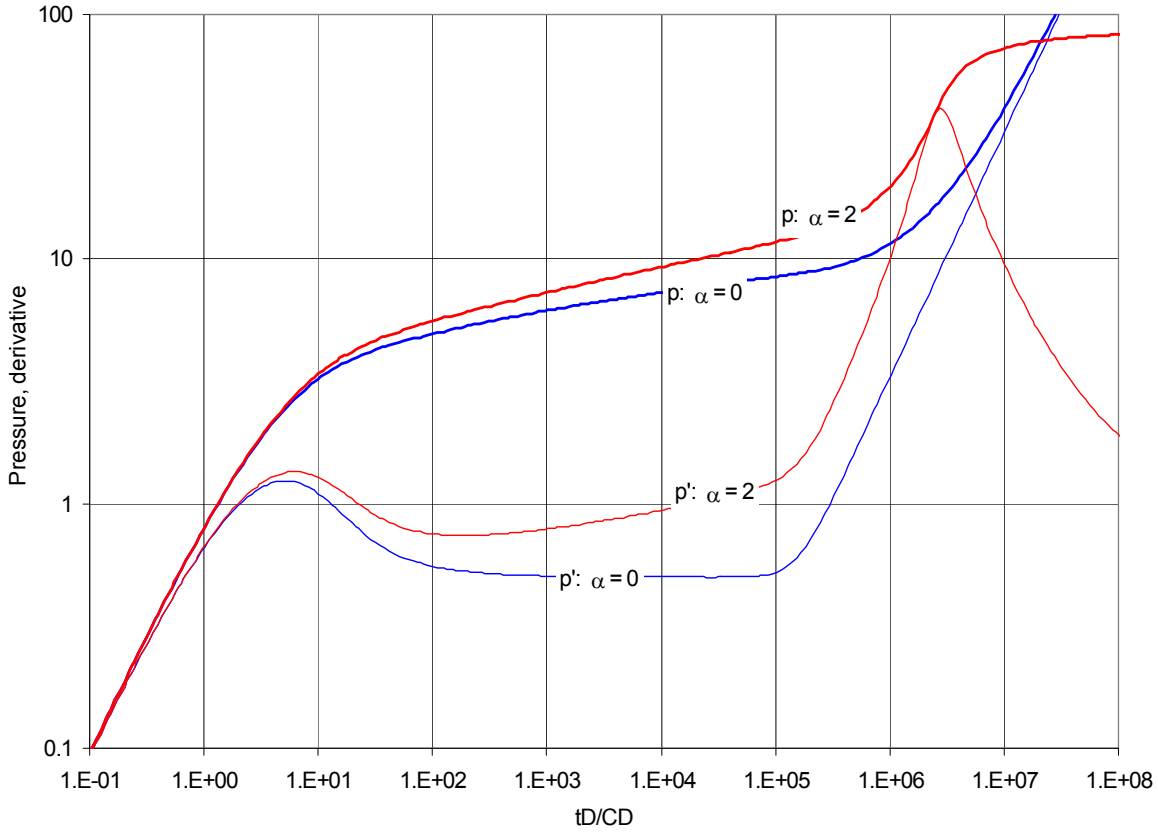

Figure 4-22. Drawdown type curves, closed outer boundary, various α

The case with stress-dependent permeability is markedly different. First, the pressure during transient flow is greater than the linear case pressure in order to compensate for ever decreasing permeability. The derivative reflects this trend. Second, as the boundary is reached both pressure and derivative begin to increase, but the increase does not continue indefinitely as in the linear case, rather at some later time pressure stabilizes at a constant

value. The derivative clearly shows it by dropping to zero. And, third, it appears that in the linear case the boundary is reached later.

In order to visualize such behavior let us consider the numerical rate calculation. In its implicit formulation rate is given by

$$\left.\frac{\partial p_D}{\partial x}\right|_{x=0} = \frac{2K_1^n}{2-\ln K_2^n + \ln K_1^n}\left[\frac{p_2^{n+1}-p_1^{n+1}}{\Delta x} - \left(\ln r_{eD}\right)^2 \frac{\Delta x \omega}{2K_1^n \kappa}\frac{p_1^{n+1}-p_1^n}{\Delta t}\right]$$

$$q_D = C_D \frac{dp_{wD}}{dt_D} - \frac{\kappa}{\ln r_{eD}}\left.\frac{\partial p_D}{\partial x}\right|_{x=0} = 1$$

For large times the rate is essentially determined by the product

$$\frac{\kappa}{\ln r_{eD}}\left.\frac{\partial p_D}{\partial x}\right|_{x=0} = \frac{\kappa}{\ln r_{eD}}\left(\frac{2K_1^n}{2-\ln K_2^n + \ln K_1^n}\right)\left(\frac{p_2^{n+1}-p_1^{n+1}}{\Delta x}\right)$$

where the two components in brackets change with time as shown in Fig. 4-23. Here blue curve is the rate, red curve is the pressure gradient, multiplied by $\frac{\kappa}{\ln r_{eD}}$, and green curve is the complex with the permeabilities. As time increases the green curve deviates from unity, as permeability near the well declines in response to declining pressure and increasing effective stress. The red curve increases, which corresponds to increasing pressure drop in the well in order to accommodate the permeability decrease and to maintain constant rate production. The product of the curves tends to unity as wellbore storage effects disappear with time.

Following the end of wellbore storage, the red and green curves change uniformly and fairly smoothly until $t_D/C_D \approx 2*10^5$, at which time the boundary is reached and pressure everywhere in the reservoir begins to increase. This rapidly increasing pressure causes respective rapid decrease of permeability, which eventually arrests pressure increase near the

wellbore and subsequently in the entire formation. At $t_D/C_D \approx 10^7$ pressure term reaches a maximum and permeability term reaches a minimum and after that both terms change respectively oppositely to each other until stabilization. From the results it appears that production at constant rate from a closed reservoir can be maintained indefinitely, which is impossible.

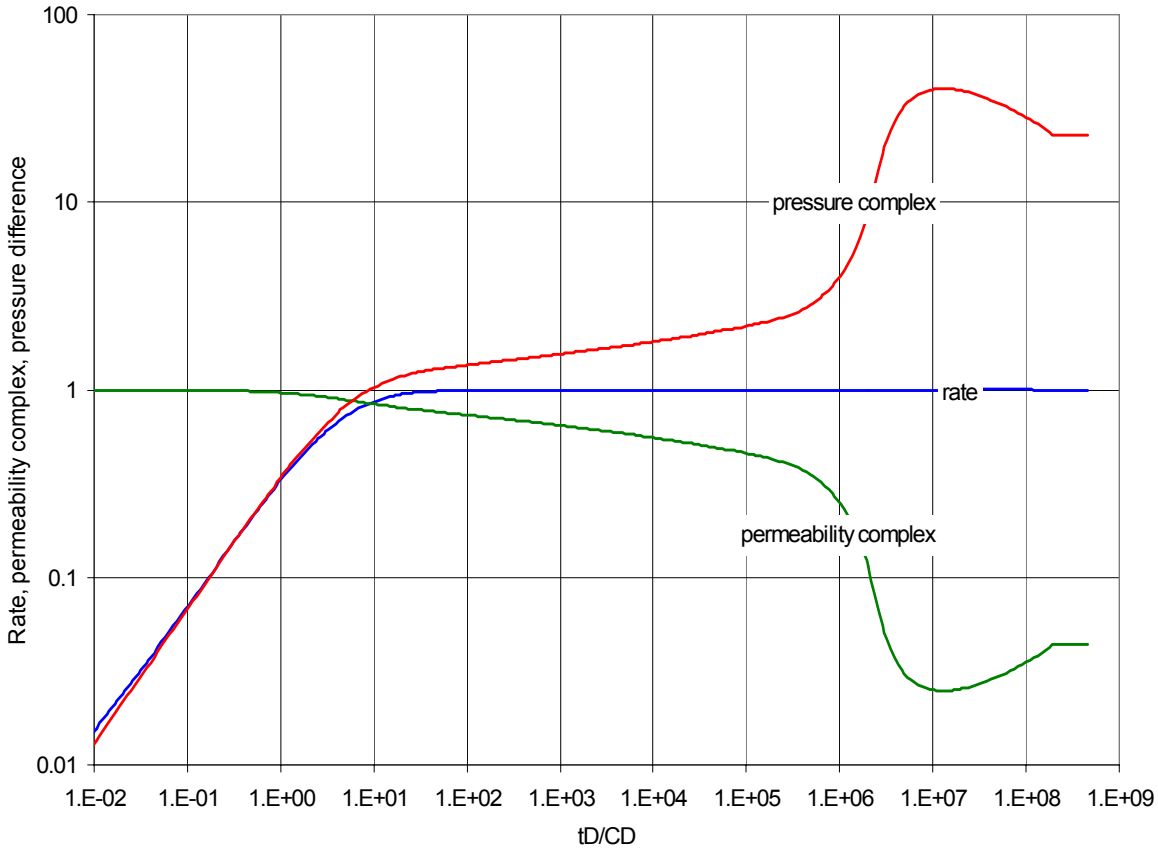

Figure 4-23. Behavior of calculated rate and its components vs. time

In order to visualize the transient processes, let us consider pressure and permeability distributions at several moments in time as given in Figs. 4-24 and 4-25, respectively.

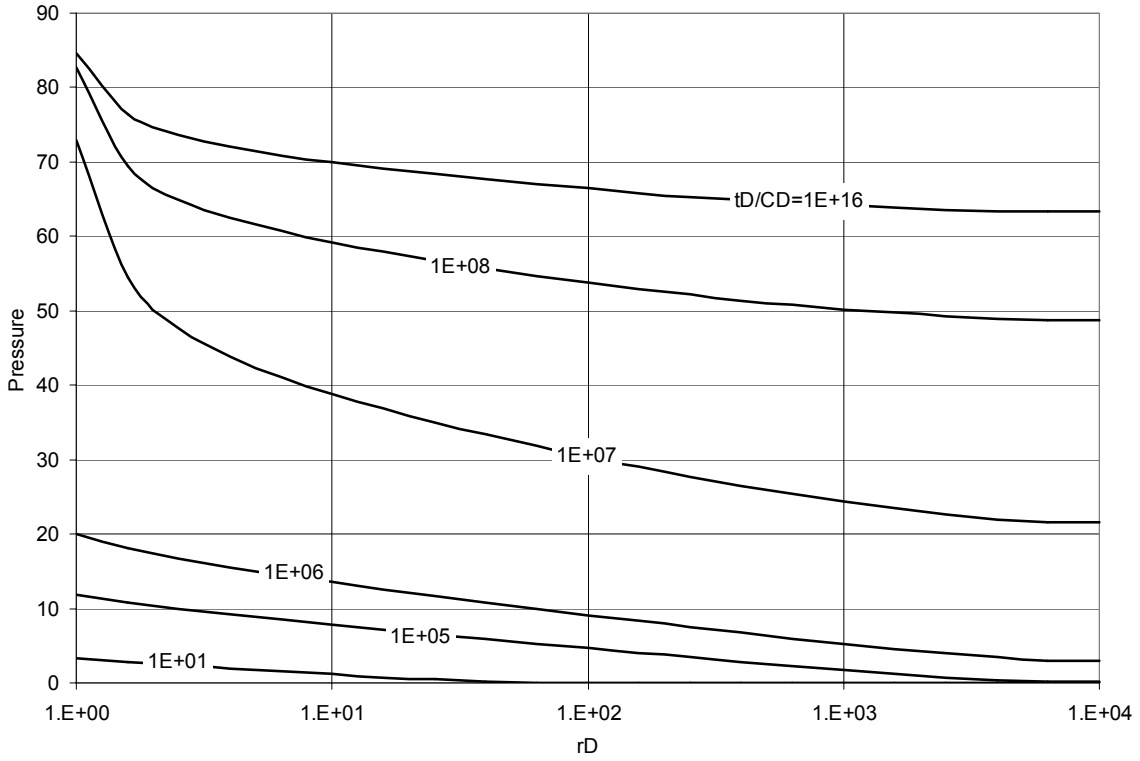

Figure 4-24. Pressure vs. distance in closed reservoir at several times and α=2

We can see that pressure gradient near the well increases up to $t_D/C_D \approx 10^7$ and then decreases. Pressure in the reservoir finally stabilizes, so that there is not a lot of difference between distributions at $t_D/C_D = 10^{10}$ and 10^{16}. Near-well permeability is eventually reduced by several orders of magnitude. Permeability everywhere in the formation is less than 10% of the initial value. Clearly, production rate cannot remain constant in such conditions. In fact, it should decrease since pressure gradient near the well decreases and so does permeability. Nevertheless, calculations show that the rate can be maintained constant. The discrepancy is due to numerical evaluation of rate, which is a product of pressure derivative and permeability term. At large times pressure gradient (multiplied by $\frac{\kappa}{\ln r_{eD}}$) is the inverse of permeability term. As a result the dimensionless rate $q_D = 1$.

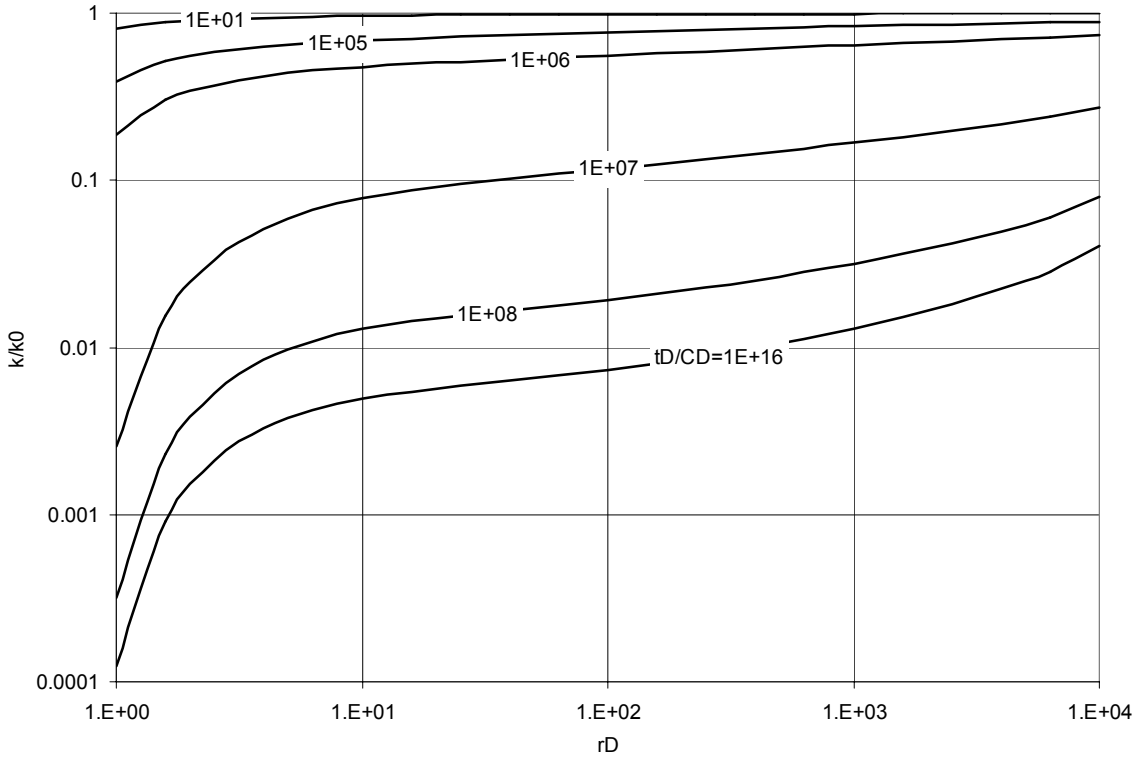

Figure 4-25. Permeability vs. distance in closed reservoir at several times and α=2

Let us consider another approach to numerical calculation of rate. Instead of approximating the pressure derivative on the well at $x = 0$, as it was shown in Chapter 3.4 we now will find the derivative on the outer boundary at $x = 1$. Using Taylor series, have

$$p(1-h) = p(1) - h\frac{\partial p(1)}{\partial x} + \frac{h^2}{2}\frac{\partial p^2(1)}{\partial x^2} + O\left(h^3\right)$$

$$\frac{\partial p(1)}{\partial x} = \frac{p(1) - p(1-h)}{h} + \frac{h}{2}\frac{\partial p^2(1)}{\partial x^2} + O\left(h^2\right)$$

Expression for the second derivative follows from the pressure equation

$$\frac{\partial}{\partial x}\left[K\frac{\partial p}{\partial x}\right] = \frac{\partial K}{\partial x}\frac{\partial p}{\partial x} + K\frac{\partial^2 p}{\partial x^2} = r_{eD}^{2x}\left(\ln r_{eD}\right)^2\frac{\omega}{\kappa}\frac{\partial p}{\partial t} = r_{eD}^2\left(\ln r_{eD}\right)^2\frac{\omega}{\kappa}\frac{\partial p}{\partial t}$$

$$\frac{\partial^2 p}{\partial x^2} = -\frac{\partial K}{K\partial x}\frac{\partial p}{\partial x} + \frac{\left(r_{eD}\ln r_{eD}\right)^2}{K}\frac{\omega}{\kappa}\frac{\partial p}{\partial t} = -\frac{\partial(\ln K)}{\partial x}\frac{\partial p}{\partial x} + \frac{\left(r_{eD}\ln r_{eD}\right)^2}{K}\frac{\omega}{\kappa}\frac{\partial p}{\partial t}$$

$$\frac{\partial p(1)}{\partial x} = \frac{p(1) - p(1-h)}{h} + \frac{h}{2}\left[-\frac{\partial(\ln K)}{\partial x}\frac{\partial p(1)}{\partial x} + \frac{\left(r_{eD}\ln r_{eD}\right)^2}{K}\frac{\omega}{\kappa}\frac{\partial p(1)}{\partial t}\right]$$

$$\frac{\partial p}{\partial x}\left[1 + \frac{h}{2}\frac{\partial(\ln K)}{\partial x}\right] = \frac{p_N - p_{N-1}}{h} + \frac{h}{2}\frac{\left(r_{eD}\ln r_{eD}\right)^2}{K}\frac{\omega}{\kappa}\frac{\partial p}{\partial t}$$

$$\left.\frac{\partial p}{\partial x}\right|_{x=1} = \frac{1}{1 + \frac{h}{2}\frac{\partial(\ln K)}{\partial x}}\left(\frac{p_N - p_{N-1}}{h} + \frac{h}{2}\frac{\left(r_{eD}\ln r_{eD}\right)^2}{K}\frac{\omega}{\kappa}\frac{\partial p}{\partial t}\right)$$

$$\left.\frac{\partial p}{\partial x}\right|_{x=1} = \frac{2}{2 + \ln K_N^n - \ln K_{N-1}^n}\left(\frac{p_N^{n+1} - p_{N-1}^{n+1}}{h} + \frac{h}{2\tau}\frac{\left(r_{eD}\ln r_{eD}\right)^2}{K_N^n}\frac{\omega}{\kappa}\left(p_N^{n+1} - p_N^n\right)\right)$$

which is similar to previous result, except for all variables are taken at $x = 1$.

Now we take the pressure equation

$$\frac{\partial}{\partial x}\left[K\frac{\partial p}{\partial x}\right] = r_{eD}^{2x}\left(\ln r_{eD}\right)^2\frac{\omega}{\kappa}\frac{\partial p}{\partial t}$$

And integrate it formally from 0 to 1

$$\int_0^1 \frac{\partial}{\partial x}\left[K\frac{\partial p}{\partial x}\right]dx = \int_0^1 r_{eD}^{2x}\left(\ln r_{eD}\right)^2\frac{\omega}{\kappa}\frac{\partial p}{\partial t}dx$$

$$\left[K\frac{\partial p}{\partial x}\right]_{x=1} - \left[K\frac{\partial p}{\partial x}\right]_{x=0} = \left(\ln r_{eD}\right)^2\frac{\omega}{\kappa}\int_0^1 r_{eD}^{2x}\frac{\partial p}{\partial t}dx$$

On the left-hand side we have the difference of pressure derivatives (essentially, rates) at the boundaries and we have an expression to calculate rate at *x*=1. We can, therefore, calculate well rate using rate on the outer boundary. To do this we need to consider integral

$$\int_0^1 r_{eD}^{2x}\frac{\partial p}{\partial t}dx = \int_0^h r_{eD}^{2x}\frac{\partial p}{\partial t}dx + \int_h^{2h} r_{eD}^{2x}\frac{\partial p}{\partial t}dx + \ldots + \int_{1-h}^1 r_{eD}^{2x}\frac{\partial p}{\partial t}dx = \sum_{i=1}^{N-1}\int_{x_i}^{x_{+1}} r_{eD}^{2x}\frac{\partial p}{\partial t}dx$$

We now replace the time derivative with its value at the midpoint of the interval

$$\sum_{i=1}^{N-1}\left(\frac{\partial p}{\partial t}\right)_{i+1/2}\int_{x_i}^{x_{+1}} r_{eD}^{2x}\,dx=\sum_{i=1}^{N-1}\left(\frac{p_i^{n+1}-p_i^n}{\tau}\right)_{i+1/2}\int_{x_i}^{x_{+1}} r_{eD}^{2x}\,dx=\frac{1}{2\tau}\sum_{i=1}^{N-1}\left(p_i^{n+1}+p_{i+1}^{n+1}-p_i^n-p_{i+1}^n\right)\int_{x_i}^{x_{+1}} r_{eD}^{2x}\,dx$$

Integrals individually are

$$\int_{x_i}^{x_{+1}} r_{eD}^{2x}\,dx=\frac{1}{2\ln r_{eD}}\left(r_{eD}^{2x_{i+1}}-r_{eD}^{2x_i}\right)$$

Therefore

$$\int_0^1 r_{eD}^{2x}\frac{\partial p}{\partial t}\,dx=\frac{1}{4\tau\ln r_{eD}}\sum_{i=1}^{N-1}\left(p_i^{n+1}+p_{i+1}^{n+1}-p_i^n-p_{i+1}^n\right)\left(r_{eD}^{2x_{i+1}}-r_{eD}^{2x_i}\right)$$

Finally, denoting $y_i=r_{eD}^{2x_{i+1}}-r_{eD}^{2x_{i-1}}$, $y_1=r_{eD}^{2x_2}-r_{eD}^{2x_1}$, $y_N=r_{eD}^{2x_N}-r_{eD}^{2x_{N-1}}$, obtain

$$\left[K\frac{\partial p}{\partial x}\right]_{x=0}=\frac{2K_N^n}{2+\ln K_N^n-\ln K_{N-1}^n}\left(\frac{p_N^{n+1}-p_{N-1}^{n+1}}{h}+\frac{h}{2\tau}\frac{\left(r_{eD}\ln r_{eD}\right)^2}{K_N^n}\frac{\omega}{\kappa}\left(p_N^{n+1}-p_N^n\right)\right)-$$

$$-\frac{\omega}{\kappa}\frac{\ln r_{eD}}{4\tau}\left[p_1^{n+1}y_1+p_2^{n+1}y_2+p_3^{n+1}y_3+\ldots-p_1^n y_1-p_2^n y_2-p_3^n y_3-\ldots\right]$$

This expression shows that production rate cannot remain constant but should decline with time. As τ increases the numerical value of the expression decreases. Indeed, when this formula was used to calculate rate, the rate steadily declined after pressure reached maximum at $t_D/C_D\approx 10^7$.

Type curves for α=0, 1, 3, and 5 are presented in Fig. 4-26 (blue, red, green, and black pairs of curves). We can see that the greater is the sensitivity of permeability to deformation, the sooner the above describe effects are observed, i.e. permeability reduction leads to infeasibility of constant rate production.

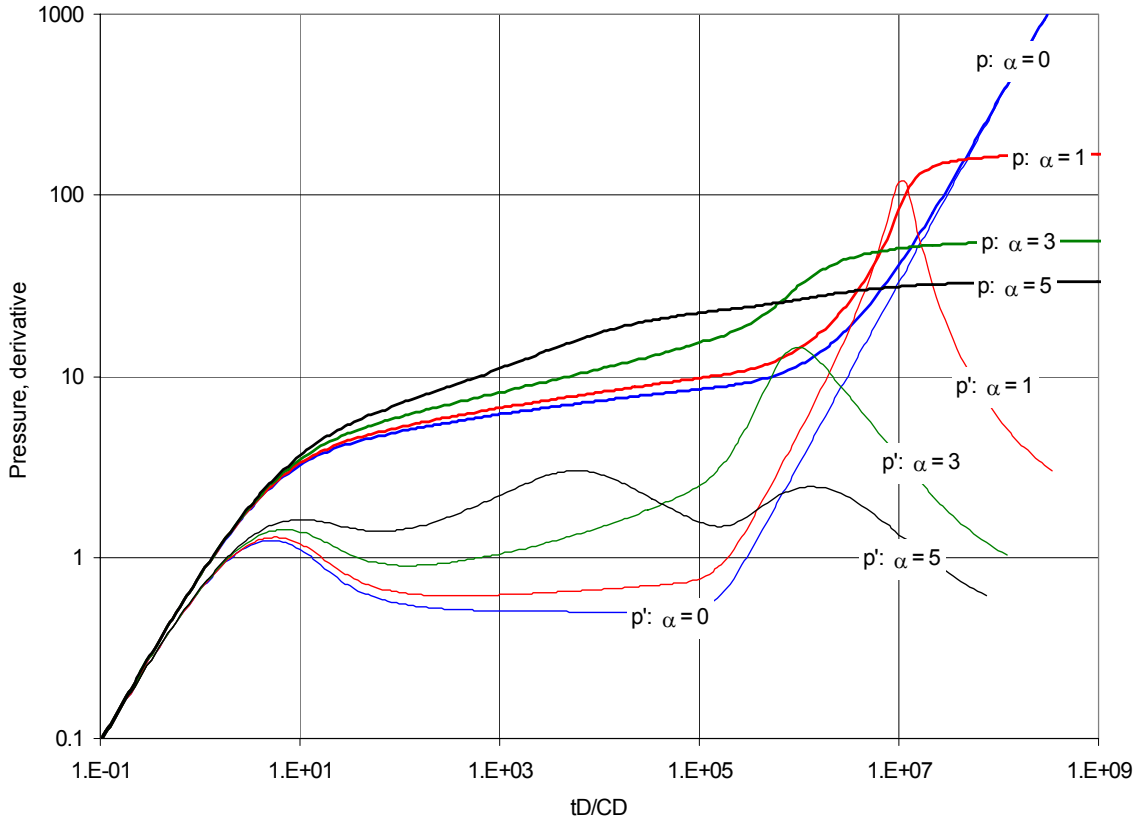

Figure 4-26. Drawdown type curves, closed reservoir, various α

4.2.4 Constant pressure drawdown, constant pressure outer boundary

The next problem considered is a case of a well put on production with constant wellbore pressure and with constant pressure circular outer boundary. The boundary is at $r_{eD} = 10{,}000$, all other parameters are the same as in the base case. Rather than observing change of pressure on the well and its derivative we now observe how production rate declines with time. At constant pressure, as suggested by several researchers (see, for example, Ref. 34) a plot of $1/q_D$ vs. time has similar trends as the considered before constant rate case where pressure difference is plotted vs. time.

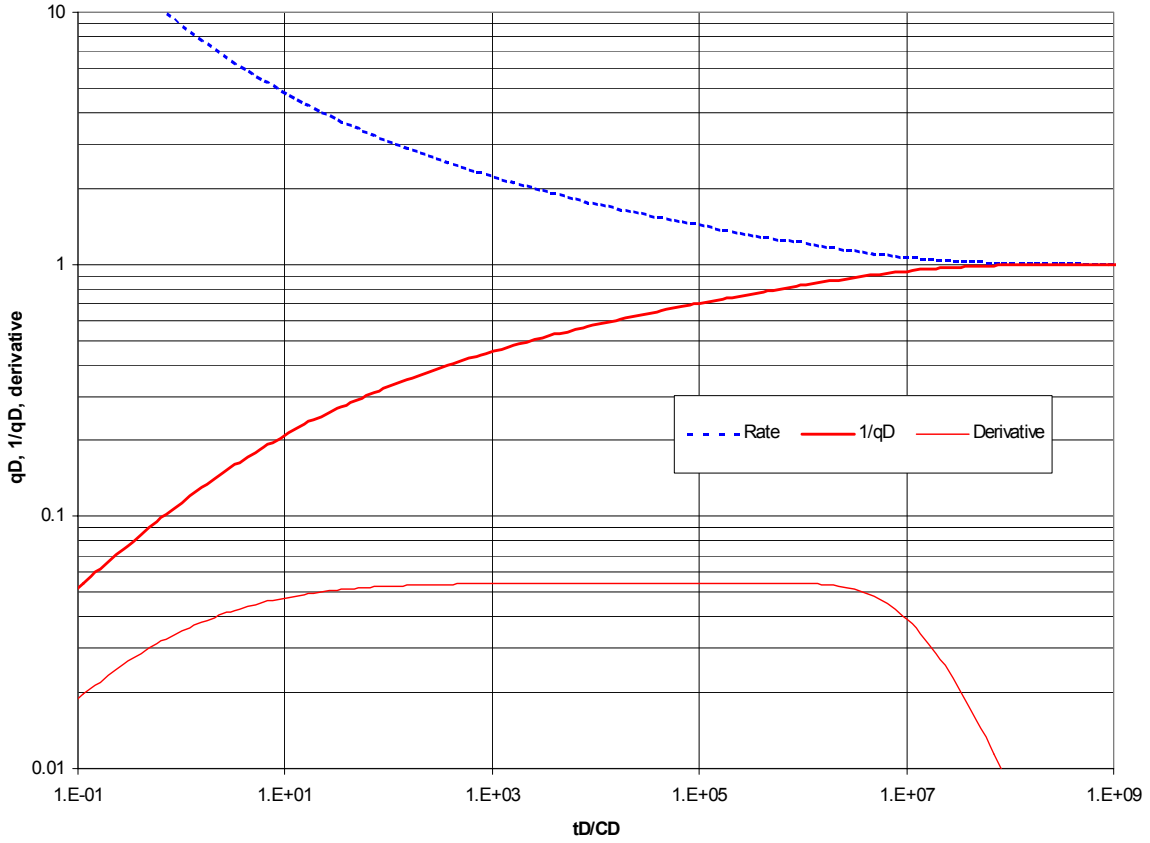

Figure 4-27. Constant pressure production, linear case

Dimensionless rate (dashed blue curve) as well as $1/q_D$ (thick red curve) and logarithmic derivative $\partial(1/q_D)/\partial(\ln t_D)$ (thin red curve) are presented in Fig. 4-27 for the linear case α=0. The magnitude of dimensionless wellbore flowing pressure is equal to $\ln(r_{eD})$, so that production rate stabilizes at q_D=1. We can see that initially $1/q_D$ increases fairly rapidly (production rate exhibits rapid decline) and after $t_D/C_D \approx 100$ increases at a constant rate, which is indicated by constant derivative. As the boundary is reached at $t_D/C_D \approx 10^6$, both production rate and $1/q_D$ flatten at constant value of 1, respectively the derivative drops to zero.

If permeability is stress-dependent with α=2, then constant pressure production at same as above $p_{wD} = \ln r_{eD}$ results in the following deviation from the linear case. Presented in Fig. 4-28 are the same variables. We can see that at steady-state production rate is lower than in the linear case. The increase of $1/q_D$ is at variable rate at all time, which is reflected by the derivative. Such behavior is due to decrease of permeability in response to caused by production pressure decrease.

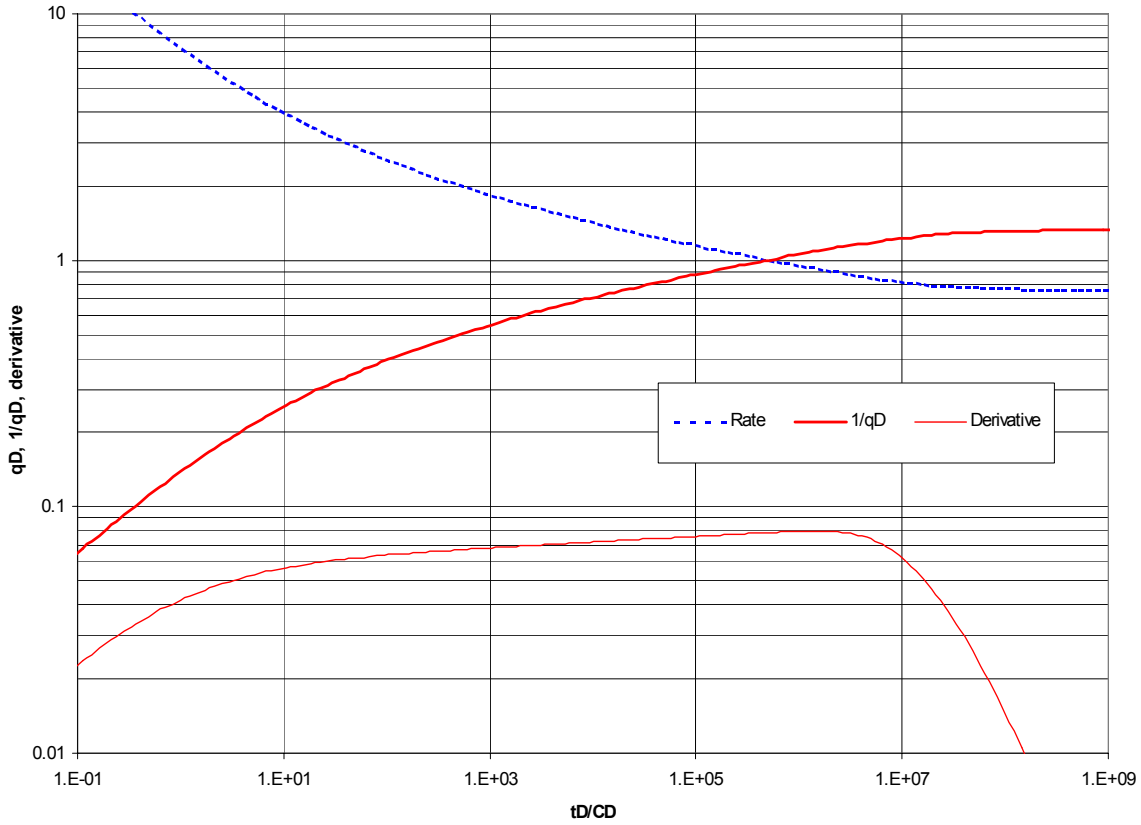

Figure 4-28. Constant pressure production, α=2

Distributions of dimensionless pressure, deformation, and permeability at several moments in time are presented in Figs. 4-29, 30, 31. The curves correspond to $t_D/C_D \approx 0.01$, 1, 100, 10^4, 10^6, and 10^{13} (stabilization), blue dashed straight line in Fig. 4-29 is steady-state linear case pressure distribution.

Let us consider the blue curves. At this early time pressure has not yet moved beyond 3-4 wellbore radii (Fig. 4-29) but the impact of the well pressure drop has been already felt at a significant distance away from the wellbore. The stress-strain state in the system has changed and as a result the formation has deformed far beyond of the zone with altered pressure (Fig. 4-30). This deformation causes reduction of permeability and, for example, at a distance of about 16 wellbore radii the permeability has dropped by 1 percent (Fig. 4-31). The reduced permeability, in turn, affects the flow and the pressure difference, which eventually stabilizes at a lower level than in the linear case.

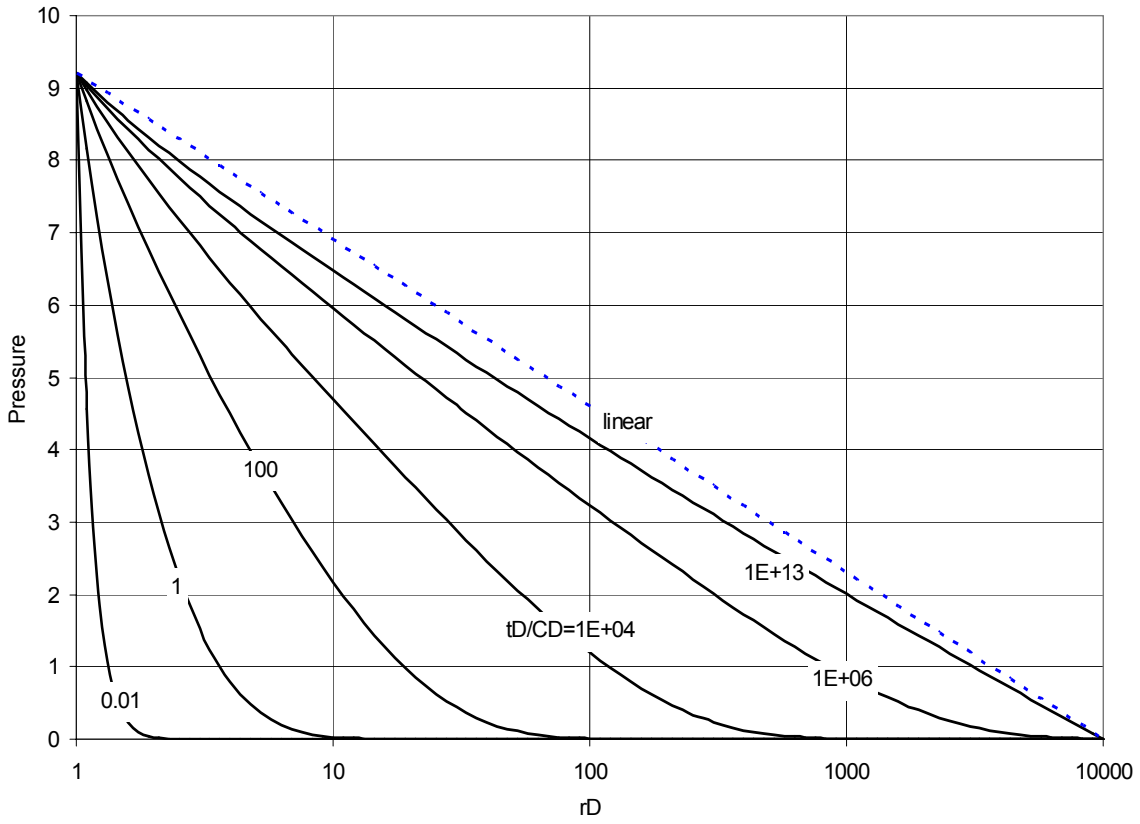

Figure 4-29. Pressure vs. distance at several times

The same behavior is observed for later times. At the onset of steady-state flow (red curves) the entire formation has been already significantly affected with respective

magnitudes of deformation and reduced permeability. For this value of α, the permeability on the well stabilizes at less than half of the initial value and on the outer boundary drops to about 90 percent of the initial value. The majority of permeability reduction occurs within the distance of about 10 dimensionless wellbore radii. Note that conventional models that account for stress change in the formation only would not predict any permeability change at the outer boundary.

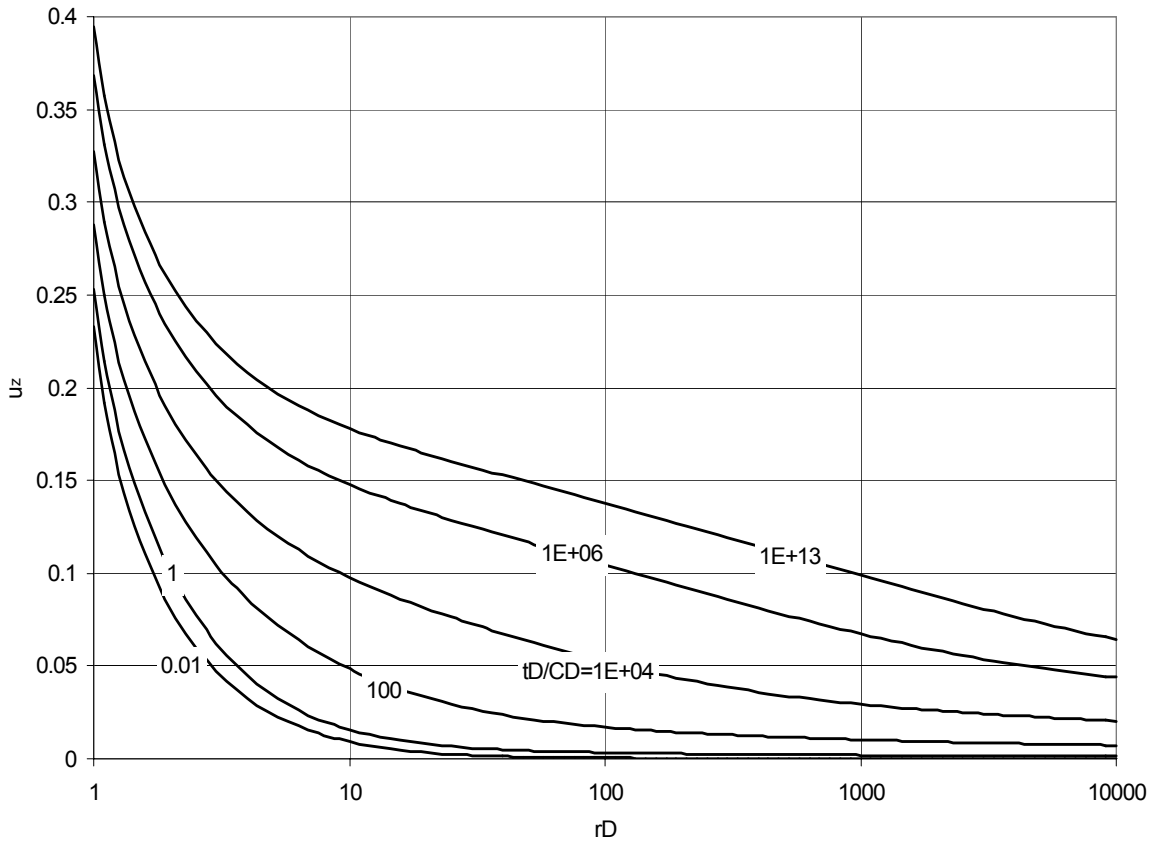

Figure 4-30. Deformation vs. distance at several times

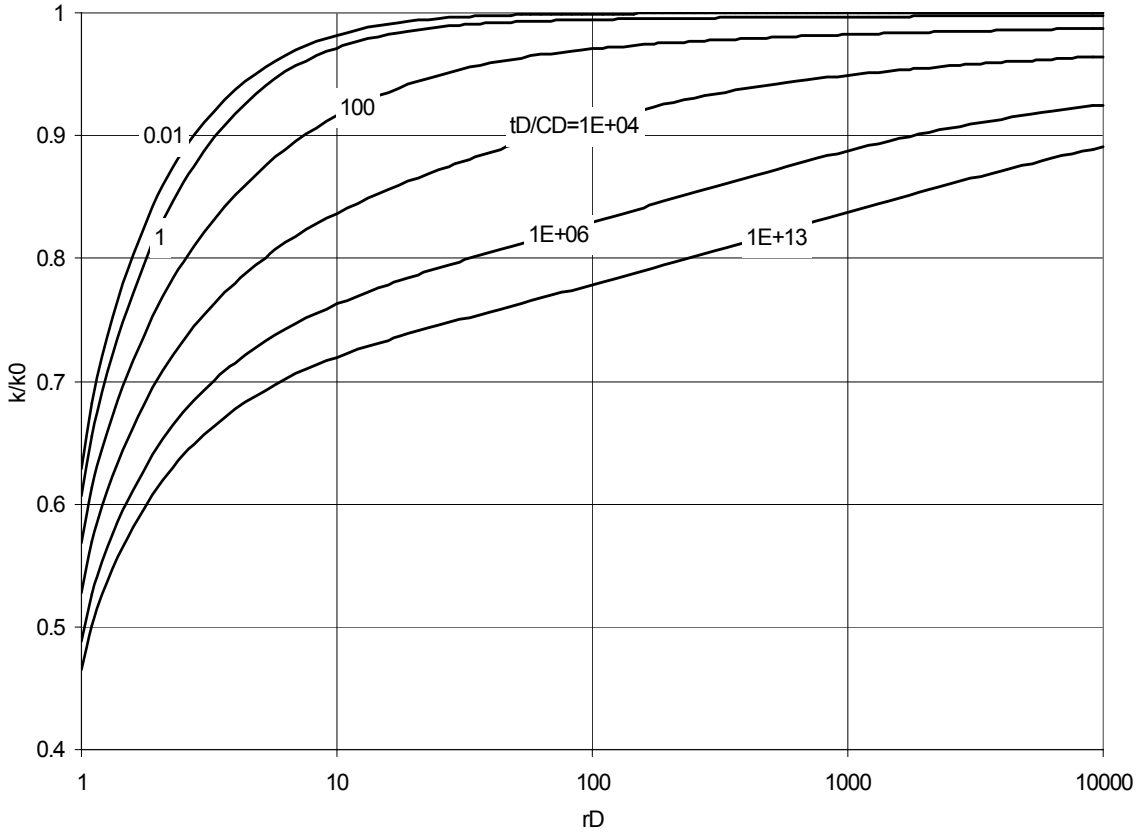

Figure 4-31. Permeability vs. distance at several times

For greater sensitivity of permeability to deformation the deviation from the linear case is, respectively, more significant. The rate type curves for α=0, 4, and 8 (blue, red, and green pairs of curves, respectively) are presented in Fig. 4-32. Clearly, the transient process of rate stabilization is affected by the magnitude of α. When sufficiently accurate measurements of production rate are available, plot of $1/q_D$ vs. time may provide indication of permeability stress-sensitivity.

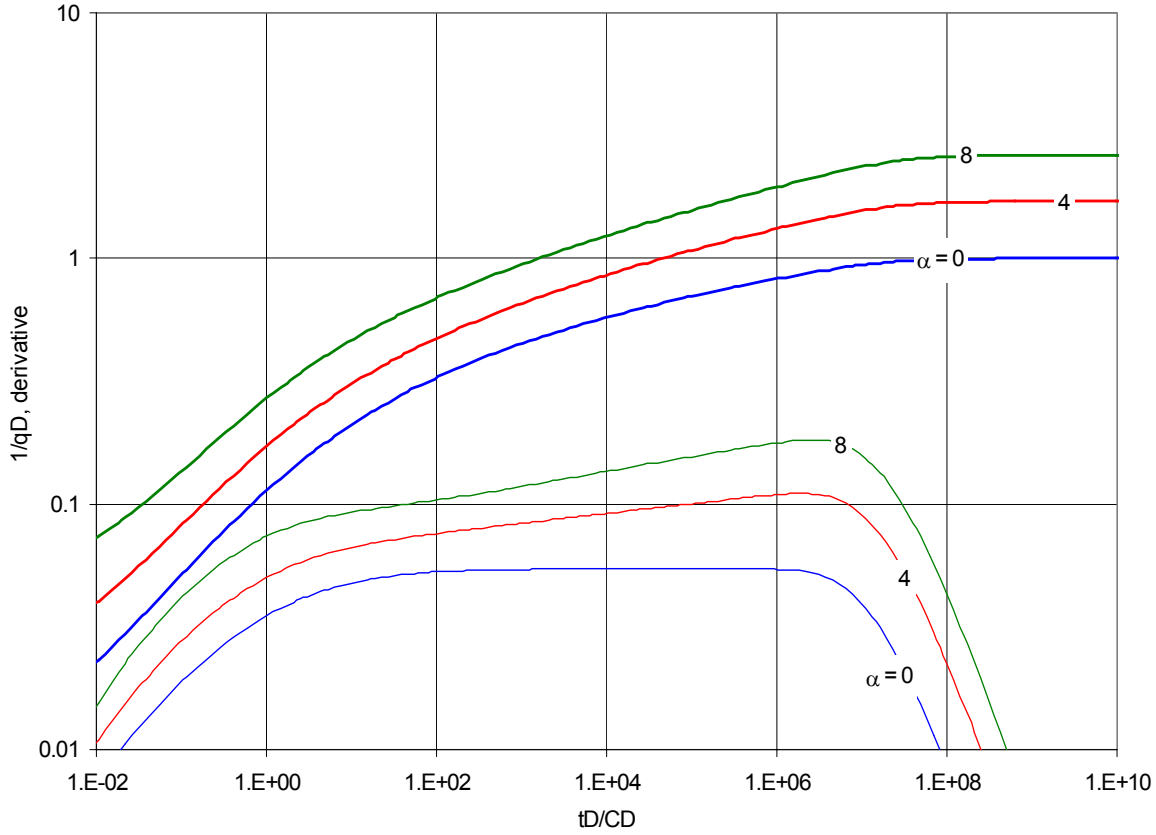

Figure 4-32. Rate type curves for various α

The steady-state rate vs. α is presented in Fig. 4-33. Increased sensitivity of permeability to deformation expectedly results in a decreased production, so that, for example, for α =10 the rate is only about 30 percent of the rate, calculated with no account for deformation.

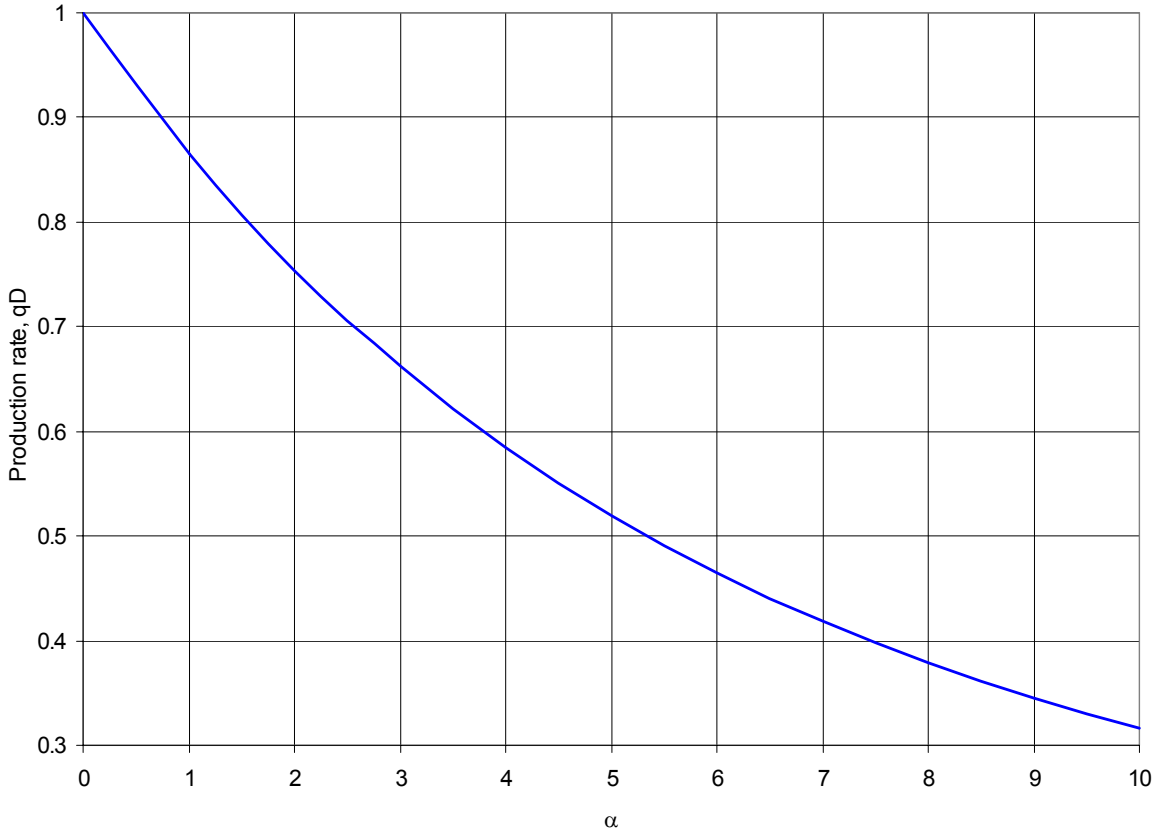

Figure 4-33. Steady-state production rate vs. α

The causes for such decrease are illustrated in Figs. 4-34 and 4-35 where we plot steady-state pressure and permeability distributions for α=0, 4, and 8 (curves colored as in Fig. 4-32). For large α the permeability near the well drops to several percent of the initial value and the pressure difference in the reservoir stabilizes at a lower level. This additional pressure drop is obviously introduced by the decreased permeability and it is plotted (normalized by the total formation pressure drop) in Fig.4-36 at steady state (values of α and curve coloring are as in Fig. 4-32). We can see that even for moderate sensitivity of permeability to deformation the additional resistance to flow is substantial, which is further aggravated by the fact that the entire area of flow is affected.

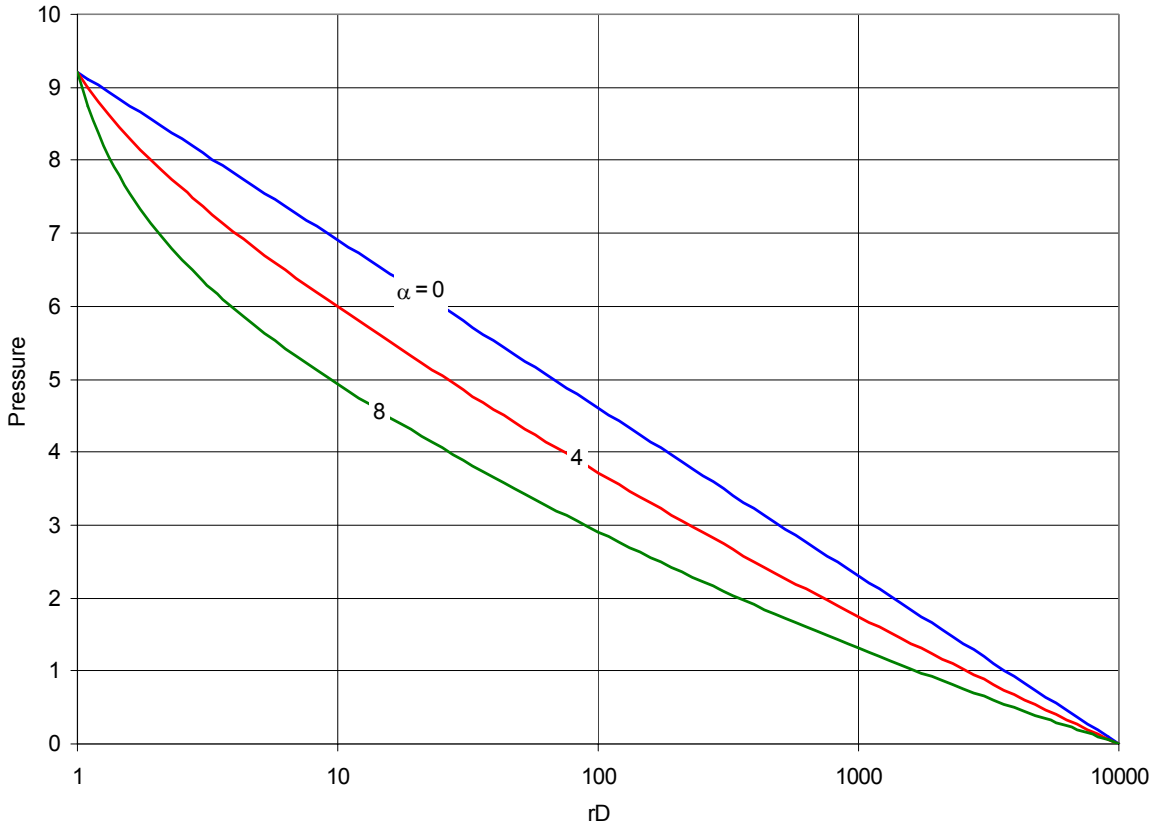

Figure 4-34. Steady-state pressure distributions for various α

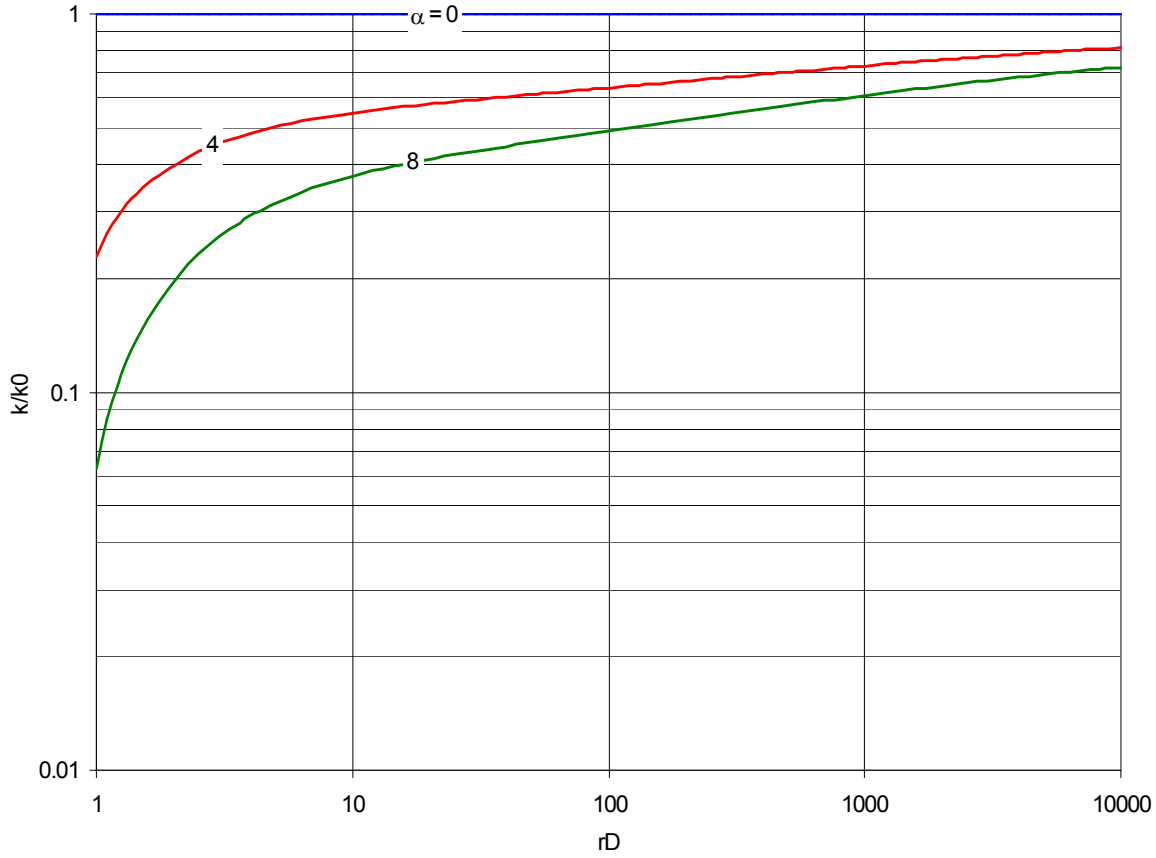

Figure 4-35. Steady-state permeability distributions for various α

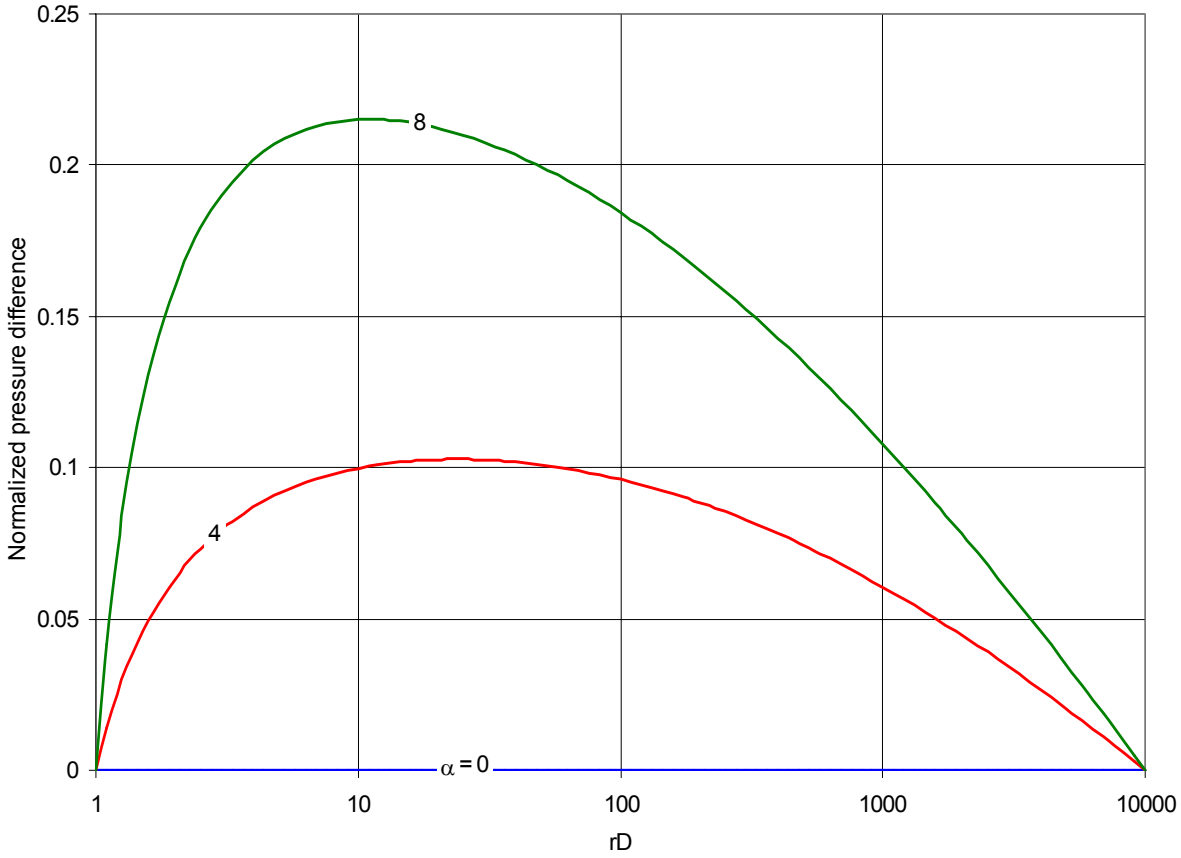

Figure 4-36. Additional steady-state pressure drop in the reservoir due to stress-sensitive permeability

Along with sensitivity of permeability to deformation the constant pressure production is affected by the value of the wellbore pressure, since its magnitude determines the pressure drop in the reservoir and deformation is a function of the effective stress. Presented in Fig.4-37 are rate type curves – $1/q_D$ and its logarithmic derivative for constant p_{wD}=1, 5, $\ln(r_{eD})$, 20, and 50 (blue, red, green, black, and pink pairs of curves, respectively). Increased drawdown leads to increase of effective stress, which results in larger deformation and for the same for all pairs of curves α=2 – in a larger permeability decrease. This, in

turn, affects the flow and production rate decreases ($1/q_D$ increases). The derivative allows to see more clearly the trend in behavior of $1/q_D$.

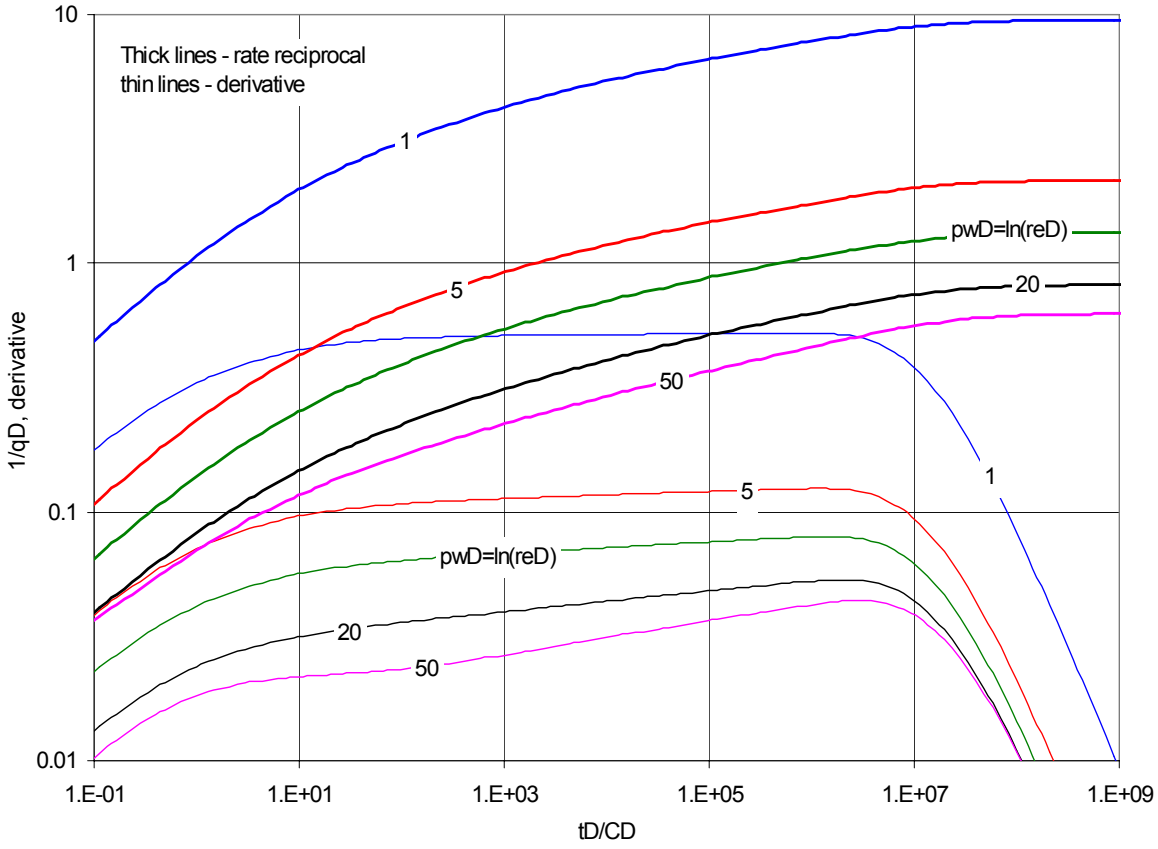

Figure 4-37. Rate type curves for various p_{wD}

A conventional way to evaluate formation capabilities is examination of an Inflow Performance Relationship (IPR). Several types of IPRs that describe different effects are available. For example, Darcy IPR for oil wells shows that rate changes linearly with drawdown for constant productivity index. It cannot be applied in the entire range of rates and pressures because it assumes single-phase flow and does not account for multiphase flow effects. These effects in oil wells can be accounted for by using either Vogel's IPR, or by calculating multiphase pseudo-pressure. The latter IPR curves are not straight-line

relationships, as is Darcy's IPR, and they account for changes in productivity index. Nevertheless, Darcy's equation and IPR are used routinely to perform quick calculations and to compare the effects of various factors on flow.

In Fig. 4-38 we use Darcy IPR to visualize the effect of permeability stress-dependence on flow rate of a well. Blue straight line is the linear case, calculated with no account for deformation. Curves from red to light green correspond to α=1, 2, 3, 4, 5, and 6. We can see that the greater is the magnitude of the drawdown and α, the greater is the deviation of an IPR from the straight-line behavior. Similar behavior is characteristic of the gas or multiphase flow, which makes it difficult to distinguish between the two. But if these trends on an IPR are observed on an oil well, produced above the bubble-point pressure, then, given that we have enough confidence in the quality of the PVT analysis and rate/pressure measurements, such deviation can be explained by the effects of deformation.

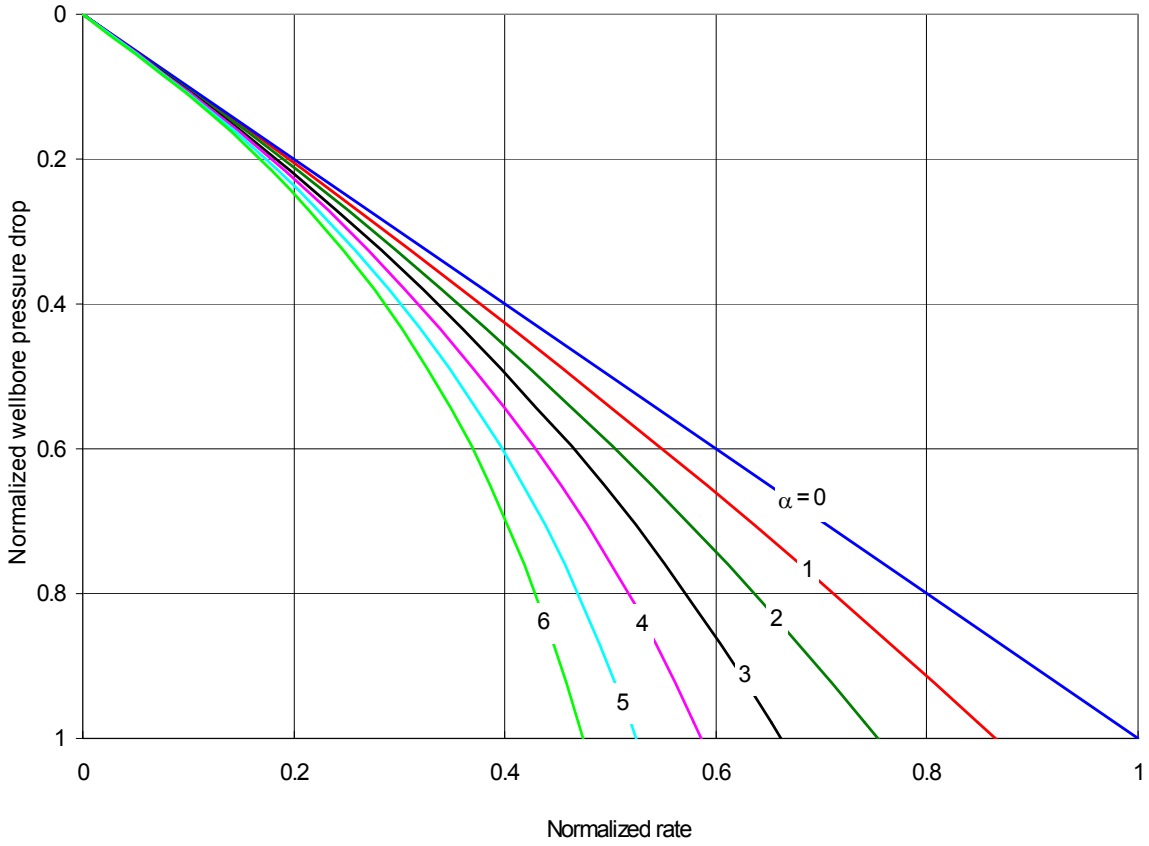

Figure 4-38. IPR curves for various α

4.2.5 Constant pressure drawdown, no-flow outer boundary

Let us next consider the case of a well put on production with constant wellbore pressure and located in the center of a closed circular drainage area. The boundary is at $r_{eD} = 10{,}000$, all other parameters are the same as in the base case. Next several graphs show how production rate declines with time for different values of the problem parameters.

In Fig. 4-39 pair of blue and red curves correspond to linear case and to the case α=2. Both cases were calculated with constant $p_{wD} = \ln r_{eD}$. As one would expect, production from a closed reservoir eventually results in decrease of rate (increase of $1/q_D$).

Transient flow regime is followed by pseudo-steady state flow, both periods are clearly identifiable.

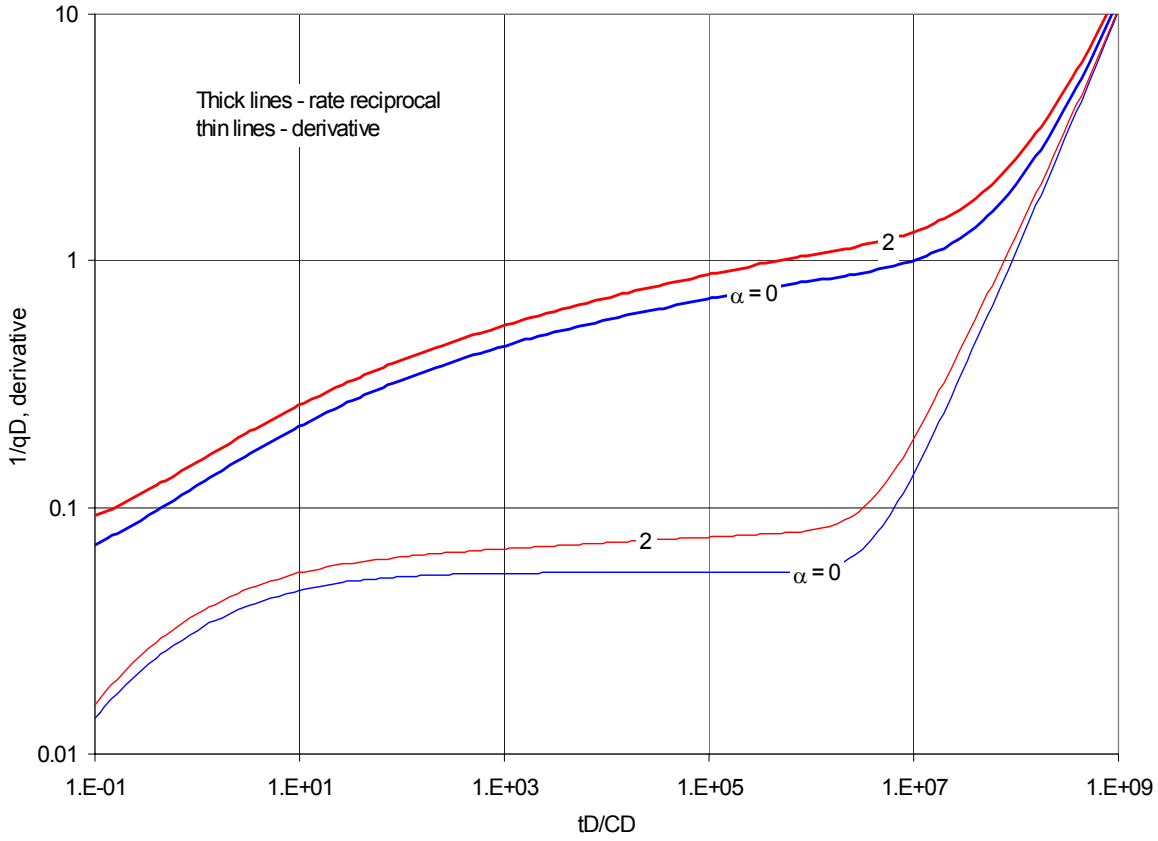

Figure 4-39. Rate type curves, closed drainage area, various α

During transient flow, prior to reaching the outer boundary, the behavior of the curves, calculated with account for deformation, is essentially the same as in the preceding problem. Let us consider distributions of pressure and permeability during transient and pseudo-steady state as presented in Figs. 4-40, 4-41. The blue curves are for $t_D/C_D \approx 0.01$, the red curves are for $t_D/C_D \approx 10^6$ and correspond to the onset of pseudo-steady state flow. All curves are approximately one log-cycle in time apart.

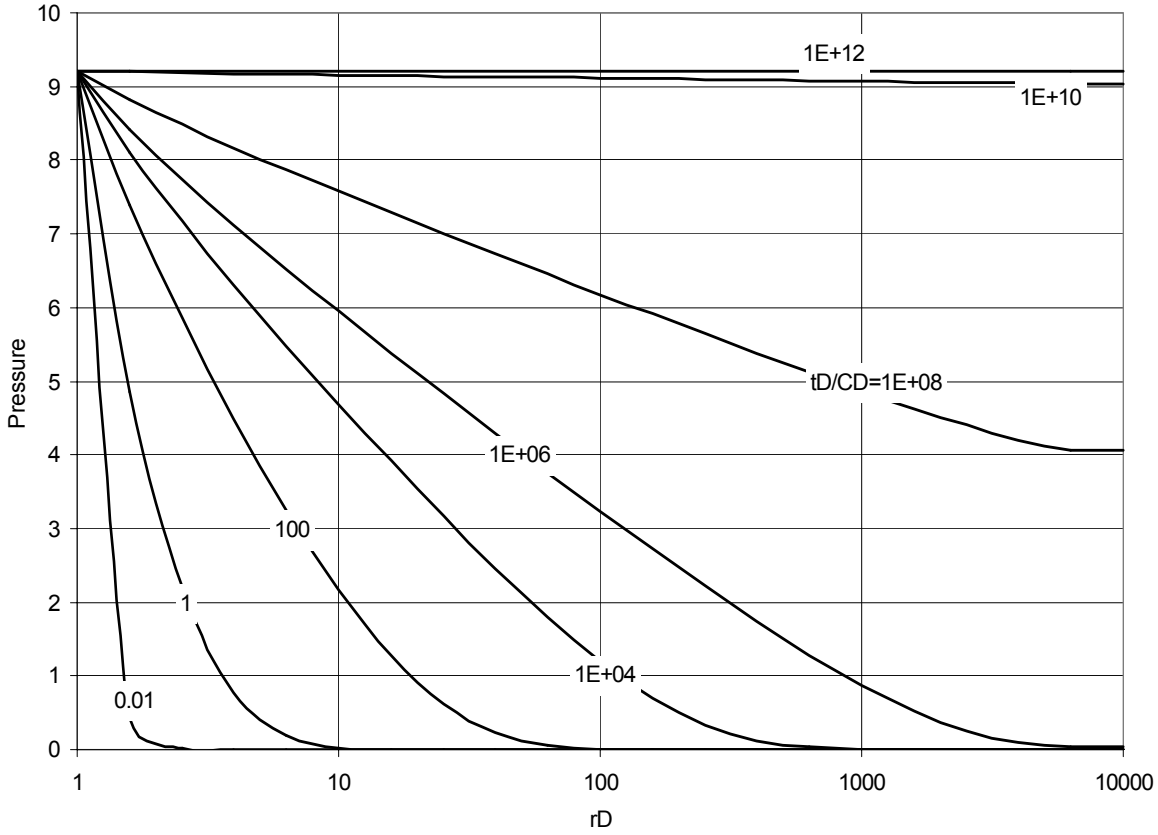

Figure 4-40. Pressure vs. distance at several times

After reaching the boundary pressure decreases everywhere in the reservoir and so does permeability. Note that even though wellbore pressure is constant, permeability on the well drops significantly in response to pressure reduction elsewhere in the reservoir. Curves for late times virtually overlay, which corresponds to rate decrease.

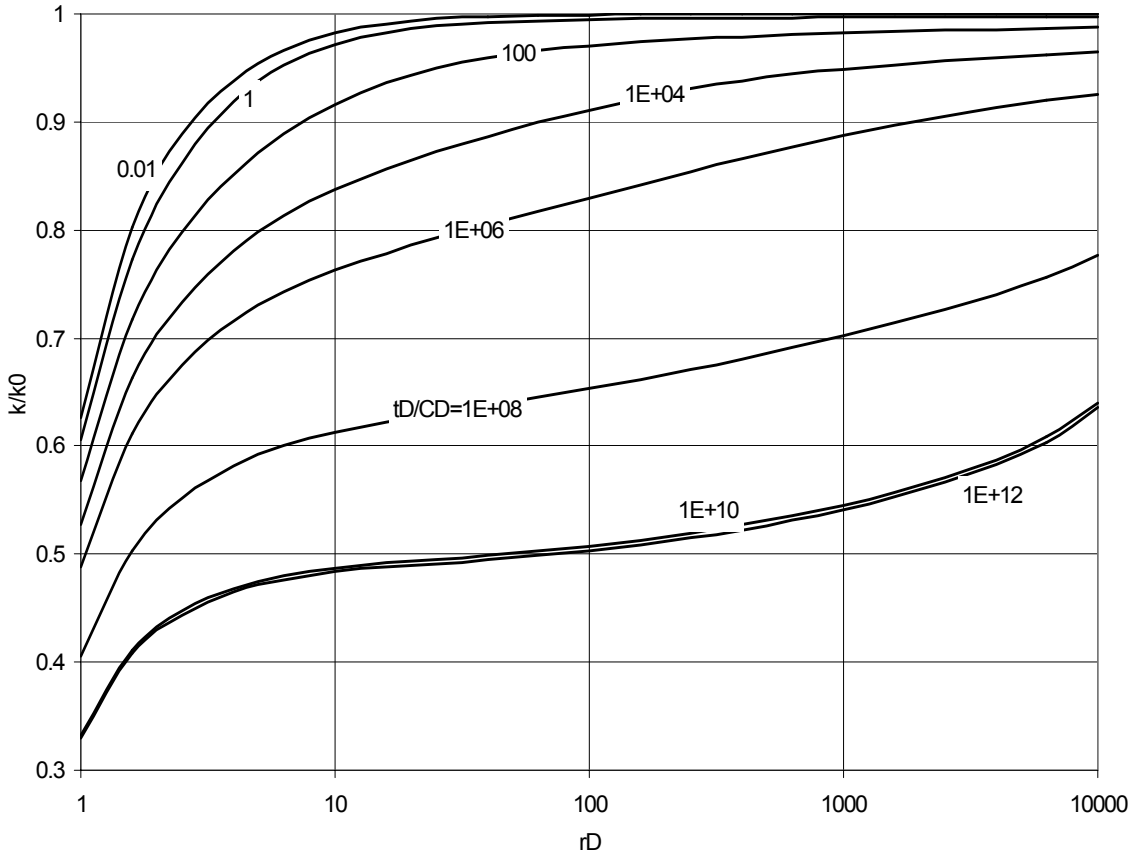

Figure 4-41. Permeability vs. distance at several times

4.3 Buildup problems

In this section we present selected results of calculation of a typical buildup test, following either a constant rate, or a constant pressure drawdown. We have already seen that commencement of production from a stress-sensitive formation causes development of a zone of reduced permeability around a well. As production continues, this zone expands into the formation, affects the fluid flow, and, respectively, the trends in the wellbore flowing pressure. One can expect, therefore, that the duration of production prior to shut-in will significantly affect wellbore pressure behavior during buildup.

Let us consider buildup in an infinite reservoir ($r_{eD} = 10^6$), following constant rate drawdown as given by the base case with $a = 0.0384$, $\alpha = 2$, $\gamma = E_1/E = 1$, $E = 10^{10}\ Pa$, $r_w/h = 0.001$, $h = 10\ m$, $C_D = 100$, $s = 0$. Suppose that at $t_D/C_D = 10^{10}$ the well is shut in for an equally extended buildup. These two flow periods are presented in Fig. 4-42. The blue curves represent drawdown, and the red curves represent buildup.

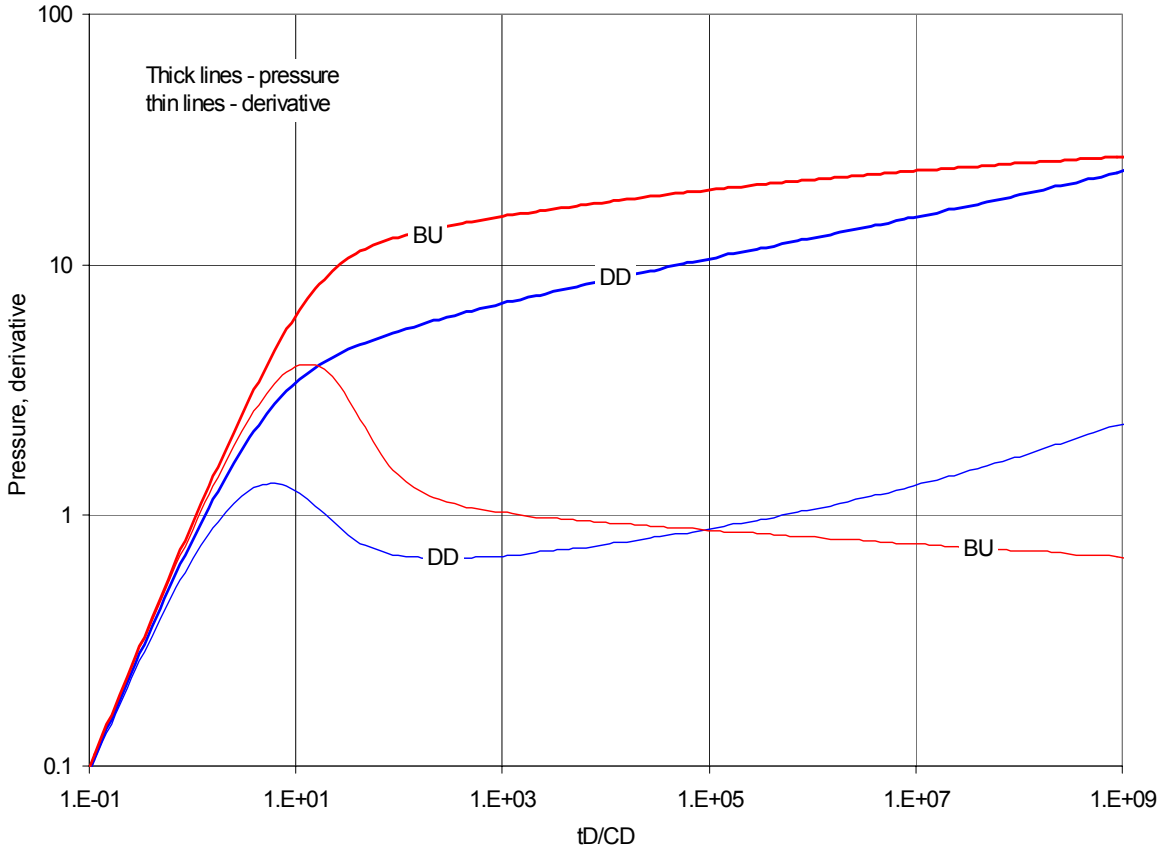

Figure 4-42. Infinite reservoir, drawdown followed by buildup, α=2

We can see that these two types of tests produce markedly different sets of curves. If interpretation of a drawdown test using conventional methods might have indicated a stimulated well, the conventional buildup interpretation would indicate a significant damage to the well. It would also appear that the magnitude of damage increases, as we are further

into the test. It is interesting to note that if buildup is terminated prior to reaching the outer boundary (which almost always will be the case in low-permeability reservoirs) the estimated reservoir pressure might be higher than the value prior to production. Obviously, conventional interpretation of both tests would provide with incorrect results. If run concurrently, the characteristic behavior as depicted here would clearly indicate stress-sensitive permeability. Such type of asymmetry of response has been observed in several reported field tests.

Let us now investigate how the production time prior to shut-in affects the shape of buildup type curves. For Figs. 4-43-4-45, well is shut-in at $t_D/C_D = 10^3$, 10^5, and 10^7, respectively. Duration of buildup is the same as of drawdown, blue and red pairs of curves correspond to drawdown and buildup, respectively. It can be seen that both pressure and derivative curves have the same characteristic features, as described above, but the difference between drawdown and buildup becomes more significant as the duration of the flow period increases.

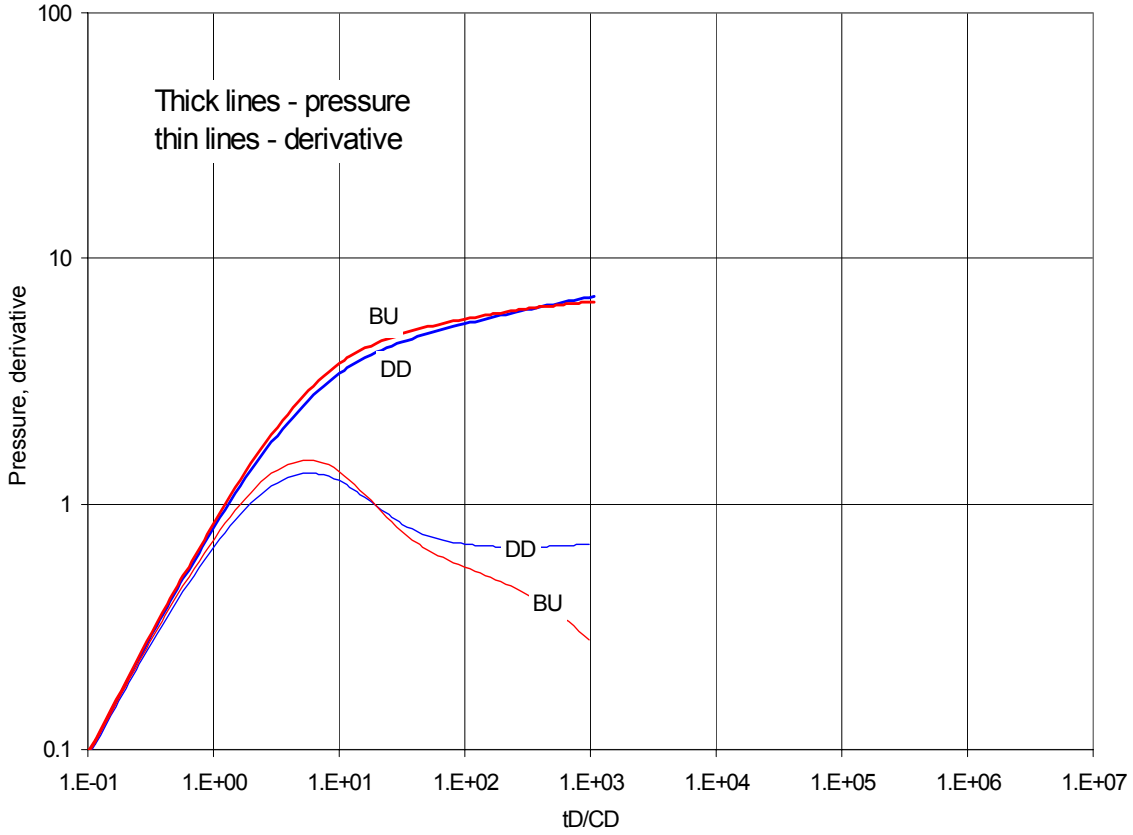

Figure 4-43. Infinite reservoir, drawdown followed by buildup. Production time 10^3

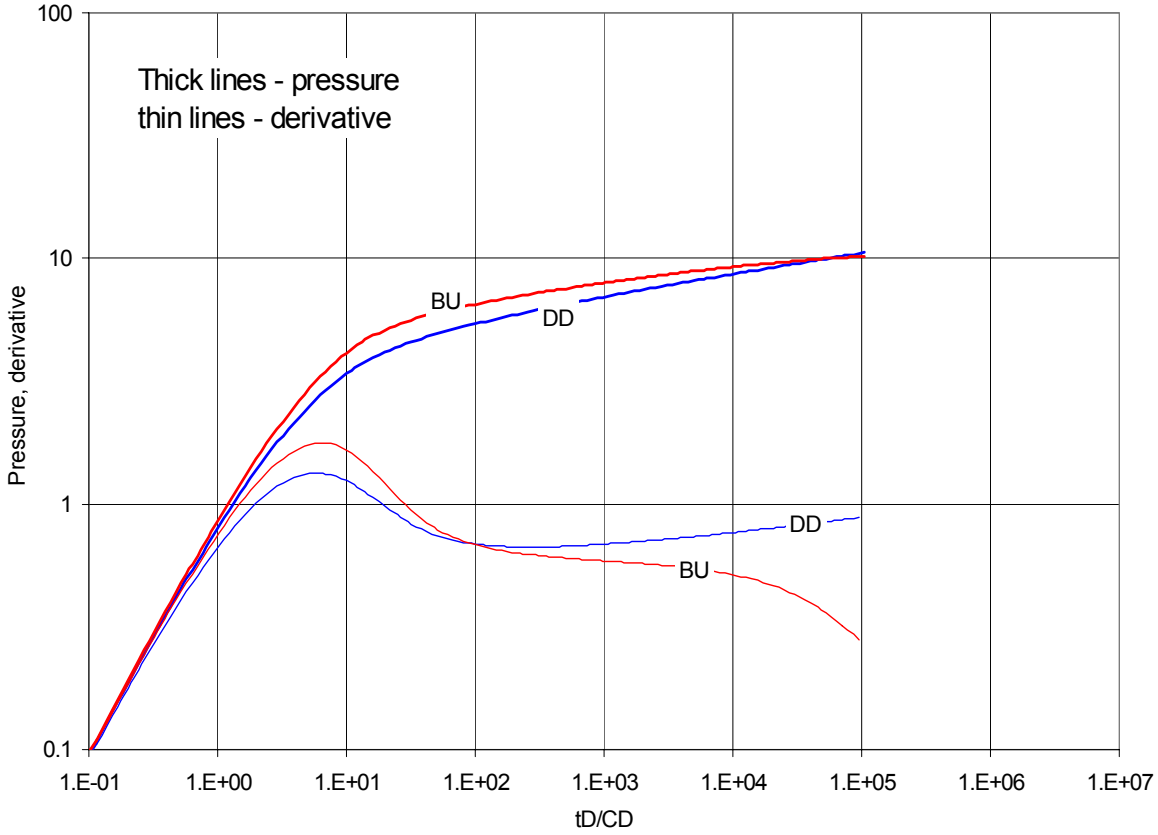

Figure 4-44. Infinite reservoir, drawdown followed by buildup. Production time 10^5

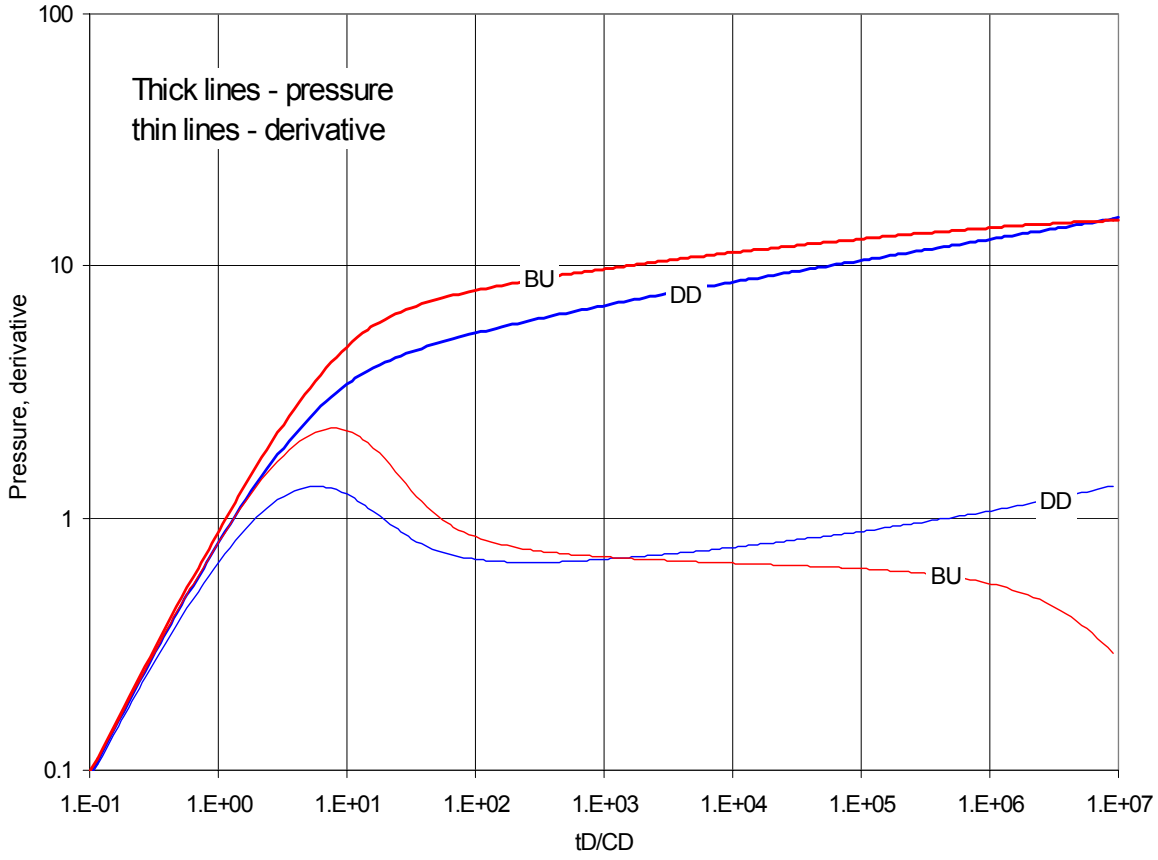

Figure 4-45. Infinite reservoir, drawdown followed by buildup. Production time 10^7

From consideration of the derivative it appears that the circular zone around the well, affected the most by the drawdown, might be erroneously recognized as drainage area of the well. Another characteristic feature is a larger separation between pressure and derivative curves in case of a longer drawdown and large separation indicates greater damage. The transition period increases with extension of drawdown which also indicates greater damage. It might be possible to identify the sensitivity of permeability to deformation as well as the conventional parameters (permeability, skin, wellbore storage coefficient) from a series of constant rate drawdown tests of increasing duration intermitted by buildup tests. The

duration of buildup tests should be long enough so that the derivative intercepts the derivative, obtained on the preceding drawdown.

It is clear that all these effects will be more pronounced if the properties of the surrounding rocks and of the reservoir allow for large deformation of the reservoir and/or the permeability is substantially sensitive to the deformation. Consider, for example, Fig. 4-46 where we illustrate what effect has the sensitivity of permeability to deformation ($\alpha = 4$) and the distance to the constant pressure reservoir radius ($r_{eD} = 10^4$). Other parameters are the same as in the previous case. As one would expect, during drawdown greater α results in larger deformation and impairment of permeability, small size of drainage area ensures that the entire area experiences a substantial permeability reduction. Shut-in pressure and derivative accordingly respond to these effects by significant deviation from the drawdown curves. The separation between buildup type curves and long transition period show severe formation damage.

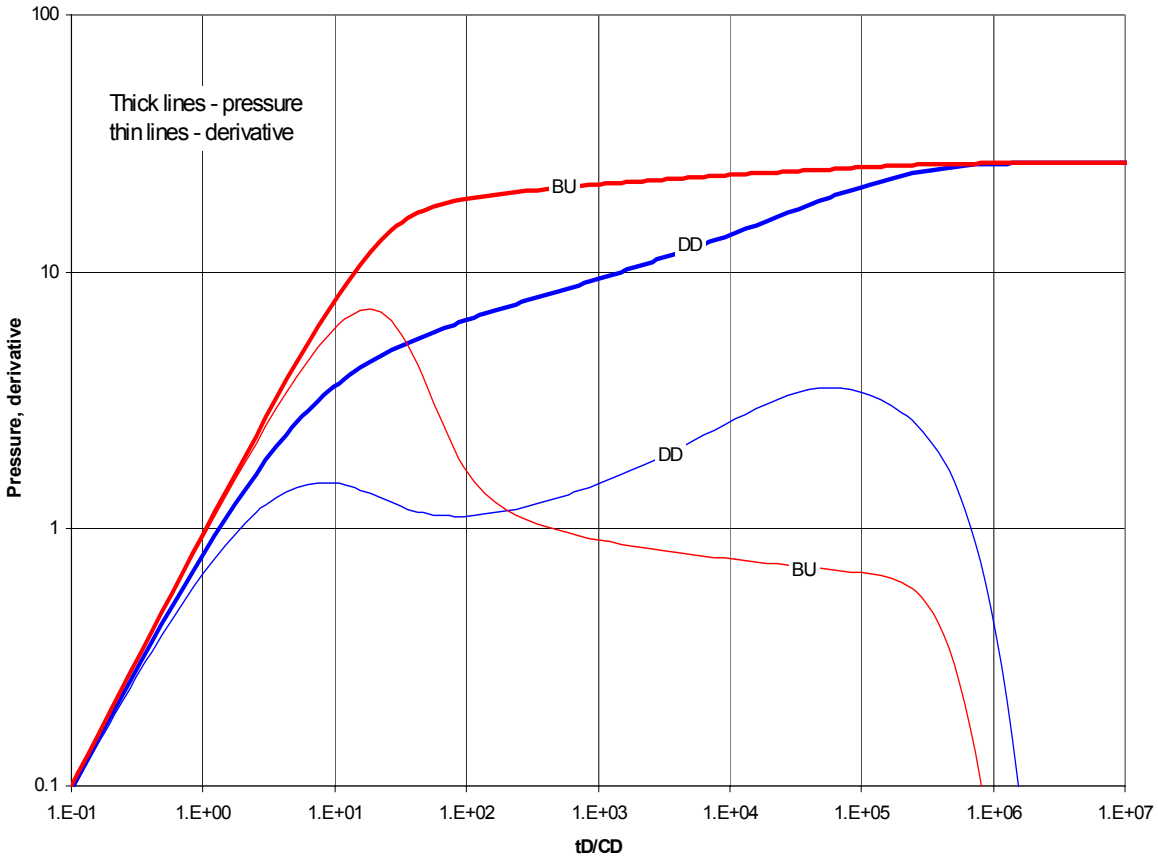

Figure 4-46. Constant pressure boundary at reD=10^4, drawdown followed by buildup, α=4

We can also note that if a well is shut-in for sufficiently long time, then the pressure builds up to the initial reservoir pressure, which coincides here with the contour constant pressure. It means that in our case of elastic deformations the permeability will fully recover to its initial value. Clearly, if a well produces from a closed reservoir with a no-flow circular boundary for extended period of time and average reservoir drops below its initial value, certain degree of permeability impairment will persist. This effect is shown in Fig. 4-47, with a no-flow boundary is located at $r_{eD} = 10^4$ and other parameters are same as for results in Fig. 4-43. The pressure builds up to a lower value. It is notable that both the separation between the buildup type curves as well as the duration of the transition period increase as a

result of substantial permeability reduction in response to declined pressure everywhere in the reservoir.

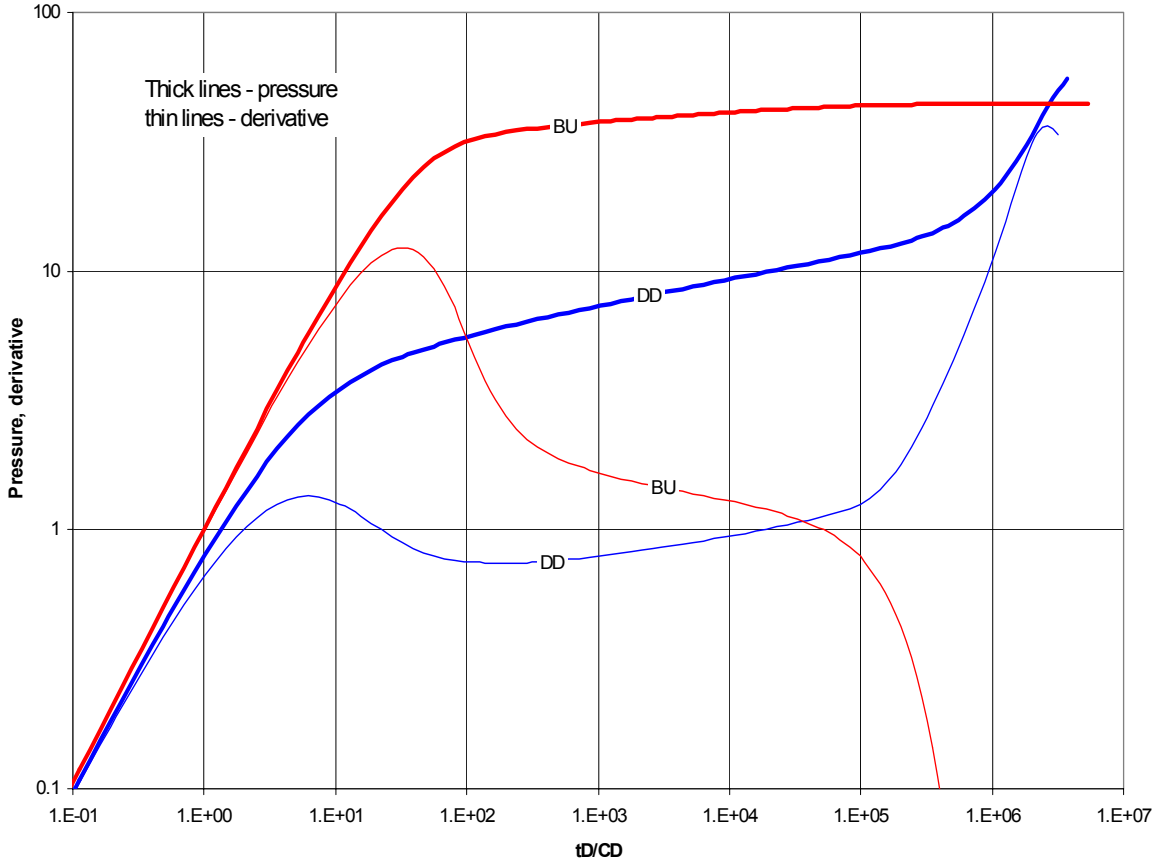

Figure 4-47. No-flow boundary at reD=10^4, drawdown followed by buildup, α= 2

4.4 Injection and falloff tests

In the examples above we have investigated how flow characteristics – wellbore pressure and production rate – change during drawdown and buildup if we account for permeability stress-dependence. It is also of interest to consider another type of a well test, injection test, and to examine how permeability stress-dependence influences the transient processes in this case. We have already shown in Section 4.1 that the response of formation

to injection is different from that of to production because of the assumed functional form of permeability dependence to deformation.

Similarly to drawdown test before we introduce base case for injection test. The values of the parameters (elastic, geometric, etc.) are the same as in the drawdown base case, except for α =-2. Type curves for linear case (blue curves) and base case (green curves) are presented in Fig. 4-48. Since for the base case permeability increases in response to injection, it requires less pressure difference to maintain constant rate and the pressure curve is lower than the respective curve in linear case. As pressure transient propagates into the formation, it changes the stress-strain state in the system reservoir-surrounding rocks, which results in permeability increase in the reservoir. This behavior can be identified from examination of the derivative – it has a downward trend as if the permeability-thickness product were increasing with increasing duration of injection. Red and black pairs of curves in Fig. 4-48 correspond to α =-1 and to -3. Clearly, for greater sensitivity of permeability to deformation these effects become more pronounced.

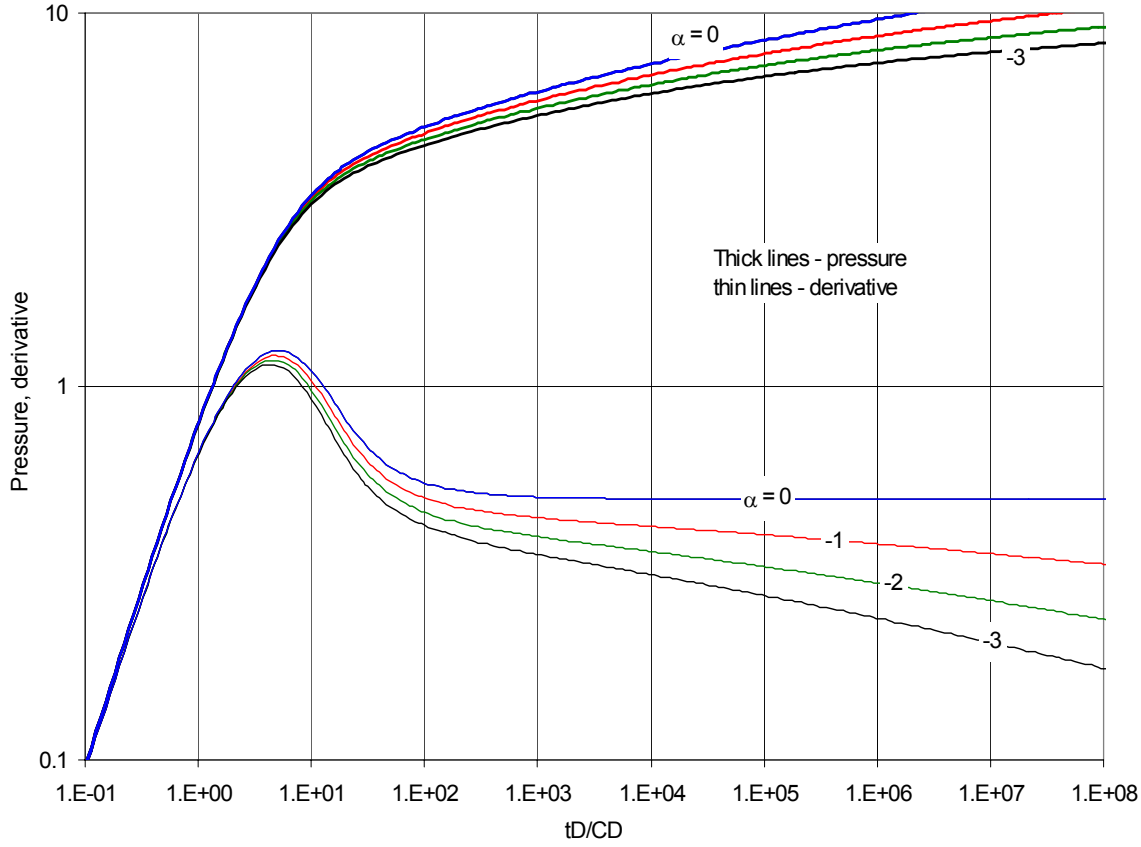

Figure 4-48. Injection type curves, various α

Similarly to drawdown test transient wellbore pressure response to constant rate injection depends on the elastic and geometric parameters of the system. Though sensitivity of permeability to deformation in case of injection probably varies in a smaller range. There is limited data on the degree of permeability increase due to injection and the available estimates should be taken with caution as in many cases the non-linear increase of permeability could be attributed to breakdown of a rock sample. Field experiments are also difficult to evaluate quantitatively.

It is reasonable to assume that after millions of years of burial and associated creep compaction, permeability of rock would not increase orders of magnitude under injection at pressures below formation parting pressure. Even with the pre-existing network of cracks

and fissures the injected fluid (water) will quickly find a preferential path, which will leave the majority of fissures at their initial sizes. Increased injection pressure might result in involving into flow of a larger number of cracks, but most of the water will still flow along the developed path which will increase the sizes of cracks and fissures mainly along this path. A fairly uniform permeability increase due to injection could be observed in a formation with reservoir pressure lower than its initial value. In such situation permeability increase can be attributed to re-opening of the cracks that were closed because of the increased effective stress due to production.

We will continue using the exponential functional dependence of permeability on deformation, but will limit the magnitude of the parameter α. Clearly, for large α we may calculate a substantial non-linear permeability increase, but such increase might be attributed to some other factors, different from the mechanism that we consider in this research. In order to estimate the range of the parameter α for the case of injection we plot in Fig. 4-49 steady-state permeability distributions vs. distance for several values of α and $r_{eD} = 10^4$. Other parameters are as in the base case.

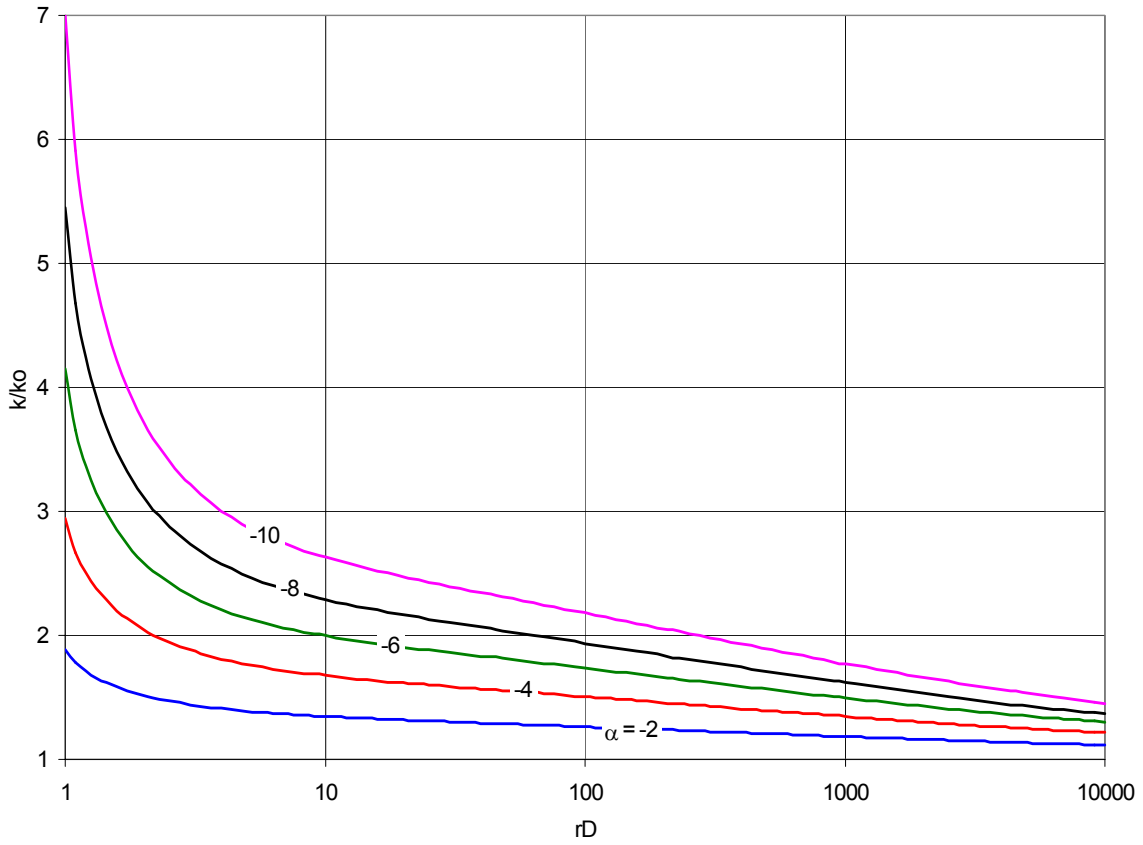

Figure 4-49. Steady-state permeability vs. distance for various α

As one would expect, greater sensitivity of permeability to deformation results in higher permeability values in the reservoir and, for example, for $\alpha = -6$ (green curve) permeability increase near the wellbore is 4-fold and at the external contour of the drainage area is about 30%. Though it is fairly easy to visualize a 4-fold permeability increase in the vicinity of a well, a significant increase of permeability further in the formation can look suspicious because of the relative permeability effects, associated with simultaneous flow of water and oil. In this research we consider flow of a single-phase fluid only. Nevertheless, the presented below several injection/falloff problems can provide certain insight into behavior of injection wells. We will also limit the magnitude of α by -4, which corresponds to about 3-fold permeability increase near the well.

In Fig. 4-50 and 4-51 the blue and red pairs curves correspond to injection and falloff, respectively. For both graphs the problem parameters are the same as in the previous case, except for $\alpha = -2$ for Fig. 4-50 and $\alpha = -4$ for Fig. 4-51.

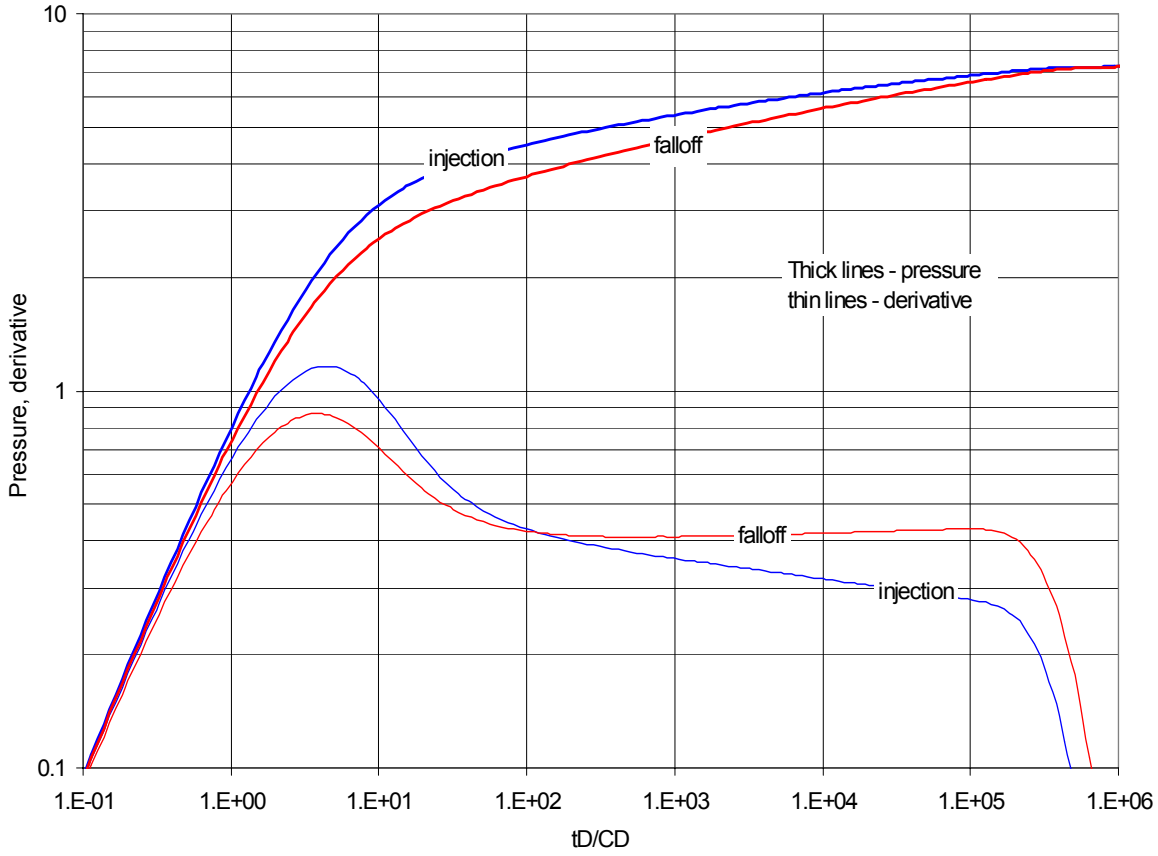

Figure 4-50. Injection followed by falloff, α=-2

It can be seen that behavior of these tests is completely different from the drawdown-buildup case. Pressure difference during injection period initially increases fairly fast and causes fast increase of permeability near the well. After this initial period, as the deformation and, therefore, permeability become limited either by the elastic properties of the reservoir or those of the surrounding rocks, pressure increases at a much slower rate, which serves as an illustration of importance of the near-wellbore zone in the flow. In fact,

increase of permeability further away in the reservoir has little effect on the pressure, as the injectivity becomes limited by the throughput capability of the near-wellbore zone. The derivative simply reflects this ever diminishing increase of pressure, and its behavior might be interpreted as increasing kh. For larger negative $\alpha = -4$ these features are more pronounced

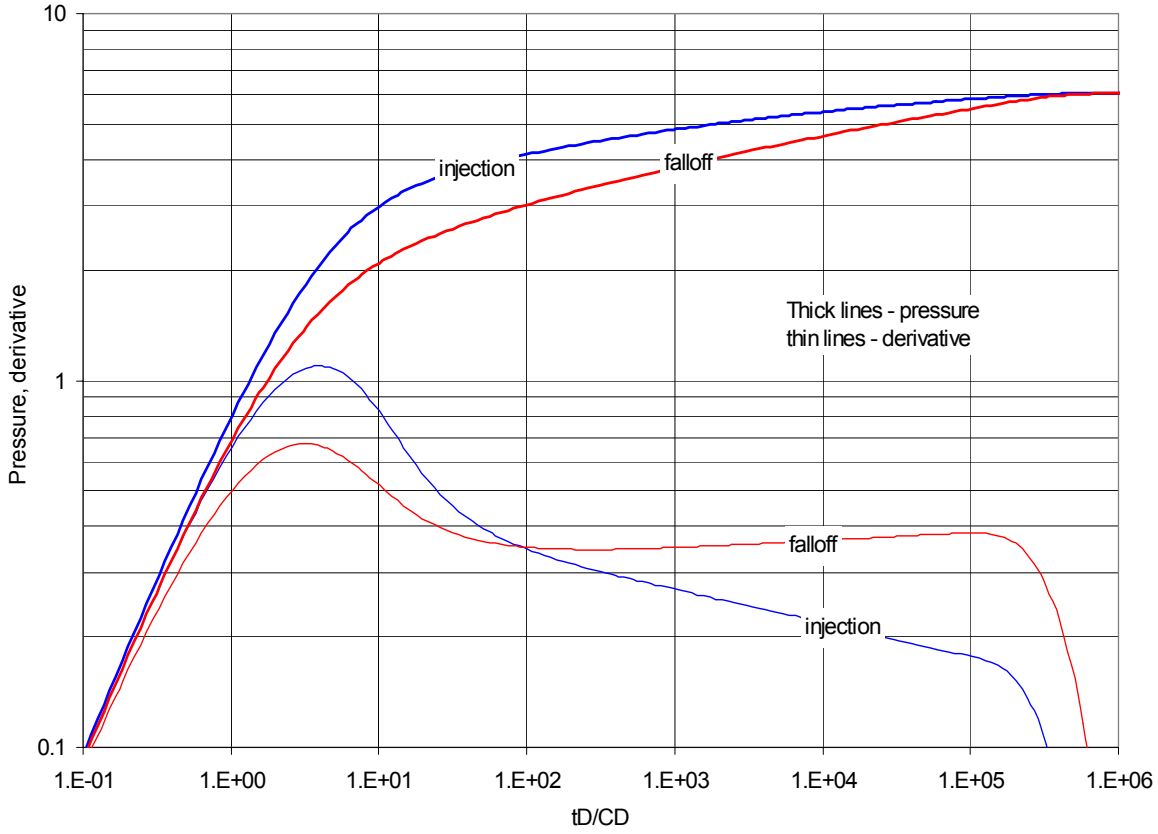

Figure 4-51. Injection followed by falloff, α=-4

Once an injection well is shut-in for pressure falloff test, the pressure starts to drop. Once the wellbore storage distortion has seized, pressure declines at a fairly constant rate (pressure difference increases steadily) with logarithm of time. The derivative is almost flat on both figures with a tendency to slight increase in the late time region. The derivative response is almost that of a homogeneous layer, because permeability near the well drops

fairly quickly and not so fast further in the reservoir. Permeability profiles along distance at several moments in time for $\alpha = -4$ are given in Fig. 4-52. The thick red curve corresponds to $t_D/C_D = 100$, i.e. to the end of the transition period following wellbore storage. We can see that after that time the permeability distributions are approximately uniform throughout the reservoir.

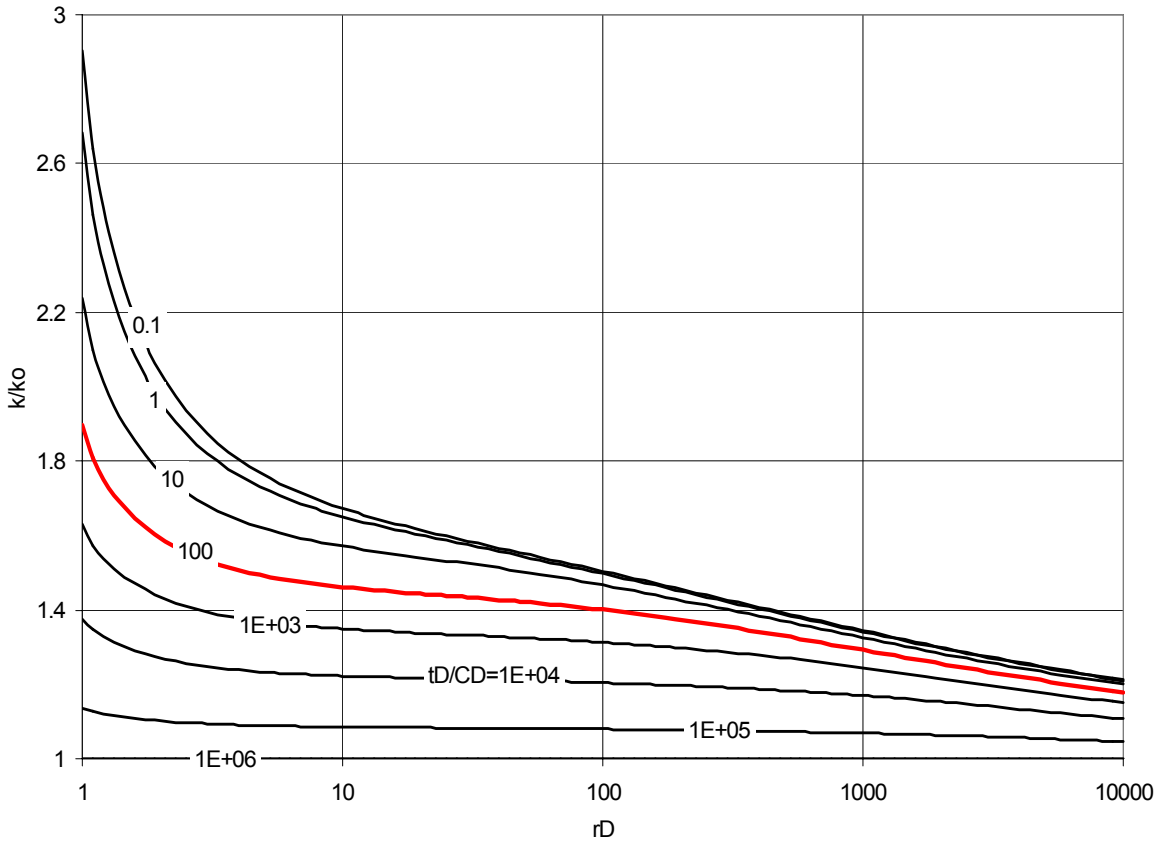

Figure 4-52. Falloff permeability distributions at several times

Analysis of a falloff test alone using conventional methods would thus provide with an estimate of permeability, which is different from the actual value. In order to illustrate this point we plot in Fig. 4-53 falloff type curves for linear case (blue curves), which is the same as a conventional method, and falloff with $\alpha = -4$ (red curves). Additionally, green curves are red curves shifted up and to the right in order to align the flat portion of the

derivative and the wellbore storage region with the type curves. This shift corresponds to the scenario that would be followed when analyzing pressure data using conventional approach.

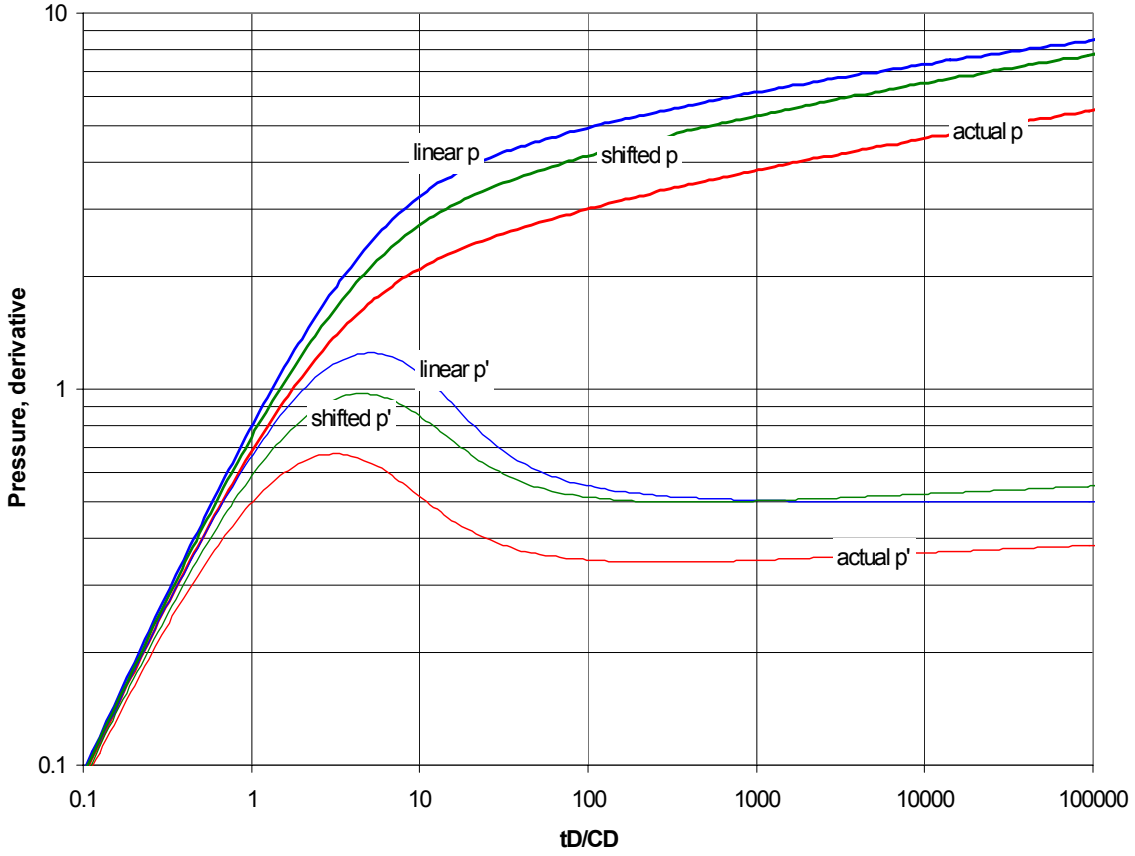

Figure 4-53. Conventional analysis applied to falloff data in a stress-sensitive formation

Let us estimate how the shifting of the data performed in order to conform to classical method affects the values of the principal parameters. First, let us recall that the dimensionless pressure and time are defined as

$$p_D = \frac{kh(p_{wi} - p)}{141.2qB\mu} \qquad \text{and} \qquad t_D = \frac{0.0002637kt}{\phi\mu c_t r_w^2}$$

The upward shift of the curves is equivalent to increase of p_D, the right shift is equivalent to increase of t_D. Both increases can be accommodated only by increase of permeability, since it is the only unknown variable in both equations. Therefore, the value of

permeability if estimated by conventional method will be greater than the actual value. The value of the wellbore storage coefficient should be correct because the same amount of shift is applied in time and pressure directions. We can also see that the value of average reservoir pressure will be determined to be higher than the true value (lower difference between the injection pressure prior to the test and falloff pressure). In order to estimate the effect of the shift on skin, recall than skin can be determined using

$$s = \frac{1}{2}\left[\frac{\Delta p_r}{(t\Delta p')_r} - \ln\left(\frac{kt_r}{1688\phi\mu c_t r_w^2}\right)\right]$$

where first term in brackets is the separation between the pressure and the derivative curve. Clearly, shifting does not affect this ratio. The second term includes permeability and since it's value was incorrectly determined to be higher than the true value, it will result in a lower estimate of skin.

In order to get an understanding of the magnitude of errors introduced by using conventional methods we have used WELLTEST software to analyze falloffs for linear case and for the case with $\alpha = -4$ (Fig. 4-51). The actual permeability and skin were 10 md and 0, respectively. Analysis of the linear case yielded correct values, while application of the conventional approach for the stress-sensitive case resulted in 14 md permeability and skin of -1. The difference between estimates of average reservoir pressure was 1,200 psi, wellbore storage coefficient was essentially the same in both analyses.

It is obvious that if formation has lower sensitivity to deformation the results, obtained using conventional approach, will be fairly close to the correct values. It is also possible to derive the correct values of permeability and skin if there is an independent estimate of the value of average reservoir pressure. In such case we can deduce the magnitudes of pressure and time shift, introduced by application of the conventional analysis

methods, and to come up with true formation permeability and, subsequently, skin. Therefore, falloff tests on injection wells appear to be very attractive practically, as these tests do not normally require long shut-in and can provide useful information even in stress-sensitive formations.

5 TWO LAYER CASE

In this chapter we examine several typical problems and show how the model allows to account for interaction of pressure fields in adjacent layers. We consider sensitivity of the flow to a number of elastic and geometric parameters of the problem. Generally, the layers may have different values of thickness, permeability, porosity, etc. As before, permeability is assumed to be an exponential function of deformation. Having calculated total deformation of the reservoir, we can obtain the values of deformation of individual layers and calculate permeability distributions in layers. Since total deformation is a sum of layers' deformations and individual deformations depend on pressure distributions in layers, it is clear that the flow in one of the layers will depend on pressure distributions in both layers.

5.1 Constant rate drawdown in an infinite reservoir

Let a well be producing at constant well rate from an reservoir comprised of two layers. A natural check of the validity of the calculations is to first assume that two layers have identical properties. Then the flow behavior of a well should coincide with the previously calculated single layer case of the same total reservoir thickness. Performed calculations indicate that in such case the two layer results are identical to the single layer results presented earlier, which gives confidence in the accuracy of the numerical implementation of the solution.

Let us first consider how the magnitude of sensitivity of permeability to deformation affects the results. We set $a = 0.0384$, $\alpha_1 = 0$, $\alpha_2 = 4$, $\gamma_j = E_j / E = 1$, $E = 10^{10}\ Pa$, $r_w / h = 0.001$, $k_j = 10\ md$, $h = 10\ m$, $h_j = 5\ m$, $C_D = 100$, $s_j = 0$ (subscript j=1, 2 denotes layer number). Infinite reservoir is modeled by setting constant pressure outer boundary at

$10^5\ m$. The results of calculations are presented in Fig. 5-1. Here green pairs of curves correspond to well pressure response for the described two layer case. The blue and red pairs of curves are for the single layer case with α=0 and 4, respectively. We can see that the two layer case deviates only slightly from the linear case with α=0 and in practice may be detected only when running a long-duration drawdown in a well equipped with permanent pressure gauge.

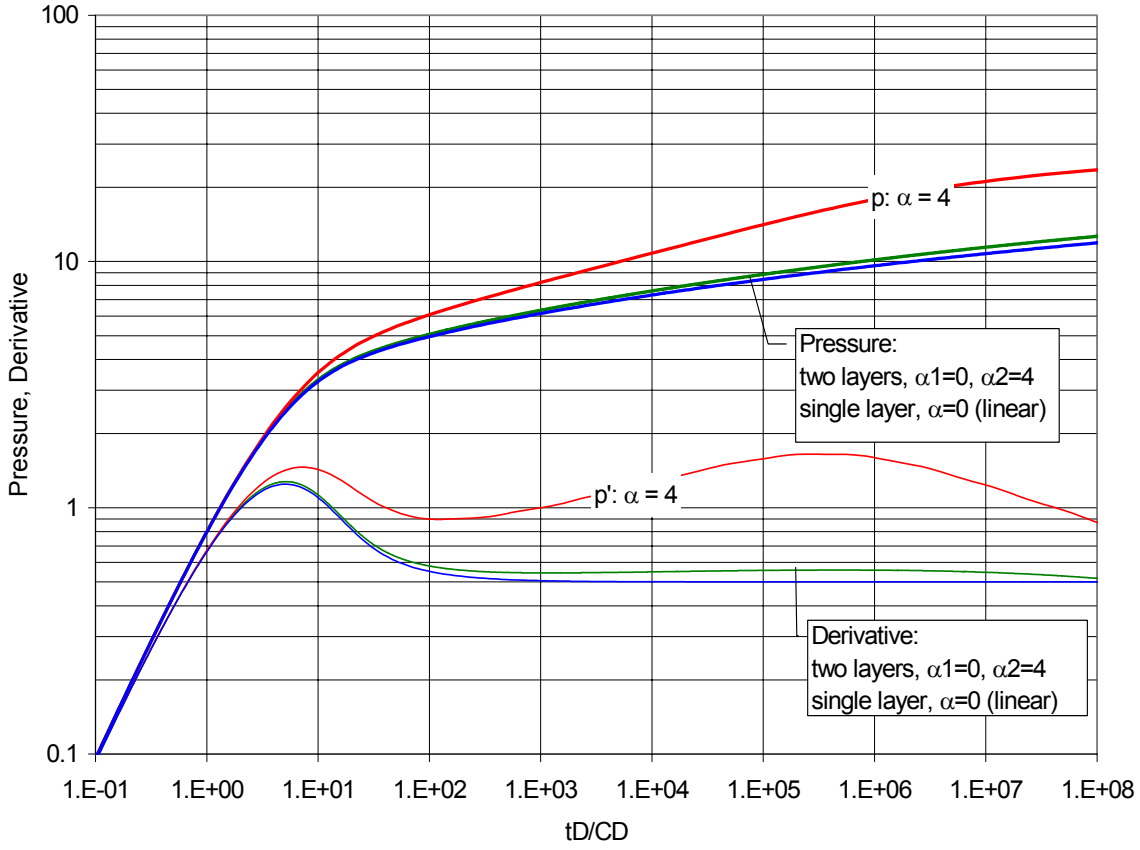

Figure 5-1. Type curves for two-layer case and two single-layer cases

Since low-permeability rocks experience more permeability reduction than high-permeability rocks, it is more interesting to consider a case with unequal initial

permeabilities. For results presented in Fig. 5-2 $k_1 = 100\ md$ and $k_2 = 1\ md$, all other parameters are the same as in the previous case.

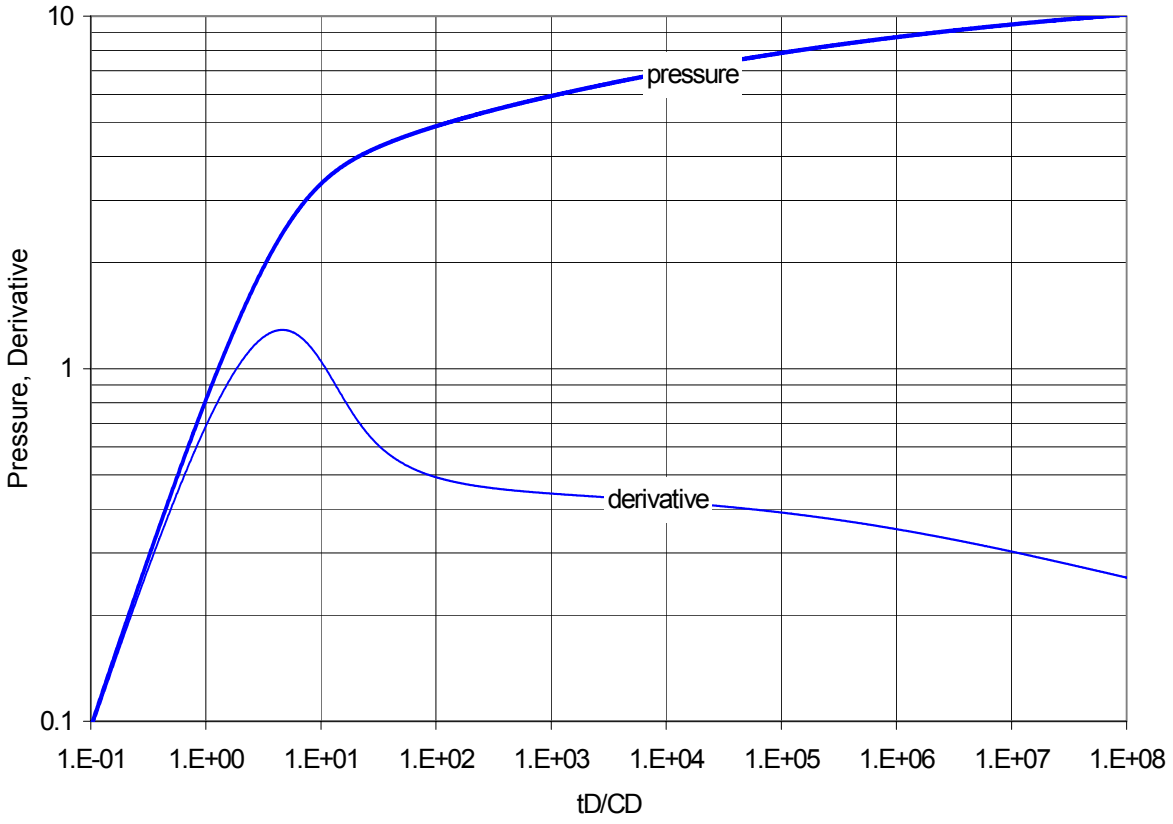

Figure 5-2. Type curves for two-layer case with equal thicknesses of layers and k_1/k_2=100

It can be seen that presence of two layers with significantly different permeability values changes the behavior of the derivative – it appears that the permeability-thickness product increases. This happens because both layers deform under increased effective stress and even though for the high-permeability layer the impact of deformation on permeability is negligible ($\alpha_1 = 0$), compaction of this layer causes some unloading of the low-permeability layer. This unloading leads to increase of permeability in low-permeability layer.

Another even more realistic case is when a relatively thin high-permeability layer is produced simultaneously with a thicker low-permeability one. The results for $h_1 = 1\,m$, $h_2 = 9\,m$ and other parameters same as in previous two cases are presented in Fig. 5-3.

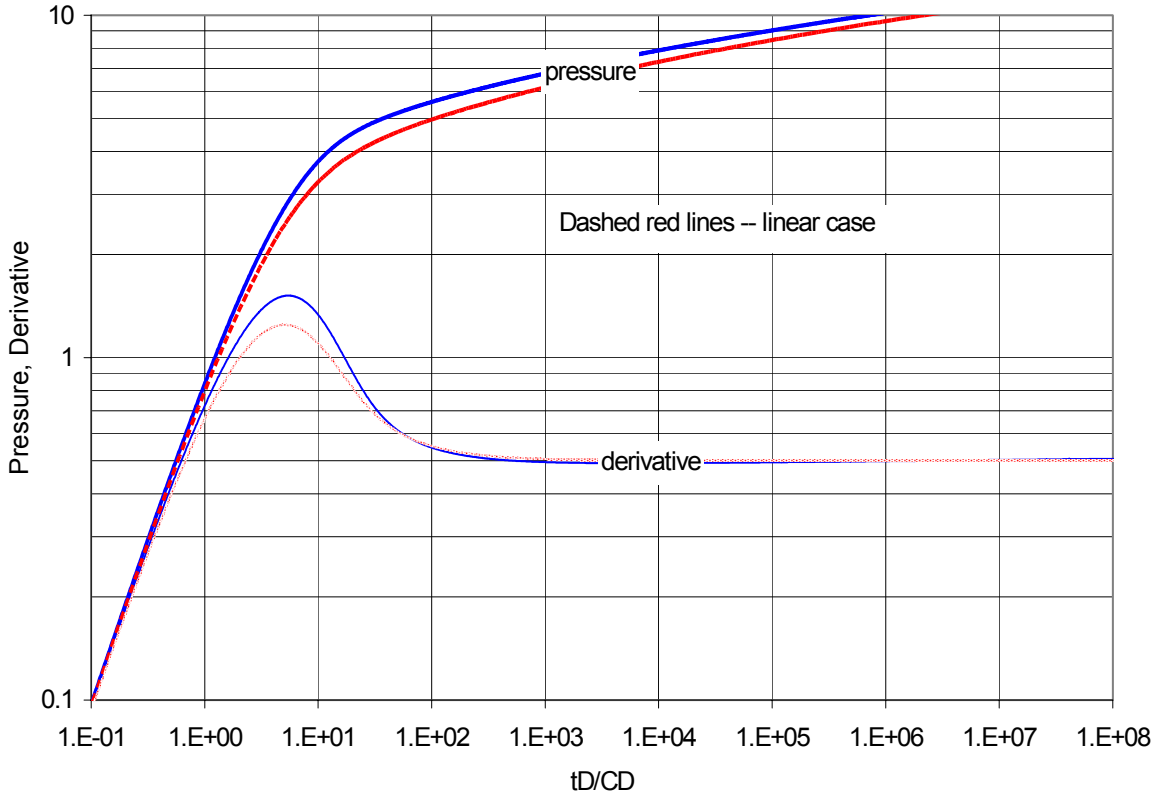

Figure 5-3. Type curves for two-layer case with $h_2/h_1=9$ and $k_1/k_2=100$

We can see that it would be impossible to distinguish this case from a case of a homogeneous reservoir -- the derivative flattens at typical 0.5. It is also clear, that if one were using conventional analysis the determined value of skin would be higher, since permeability reduction manifests itself as increased resistance to fluid flow. The practical implications of such error are obvious. For example, a futile workover with the goal of eliminating damage skin might be performed.

To visualize the transient processes that occur in the latter case, we present results of calculation of pressure, deformation, and permeability distributions in the two layers at several moments in time. In Fig. 5-4, the left and right groups of graphs are the distributions of the above listed parameters at $t_D \approx 0.1$ and at $t_D \approx 1$. The solid blue lines represent the first layer of thickness $h_1 = 1\ m$ and initial permeability $k_{01} = 100\ md$. The dashed red lines represent the second thicker low-permeability layer. In Figs. 5-5 through 5-8 we present the same characteristics of flow at later times.

Let us consider $t_D \approx 0.1$ (left group of graphs in Fig. 5-4). Pressure in both layers has traveled a certain distance into the formation in response to constant rate production (first graph). Reduced pressure in the vicinity of the well causes deformation of the reservoir and the deformations of the individual layers are given on the second graph. We can see that the first layer deforms to a greater degree, as one would expect, given that pressure in this layer has dropped to a greater degree and in a larger area around the well. The deformation of the first layer is substantial and causes unloading of the low-permeability second layer – it actually experiences negative (tensile) deformations. Since we have assumed that permeability of the first layer is not sensitive to deformation, its dimensionless permeability remains the same, while dimensionless permeability of the second layer increases in response to unloading (third graph).

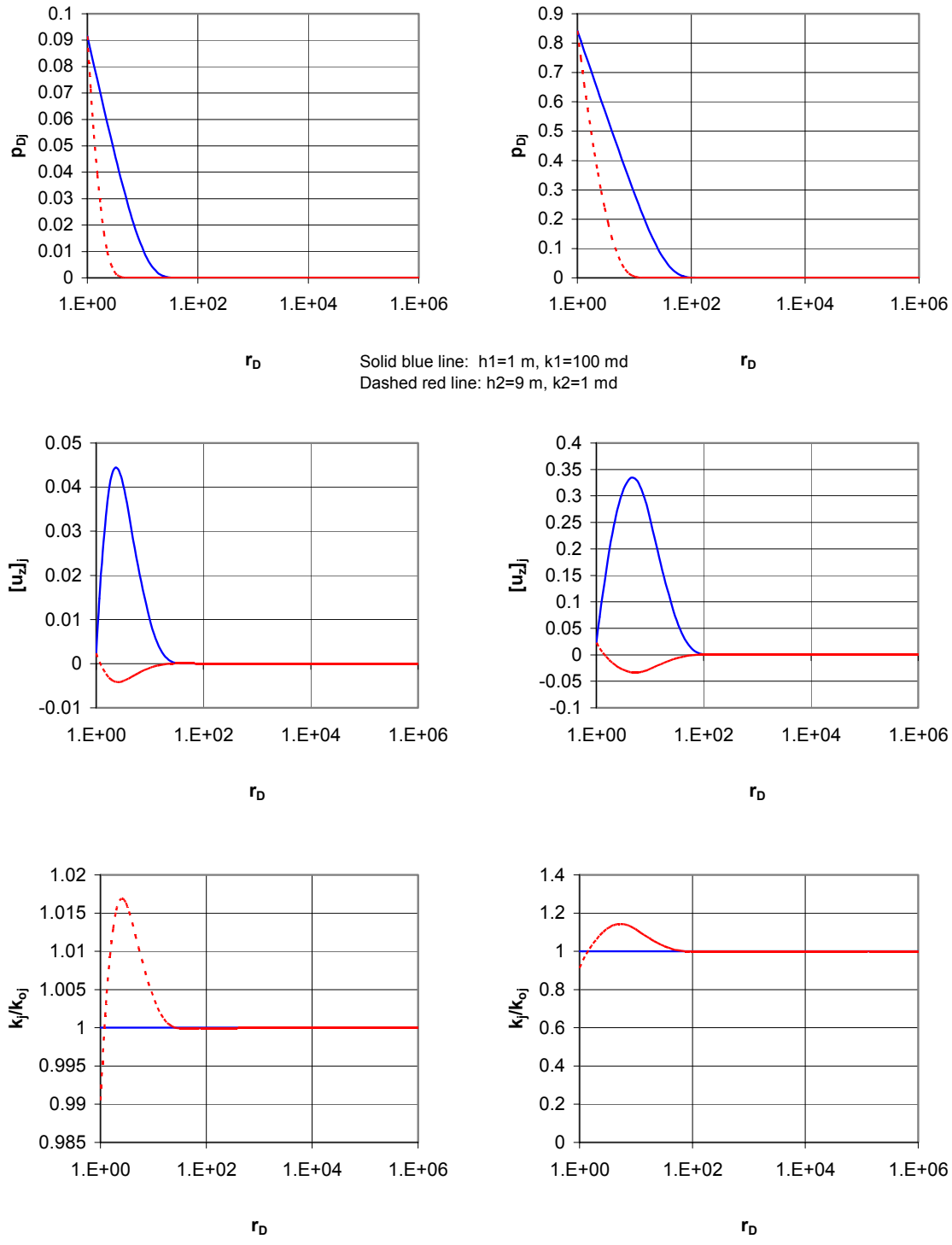

Figure 5-4. Distributions of pressure, deformation, and permeability vs. distance at $t_D/C_D \approx 0.1$ (left) and $t_D/C_D \approx 1$ (right group)

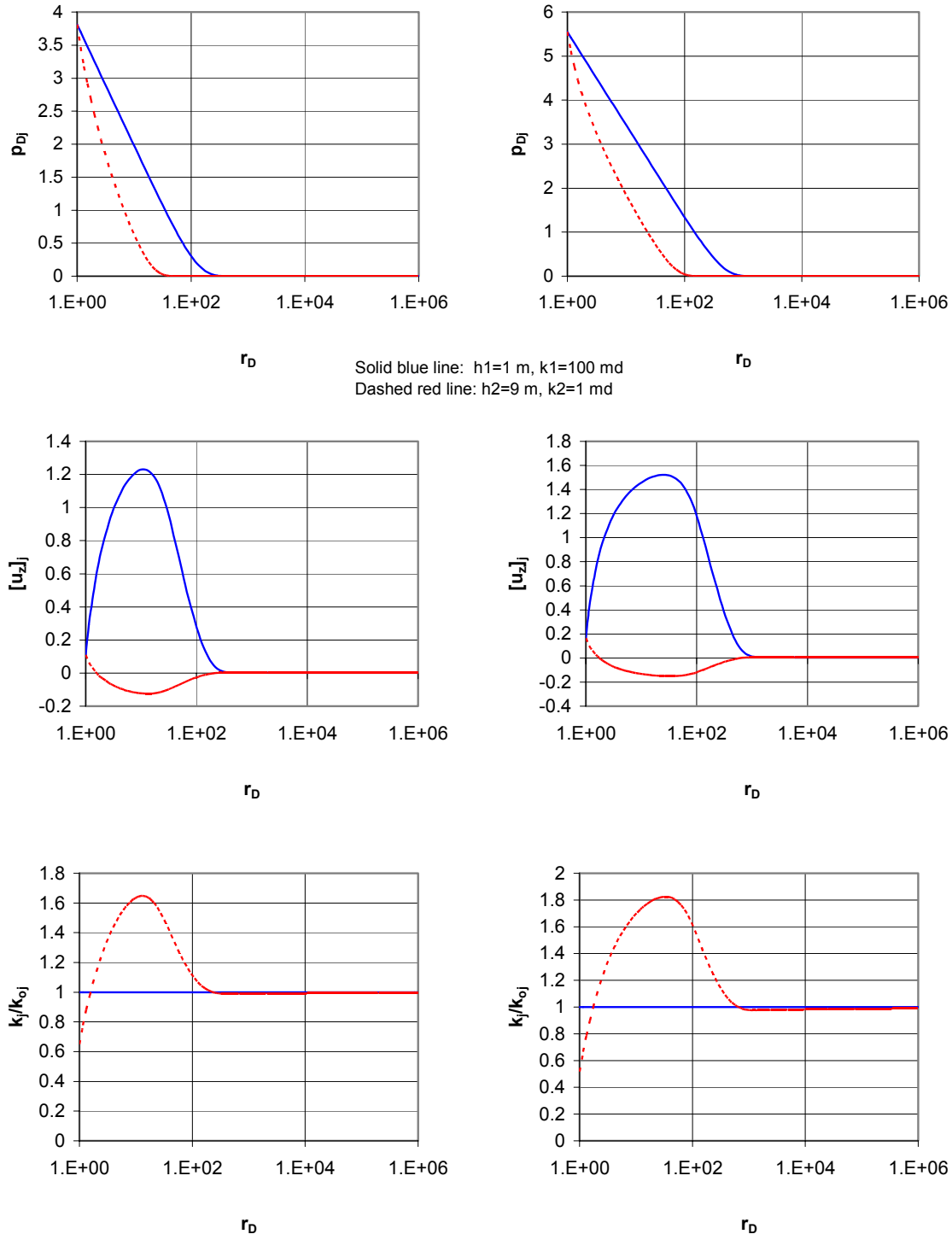

Figure 5-5. Distributions of pressure, deformation, and permeability vs. distance at $t_D/C_D \approx 10$ (left) and $t_D/C_D \approx 100$ (right group)

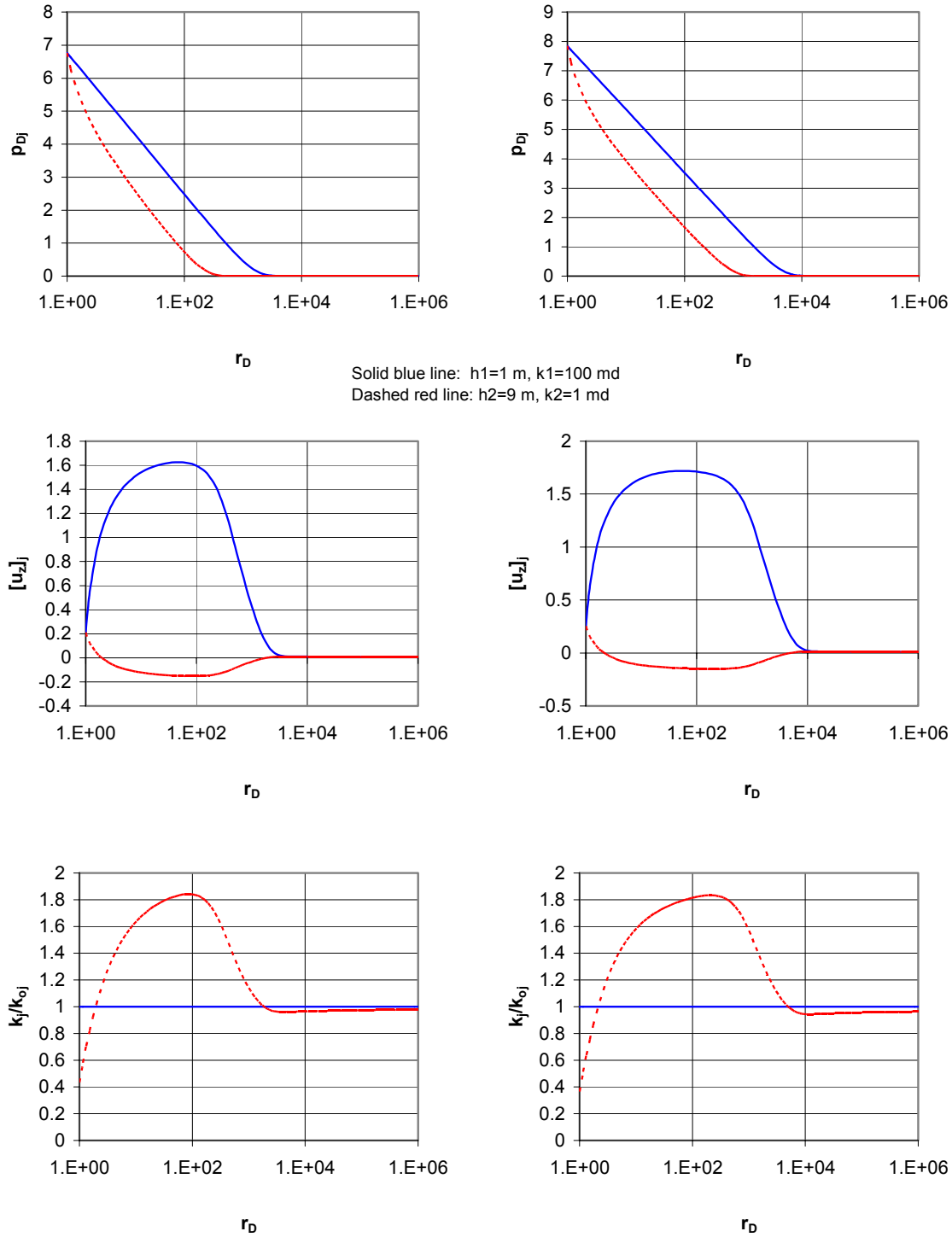

Figure 5-6. Distributions of pressure, deformation, and permeability vs. distance at $t_D/C_D \approx$1E+3 (left) and $t_D/C_D \approx$1E+4 (right group)

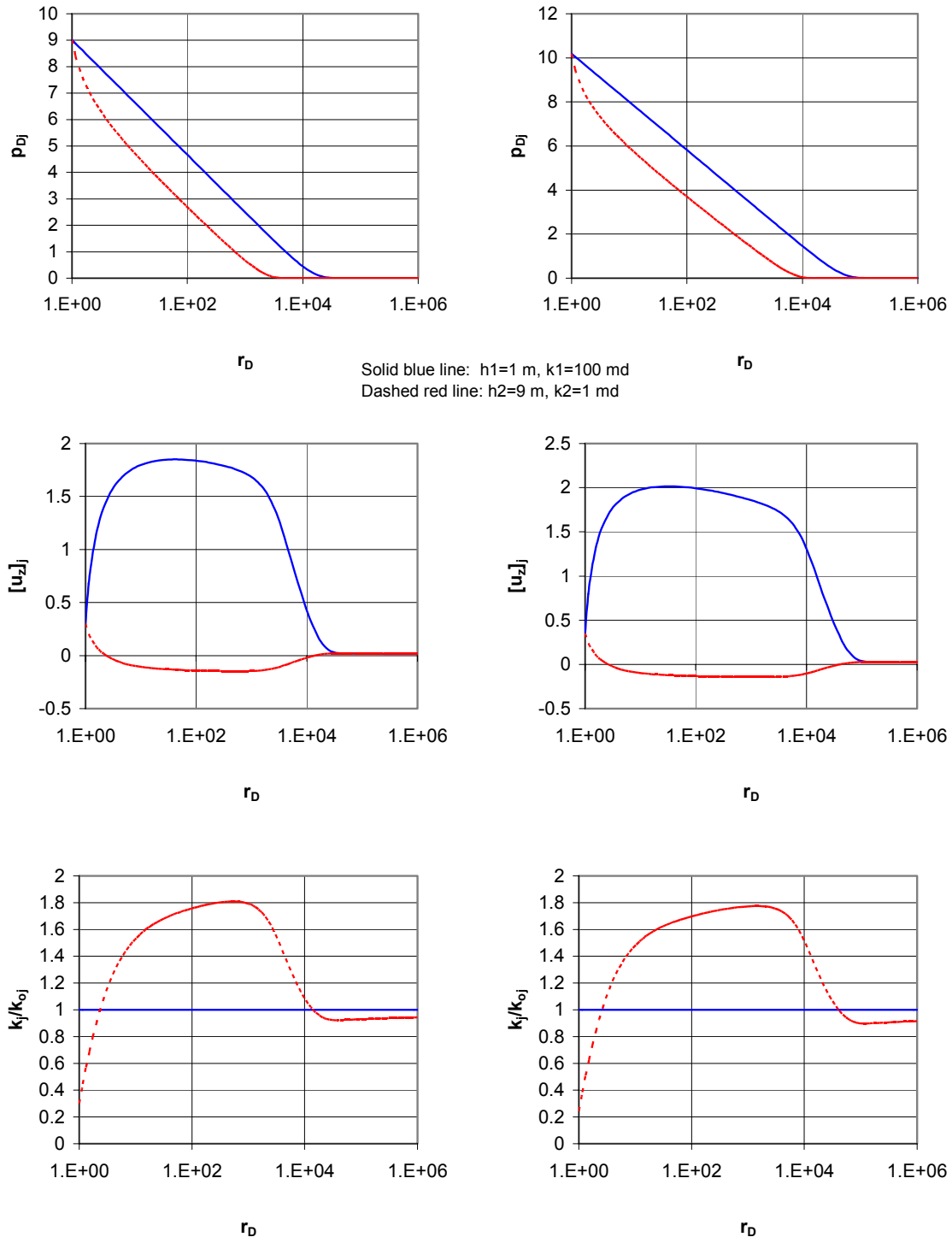

Figure 5-7. Distributions of pressure, deformation, and permeability vs. distance at t_D/C_D ≈1E+5 (left) and t_D/C_D ≈1E+6 (right group)

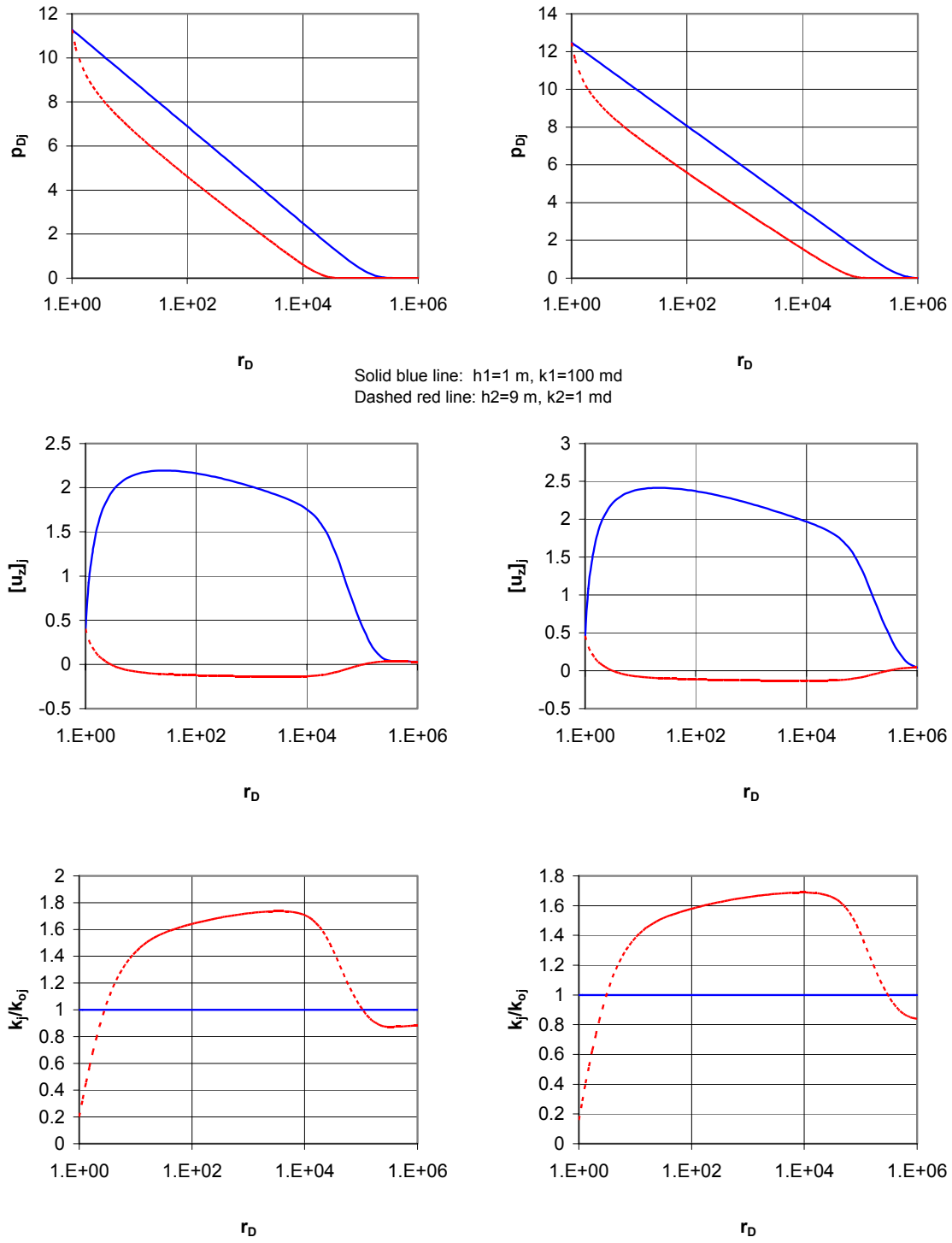

Figure 5-8. Distributions of pressure, deformation, and permeability vs. distance at $t_D/C_D \approx$1E+7 (left) and $t_D/C_D \approx$1E+8 (right group)

The same trends are present on subsequent graphs for later times. Compaction of the first layer in response to pressure propagation into the formation leads to unloading of the second layer and its permeability increases. At the same time, the deformation of both layers in the vicinity of the wellbore is positive, i.e. both layers experience compaction. The permeability of the second stress-sensitive layer within a small area around the wellbore (3-5 wellbore radii) decreases, which shows up as increased skin on the diagnostic plot. Further away in the formation, within the zone affected by the well production, the permeability of the low-permeability layer is greater than the initial value. Finally, outside of this zone the reservoir experiences compaction and permeability of the second layer is less than the initial value. The plots illustrate that the deformations of individual layers depend on the magnitude of pressures in the layers, and also on the pressure difference, i.e. on interaction of pressure fields in layers.

5.2 Constant rate drawdown in a finite reservoir (constant pressure, or no-flow outer boundary)

Pressure behavior during a constant rate drawdown in a finite reservoir initially follows the trends, described in the previous example. The infinite reservoir in this example was modeled by setting a constant pressure outer boundary at $r_{eD} = 10^6$. From the group of graphs on the right side of Fig. 5-8, it is clear that the outer boundary should be reached somewhat later than $t_D / C_D = 10^8$. Let us consider what happens at later times. Pressure, deformation and permeability distributions are given in Figs. 5-9 – 5-11.

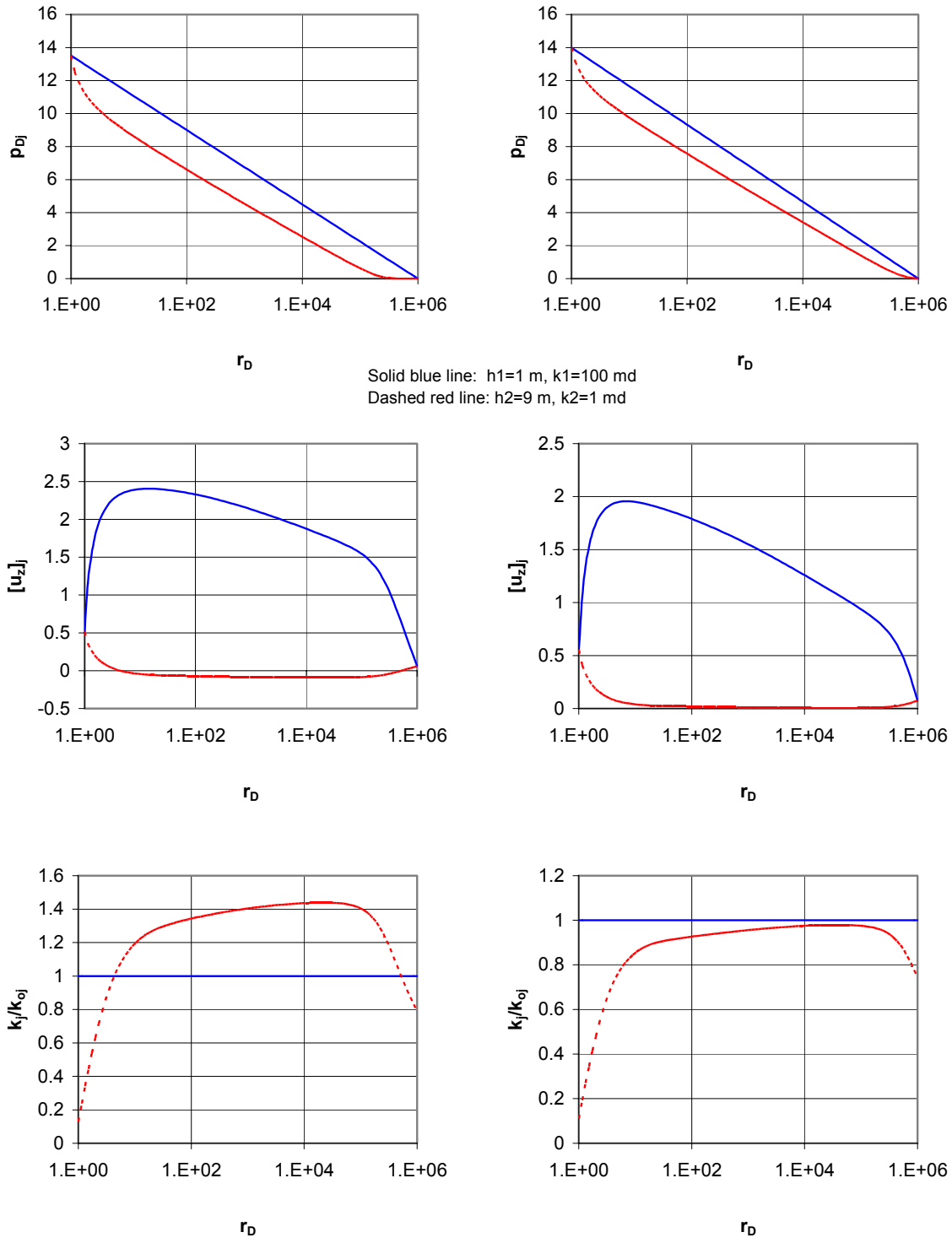

Figure 5-9. Distributions of pressure, deformation, and permeability vs. distance at $t_D/C_D \approx$1E+9 (left) and $t_D/C_D \approx$1E+10 (right group)

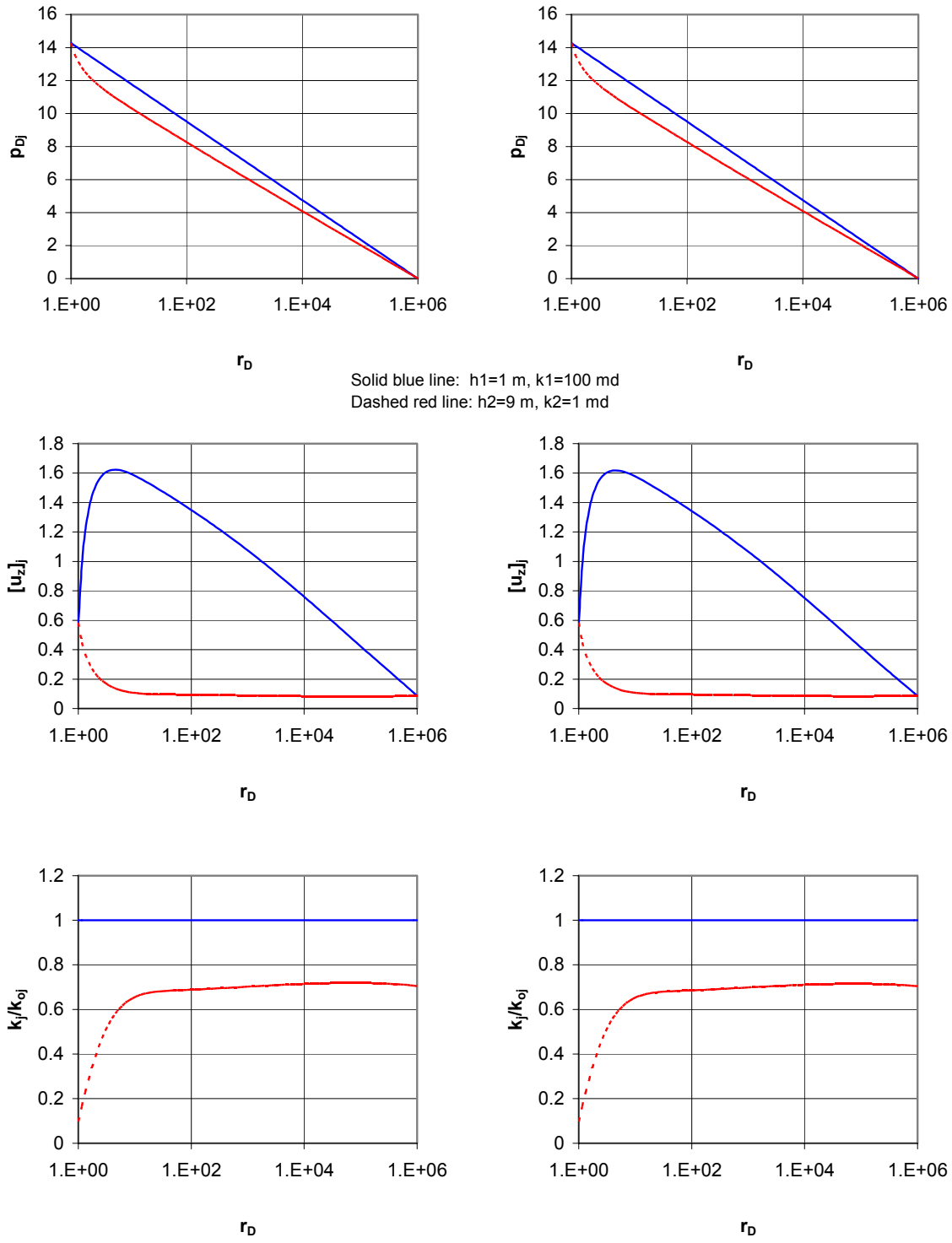

Figure 5-10. Distributions of pressure, deformation, and permeability vs. distance at $t_D/C_D \approx$1E+11 (left) and $t_D/C_D \approx$1E+12 (right group)

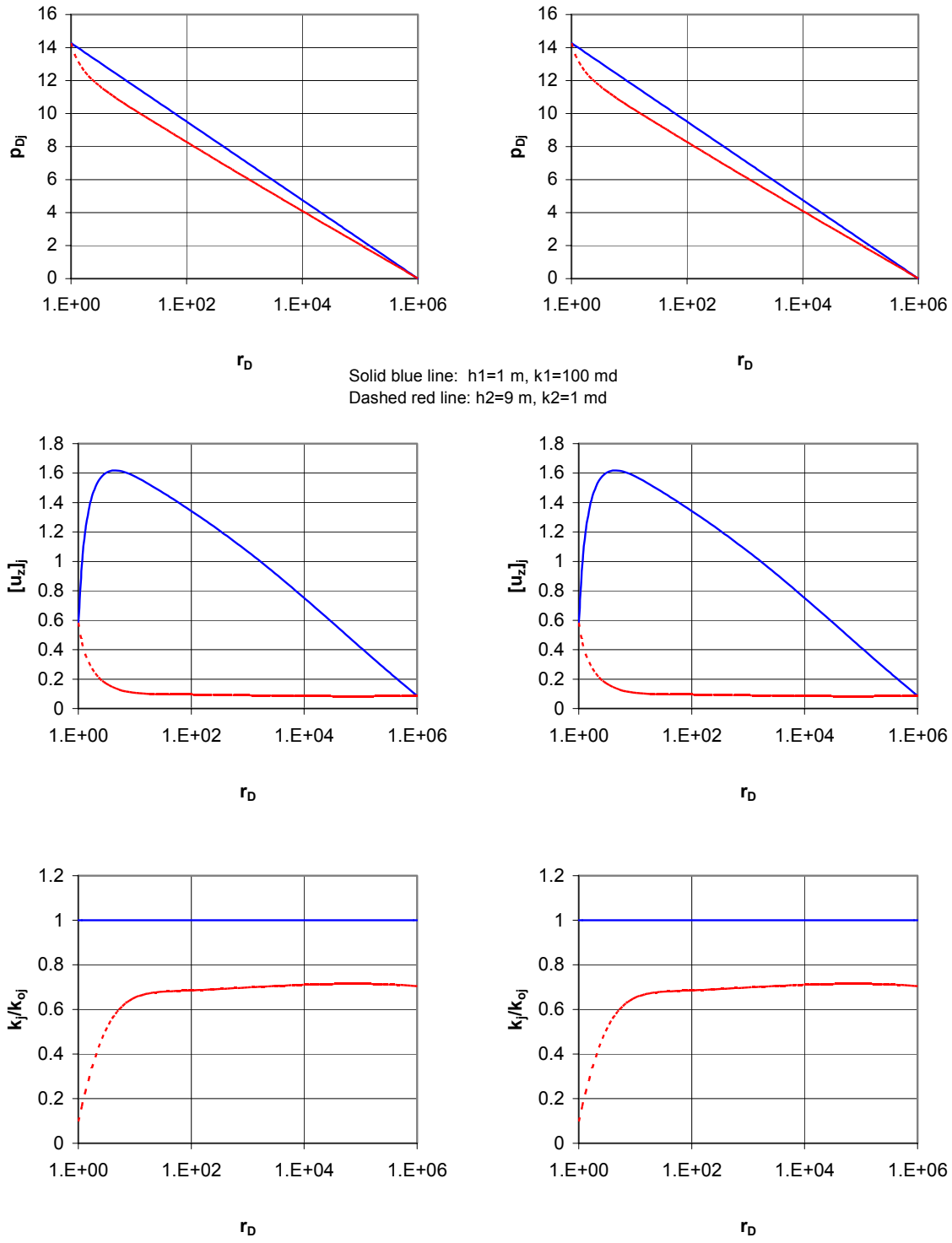

Figure 5-11. Distributions of pressure, deformation, and permeability vs. distance at $t_D/C_D \approx$1E+13 (left) and $t_D/C_D \approx$1E+14 (right group)

We can see that once the boundary is reached, the distributions of all characteristics change. Pressure in the low-permeability layer stabilizes at a level which is lower than the typical logarithmic distribution. Both layers experience compaction – the deformation is positive in the entire formation. Permeability of the stress-sensitive layer stabilizes at a fairly uniform level everywhere in the reservoir, except for the near-wellbore zone. In this zone permeability drops from about 70% of the initial value to 10% on the well contour. This distribution is quite different from the single-layer case. In Fig. 5-12 we present stabilized permeability distribution for a 10 m thick single-layer with same values of other elastic and geometric parameters along with the steady-state permeability distributions of the two-layer case (as in Fig. 5-11).

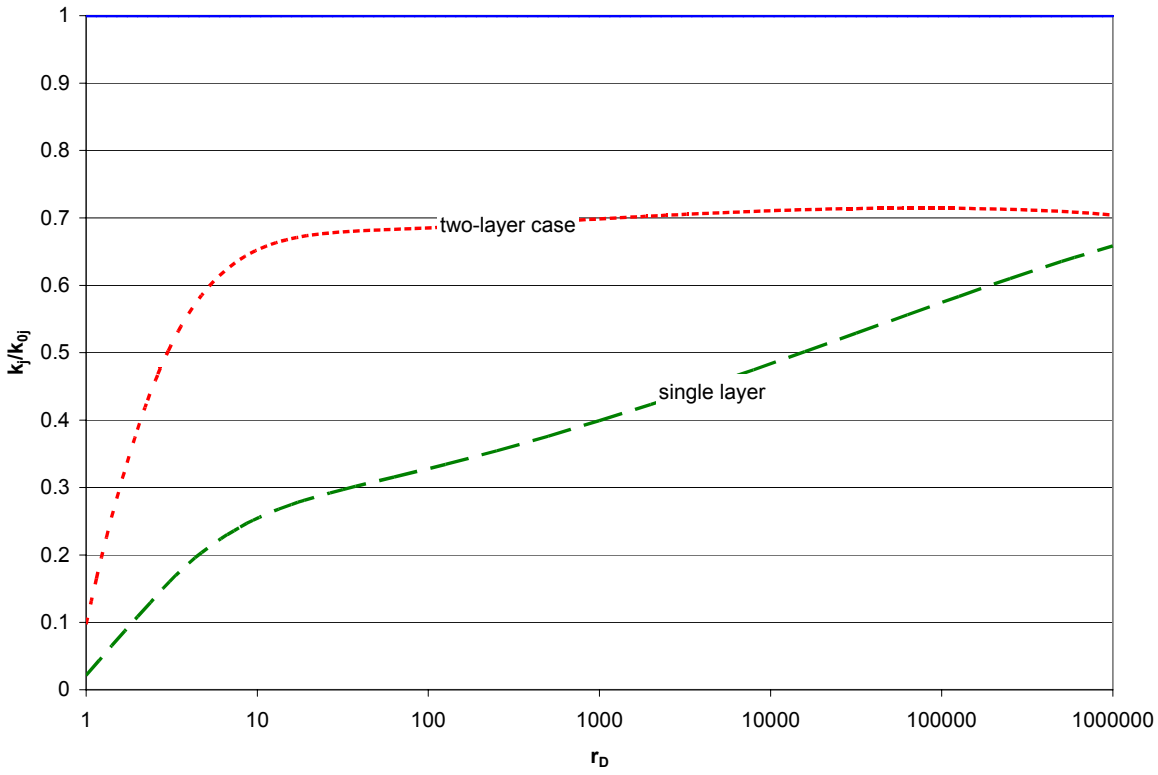

Figure 5-12. Steady-state permeability distributions for one- and two-layer cases

We can see that in comparison with the single-layer case, the presence of a high-permeability layer has a positive effect on the flow in the low-permeability layer as compaction of the former leads to unloading of the latter. Permeability decrease in the near-wellbore zone is still significant and will exacerbate any damage skin, if present.

In the case of a no-flow outer boundary, the above described effect of unloading of the low-permeability layer persists after pressure in the high-permeability layer reaches the outer boundary. As a consequence, the dimensionless permeability of the low-permeability layer increases in the formation by an order of magnitude or more. Near the wellbore, however, it continues to decrease with time. These results for $r_{eD} = 10^4$ and other parameters same as in the previous example are presented in Fig. 5-13 (type curves) and Fig. 5-14 – 5-18 (pressure, deformation, and permeability distributions vs. distance at several moments in time). Let us consider Fig. 5-13. Prior to the pressure in the high-permeability thinner layer reaching the closed boundary, the type curves have familiar features. Once the boundary has been reached at approximately $t_D/C_D = 10^4$, the derivative starts to increase in response to increasing pressure. As the deviation of pressure in the high-permeability layer from the initial pressure increases and the difference between pressures in layers increases, substantial unloading of the thicker low-permeability layer will occur and its permeability away from the well will increase (see left group of graphs in Fig. 5-17), while on the well contour it remains at approximately same low value. Since near-well permeability determines the flow rate, the permeability improvement elsewhere in the reservoir is inconsequential. At about $t_D/C_D = 2*10^5$ the boundary is reached in the low-permeability layer and for a period of time the pressure curve flattens (derivative drops). Up to and during this time it is still possible to maintain constant rate production, but eventually (at $t_D/C_D \approx 6*10^5$) the

pressure drops to such a degree that flow rate declines. The second flattening of the pressure curve occurs at about $t_D/C_D = 10^7$ and corresponds to the time when near-well permeability in the low-permeability layer is reduced to about 1-2% of the initial value, therefore, effectively choking this layer, and when the magnitude of drawdown in the high-permeability layer becomes negligible. At this time the flow rate essentially drops to zero.

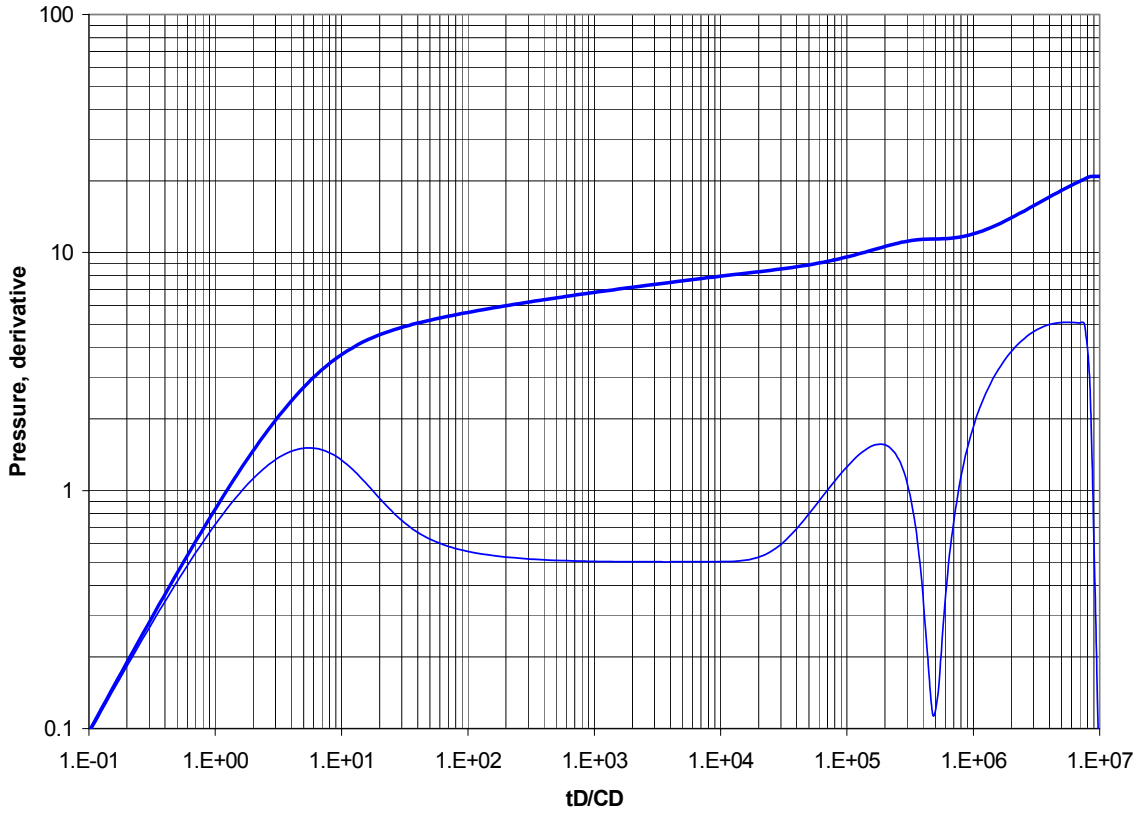

Figure 5-13. Type curves for constant rate drawdown in closed drainage area. Two-layer case with $h_2/h_1=9$ and $k_1/k_2=100$

Note again that until the boundary has not been reached the behavior of pressure and derivative curves with time is indistinguishable from a conventional linear case.

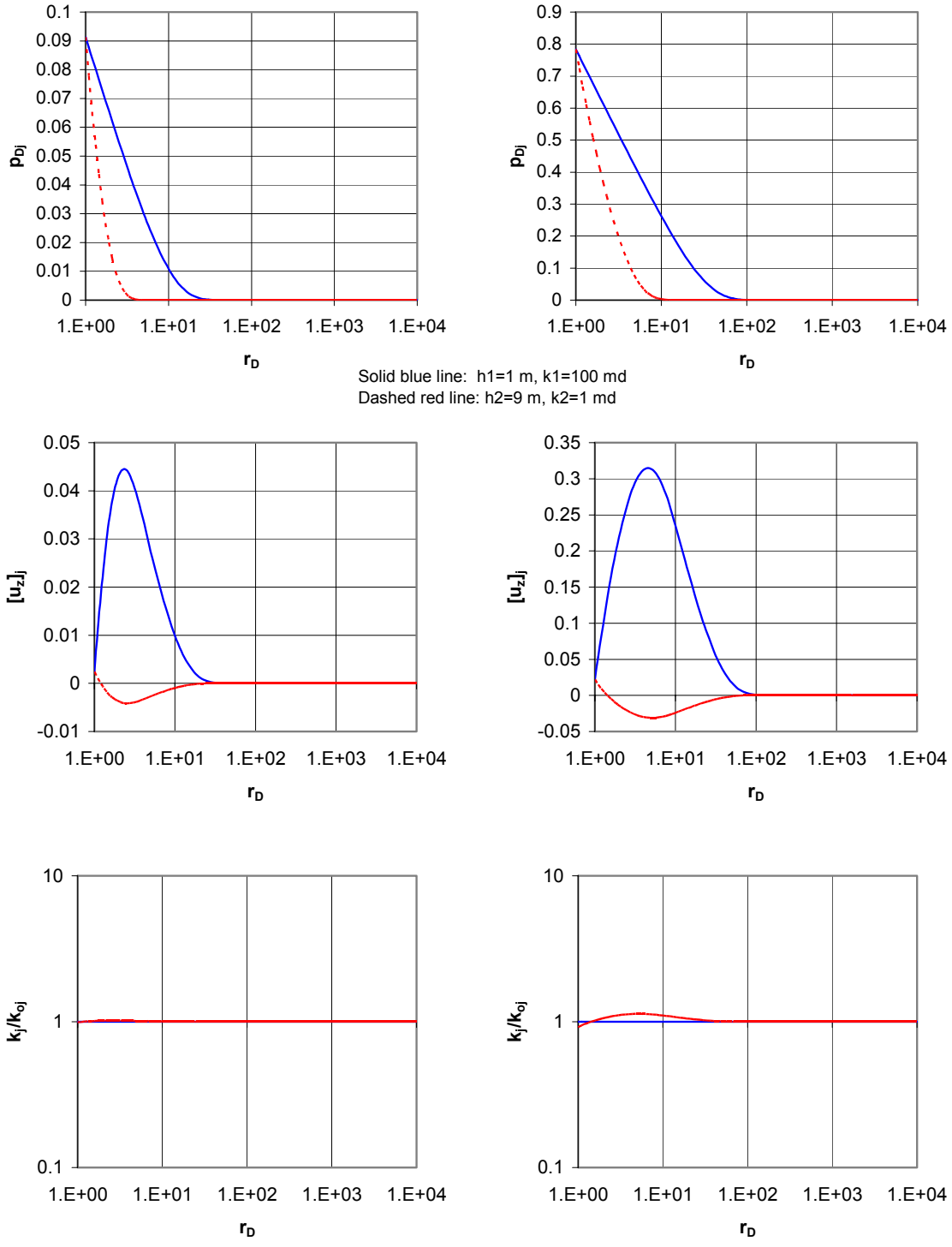

Figure 5-14. Closed drainage area. Distributions of pressure, deformation, and permeability vs. distance at $t_D/C_D \approx 0.1$ (left) and $t_D/C_D \approx 1$ (right group)

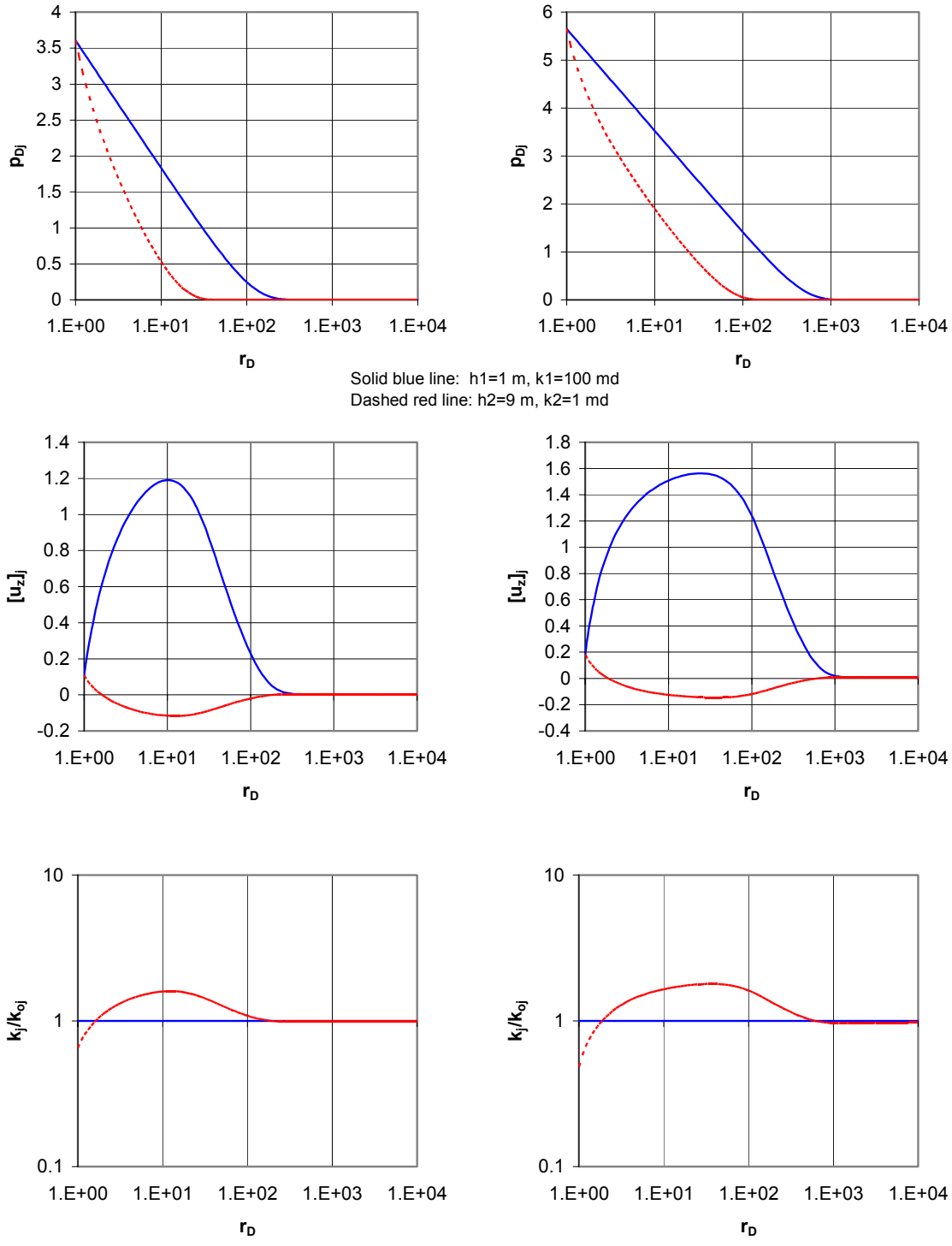

Figure 5-15. Closed drainage area. Distributions of pressure, deformation, and permeability vs. distance at $t_D/C_D \approx 10$ (left) and $t_D/C_D \approx 100$ (right group)

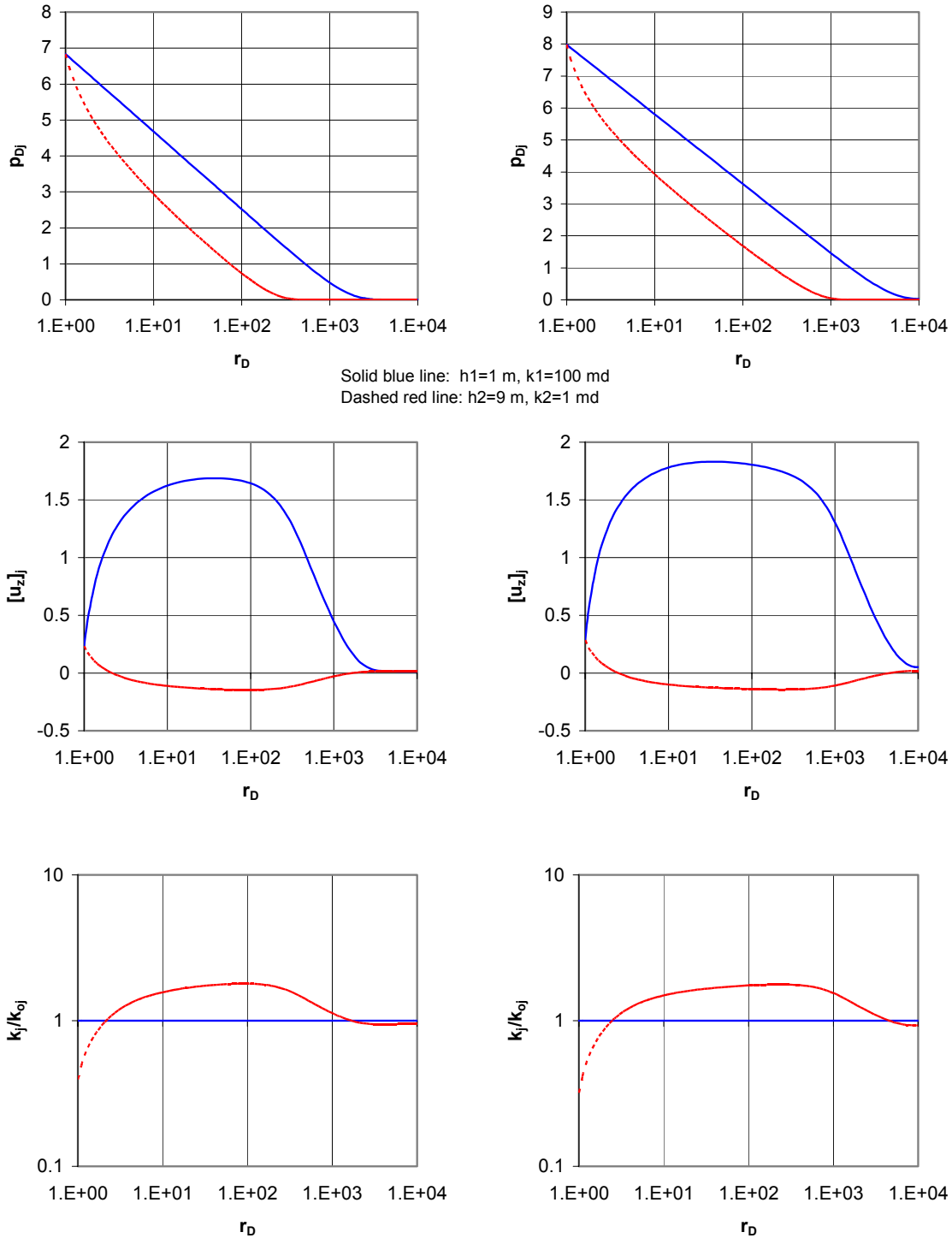

Figure 5-16. Closed drainage area. Distributions of pressure, deformation, and permeability vs. distance at t_D/C_D ≈1E+3 (left) and t_D/C_D ≈1E+4 (right group)

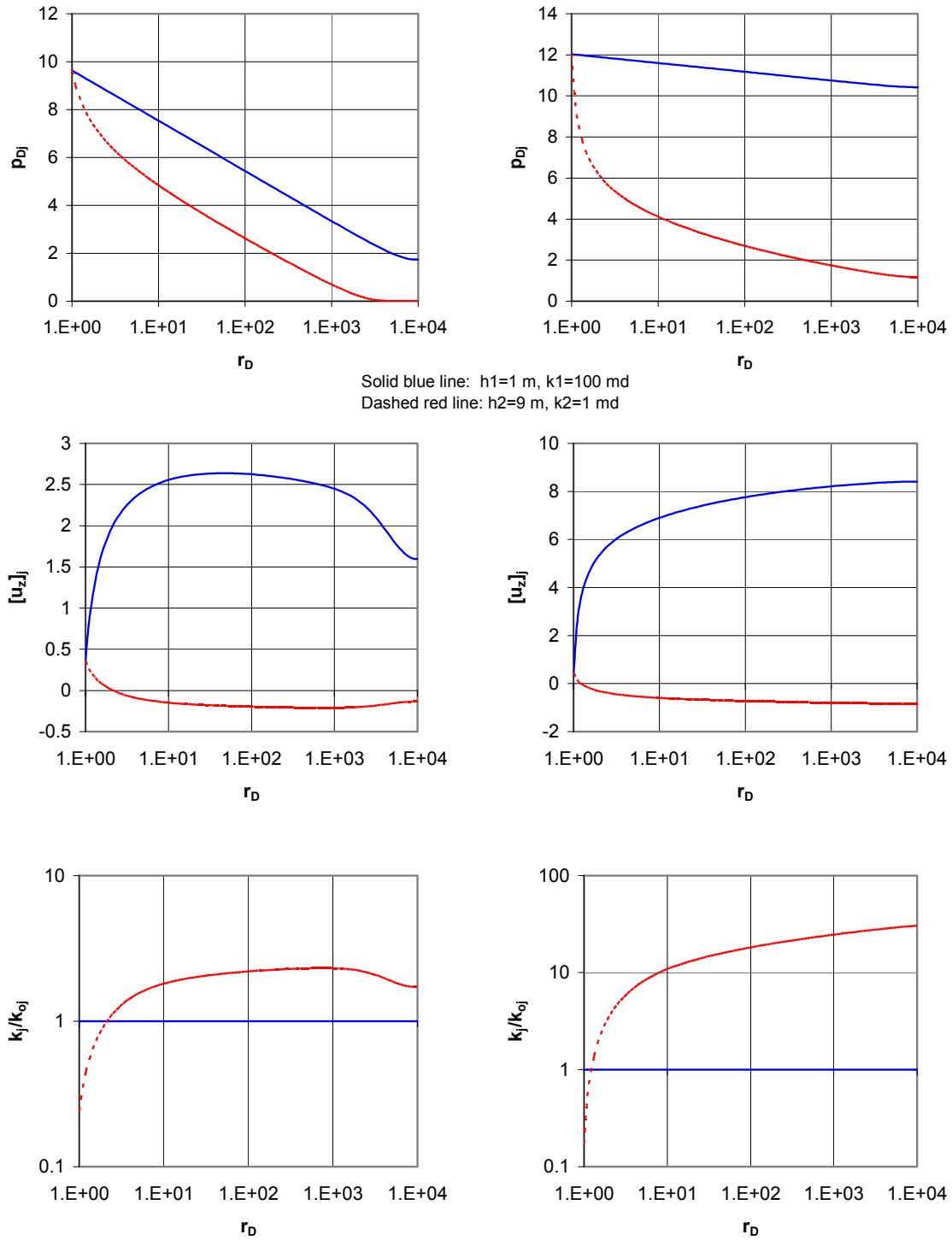

Figure 5-17. Closed drainage area. Distributions of pressure, deformation, and permeability vs. distance at t_D/C_D ≈1E+5 (left) and t_D/C_D ≈1E+6 (right group)

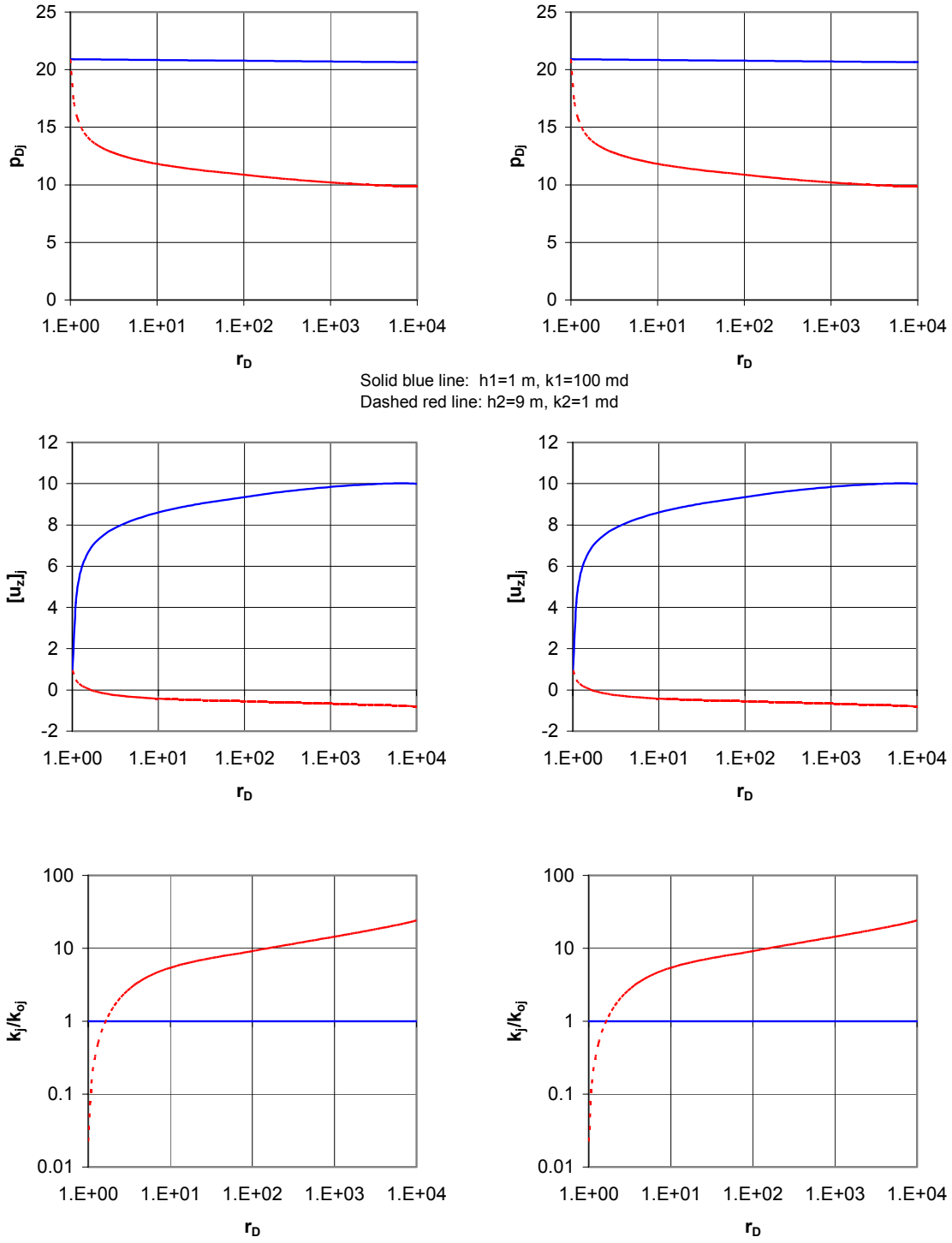

Figure 5-18. Closed drainage area. Distributions of pressure, deformation, and permeability vs. distance at t_D/C_D ≈1E+7 (left) and t_D/C_D ≈3E+7 (right group)

5.3 Constant pressure drawdown in a finite reservoir with constant pressure outer boundary

The next problem we consider is constant pressure production from a circular reservoir with constant pressure outer boundary. The reservoir is comprised of two layers. We will focus here mainly on the steady-state flow rate, as the transient processes of stabilization have been described earlier and are qualitatively the same in this case.

As in the previous examples, let $a = 0.0384$, $\gamma_j = E_j / E = 1$, $E = 10^{10}\ Pa$, $r_w / h = 0.001$, $h = 10\ m$, $C_D = 100$, $r_{eD} = 10^4$, $s_j = 0$ (subscript j=1, 2 denotes layer number). Also, $k_1 = 100\ md$, $k_2 = 1\ md$, $h_1 = 1\ m$, $h_2 = 9\ m$, $\alpha_1 = 0$, $\alpha_2 = 4$. The inflow performance curve for this case is presented in Fig. 5-19 along with Darcy straight-line IPR (dotted line). We can see that the difference between the two IPRs is negligible. On the same graph we present as dashed curve the results for a case with $k_1 = 10\ md$, $k_2 = 1\ md$, $h_1 = 1\ m$, $h_2 = 9\ m$, $\alpha_1 = 1$, $\alpha_2 = 4$. In the latter case permeability of both layers is sensitive to deformation with the value of parameter α_1 in line with the magnitude of the initial layer permeability. We can see that in this case the deviation from the straight line is significant since the magnitudes of individual layers' flow rates are now comparable and both layers experience permeability reduction. The interaction of pressures in layers results in higher flow rate for the same magnitude of drawdown as compared to a single-layer case with $\alpha = 4$ (see respective curve in Fig. 4-38). The presence of a thin higher-permeability layer causes unloading of low-permeability layer and the total rate increases.

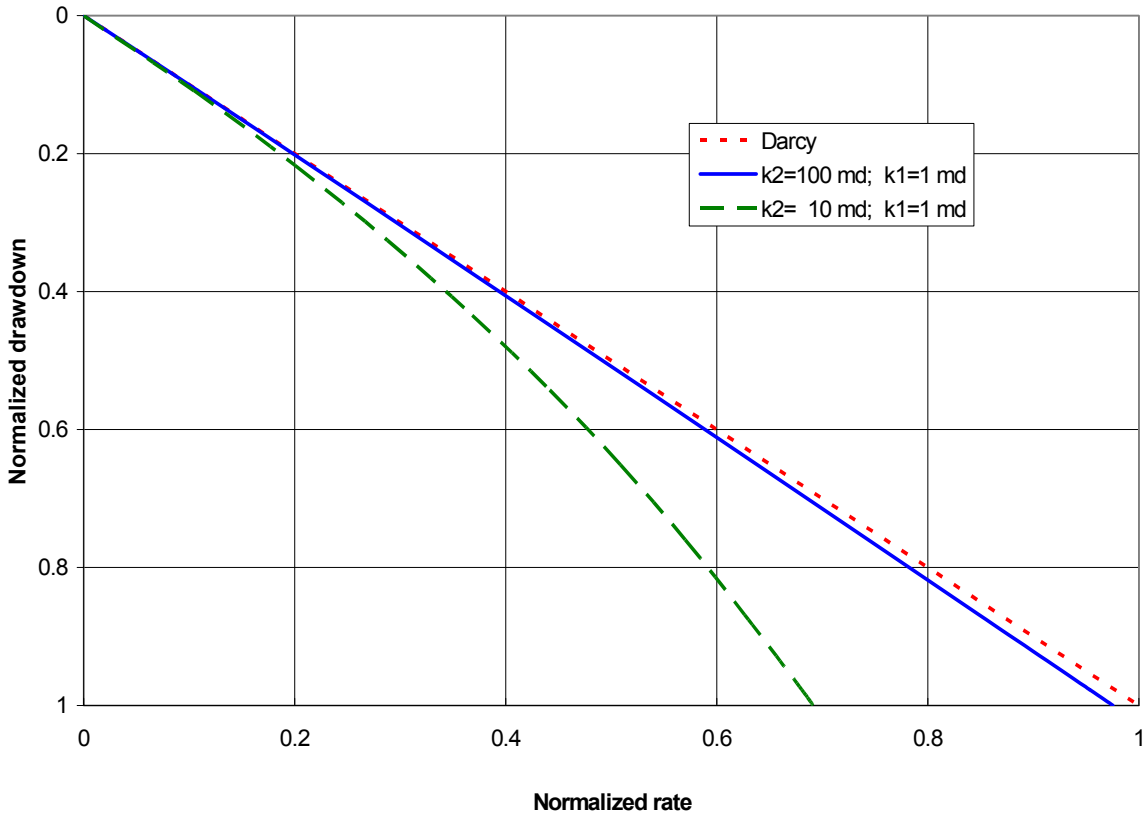

Figure 5-19. Comparison of a two-layer case IPR with Darcy IPR

Overall, it is clear that presence of a high-permeability layer, in which permeability does not change noticeably with change of effective stress, masks the stress-sensitive behavior of low-permeability layer when both layers are produced simultaneously. If the permeability contrast between the two layers is not significant then it may be possible to detect the characteristic qualitative response of a stress-sensitive reservoir, given, of course, that we are able to confidently isolate the pressure- and rate-dependent effects (multiphase flow and non-Darcy flow).

5.4 Buildup following constant rate/pressure drawdown in a finite two-layer reservoir with constant pressure outer boundary

Just as it was observed earlier in the single-layer case, a drawdown test followed by a buildup test can provide a much better indication of the stress-sensitive behavior. Depending on the duration of the drawdown and, respectively, the area around a well that was affected, buildup response does reflect the altered permeability in this zone.

Consider the case with $a = 0.0384$, $\gamma_j = E_j / E = 1$, $E = 10^{10}\ Pa$, $r_w / h = 0.001$, $h = 10\ m$, $C_D = 100$, $r_{eD} = 10^4$, $s_j = 0$, $k_1 = 10\ md$, $k_2 = 1\ md$, $h_1 = 1\ m$, $h_2 = 9\ m$, $\alpha_1 = 1$, $\alpha_2 = 4$ (subscript *j*=1, 2 denotes layer number). The type curves are presented in Fig. 5-20 and have all the characteristic features, described earlier. During drawdown the pressure difference increases fairly slowly because of the expanding zone with altered permeability. The derivative reflects the permeability reduction by an upward trend, which can be interpreted as decreasing skin. Since flow rate is proportional to *kh* and inversely proportional to skin, it is obvious that for constant rate decrease of *kh* should be accompanied by decrease of skin and vice versa.

During a pressure buildup, the permeability in both layers improves in response to decreasing pressure difference in the formation. Such behavior leaves characteristic signature trend on the type curves. The pressure difference in the well increases fairly rapidly and the derivative behaves as if the permeability-thickness product were increasing. As before, a combination of drawdown and buildup test provides a clear qualitative indication of formation stress-sensitivity.

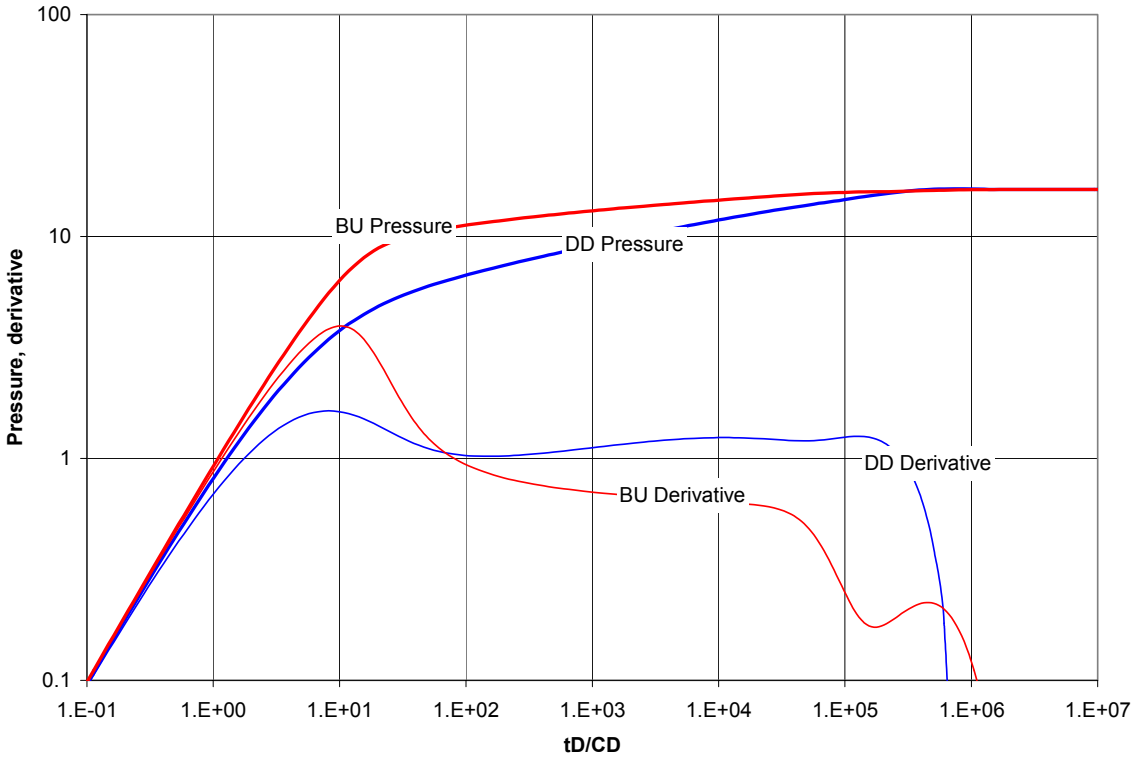

Figure 5-20. Drawdown followed by buildup in a two-layer reservoir

It is of interest to review the transient processes of stabilization of pressure, deformation, and permeability. The distributions of these parameters vs. distance for several moments in time are presented in Figs. 5-21 through 5-25 (drawdown) and Figs. 5-26 through 5-30 (buildup). The dashed curves correspond to the second layer. The series of graphs illustrate the interaction of pressure fields in layers, what impact it has on permeability distributions, and allow to visualize the effects that eventually result in the behavior observed on the type curves.

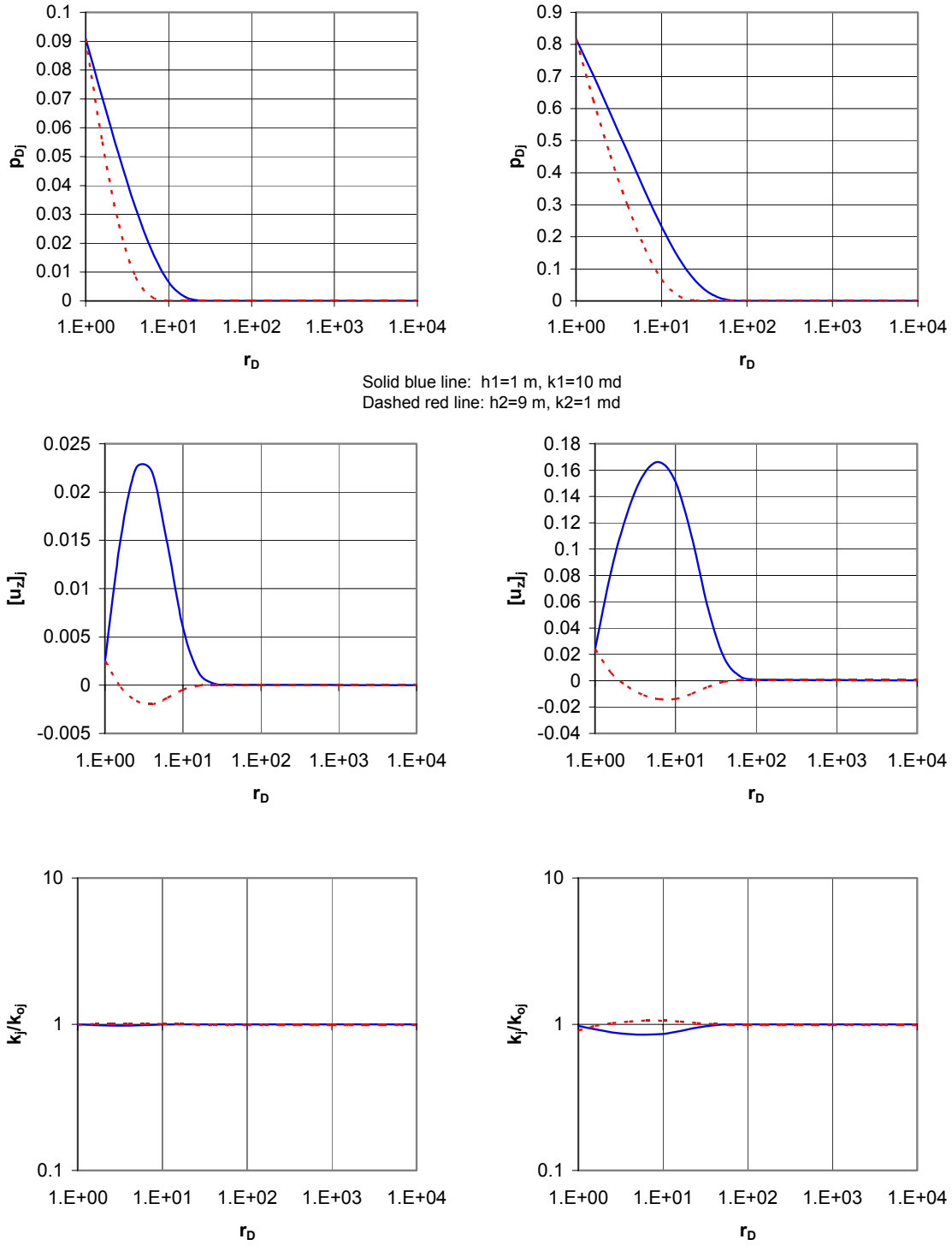

Figure 5-21. Drawdown. Distributions of pressure, deformation, and permeability vs. distance at $t_D/C_D \approx 0.1$ (left) and $t_D/C_D \approx 1$ (right group)

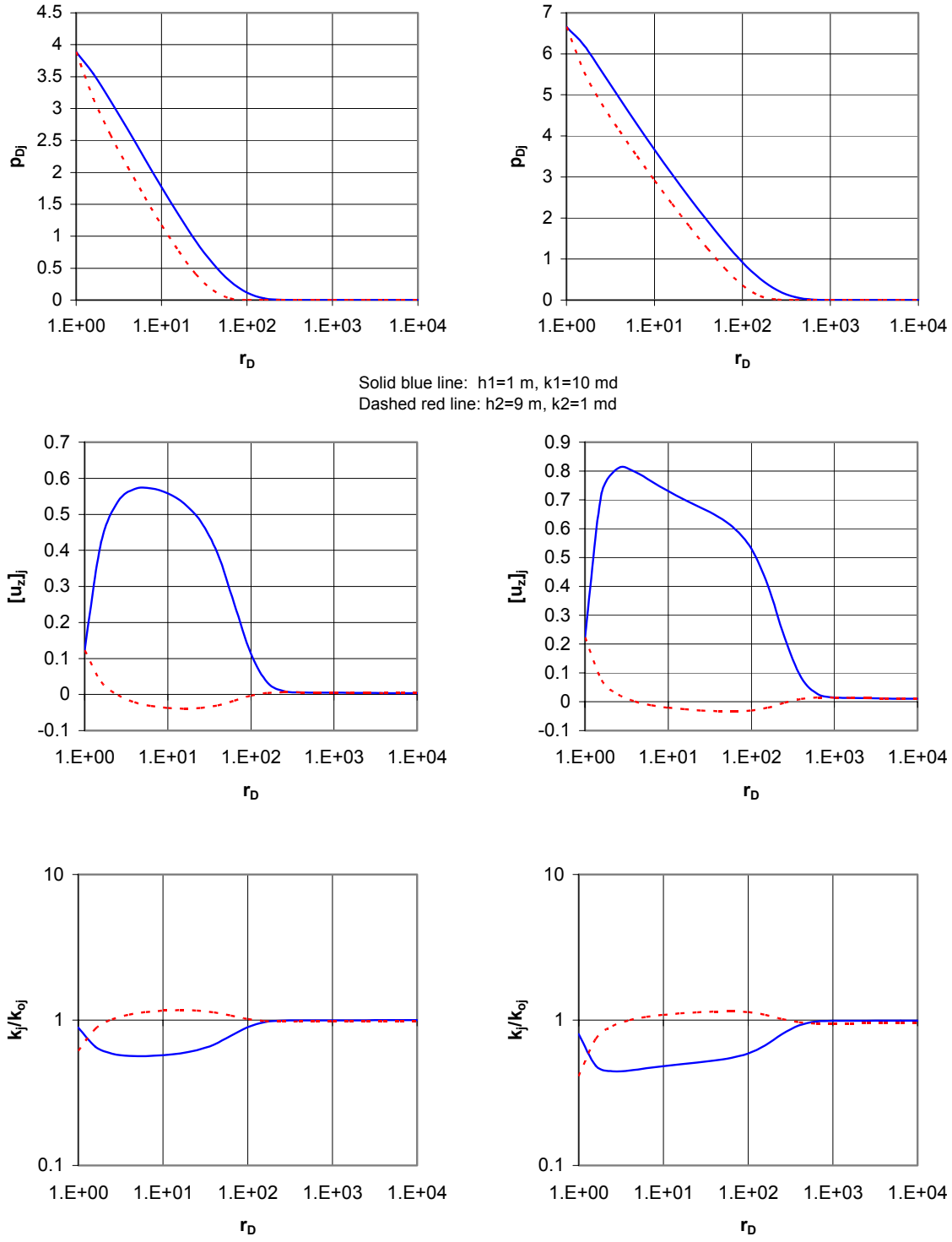

Figure 5-22. Drawdown. Distributions of pressure, deformation, and permeability vs. distance at $t_D/C_D \approx 10$ (left) and $t_D/C_D \approx 100$ (right group)

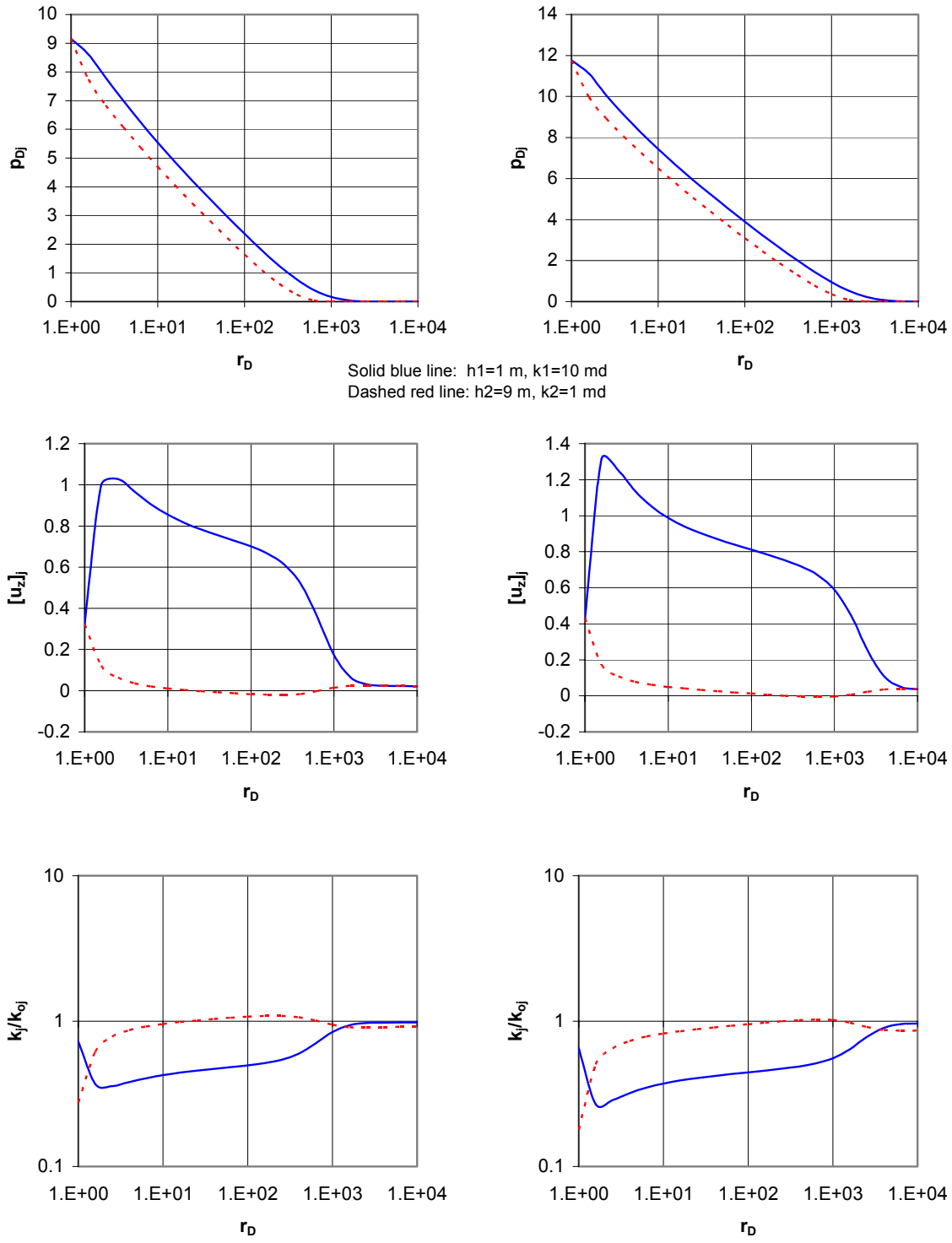

Figure 5-23. Drawdown. Distributions of pressure, deformation, and permeability vs. distance at $t_D/C_D \approx$1E+3 (left) and $t_D/C_D \approx$1E+4 (right group)

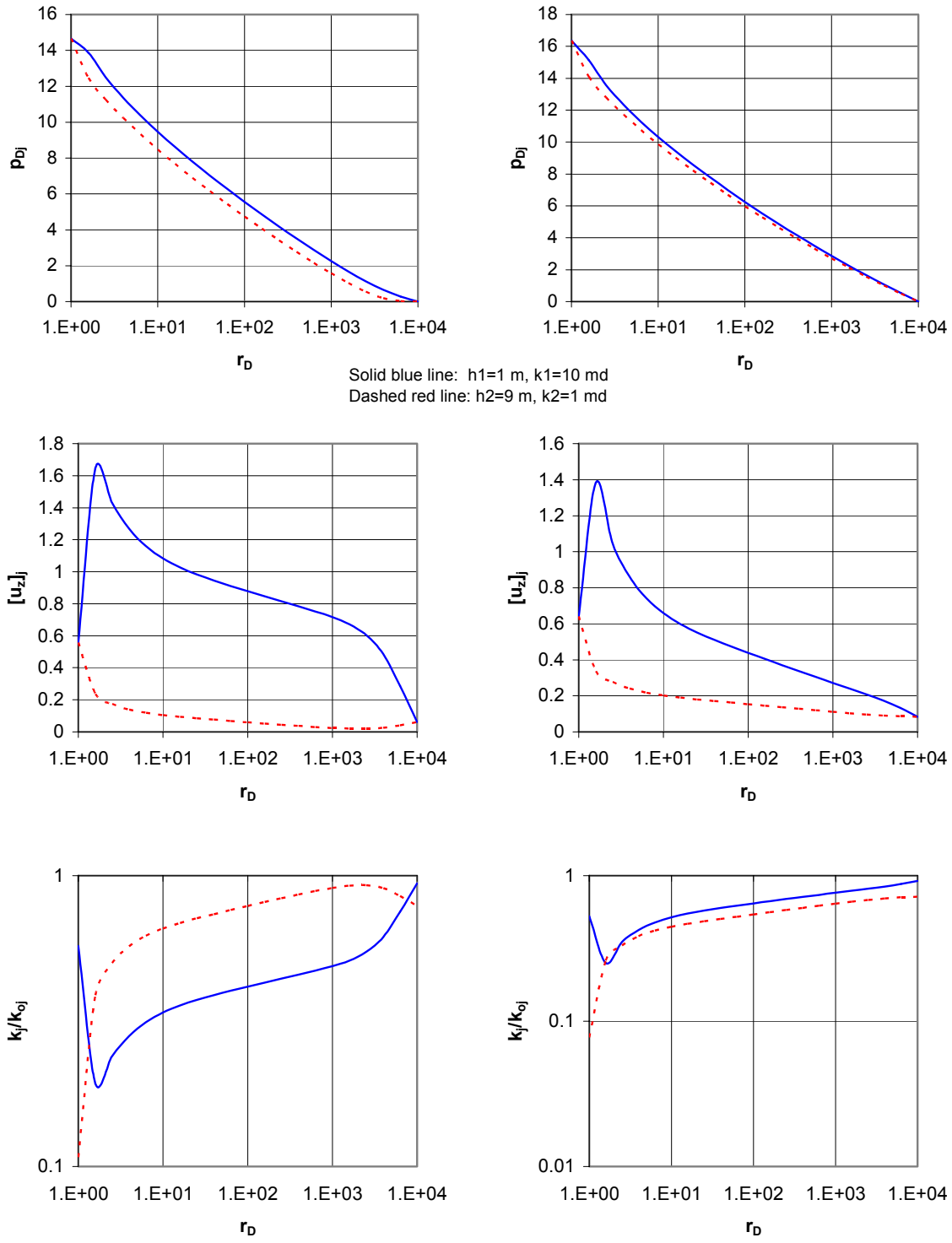

Figure 5-24. Drawdown. Distributions of pressure, deformation, and permeability vs. distance at t_D/C_D ≈1E+5 (left) and t_D/C_D ≈1E+6 (right group)

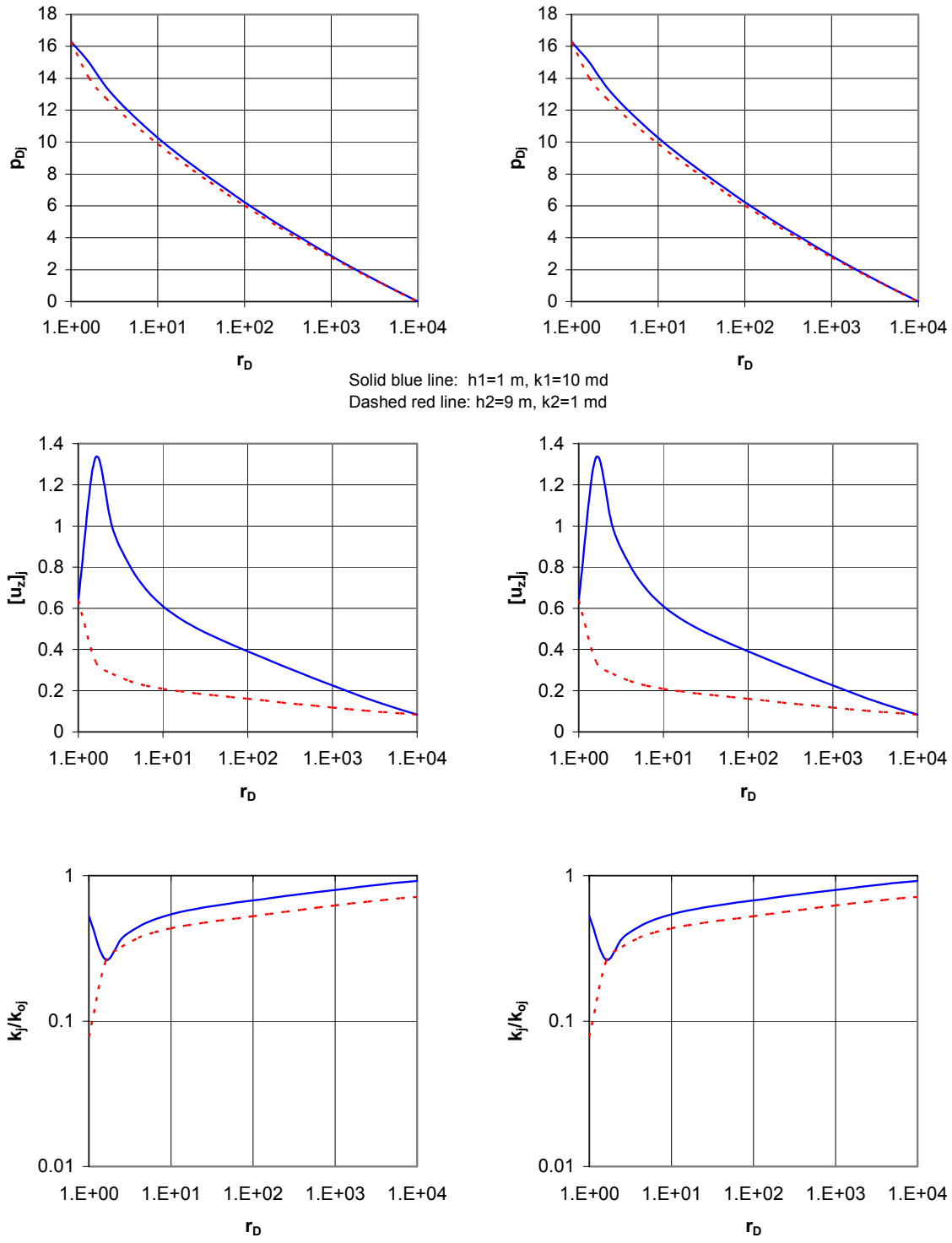

Figure 5-25. Drawdown. Distributions of pressure, deformation, and permeability vs. distance at $t_D/C_D \approx$1E+7 (left) and $t_D/C_D \approx$1E+8 (right group)

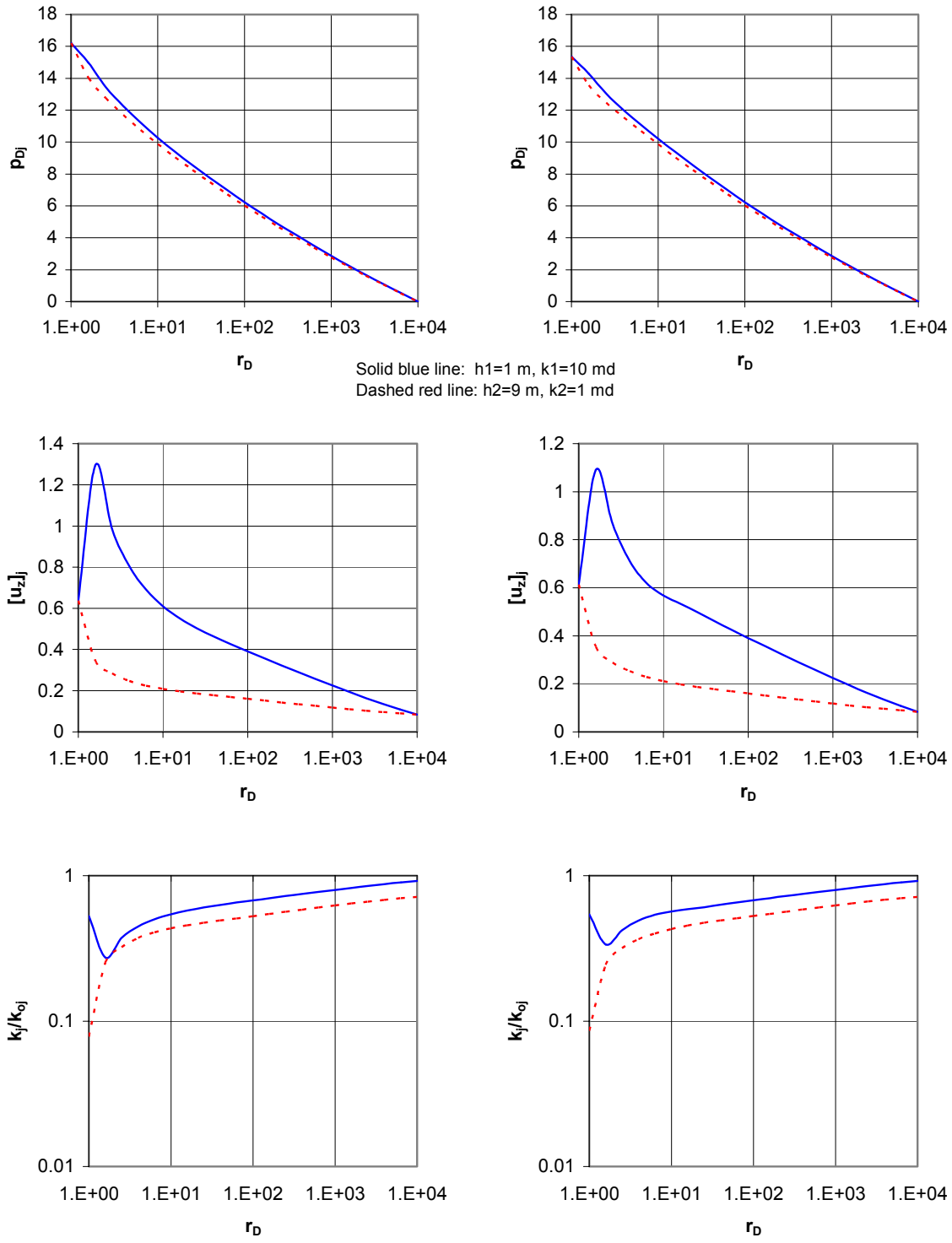

Figure 5-26. Buildup. Distributions of pressure, deformation, and permeability vs. distance at $t_D/C_D \approx 0.1$ (left) and $t_D/C_D \approx 1$ (right group)

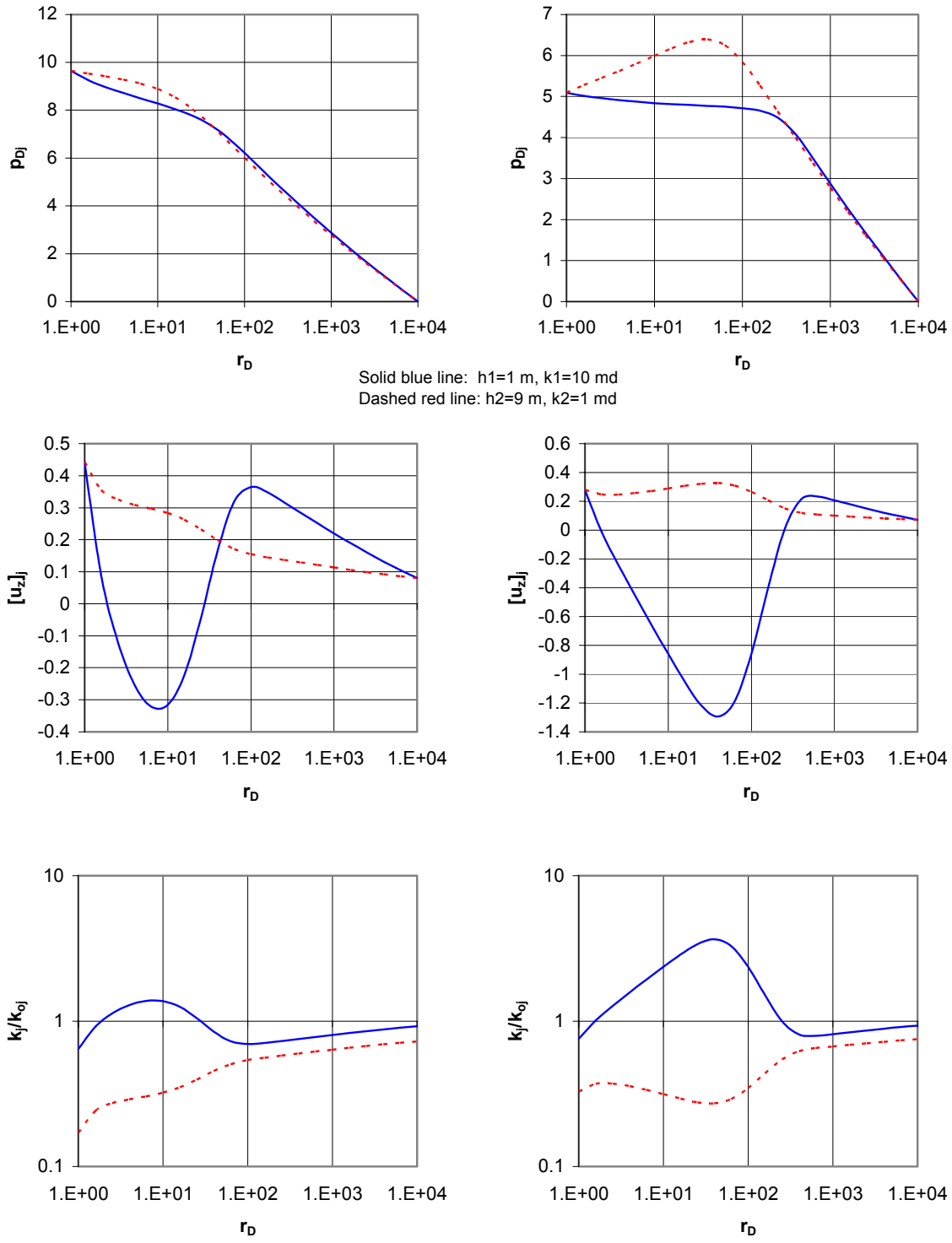

Figure 5-27. Buildup. Distributions of pressure, deformation, and permeability vs. distance at $t_D/C_D \approx 10$ (left) and $t_D/C_D \approx 100$ (right group)

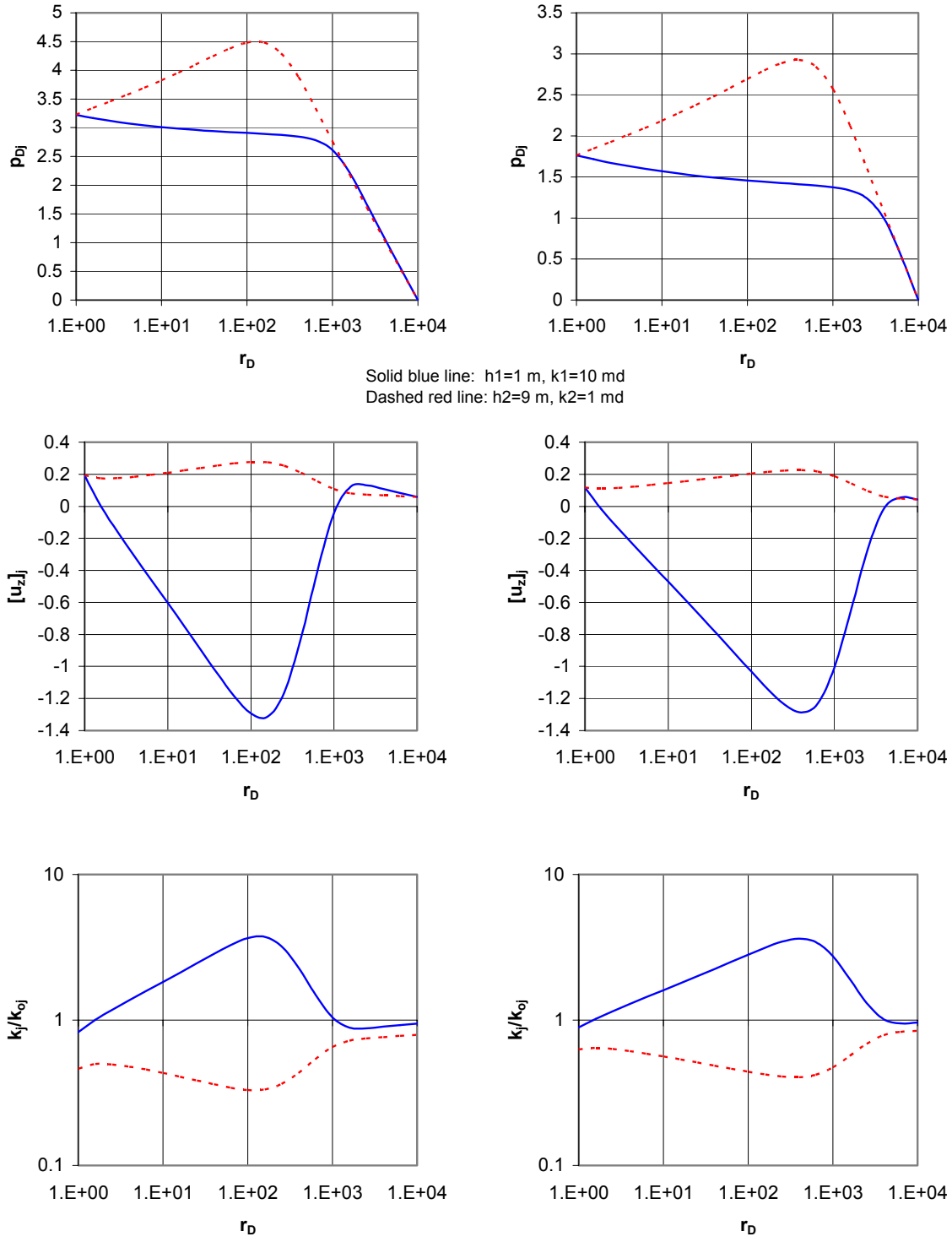

Figure 5-28. Buildup. Distributions of pressure, deformation, and permeability vs. distance at t_D/C_D ≈1E+3 (left) and t_D/C_D ≈1E+4 (right group)

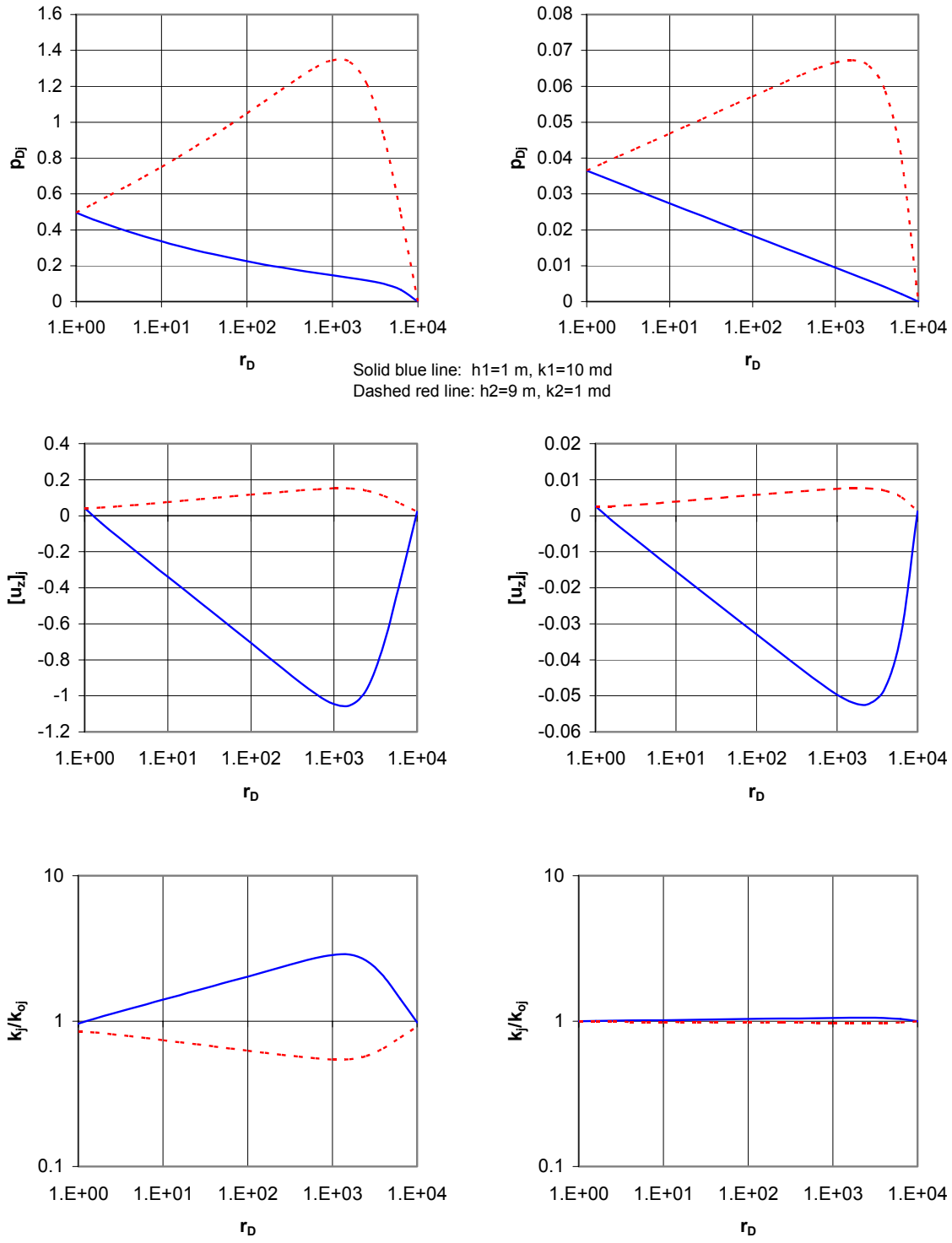

Figure 5-29. Buildup. Distributions of pressure, deformation, and permeability vs. distance at $t_D/C_D \approx$1E+5 (left) and $t_D/C_D \approx$1E+6 (right group)

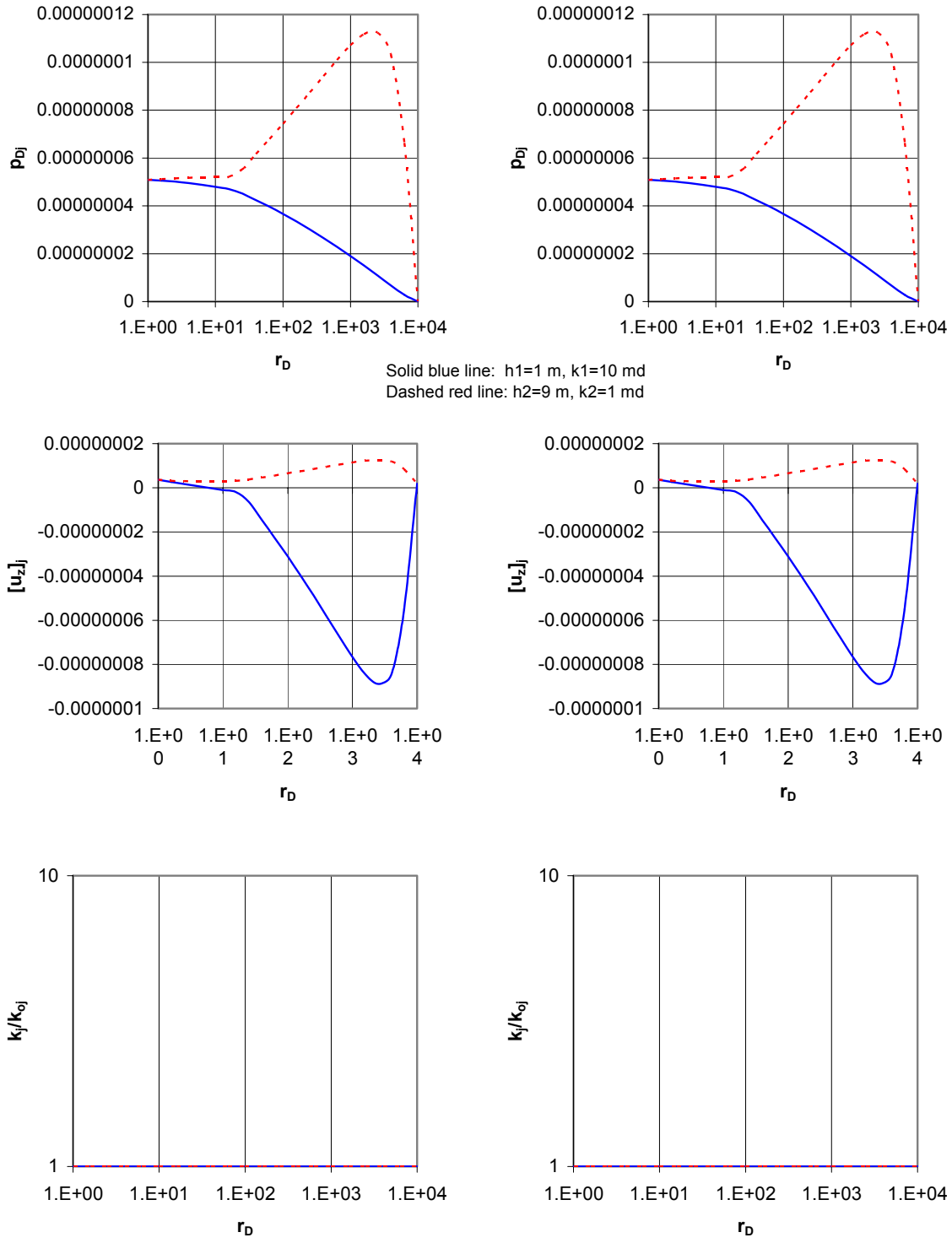

Figure 5-30. Buildup. Distributions of pressure, deformation, and permeability vs. distance at $t_D/C_D \approx$1E+7 (left) and $t_D/C_D \approx$1E+8 (right group)

5.5 Water injection into a two-layer reservoir at different injection pressures in individual layers

We do not present in detail the cases of injection and falloff tests, as behavior of these tests is consistent with already presented results. It is interesting though to consider the situation that was described in the introduction. According to a series of field tests, injection at increased pressures in one of the layers while maintaining the same injection pressure in the other layer had resulted in a decrease of the volume of water accepted by the layer with constant injection pressure. This could be an indication of interaction of pressure fields in separate layers, which would cause, according to our model, deformation (inflation) of the layer with increased injection pressure and respective compaction of the layer with constant injection pressure. The deformation would cause appropriate change of permeability, specifically its decrease in the layer with constant injection pressure.

Let us consider a two-layer reservoir with the following elastic and geometric parameters: $a = 0.0384$, $\gamma_j = E_j / E = 1$, $E = 10^{10}\ Pa$, $r_w / h = 0.001$, $h = 10\ m$, $h_j = 5\ m$, $C_D = 100$, constant pressure outer boundary is at $r_{eD} = 10^4$, $s_j = 0$, $k_j = 10\ md$, $\alpha_j = -2$ (subscript j=1, 2 denotes layer number). Also dimensionless injection pressure in the first layer is $p_{wD}^1 = 3$ and let us vary injection pressure in the second layer and observe how the volumes injected in each layer change. In Fig. 5-31 we present the behavior of dimensionless injection rates in each layer vs. dimensionless time. For the blue and red curves $p_{wD}^2 = 1$ and for the green and black curves $p_{wD}^2 = 5$.

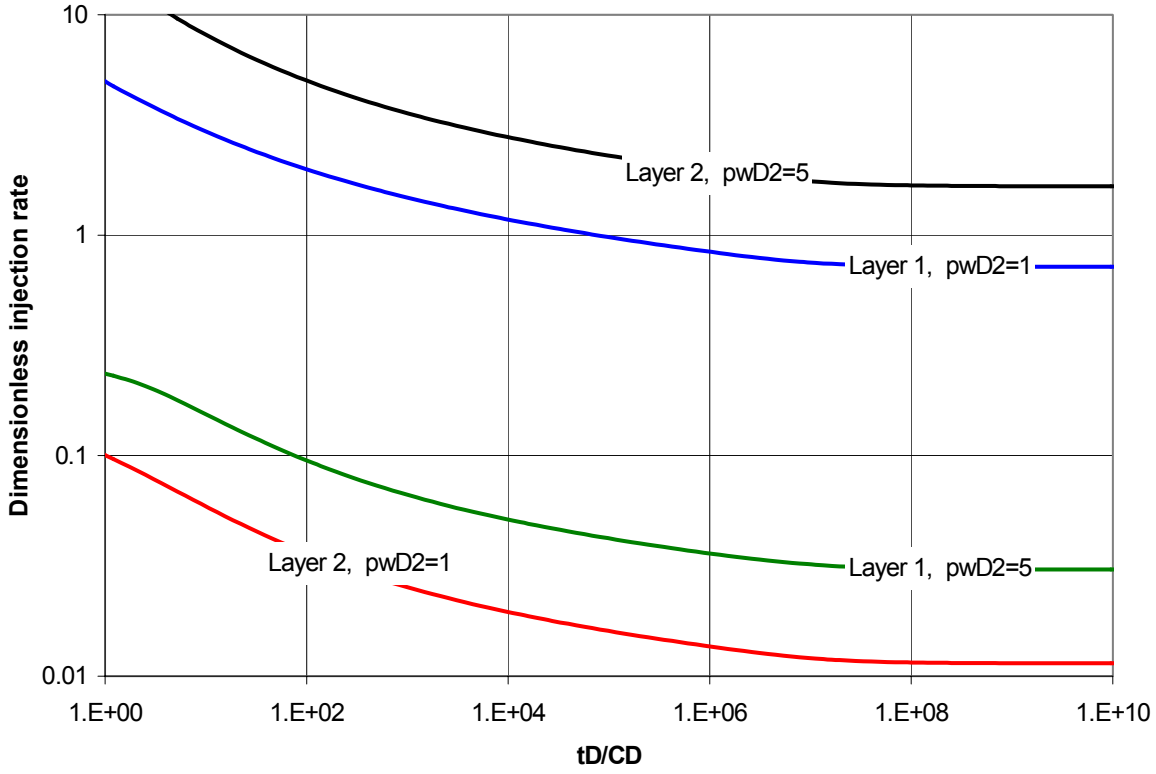

Figure 5-31. Stabilization of injection rates for constant injection pressure in the first layer and varied injection pressure in the second layer

We can see that the amount of fluid a layer accepts depends on the magnitudes of the injection pressures in both layers. At lower $p^2_{wD} = 1$ the injection rate in the first layer (blue curve) is smaller than in the second layer (red curve). Regardless of the fact that the properties of both layers are identical, the stabilized injection rates differ quite significantly and in non-linear fashion. Higher injection pressure in the second layer causes its inflation and respective compaction of the first layer with lower $p^1_{wD} = 3$ (green and black curves).

Steady-state injection rates in both layers for constant $p^1_{wD} = 3$ vs. p^2_{wD} are presented in Fig. 5-32. The solid blue and dashed red curves correspond to the first and second layer, respectively.

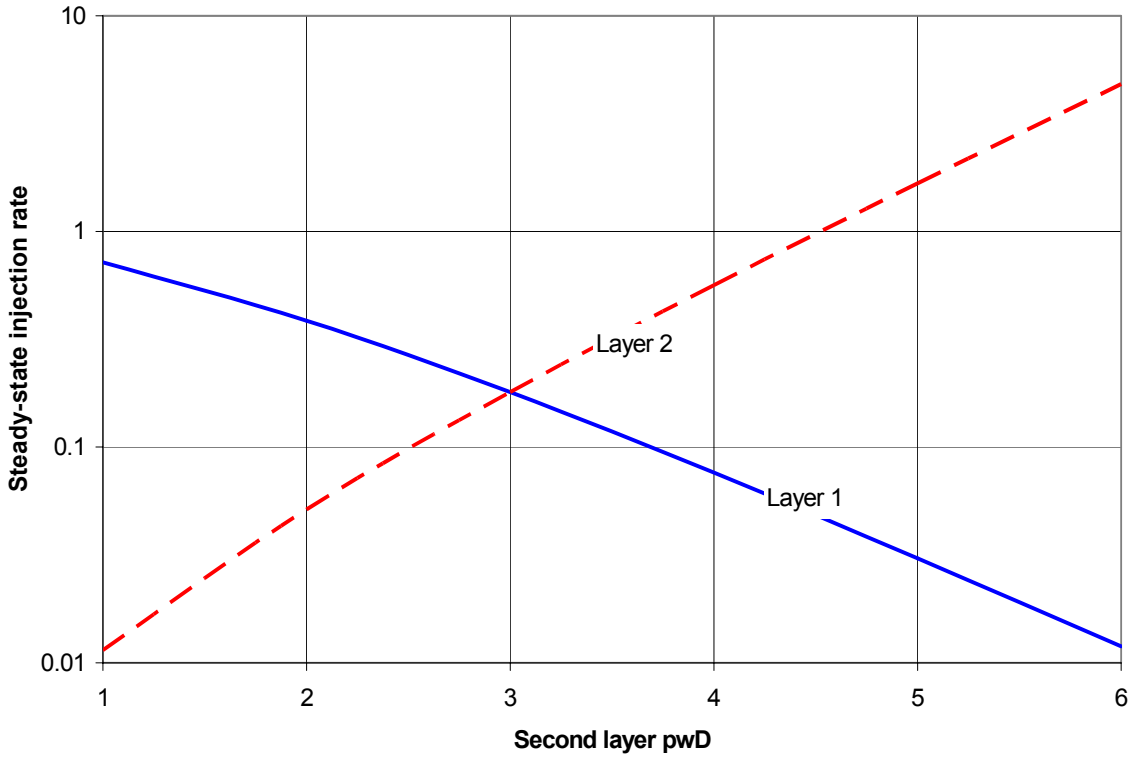

Figure 5-32. Layers' injection rates vs. injection pressure in the second layer for constant injection pressure in the first layer

The results qualitatively agree with the field tests thus suggesting a possible explanation of the observed behavior.

6 THREE LAYER CASE

As stated earlier, we can model a reservoir with an arbitrary number of layers. In this chapter we present several typical problems that have been calculated for a three-layer reservoir. As one would expect, based on examination of the two-layer cases, the increased number of layers should make the characteristic features of the single-layer type curves even less obvious, more so if the layers' properties are significantly different.

6.1 Constant rate drawdown followed by buildup in a finite reservoir with constant pressure outer boundary

Let us consider a three-layer reservoir with $a = 0.0384$, $\gamma_j = E_j / E = 1$, $E = 10^{10}\ Pa$, $r_w / h = 0.001$, $h = 10\ m$, $C_D = 100$, constant pressure outer boundary is at $r_{eD} = 10^4$, and $s_j = 0$ (subscript j denotes layer number). The layers have different thicknesses, initial permeabilities, and sensitivities of permeability to deformation. These values are as follows: $h_1 = 1\ m$, $k_1 = 100\ md$, $\alpha_1 = 0$; $h_2 = 2\ m$, $k_2 = 10\ md$, $\alpha_2 = 1$; $h_3 = 7\ m$, $k_3 = 1\ md$, $\alpha_3 = 4$ (the highest-permeability layer having the least thickness and negligible sensitivity of permeability to deformation).

The type curves for this case are presented in Fig. 6-1 (blue solid curves – drawdown, red dashed curves – buildup). We can see that as in the two-layer case, large permeability contrast and respective values of sensitivity of permeability to deformation makes this case virtually indistinguishable from a linear case with no account for deformation.

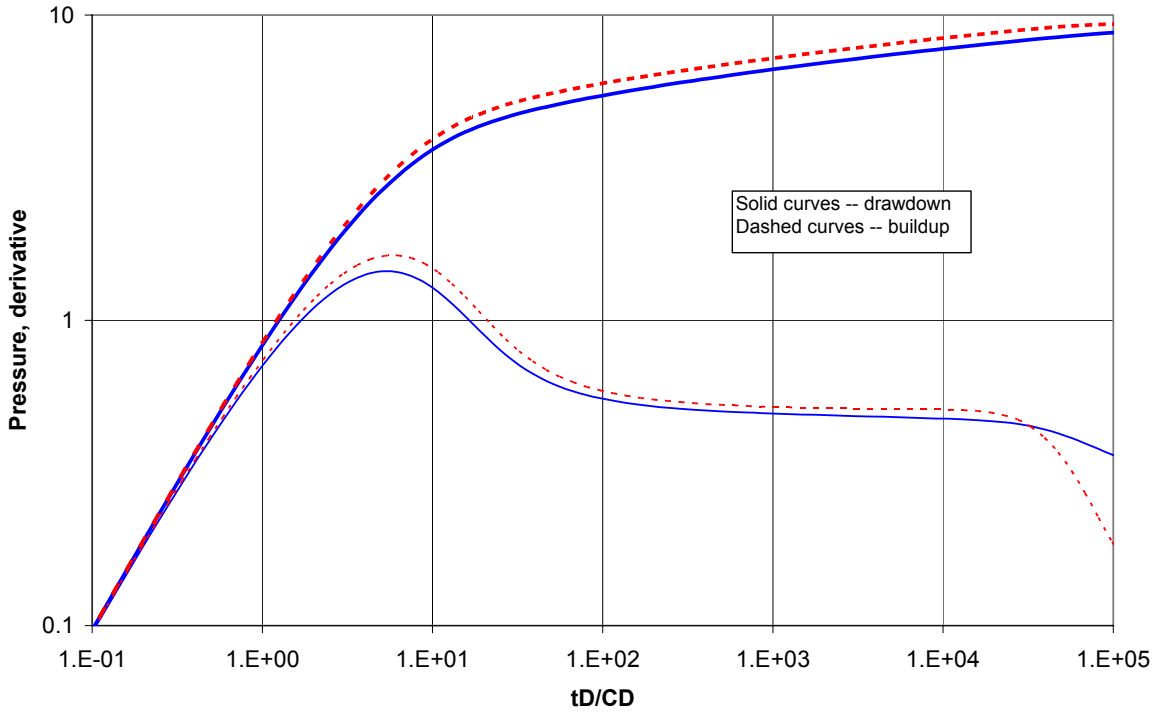

Figure 6-1. Drawdown followed by buildup in a three-layer reservoir. Thick high permeability layer

It has been shown earlier that the results depend also on a layer thickness and thin layers deform to a lesser degree. In Fig. 6-2, we present the results for the case when high-permeability layer is 0.1 m thick, $h_2 = 1\,m$, $h_3 = 8.9\,m$, and all other parameters are the same as in the previous example. The high-permeability layer deforms less, the lower-permeability layers experience less unloading and the buildup type curves qualitatively resemble more the type curves for a single-layer case.

If permeability contrast among layer is relatively small and, respectively, the layers' permeabilities have not negligible sensitivity to deformation, then the difference between drawdown and buildup curves becomes larger. This is shown in Fig. 6-3 where we present the results for the case with $h_1 = 1\,m$, $k_1 = 10\,md$, $\alpha_1 = 1$; $h_2 = 2\,m$, $k_2 = 5\,md$, $\alpha_2 = 2$;

$h_3 = 7\ m$, $k_3 = 1\ md$, $\alpha_3 = 4$. The rest of the parameters are the same as in previous two examples.

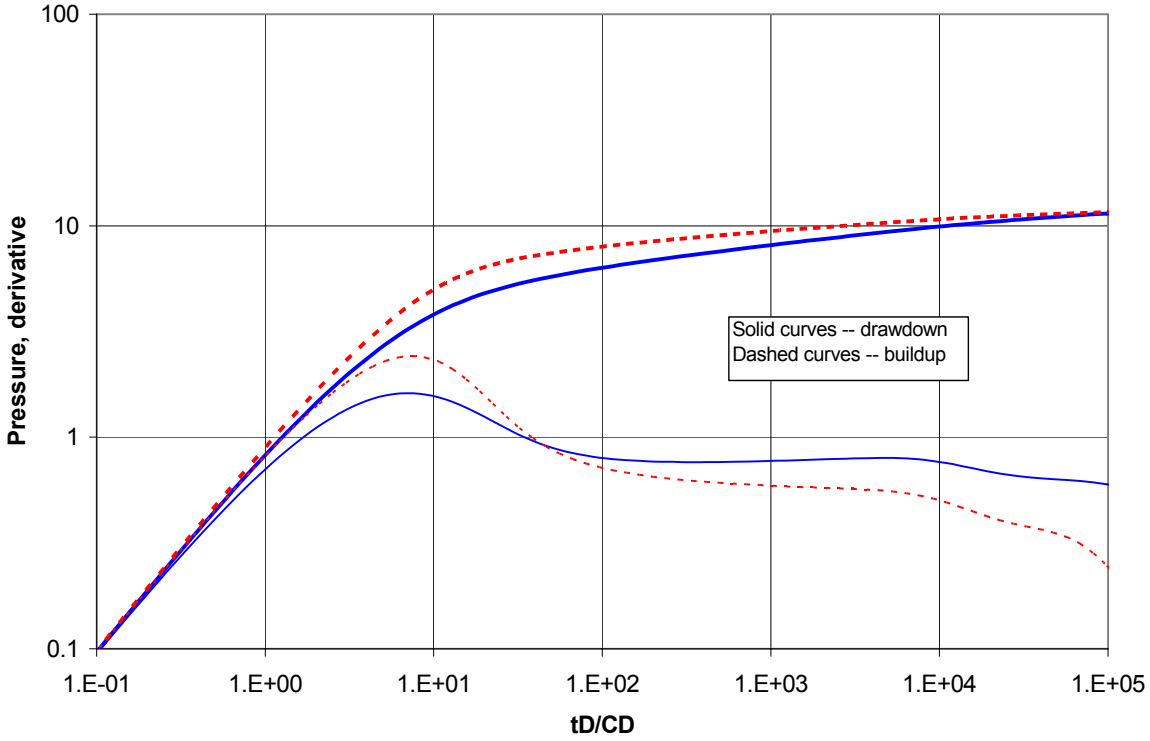

Figure 6-2. Drawdown followed by buildup in a three-layer reservoir. Thin high permeability layer

We should note again that it is practically impossible to infer stress-sensitive behavior from drawdown curves alone. This means that for confident identification of the effect under consideration and for its quantitative description one would need an extended flow period, so that a large are around a well is affected by the drawdown, followed by a shut-in period, which is long enough for the downward trend on the derivative to be established. One would also need to have some evidence of layering of the reservoir and some crude estimates of layers' permeability values.

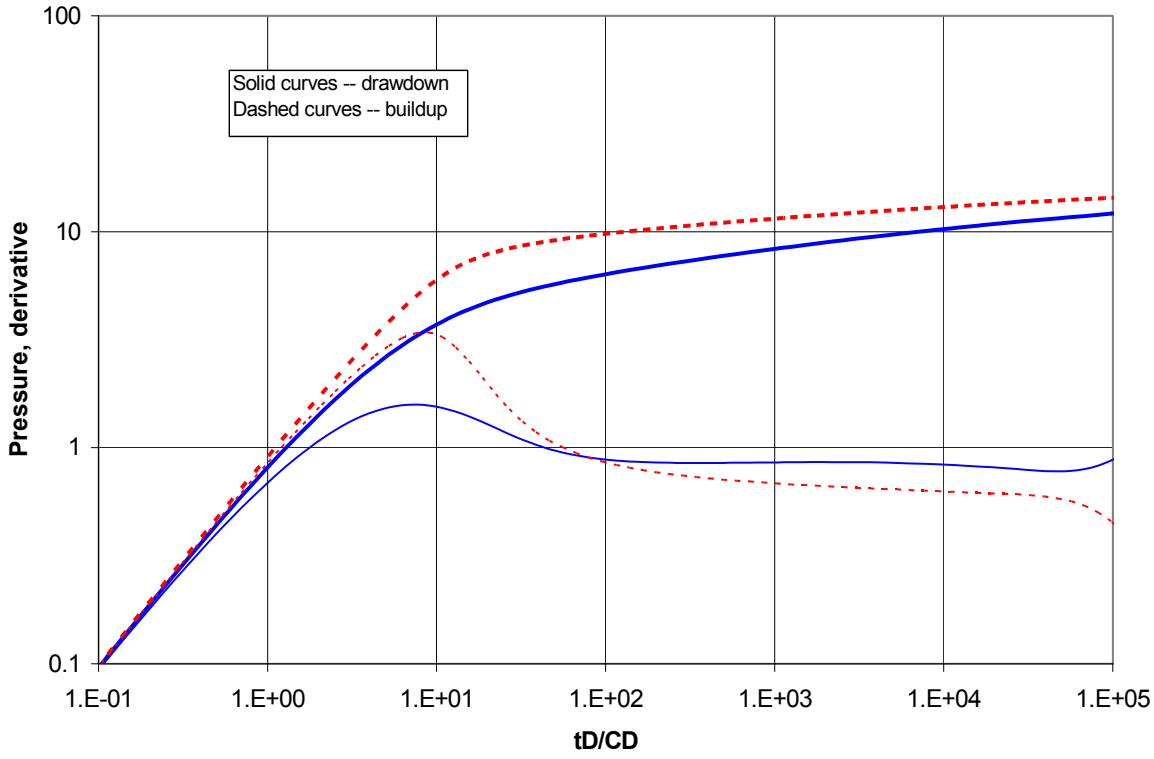

Figure 6-3. Drawdown followed by buildup in a three-layer reservoir. Low permeability contrast

The type curve behavior of a three-layer system, as evident from the above three examples, is in accordance with the previous results, so we will not consider any other drawdown/buildup problems.

6.2 Water injection into two layers, separated by an impermeable layer, at different injection pressures in individual layers

Let us again consider the case of water injection into two layers at different magnitudes of injection pressure in individual layers. Field tests have shown that the volume of water that any particular layer accepts depends on pressures in both layers. Increase of

injection pressure in one of the layers results in decrease of the volume accepted by the other layer, even though the injection pressure in that layer is kept constant. The layers may be several meters apart.

We consider a three-layer reservoir with $a = 0.0384$, $\gamma_j = E_j / E = 1$, $E = 10^{10}\ Pa$, $r_w / h = 0.001$, $h = 10\ m$, $C_D = 100$, constant pressure outer boundary is at $r_{eD} = 10^4$, and $s_j = 0$ (subscript j denotes layer number). The two permeable layers with identical properties are separated by a thicker impermeable layer. Let $h_1 = h_3 = 5\ m$, $k_1 = k_3 = 10\ md$, $\alpha_1 = \alpha_3 = -2$; $k_2 = 1e-15\ md$, $\alpha_2 = 0$. The injection is at constant $p_{wD}^3 = 3$ in the bottom layer, injection pressure in the first layer varies between 1 and 6. Since the middle layer is impermeable, does not accept any water, and pressure in it does not change, any interaction between two permeable layers is possible by means of deformation of all three layers.

Let us see what effect has the thickness of the impermeable layer. For results presented in Fig. 6-4 $h_2 = 0, 10, 20\ m$ from top to bottom graph, respectively. Solid blue line corresponds to the third layer with constant injection pressure, dashed red line corresponds to the first layer. For zero thickness of the middle layer the results coincide with the two-layer case, presented earlier. As thickness of the impermeable layer increases, the interaction between permeable layers becomes less. We can see that even though the distance between the producing layers may be substantial they still do affect each other and exhibit the observed in the field experiments trend.

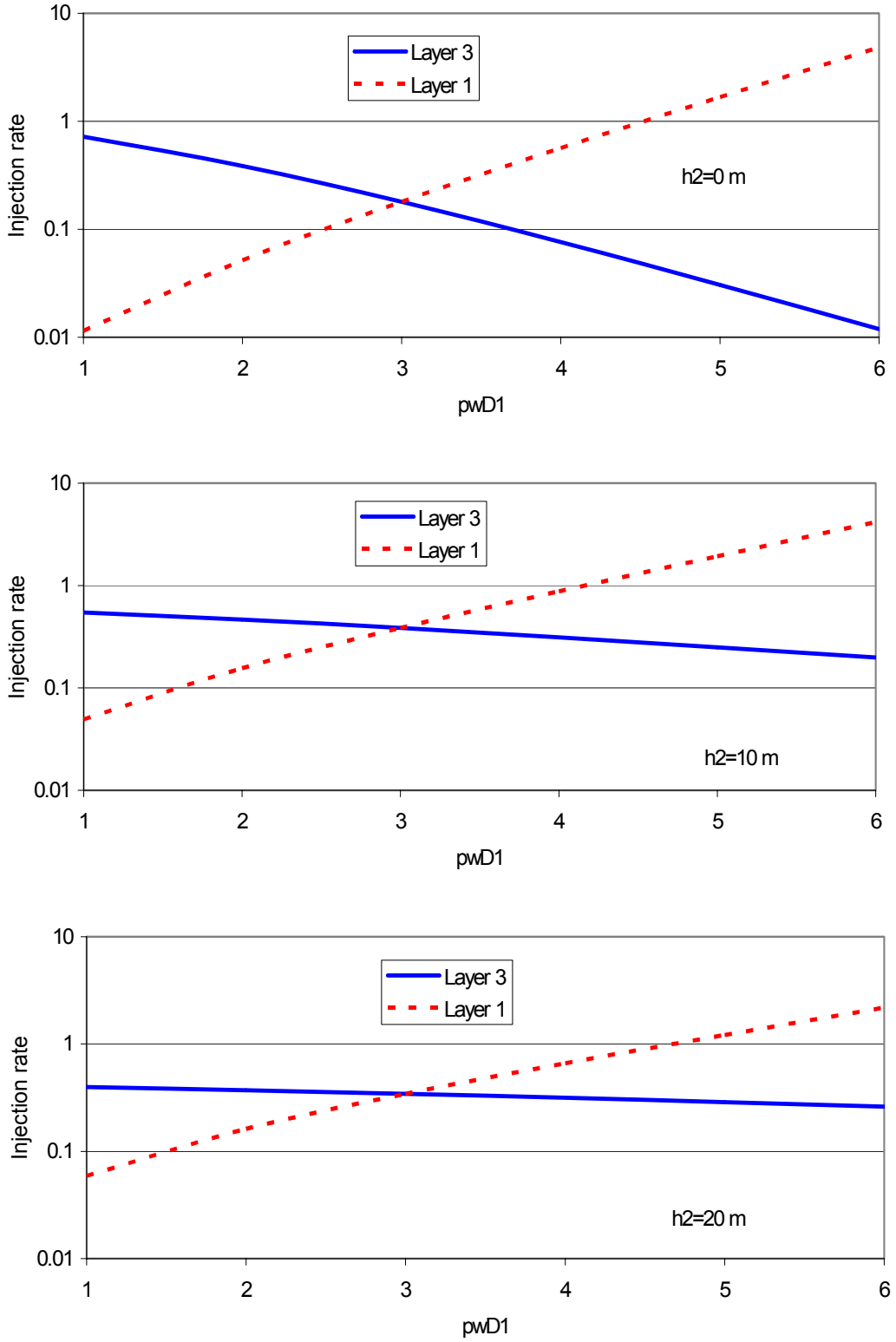

Figure 6-4. Three-layer case. Various thicknesses of impermeable middle layer

7 MULTILAYER CASE

Comparison of single-, two-, and three-layer cases shows that the presence of several layers tends to mask the characteristic behavior of the single-layer type curves, more so when the layers' properties (such as permeability) vary significantly from layer to layer. In fact, as the heterogeneity increases the results become more similar to the linear case, i.e. calculated without accounting for stress-dependence. The interaction of pressures in layers can be easily understood if we recall the formula for vertical deformation of an individual layer.

$$\left[u_z^j\right] = \frac{\left[u_z\right] - \eta \sum_{k=1}^{n} \frac{p_k}{c_k}}{c_j \sum_{k=1}^{n} \frac{1}{c_k}} + \eta \frac{p_j}{c_j} \tag{7.1}$$

At any given point in the reservoir, the first term in the expression above is essentially the same for all layers if the magnitudes of layers Young's moduli and thicknesses are close. The principal difference among layers is attributed to the last term, $\eta\, p_j / c_j$. During drawdown, the radius of investigation in a higher-permeability layer is greater and pressure difference is greater in the high-permeability layer at any point and at any moment in time. According to Eq. 7.1 the deformation of the high-permeability layer is also greater than that of lower-permeability layers. Greater deformation results in a certain degree of "unloading" of lower-permeability layers and an improvement, or at least in a lesser damage, to their permeabilities. The higher-permeability layer, on the other hand, suffers certain permeability reduction. As a result of these deformation effects, the pressure in the lower-permeability layers tends to catch-up with pressure in the higher-permeability layers, as the former experiences permeability improvement and the latter – degradation. The net effect is that pressure disturbance moves into the formation approximately uniformly in all layers. As the

permeability contrast among layers increases and as the thickness of the high-permeability layer increases the effect is more pronounced.

Elsewhere in the reservoir the deformation effects tend to reduce the permeability contrast, but on the well contour, the magnitude of deformation is the same in all layers (if elastic moduli and thicknesses are the same) or at least comparable across layers, and highest- and lowest-permeability layers suffer least and most permeability reduction, respectively. The created deformational choke greatly impedes flow from the low-permeability layer. Even though far-field permeability in it might be improved, the input of this layer into well flow rate is very low

Let us consider a 6-layer reservoir with the following properties: $a = 0.0384$, $\gamma_j = E_j / E = 1$, $E = 10^{10}\ Pa$, $r_w / h = 0.001$, $h = 10\ m$, $C_D = 100$, constant pressure outer boundary is at $r_{eD} = 10^4$, and $s_j = 0$. Sensitivity of a layer to deformation depends on the magnitude of the initial permeability. These parameters are shown in Table 7-1.

Table 7-1. Parameters for the 6-layer case

h, m	k_0, md	α	h, m	k_0, md	α
5	1	4	1	4	3
1	2	3.67	1	5	2.67
1	3	3.33	1	6	2.33

The drawdown and buildup type curves are presented in Fig. 7-1. We can see that it might be difficult to distinguish this case from a single-layer linear case if only short-duration drawdown or buildup data are available. The combination of the two tests of sufficient

duration might allow for interpretation. The individual layers' parameters is practically impossible to determine.

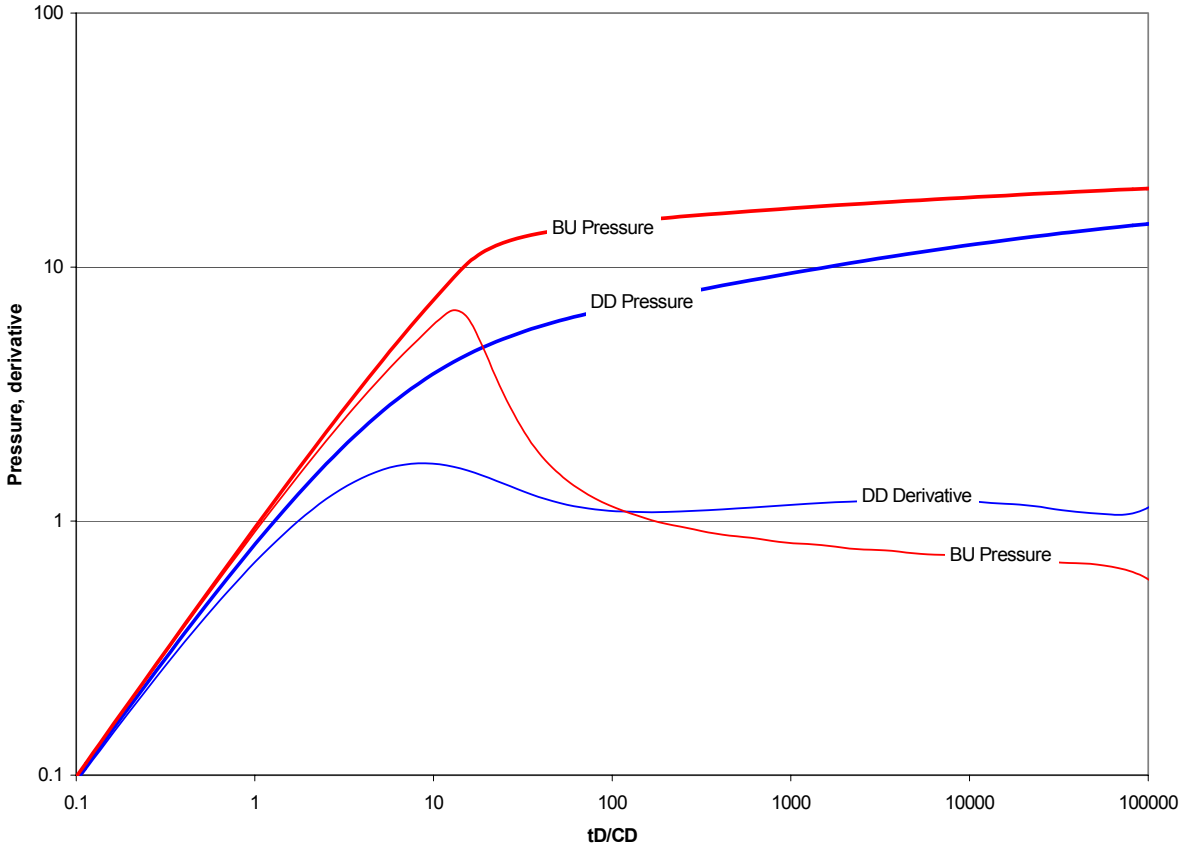

Figure 7-1. 6-layer case

Though not discussed in any detail, possible crossflow between adjacent layers can significantly change the processes of stabilization of the major parameters. In the program the crossflow is incorporated as an additional term of the form $CF_j^{j+1}\left(p_{jD} - p_{j+1D}\right)$ in the pressure equation, where CF_j^{j+1} is the dimensionless crossflow coefficient between adjacent layers. The greater is this coefficient and the greater is the permeability contrast and, respectively, the contrast of sensitivities of permeability to deformation in adjacent layers, the closer are the type curves to the linear case.

8 FIELD CASE

8.1 Account for pressure-dependent fluid properties and stress-sensitivity

Prior to proceeding to the field case, let us include in calculations the fluid properties and examine how dependence of oil and gas properties on pressure and temperature affect the results. We have incorporated correlations, which allow calculating oil or gas viscosity, formation volume factor, etc. into the code and have performed several runs in order to evaluate how accounting for changing fluid properties in addition to accounting for permeability dependence on deformation affects the results.

The variation of oil viscosity was included into the calculation of the non-linear term in the pressure equation

$$\frac{1}{r_D}\frac{\partial}{\partial r_D}\left[r_D\frac{K_j}{\mu_o^*(p)}\frac{\partial p_{jD}}{\partial r_D}\right]=\frac{\omega_j}{\kappa_j}\frac{\partial p_{jD}}{\partial t_D}$$

where $\mu_o^*(p)$ is ratio of oil viscosity at a particular value of pressure to the value at the initial pressure. For simplicity, we did not consider variation of oil or formation compressibility and oil formation volume factor.

The parameters for the example single-layer case are given in Table 8-1.

Table 8-1. Parameters for the case with account for variation of fluid properties

Initial reservoir pressure, psia	4,000	Permeability, md	10
Formation temperature, oF	200	Net pay thickness, ft	30.5
Oil gravity, oAPI	40	Wellbore radius, ft	0.328
Gas specific gravity	0.7	Reservoir radius, ft	3,281
Solution GOR, scf/bbl	800	Skin factor	0

Additionally, $a=0.0384$, $\gamma_j=E_j/E=1$, $E=10^{10}\ Pa$, $C_D=100$, no gas impurities. We have also required 10% retained permeability at the largest drawdown, which

corresponds in this case to $\alpha = 1.6$ at $q = 1{,}600\ BOPD$. Since parameter α is proportional to production rate, its magnitude was scaled accordingly to values of rate.

In Fig. 8-1 we present results of calculation of IPRs when accounting only for variation of oil viscosity (dashed blue curve), only for permeability sensitivity to deformation (solid green curve), and for both factors (dotted red curve).

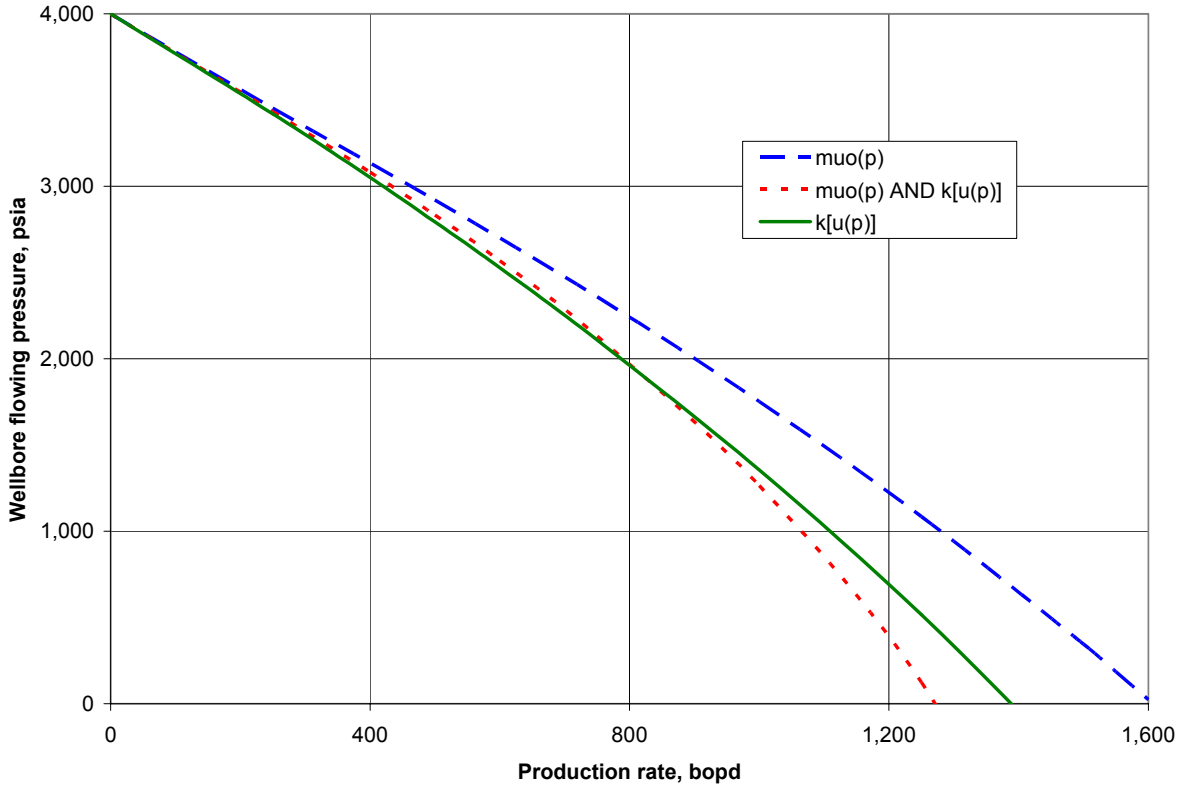

Figure 8-1. Sandface IPRs for the three cases

We can see that permeability stress-dependence results in substantial deviation of an IPR from a conventional case when only variation of oil viscosity is considered. For bottomhole pressures significantly below the bubble-point (3,318 psia) the deviation is larger, as the oil viscosity increases and the magnitude of the non-linear pressure- and deformation-dependent term in the equation of flow further decreases. It should be also

noted that in this case for the conditions of predominantly single-phase formation flow with a small zone of gas liberation around the wellbore, the effect of permeability stress-dependence is much greater than the effect of pressure-dependent fluid properties. For more accurate description of simultaneous flow of oil and gas we need to account also for changing relative permeabilities which would result in additional and approximately the same deviation of all curves in Fig. 8-1.

Properties of gases, on the other hand, normally vary in a much broader range. In order to accurately account for the variations, one should use adjusted pseudo-pressure and pseudo-time. The form of the dimensionless flow equation remains the same and solutions developed for flow of liquid apply. However, when performing analysis one must plot actual data in adjusted variables.

When considering the field case, we assume that deformation is the same as before function of the adjusted pseudo-pressure, since the numerical values of dimensionless pressure in liquid case and of adjusted pseudo-pressure coincide, and permeability depends on deformation.

8.2 Field description

The Opon gas field is located in the La Paz formation in Colombia and produces lean retrograde gas with dew point pressure of about 9,000 psi and 45o API condensate gravity (all information is as of 1995). The area is characterized by high tectonic stresses – 1.3 psi/ft, the reservoir is over pressured at 1 psi/ft. As a result of thrust faulting this single-layer homogeneous reservoir is highly fractured. Common problems in the field include perforation failure, there is also concern about reservoir stability and possible earthquakes.

According to results of core analysis matrix permeability ranges from 0.005 to 0.2 md, core porosity ranges from 5 to 9%. While simulating depletion core permeability is sensitive to increasing stress. Results of pressure transient analysis indicate permeability-thickness product in the range from 1,000 to 2,100 md-ft, which along with the core analysis indicates high density of natural fractures. Some other data is provided in Table 8-2.

Table 8-2. Opon field data

Field name	Opon field
Reservoir age	Eocene
Stratigraphic unit	La Paz formation
Geologic setting	Braided fluvial
Lithology	Sandstone and shale
Porosity type	Intergranular, feldspar dissolution
Trapping mechanism	North-plunging fault bend anticline
Structural size, acres	7,750
Gas column, ft	3,600
Average porosity, %	7.4
Average Sw, %	35
Average gross thickness, ft	1,900
Average pay thickness, ft	775
Gas gravity	0.725 (recombined)
Dew point pressure, psia	8,640
Average well depth, ft	12,500
Reservoir pressure Opon #3 / Opon #4, psi	11,100 (-9,186’ subsea) / 10,850 (-9,128’)
Reservoir temperature, oF	210
Estimated field reserves	2.2 TCF and 94 MMBC
Production test results Opon #3	45 MMSCFD and 2,000 BCPD
Production test results Opon #4	58 MMSCFD and 1,900 BCPD

A single isochronal test data set is available (Fig. 8-2). The quality of the data prevents from obtaining a confident type-curve match, though certain qualitative features can be noted.

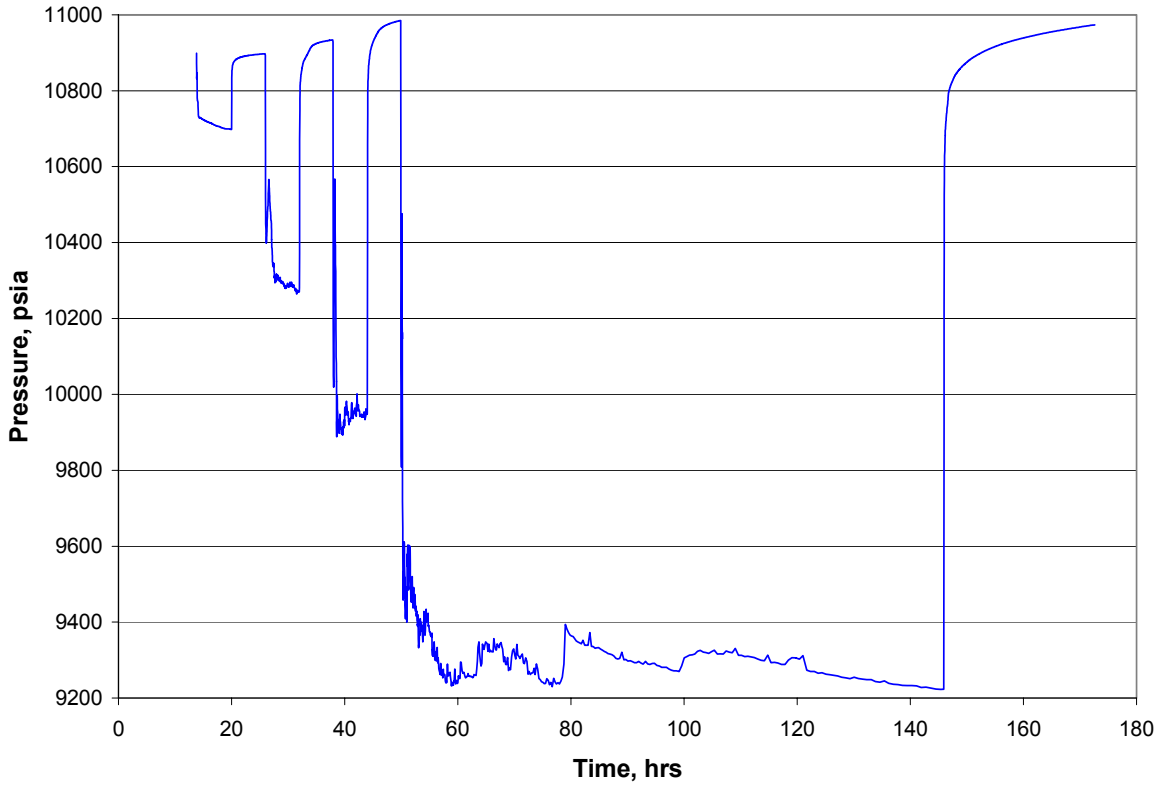

Figure 8-2. Opon #3. Modified isochronal test

In Fig. 8-3 we present an attempt to match the first drawdown data. Clearly the data is far too noisy (other flow periods are even worse), though one might see an upward trend on the derivative.

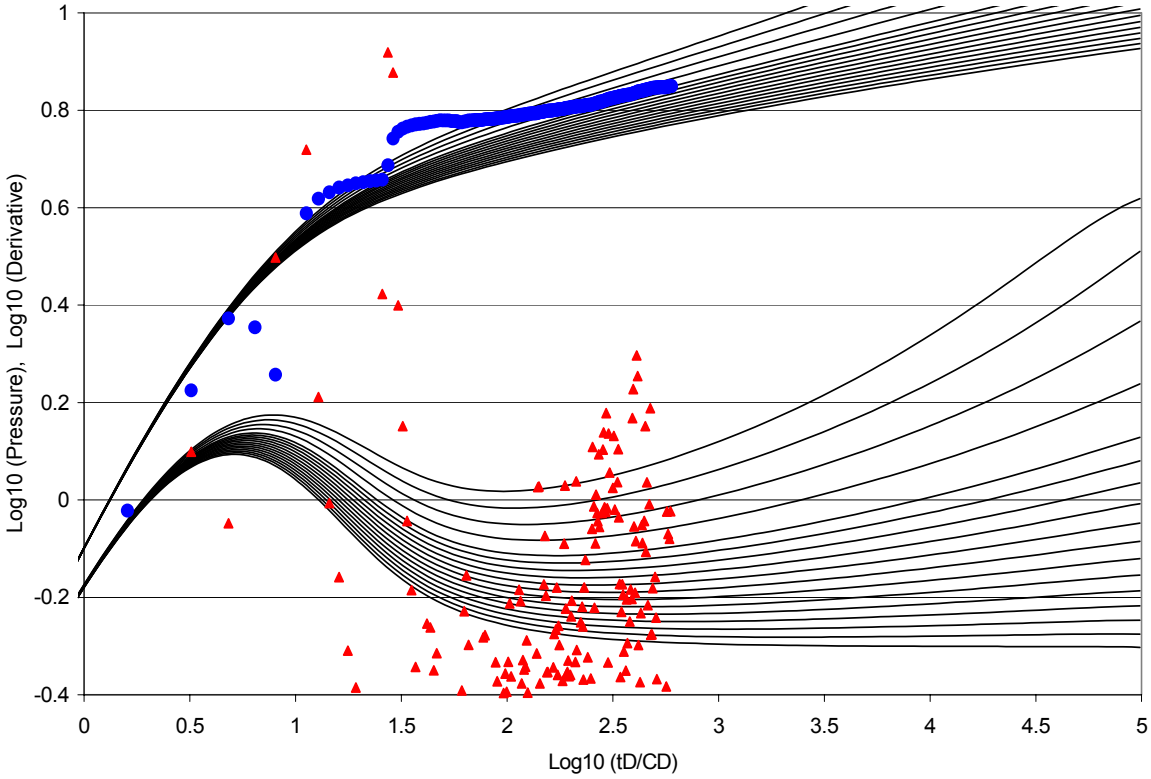

Figure 8-3. Type curve analysis of the first flow period

The buildup data is less noisy but lack of early time data prevents from a confident match (see Figs. 8-4 – 8-7). The (arguably) recognizable downward trend on the derivative is in line with prediction of our model. Late data exhibit a more discernable drop, which may be indicative of the end of the zone of altered permeability, created by the first drawdown. Sensitivity of permeability to deformation appears to be fairly high (lowest type curves correspond to the linear case $\alpha = 0$, highest – to $\alpha = 4$).

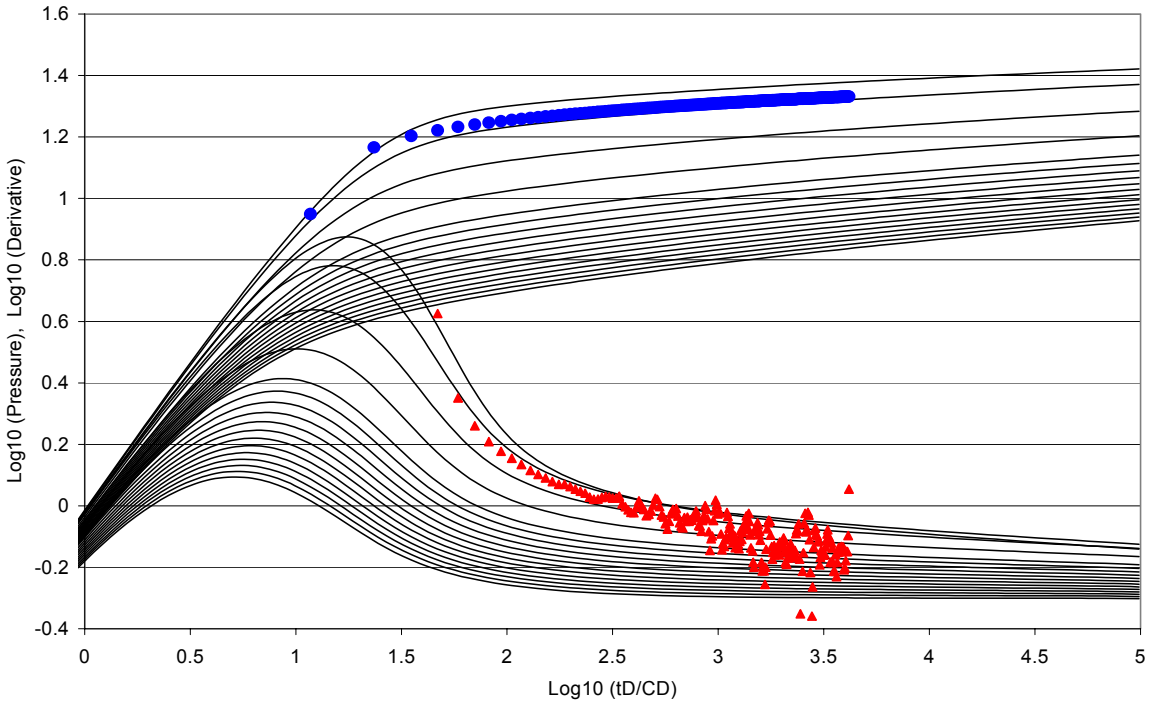

Figure 8-4. First buildup

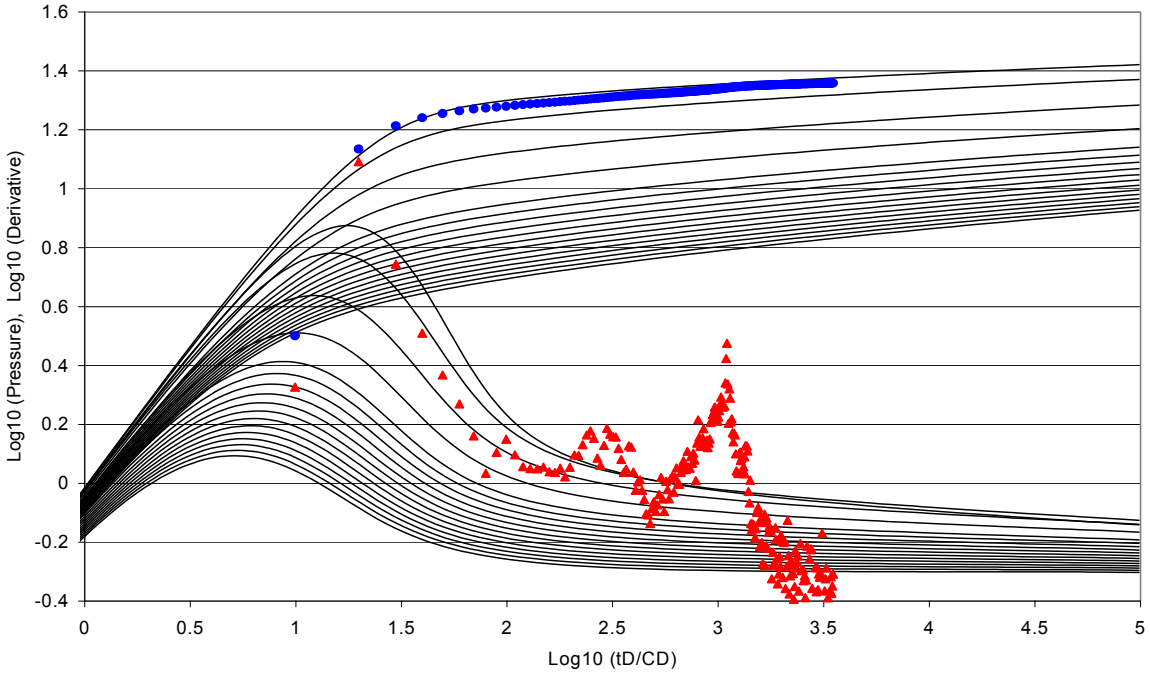

Figure 8-5. Second buildup

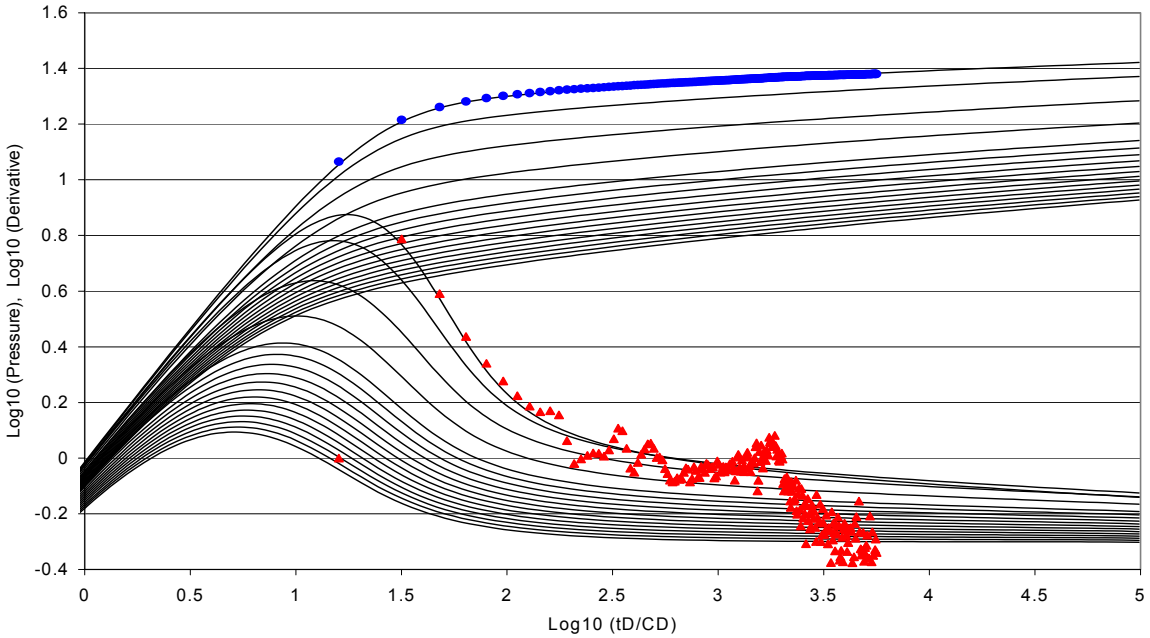

Figure 8-6. Third buildup

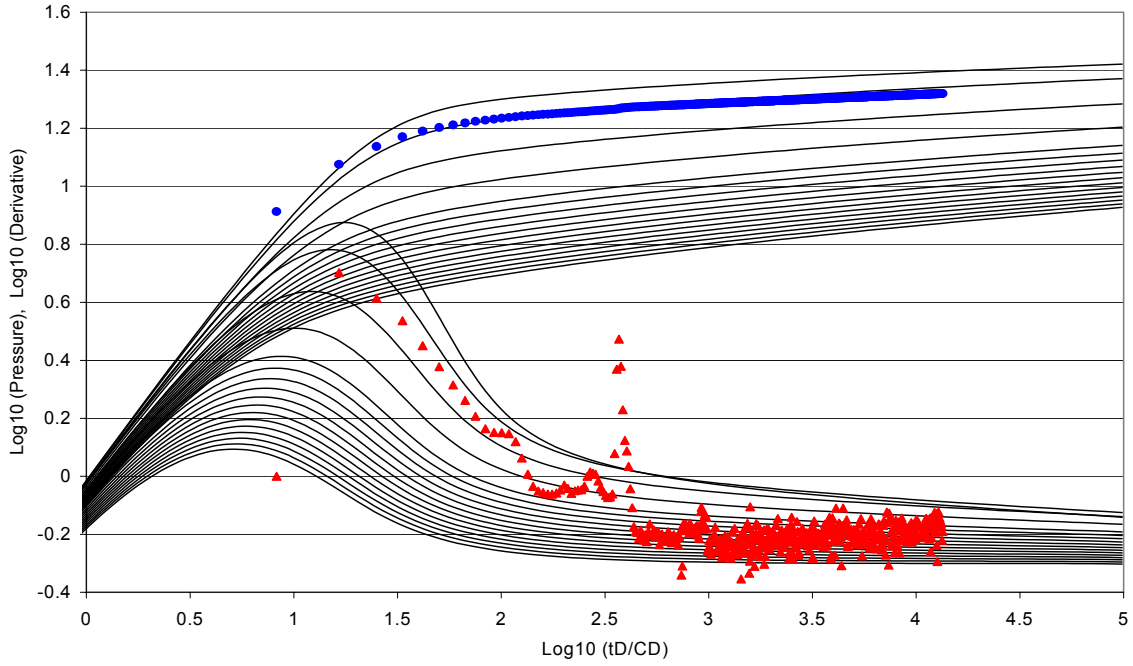

Figure 8-7. Fourth (extended) buildup

Other buildup periods also show the downward trend on the derivative, which gives certain assurance in the validity of the model, but confident analysis is impossible in absence of quality data in the drawdown periods and early-time data in the buildup periods. The data requirements are as follows. We need at least two flow periods followed by two buildups. During the first flow period the flow rate should be fairly low and the duration of the first buildup should be preferably the same as duration of the first drawdown in order for permeability to restore to its initial value. The magnitude of the second flow rate should be higher than that of the first flow period, but preferably low enough to minimize the multi-phase and non-Darcy flow effects . Duration of both flow periods should be long enough in order to observe the data undistorted by the wellbore storage. The second buildup can be of shorter duration and can be terminated as soon the downward trend in the middle-time region is observed.

The data then should plotted using appropriate plotting functions and type curve match should be performed. From the match two values of α will be obtained, which will be in the same proportion as the respective flow rates. Since $\alpha = \beta \frac{\eta}{E} \frac{q_t \mu}{2\pi (kh)_t}$, we will be able to determine the sensitivity of permeability to deformation and the permeability-thickness product. Skin factor in its conventional sense of an additional pressure drop on the well contour can not be determined, rather we will calculate permeability impairment in the near-wellbore zone accordingly to the sensitivity of permeability to deformation. The value of average reservoir pressure can be determined fairly accurately for small sensitivity of permeability to deformation if one extrapolates drawdown and respective buildup data until pressure curves intersect. In general, the value of average reservoir pressure will be overestimated.

Once the parameters have been determined, one can make a decision on the optimal magnitude of the drawdown on the well. In some cases it will make economic sense to limit the production rate, as it will result in less permeability reduction and less reservoir drawdown needed to maintain this rate. Fracturing can be very beneficial in the sense that it allows economically produce a well with low drawdown.

We have seen that the majority of permeability reduction occurs in the near-wellbore zone. This reduction is the greater the lower is the permeability of this zone, which makes the problems of introduced near-wellbore damage and of fines migration more acute.

9 CONCLUSIONS

The developed model of fluid flow in a deformable reservoir incorporates elastic properties of the system "reservoir – surrounding rock mass" to calculate deformations in this system due to pore pressure change caused by well operation. We use a formal model of a uniform reservoir with permeability assumed to be a strong function of vertical deformation of the reservoir. This approach is suitable to describe the behavior of a naturally fractured reservoir and some other possible situations. Solution to problems of fluid flow in deformable multi-layer reservoir with account for wellbore storage, skin, and crossflow between layers were obtained by finite-difference methods. We have solved numerically several problems with typical boundary conditions and made the following conclusions.

- The deformation of a reservoir depends on the elastic properties of the entire system comprised of the reservoir itself and the embedding rock mass.
- The behavior of a drawdown (injection) test is inconsistent with a buildup (falloff) test. The respective tests should be analyzed with different sets of type curves.
- The processes of production and injection are asymmetric.
- During drawdown/buildup test, the permeability-thickness product in a stress-sensitive reservoir appears to be decreasing/increasing with time as the test continues.
- The presence of several layers with different properties tends to mask the characteristic drawdown response and to a lesser degree the characteristic buildup response. The greater is the properties contrast of the layers, the more the behavior of both tests is obscured. These effects are due to the interaction of the pressure and deformation fields in individual layers.

- The drawdown response of a highly heterogeneous reservoir with stress-dependent permeability is practically indistinguishable from the response of a homogeneous reservoir with no stress-dependence. The buildup response may still provide a qualitative indication of permeability stress-sensitivity.
- In order to estimate the parameters of a stress-sensitive reservoir at least two drawdown-buildup sequences are required. The magnitudes of flow rates during drawdown periods must be selected so that to minimize the multi-phase and non-Darcy flow effects at the largest possible difference between the two rates.
- The results qualitatively agree with the field data, thus suggesting an explanation to phenomena observed in practice. For quantitative analysis the tests should designed and run accordingly to the recommended here procedure.

REFERENCES

1. Diyashev, R.N., Kosterin, A.V., and Scvortsov, E.V.: *Fluid Flow in Deformable Oil Reservoirs*, Kazan Math. Society, Kazan, Russia (1999).

2. Yentov, V.M., and Malakhova, T.A.: "On Change of Stress-Strain State of Rock Mass, Caused by Pressure Change in Fluid-Saturated Reservoir", *Izvestiya Akademii Nauk SSSR, Mekhanika Tverdogo Tela*, (1974) No 6,.

3. Raghavan, R., Scorer, J.D.T., and Miller, F.G.: "An Investigation by Numerical Methods of the Effect of Pressure-Dependent Rock and Fluid Properties on Well Flow Tests", paper SPE 2617 presented at 1969 SPE Annual Fall Meeting, Denver, Colorado, 28 September – 1 October.

4. Vairogs, J., Hearn, C.L., Dareing, D.W., and Rhoades, V.W.: "Effect of Rock Stress on Gas Production From Low-Permeability Reservoirs", paper SPE 3001 presented at 1970 SPE Annual Fall Meeting, Houston, Texas, 4-7 October.

5. Vairogs, J., and Rhoades, V.W.: "Pressure Transient Tests in Formations Having Stress-Sensitive Permeability", paper SPE 4050 presented at 1972 SPE-AIME Annual Fall Meeting, San Antonio, Texas, 8-11 October.

6. Evers, J.F., and Soeiinah, E.: "Transient Tests and Long-Range Performance Predictions in Stress-Sensitive Gas Reservoirs", paper SPE 5423 presented at 1975 SPE-AIME Northern Plains Regional Meeting, Omaha, Nebraska, 15-18 May.

7. Pedrosa, O.A.: "Pressure Transient Response in Stress-Sensitive Formations", paper SPE 15115 presented at the 1986 SPE California Regional Meeting, Oakland, California, 2-4 April.

8. Celis, V., Silva, R., Ramones, M., Intevep, S.A., and Guerra, J.: "A New Model for Pressure Transient Analysis in Stress Sensitive Naturally Fractured Reservoirs", paper SPE 23668 presented at the 1992 Second Latin American Petroleum Engineering Conference, Caracas, Venezuela, 8-11 March.

9. Buchsteiner, H., Warpinski, N.R., and Economides, M..J.: "Stress-Induced Permeability Reduction in Fissured Reservoirs", paper SPE 26513 presented at the 1993 SPE Annual Technical Conference and Exhibition, Houston, Texas, 3-6 October.

10. Economides, M..J., Buchsteiner, H., and Warpinski, N.R.: "Step-Pressure Test for Stress-Sensitive Permeability Determination", paper SPE 27380 presented at the 1994 SPE Intl. Symposium on Formation Damage Control, Lafayette, Louisiana, 7-10 February.

11. Zhang, M.Y., and Ambastha, A.K.: "New Insights in Pressure-Transient Analysis for Stress-Sensitive Reservoirs", paper SPE 28420 presented at the 1994 SPE Annual Technical Conference and Exhibition, New Orleans, Louisiana, 25-28 September.

12. Ostensen, R.W.: "The Effect of Stress-Dependent Permeability on Gas Production and Well Testing", paper SPE 11220 presented at the 1982 SPE Annual Fall Meeting, New Orleans, Louisiana, 26-29 September.

13. Ostensen, R.W.: "Microcrack Permeability in Tight Gas Sandstone", paper SPE 10924, *SPEJ* (December 1983).

14. Ganghi, A.F.: "Variation of Whole and Fractured Porous Rock Permeability with Confining Pressure", *Intl. J. Rock Mech. Min. Sci. & Geomech.,* Vol. 15, Pergamon Press (1978).

15. Cuisiat, F., Gutierrez, M., Lewis, R.W., and Masters, I.: "Petroleum Reservoir Simulation Coupling Flow and Deformation", paper SPE 50636 presented at SPE Europec'98, The Hague, The Netherlands, 20-22 October.

16. Osorio, J.G., Wills, A., and Alcalde, O.R.: "A Numerical Model to Study the Formation Damage by Rock Deformation from Well Test Analysis", paper SPE 73742 presented at the 2002 SPE International Symposium and Exhibition on Formation Damage Control, Lafayette, Louisiana, 20-21 February.

17. Chin, L.Y., Raghavan, R., and Thomas, L.K.: "Fully Coupled Geomechanics and Fluid-Flow Analysis of Wells With Stress-Dependent Permeability", paper SPE 58968, *SPEJ* (March 2000) 5 (1).

18. Yentov, V.M., Malakhova, T.A., and Marmorshtein, L.M.: "Influence of Fluid Pressure Change in a Reservoir on Flow Characteristics of Adjacent Layers", *Izvestiya VUZov, Neft' I Gaz* (1977) 4.

19. Zazovskii, A.F.: "Stress State in the Vicinity of a Production Well in a Fluid-Saturated Reservoir", *Izvestiya Akademii Nauk SSSR, Mekhanika Tverdogo Tela* (1980) 3.

20. Nikolayevskii, V.N., and Ramazanov, T.K.: "Stress State in Rock Mass and Non-Local Transient Flow in Reservoir", *Izvestiya Akademii Nauk SSSR, Mekhanika Tverdogo Tela* (1977) 3.

21. Nikolayevskii, V.N., and Ramazanov, T.K.: "Fluid Flow and Stress-Strain State of a Reservoir", *Izvestiya SO Akademii Nauk SSSR, FTPRPI* (1982) 5.

22. Lewis, R.W., Schrefler, B.A., and Simoni, L.: "Coupling versus Uncoupling in Soil Consolidation", *Intl. J. for Numerical and Analytical Methods in Geomechanics* (1991) 15.

23. Dobrinin, V.M.: *Deformations and Alteration of Physical Properties of Hydrocarbons-Bearing Rocks*, Nedra, Moscow (1970).

24. Lewis, R.W., Roberts, G.K., and Zienkiewicz, O.C.: "A Non Linear Flow and Deformation Analysis of Consolidation Problems", Proc. of 2nd Intl. Conf. Numerical Methods in Geomechanics, Blacksburg, Virginia, 1976.

25. Gubanov, B.F. "*Investigation and Development of Methods and Technology of Stimulation to Increase Volumetric Recovery Efficiency*", D. Tech. Sci Dissertation., Moscow (1981).

26. Gubanov, B.F., and Zheltov, Yu.P.: "Application of High Injection Pressures in Reservoir Management", *Trudi VNII* (1968) 54.

27. Chernikov, O.A., Andreeva, Yu.I., and Il'in, V.Ya.: "Influence of Pressure on Flow Characteristics of Sandstones and Carbonates", *Problems of Petroleum Geology, IGRGI* (1977) 14.

28. Blinov, A.F., and Zainullin, N.G.: "Spinner Measurements on Injection Wells in Romashkino Field", in *Problems of Geology, Hydrodynamics, and Physics of Reservoirs*, Nedra, Moscow (1965).

29. Diyashev, R.N.: *Commingled Development of Oil Reservoirs*, Nedra, Moscow (1984).

30. Novatskii, V.: *Elasticity Theory*, Mir, Moscow (1975).

31. Gradshtein, I.S., and Ryzhik, Ya.S.: *Tablitsi Integralov, Summ, Ryadov i Proizvedenii*, Nauka, Moscow (1964).

32. Ehlig-Economides, C. A., and Joseph, J. A.: "A New Test for Determination of Individual Layer Properties in a Multilayered Reservoir", paper SPE 14167 presented at the

1985 SPE Annual Technical Conference and Exhibition, Las Vegas, Nevada, 22-25 September.

33. Press, W.H., Teukolsky, S.A., Vetterling, W.T., and Flannery, B.P.: "*Numerical Recipes in FORTRAN: The Art of Scientific Computing*", Cambridge University Press, New York City (1992).

34. Ehlig-Economides, C.A., and Ramey, H.J., Jr.: "Transient Rate Decline Analysis for Wells Produced at Constant Pressure", *SPEJ* (February 1981).

APPENDIX

Driver

```
Option Explicit
Option Base 1
Public nx As Integer, nl As Integer, ntau As Integer, m As Integer
Public tauInit As Double, tau As Double, tauMult As Double, TotalTime As
Double, sa() As Double
Public dx As Double, reD As Double, rD() As Double, u() As Double, Eo As
Double, CD As Double, pwD As Double, p_mult As Double
Public MaxT As Double, MaxP As Double, ConstantPwD As Double, qq As
Double, pwDinit As Double, q As Double, pres As Double, muo As Double
Public bDone As Boolean, bConstantQ As Boolean, bNoFlow As Boolean,
bSparse As Boolean
Public Points As Collection, Layers As Collection, Reservoir As
cls05Reservoir
Public Initialize As cls01Initialize, FlProp As cls02FlProp, Layer As
cls03Layer, Point As cls04Point
Public ExitCriteria As clsExitCriteria, Newton As clsNewton
Public Vector As clsVector, Matrix As clsMatrix, Outp As clsOut
Public VEH As clsVEH, bDrawDown As Boolean, bBuildUp As Boolean, bBoth As
Boolean, PrintFrequency As Integer

Sub MainProg()
Dim timestart As Double, x() As Double, check As Boolean, niter As Integer
'    On Error GoTo 3
    Set Initialize = New cls01Initialize
    timestart = Timer
1   Call Initialize.WhatToRun(x)
    While Not bDone
        ntau = ntau + 1
        TotalTime = TotalTime + tau
        If bConstantQ Then
            Call Newton.Run(x, check, niter)
        Else
            While Not ExitCriteria.bConverged(x)
                Call Reservoir.SetLayersPressure(x)
                Reservoir.Pressure
                Call Reservoir.Deformation(0, 0)
                Reservoir.CalculateLayersPermeability
                Call Vector.Progonka(x)
            Wend
        End If
        Reservoir.UpdateLayersPressure
        Outp.Intermediate
        tau = tau * tauMult
        Call ExitCriteria.Evaluate(x)
    Wend
    Sheets("Input").Cells(30, 2) = Timer - timestart
    Exit Sub
    If bBoth Then GoTo 1
    Exit Sub
3   Sheets("Input").Cells(30, 2) = "Error"
End Sub
--------------------------------------------------------------------------
---------------------------------
```

Initialization

```
Option Explicit
Option Base 1
Private ms_ftype As String, md_Pb As Double, md_H2S As Double, md_CO2 As
Double, md_N2 As Double, md_T As Double
Private md_API As Double, md_SGG As Double, md_Rsb As Double, md_Rs As
Double
Private mb_bProd As Boolean, md_LayerParams() As Double, md_kht As Double,
md_phiht As Double, md_1ci As Double
Private md_pres As Double, md_qwell As Double

Sub Class_Initialize()
    ReadSpreadsheetData
    InitializeFileReader
    PerformAuxCalculations
    InitializeFluidProperties
    InitializeLayers
    InitializePoints
    InitializeReservoir
    Set ExitCriteria = New clsExitCriteria
    Set Outp = New clsOut
    Set Vector = New clsVector
    Set Matrix = New clsMatrix
    Set Newton = New clsNewton
    Set VEH = New clsVEH
End Sub
Private Sub ReadSpreadsheetData()
Dim item As Variant, j As Integer, rw As Double, re As Double
    Sheets("Input").Activate
    For Each item In ActiveWorkbook.Names
        Select Case item.Name
            Case Is = "q":      md_qwell = Range(item.Name).Value
            Case Is = "pres":   pres = Range(item.Name).Value
            Case Is = "CD":     CD = Range(item.Name).Value
            Case Is = "pwD":    ConstantPwD = Range(item.Name).Value
            Case Is = "tau":    tauInit = Range(item.Name).Value
            Case Is = "taum":   tauMult = Range(item.Name).Value
            Case Is = "tmax":   MaxT = Range(item.Name).Value
            Case Is = "pmax":   MaxP = Range(item.Name).Value
            Case Is = "E":      Eo = Range(item.Name).Value
            Case Is = "nl":     nl = Range(item.Name).Value
            Case Is = "brw":    bConstantQ = Range(item.Name).Value
            Case Is = "bre":    bNoFlow = Range(item.Name).Value
            Case Is = "both":   bBoth = Range(item.Name).Value
            Case Is = "rw":     rw = Range(item.Name).Value
            Case Is = "re":     re = Range(item.Name).Value

            Case Is = "prod":   mb_bProd = Range(item.Name).Value
            Case Is = "API":    md_API = Range(item.Name).Value
            Case Is = "SGG":    md_SGG = Range(item.Name).Value
            Case Is = "Rsb":    md_Rsb = Range(item.Name).Value
            Case Is = "yH2S":   md_H2S = Range(item.Name).Value
            Case Is = "yCO2":   md_CO2 = Range(item.Name).Value
            Case Is = "yN2":    md_N2 = Range(item.Name).Value
            Case Is = "Pb":     md_Pb = Range(item.Name).Value
            Case Is = "T":      md_T = Range(item.Name).Value
```

```
            Case Is = "fltype": ms_ftype = Range(item.Name).Value
            Case Else
        End Select
    Next item
    reD = re / rw
    md_kht = 0#
    md_phiht = 0#
    md_1ci = 0#
    ReDim md_LayerParams(nl, 7)
    Cells(9, 8).Select
    For j = 1 To nl
        md_LayerParams(j, 1) = ActiveCell.Offset(j - 1, 0)      'h
        md_LayerParams(j, 2) = ActiveCell.Offset(j - 1, 1)      'phi
        md_LayerParams(j, 3) = ActiveCell.Offset(j - 1, 2)      'k
        md_LayerParams(j, 4) = ActiveCell.Offset(j - 1, 3)      'E
        md_LayerParams(j, 5) = ActiveCell.Offset(j - 1, 4)      's
        md_LayerParams(j, 6) = ActiveCell.Offset(j - 1, 5)      'alfa
        md_LayerParams(j, 7) = ActiveCell.Offset(j - 1, 7)      'xFlow
        md_kht = md_kht + md_LayerParams(j, 3) * md_LayerParams(j, 1)
        md_phiht = md_phiht + md_LayerParams(j, 2) * md_LayerParams(j, 1)
        md_1ci = md_1ci + md_LayerParams(j, 1) / (md_LayerParams(j, 4) /
Eo)
    Next j
End Sub
Private Sub PerformAuxCalculations()
Dim a As Double, i As Integer
    a = 1#
    i = 0
    While a < 10#
        i = i + 1
        a = a * tauMult
    Wend
    PrintFrequency = Application.WorksheetFunction.Max(1, CInt(i / 10))
    If mb_bProd Then                                    'production
        qq = 1#
    ElseIf Not mb_bProd Then                            'injection
        qq = -1#
    End If
    If Not bConstantQ Then qq = 0#
    dx = 1# / (nx - 1)
    ReDim rD(nx)
    For i = 1 To nx
        rD(i) = CDbl(i - 1) * dx
    Next i
    m = nx * nl
    bDrawDown = False
    bBuildUp = False
End Sub
Private Sub InitializeLayers()
Dim j As Integer, lParams() As Double
    Set Layers = New Collection
    For j = 1 To nl
        Set Layer = New cls03Layer
        ReDim lParams(7)
        lParams(1) = md_LayerParams(j, 1):  lParams(2) = md_LayerParams(j,
2):  lParams(3) = md_LayerParams(j, 3)
```

```
        lParams(4) = md_LayerParams(j, 4):  lParams(5) = md_LayerParams(j,
5):  lParams(6) = md_LayerParams(j, 6)
        lParams(7) = md_LayerParams(j, 7)
        Call Layer.SetConstantParameters(lParams, md_kht, md_phiht)
        Layers.Add Layer
    Next j
End Sub
Private Sub InitializeReservoir()
    Set Reservoir = New cls05Reservoir
    Reservoir.oneci = md_1ci
End Sub
Private Sub InitializeFluidProperties()
    Set FlProp = New cls02FlProp
    Call FlProp.ReadData(md_API, md_SGG, md_Pb, md_Rsb, md_H2S, md_CO2,
md_N2, md_T, ms_ftype)
    p_mult = (md_qwell * 1.84027) * FlProp.muo(pres) / 2# /
Application.WorksheetFunction.Pi() / (md_kht * 0.001 * 100#)
End Sub
Private Sub InitializePoints()
Dim Point As cls04Point, i As Integer, j As Integer, a1 As Double, a2 As
Double
    Set Points = New Collection
    For i = 1 To nx
        Input #1, j, a1, a2
        Set Point = New cls04Point
        Point.number = j
        Point.small = a1
        Point.ints = a2
        Points.Add Point
    Next i
    For Each Point In Points
        With Point
            .SetArrays
            For i = 1 To .number
                Input #1, a1, a2
                .xx(i) = a1
                .yy(i) = a2
            Next i
        End With
    Next
    Close #1
End Sub
Private Sub InitializeFileReader()
Dim aCalc As Single, aRead As Single, DataPath As String, FoundFile As
String
    DataPath = ThisWorkbook.Path & "\Data\reD=" & CStr(reD)
    aCalc = CStr(Cells(21, 8))
    FoundFile = Dir(DataPath & "\??????????????????????.txt")
    Do While FoundFile <> ""
        Open DataPath & "\" & FoundFile For Input As #1
        Input #1, nx, aRead
        If Abs(1# - aCalc / aRead) * 100# < 0.001 Then Exit Sub
        Close #1
        FoundFile = Dir()
    Loop
End Sub
Private Sub BuildUp()
```

```
    tau = tauInit
    ntau = 0
    TotalTime = 0#
    qq = 0#
    bDone = False
    bDrawDown = False
    bBuildUp = True
    bConstantQ = True
    qq = 0#
    pwDinit = pwD
End Sub
Private Sub DrawDown()
    tau = tauInit
    ntau = 0
    TotalTime = 0#
    bDone = False
    bDrawDown = True
    bBuildUp = False
    If bConstantQ Then
        pwDinit = 0#
    Else
        pwDinit = ConstantPwD
    End If
End Sub
Sub WhatToRun(x)
    ReDim x(m)
    If bBoth And Not bDrawDown Then
        DrawDown
    ElseIf (bBoth And bDrawDown) Or Not bBoth Then
        BuildUp
'        Call Output.Retrieve(x)
        bBoth = False
    End If
    pwD = pwDinit
End Sub
```

Fluid properties

```
Option Explicit
Option Base 1
Private md_API As Double, md_SGG As Double, md_Rsb As Double, md_H2S As
Double, md_CO2 As Double, md_N2 As Double
Private md_Tsc As Double, md_Psc As Double, md_T As Double, md_Pb As
Double, md_STO As Double
Sub Class_Initialize()
    md_Tsc = 60#
    md_Psc = 14.696
End Sub
Sub ReadData(API, SGG, Pb, Rsb, H2S, CO2, N2, T, ftype)
    md_API = API:   md_SGG = SGG:   md_Rsb = Rsb:   md_H2S = H2S:   md_CO2
= CO2:   md_N2 = N2
    md_T = T:       md_STO = 141.5 / (md_API + 131.5):
    If Pb = 0# Then
        md_Pb = Pbub
    Else
        md_Pb = Pb
    End If
```

```
End Sub
Property Get co(p) As Double
   If p < md_Pb Then
'        co = Exp(-7.633 - 1.497 * Log(p) + 1.115 * Log(md_T + 459.67) +
0.533 * Log(md_API))
'        If md_Rsb <> 0 Then co = co * Exp(0.184 * Log(md_Rsb))
        co = Exp(-7.573 - 1.45 * Log(p) - 0.383 * Log(md_Pb) + 1.402 *
Log(md_T + 459.67) + 0.256 * Log(md_API))
        If md_Rsb <> 0 Then co = co * Exp(0.449 * Log(md_Rsb))
    Else
        co = (-1433# + 5# * md_Rsb + 17.3 * md_T - 1180# * md_SGG + 12.61
* md_API) * 0.00001 / p
    End If
End Property
Property Get muo(p) As Double
    muo = 10 ^ (10 ^ (1.8653 - 0.025086 * md_API - 0.5644 * Log(md_T) /
Log(10#))) - 1#
    muo = (10.715 * (Rso(p) + 100#) ^ -0.515) * muo ^ (5.44 * (Rso(p) +
150#) ^ -0.338)
    If p > md_Pb Then muo = muo * (p / md_Pb) ^ (2.6 * p ^ 1.187 * Exp(-
11.513 - 0.0000898 * p))
End Property
Property Get Rso(p) As Double
Dim alpha As Double, beta As Double, gamma As Double, pr As Double, Rsr As
Double
    If p < md_Pb Then
        pr = (p - 14.7) / (md_Pb - 14.7)
        alpha = 0.000000973 * md_SGG ^ 1.672608 * md_API ^ 0.92987 * md_T
^ 0.247235 * (md_Pb - 14.7) ^ 1.056052
        beta = 0.022339 * md_SGG ^ -1.00475 * md_API ^ 0.337711 * md_T ^
0.132795 * (md_Pb - 14.7) ^ 0.302065
        gamma = 0.725167 * md_SGG ^ -1.48548 * md_API ^ -0.164741 * md_T ^
-0.09133 * (md_Pb - 14.7) ^ 0.047094
        Rsr = alpha * pr ^ beta + (1# - alpha) * pr ^ gamma
        Rso = md_Rsb * Rsr
        If Rso < 0# Then Rso = 0#
    Else
        Rso = md_Rsb
    End If
End Property
Property Get Bo(p) As Double
Dim DRO As Double
    If p < md_Pb Then
        DRO = rhoo(p)
        Bo = (63.37 * md_STO + 0.01357 * Rso(p) * md_SGG) / DRO
    Else
        DRO = rhoo(md_Pb)
        Bo = (63.37 * md_STO + 0.01357 * Rso(p) * md_SGG) / DRO
        Bo = Bo * Exp(co(p) * (md_Pb - p))
    End If
End Property
Property Get rhoo(p) As Double
Dim iter As Integer, ddone As Boolean, DA As Double, DN As Double
    iter = 0
    ddone = False
    DN = 52.8 - 0.01 * Rso(p)
    While Not ddone
```

```
        iter = iter + 1
        DA = -49.893 + (85.0149 - (3.70373 - 0.047981 * DN) * DN) * md_SGG
+ (2.98914 - 0.035688 * DN) * DN
        rhoo = (Rso(p) * md_SGG + 4600# * md_STO) / (73.71 + Rso(p) *
md_SGG / DA)
        If Abs(rhoo - DN) < 0.000001 Then
            ddone = True
        Else
            DN = rhoo
        End If
        If iter > 100 Then
            ddone = True
            Debug.Print "WARNING -- DENSITY CALCULATION DID NOT CONVERGE"
        End If
    Wend
    If p < md_Pb Then
        rhoo = rhoo + (0.167 + 16.81 * 10 ^ (-0.0425 * rhoo)) * (p /
1000#) _
                    - 0.01 * (0.299 + 263 * 10 ^ (-0.0603 * rhoo)) *
(p / 1000#) ^ 2
    Else
        rhoo = rhoo + (0.167 + 16.81 * 10 ^ (-0.0425 * rhoo)) * (md_Pb /
1000#) _
                    - 0.01 * (0.299 + 263# * 10 ^ (-0.0603 * rhoo)) *
(md_Pb / 1000#) ^ 2
    End If
    rhoo = rhoo - (0.00302 + 1.505 * rhoo ^ (-0.951)) * (md_T - md_Tsc) ^
0.938 _
                + (0.0233 * 10 ^ (-0.0161 * rhoo)) * (md_T - md_Tsc)
^ 0.475
    If p > md_Pb Then rhoo = rhoo * Exp(co(p) * (p - md_Pb))
End Property
Property Get Pbub() As Double
Dim VX As Double, VY As Double
    VX = 0.013098 * md_T ^ 0.282372 - 0.0000082 * md_API ^ 2.176124
    VY = md_Rsb ^ 0.081465 * md_SGG ^ -0.161488 * 10 ^ VX - 0.740152
    Pbub = 1091.47 * VY ^ 5.354891
End Property
Property Get dRso_dp(p, Pb, Rsb, API, gasgrav, Tf) As Double
Dim pr As Double
    pr = (p - 14.7) / (md_Pb - 14.7)
    If pr <= 1# Then
        VA = 0.000000973 * md_SGG ^ 1.672608 * md_API ^ 0.92987 * md_T ^
0.247235 * (md_Pb - 14.7) ^ 1.056052
        VB = 0.022339 * md_SGG ^ (-1.00475) * md_API ^ 0.337711 * md_T ^
0.132795 * (md_Pb - 14.7) ^ 0.302065
        VC = 0.725167 * md_SGG ^ (-1.48548) * md_API ^ -0.164741 * md_T ^
(-0.09133) * (md_Pb - 14.7) ^ 0.047094
        dRso_dp = md_Rsb / (md_Pb - 14.7) * (VB * VA * pr ^ (VB - 1#) + VC
* (1# - VA) * pr ^ (VC - 1#))
    Else
        dRso_dp = 0#
    End If
End Property
Property Get dBo_dp(p) As Double
Dim pr As Double
    pr = (p - 14.7) / (md_Pb - 14.7)
```

```
    If pr <= 1# Then
        dBo_dp = 1.2 * (0.00012) * (Sqr(md_SGG / md_STO) * md_Rs + 1.25 *
md_T) ^ 0.2 * Sqr(md_SGG / md_STO) * dRso_dp(p)
    Else
        dBo_dp = 0#
    End If
End Property
Property Get Bg(p) As Double
    Bg = (zfucktor(p) * (md_T + 460#) / p) * (md_Psc / (md_Tsc + 460#)) *
1000# / 5.61458333
End Property
Property Get cg(p)
Dim zj As Double, zk As Double, pTc As Double, pPc As Double, pTr As
Double, pPr As Double
Dim za As Double, zb As Double, zc As Double, zd As Double, dzB_dpr As
Double, dz_dpr As Double, z As Double
    zj = md_H2S * -0.4582 * 672.12 / 1300 + md_CO2 * -0.90348 * 547.58 /
1071 + md_N2 * -0.66026 * 227.16 / 493.1 + _
        0.11582 + md_SGG * (0.70729 + md_SGG * -0.099397)
    zk = md_H2S * -0.06534 * 672.12 / Sqr(1300#) + md_CO2 * -0.42113 *
547.58 / Sqr(1071#) + _
        md_N2 * -0.91249 * 227.16 / Sqr(493.1) + 3.8216 + md_SGG * (17.438
+ md_SGG * -3.2191)
    pTc = zk * zk / zj
    pPc = pTc / zj
    pTr = (md_T + 460#) / pTc
    pPr = p / pPc
    za = 1.39 * Sqr(pTr - 0.92) - 0.36 * pTr - 0.101
    zb = (0.62 - 0.23 * pTr) * pPr + (0.066 / (pTr - 0.86) - 0.037) * pPr
^ 2 + 0.32 * pPr ^ 6 / 10 ^ (9# * (pTr - 1))
    zc = 0.132 - 0.32 * Application.WorksheetFunction.Log10(pTr)
    zd = Exp(0.3106 + pTr * (-0.49 * pTr * 0.1824))
    dzB_dpr = (0.62 - 0.23 * pTr) + 2# * (0.066 / (pTr - 0.86) - 0.037) *
pPr + 6# * 0.32 * pPr ^ 5 / 10 ^ (9# * (pTr - 1#))
    dz_dpr = -(1# - za) * Exp(-zb) * dzB_dpr + zd * zc * pPr ^ (zd - 1#)
    z = za + (1# - za) / Exp(zb) + zc * pPr ^ zd
    cg = 1# / p - dz_dpr / (pPc * z)
End Property
Property Get mug(p) As Double
Dim Corr_h2s As Double, Corr_co2 As Double, Corr_n2 As Double, Lg10SG As
Double
Dim alpha As Double, beta As Double, gamma As Double, tr As Double, Ma As
Double, DG As Double, DG1  As Double
    Lg10SG = Log(md_SGG) / Log(10#)
    Corr_h2s = md_H2S * (3.73 + 8.49 * Lg10SG) / 1000#
    Corr_co2 = md_CO2 * (6.24 + 9.08 * Lg10SG) / 1000#
    Corr_n2 = md_N2 * (9.59 + 8.48 * Lg10SG) / 1000#
    mug = (17.09 - 2.062 * md_SGG) * md_T / 1000000# + (8.188 - 6.15 *
Lg10SG) / 1000# + Corr_h2s + Corr_co2 + Corr_n2
    tr = md_T + 459.67
    Ma = 28.9625 * md_SGG
    DG = p * Ma / zfucktor(p) / 10.732 / tr / 62.368
    alpha = ((9.379 + 0.01607 * Ma) * tr ^ 1.5) / (209.2 + 19.26 * Ma +
tr)
    beta = 3.448 + 986.4 / tr + 0.01009 * Ma
    gamma = 2.447 - 0.2224 * beta
    DG1 = 14.696 * Ma / 10.732 / tr / 62.368
```

```
    mug = mug * Exp(beta * (DG ^ gamma - DG1 ^ gamma))
End Property
Property Get zfucktor(p) As Double
Dim iter As Integer, ddone As Boolean, j As Double, k As Double, pPc As
Double, pr As Double, TPC As Double
Dim c0 As Double, c1 As Double, c2 As Double, c3 As Double, c4 As Double
Dim dr As Double, dr0 As Double, dr2 As Double, dr5 As Double, dp As
Double, pp As Double
Dim t1 As Double, t2 As Double, t3 As Double, t4 As Double, t5 As Double,
t6 As Double
Dim tr As Double, tr2 As Double, tr3 As Double, tr4 As Double
    j = 0.1158157 + (0.7072878 - 0.0993966 * md_SGG) * md_SGG - 0.2368944
* md_H2S - 0.4619311 * md_CO2 - 0.3041646 * md_N2
    k = 3.821599 + (17.43771 - 3.219084 * md_SGG) * md_SGG - 1.218021 *
md_H2S - 7.046435 * md_CO2 - 9.334518 * md_N2
    TPC = k * k / j
    pPc = TPC / j
    tr = (md_T + 459.67) / TPC
    pr = p / pPc
    If tr < 1# Then MsgBox "WARNING -- TR < 1.0"
    tr2 = tr * tr
    tr3 = tr2 * tr
    tr4 = tr2 * tr2
    c1 = -0.7361 + 0.1844 / tr
    c0 = 0.3265 * tr - 1.07 - 0.5339 / tr2 + 0.01569 / tr3 - 0.05165 / tr4
    c2 = 0.5475 * tr + c1
    c3 = -0.1056 * c1
    c4 = 0.6134 / tr2
    dr = 1#
    iter = 0
    ddone = False
    Do While Not ddone
        dr0 = dr
        dr2 = dr * dr
        dr5 = dr2 * dr2 * dr
        t1 = c0 * dr
        t2 = c2 * dr2
        t3 = c3 * dr5
        t4 = c4 * dr2
        t5 = 0.721 * dr2
        t6 = Exp(-t5)
        pp = (tr + t1 + t2 + t3) * dr + t4 * dr * (1# + t5) * t6
        dp = tr + 2# * t1 + 3# * t2 + 6# * t3 + t4 * t6 * (3# + 3# * t5 -
2# * t5 ^ 2)
        dr = dr0 - (pp - 0.27 * pr) / dp
        If dr <= 0# Then
            dr = 0.5 * dr0
        ElseIf dr >= 3# Then
            dr = dr0 + 0.9 * (3# - dr0)
        End If
        If Abs(dr - dr0) < 0.000001 Then ddone = True
        iter = iter + 1
        If iter > 100 Then
            ddone = True
            Debug.Print "WARNING -- DENSITY CALCULATION DID NOT CONVERGE"
        End If
    Loop
```

```
    zfucktor = 0.27 * pr / (dr * tr)
End Property
```

Layer Class

```
Option Explicit
Option Base 1
Private md_k As Double, md_phi As Double, md_E As Double, md_h As Double,
md_s As Double, md_alpha As Double
Private md_kappa As Double, md_omega As Double, md_lambda As Double,
md_gamma As Double, md_hgamma As Double
Private md_q As Double, md_z() As Double, md_p() As Double, md_pnew() As
Double, md_u() As Double, md_perm() As Double
Private md_t0 As Double, md_t1 As Double, md_t2 As Double, md_t3 As
Double, md_t4 As Double, md_t5 As Double, md_t6 As Double
Private md_a() As Double, md_b() As Double, md_c() As Double, md_d() As
Double, md_zz() As Double
Private md_aa As Double, md_sigma As Double, md_sigma1 As Double, md_Xflow
As Double
Sub Class_Initialize()
Dim i As Integer
    ReDim md_p(nx):     ReDim md_pnew(nx):      ReDim md_u(nx):     ReDim
md_z(nx):     ReDim md_perm(nx)
    For i = 1 To nx
        md_perm(i) = 1#
        md_z(i) = reD ^ (2# * dx * (i - 1))
    Next i
    ReDim md_zz(nx):    md_zz(1) = md_z(2) - md_z(1):
md_zz(nx) = md_z(nx) - md_z(nx - 1)
    For i = 2 To nx - 1
        md_zz(i) = md_z(i + 1) - md_z(i - 1)
    Next i
End Sub
Sub SetConstantParameters(LayerParams, kht, phiht)
    md_h = LayerParams(1)
    md_phi = LayerParams(2)
    md_k = LayerParams(3)
    md_E = LayerParams(4)
    md_s = LayerParams(5)
    md_alpha = LayerParams(6)
    md_Xflow = LayerParams(7)

    md_kappa = md_k * md_h / kht
    md_omega = md_phi * md_h / phiht
    md_lambda = Log(reD) ^ 2 * md_omega / md_kappa * dx ^ 2
    md_gamma = md_E / Eo
    md_hgamma = md_h / md_gamma
    md_q = md_k * md_h / kht
    md_sigma = 0.7
    md_sigma1 = 1# - md_sigma
End Sub
Property Get hgamma() As Double
    hgamma = md_hgamma
End Property
Property Get q() As Double
    q = md_q
End Property
Property Get pnew(Index As Integer) As Double
```

```
    pnew = md_pnew(Index)
End Property
Property Get ul(Index As Integer) As Double
    ul = md_u(Index)
End Property
Property Get perm(Index As Integer) As Double
    perm = md_perm(Index)
End Property
Sub Permeability()
Dim i As Integer, ptrue As Double
    For i = 1 To nx
        md_u(i) = (u(i) + md_pnew(i)) / md_gamma
        ptrue = (pres / 14.696 - md_pnew(i) * p_mult * md_h) * 14.696
        md_perm(i) = Exp(-md_alpha * md_u(i)) / FlProp.muo(ptrue) *
FlProp.muo(pres)
    Next i
End Sub
Private Sub CalculateVariableParameters()
    md_t0 = 2# * md_perm(1) / (2# - Log(md_perm(2)) + Log(md_perm(1)))
    md_t1 = md_t0 * md_kappa / Log(reD) / dx
    md_t2 = md_t0 * dx / tau * md_omega * Log(reD) / 2# / md_perm(1)
    md_t3 = md_lambda / tau
End Sub
Sub CalculateArrays()
    CalculateVariableParameters
    GenerateArray
    GenerateInnerBC
    If Not bConstantQ Then tridag
End Sub
Private Sub GenerateInnerBC()
Dim qImplicit As Double, qExplicit As Double, deriv As Double
    If bConstantQ Then
        qImplicit = -(md_t1 + md_t2) * md_pnew(1) + md_t1 * md_pnew(2) +
md_t2 * md_p(1)
        qExplicit = -md_t2 * md_pnew(1) - (md_t1 - md_t2) * md_p(1) +
md_t1 * md_p(2)
        md_aa = md_sigma * qImplicit + md_sigma1 * qExplicit
        deriv = CD / tau * (-md_pnew(1) + pwD)
        md_a(1) = deriv + md_aa
    Else
        md_b(1) = 1#
        md_d(1) = ConstantPwD
    End If
End Sub
Sub RetrieveArray(a, aa)
    a = md_a:     aa = md_aa
End Sub
Sub pqAndPwd()
    md_q = -(md_t1 + md_t2) * md_pnew(1) + md_t1 * md_pnew(2) + md_t2 *
md_p(1)
    If bConstantQ Then
        pwD = md_pnew(1) + md_s / md_kappa * md_q
    Else
        pwD = ConstantPwD
        md_pnew(1) = pwD + md_s / md_kappa * md_q
    End If
    md_p = md_pnew
```

```
End Sub
Private Sub GenerateArray()
Dim i As Integer, am As Double, ap As Double, g As Double, a As Double, b
As Double, c As Double, d As Double
    ReDim md_a(nx):     ReDim md_b(nx):     ReDim md_c(nx):     ReDim
md_d(nx)
    For i = 2 To nx - 1
        g = md_t3 * md_z(i)
        am = (md_perm(i) + md_perm(i - 1)) * 0.5
        ap = (md_perm(i) + md_perm(i + 1)) * 0.5
        a = am * md_sigma
        c = ap * md_sigma
        b = -(a + c) - g
        d = -g * md_p(i) + am * (md_p(i) - md_p(i - 1)) * md_sigma1 - ap *
(md_p(i + 1) - md_p(i)) * md_sigma1
        If bConstantQ Then
            md_a(i) = a * md_pnew(i - 1) + b * md_pnew(i) + c * md_pnew(i
+ 1) - d
        Else
            md_a(i) = a:        md_b(i) = b:        md_c(i) = c:
md_d(i) = -d
        End If
    Next i
    If bConstantQ Then
        md_a(nx) = -md_pnew(nx)
        If bNoFlow Then md_a(nx) = md_a(nx) + md_pnew(nx - 1)
    Else
        md_b(nx) = 1#
        If bNoFlow Then md_a(nx) = -1#
'        If bNoFlow Then md_d(nx) = -1#
    End If
End Sub
Property Let pnew(Index As Integer, ByVal pnewVal As Double)
    md_pnew(Index) = pnewVal
End Property
Sub RetrievePKU(a1, a2, a3)
    a1 = md_pnew:    a2 = md_perm:    a3 = md_u
End Sub
Sub RetrievePnew(a1)
    a1 = md_pnew
End Sub
Sub tridag()
Dim j As Integer, bet As Double, gam(500) As Double
    If md_b(1) = 0# Then MsgBox "tridag: rewrite equations"
    bet = md_b(1)
    md_pnew(1) = md_d(1) / bet
    For j = 2 To nx
        gam(j) = md_c(j - 1) / bet
        bet = md_b(j) - md_a(j) * gam(j)
        If bet = 0# Then MsgBox "pause 'tridag failed"
        md_pnew(j) = (md_d(j) - md_a(j) * md_pnew(j - 1)) / bet
    Next j
    For j = nx - 1 To 1 Step -1
        md_pnew(j) = md_pnew(j) - gam(j + 1) * md_pnew(j + 1)
    Next j
End Sub
```

Point Class

```
Option Explicit
Option Base 1
Private mi_number As Integer, md_small As Double, md_ints As Double
Private md_xx() As Double, md_yy() As Double, md_pane() As Double
Property Let number(numberVal As Integer)
    mi_number = numberVal
End Property
Property Get number() As Integer
    number = mi_number
End Property
Property Let small(smallVal As Double)
    md_small = smallVal
End Property
Property Get small() As Double
    small = md_small
End Property
Property Let ints(intsVal As Double)
    md_ints = intsVal
End Property
Property Get ints() As Double
    ints = md_ints
End Property
Sub SetArrays()
    ReDim md_xx(mi_number)
    ReDim md_yy(mi_number)
    ReDim md_pane(mi_number)
End Sub
Property Get xx(Index As Integer) As Double
    xx = md_xx(Index)
End Property
Property Let xx(Index As Integer, ByVal xxVal As Double)
    md_xx(Index) = xxVal
End Property
Property Get yy(Index As Integer) As Double
    yy = md_yy(Index)
End Property
Property Let yy(Index As Integer, ByVal yyVal As Double)
    md_yy(Index) = yyVal
End Property
Property Get pane(Index As Integer) As Double         'these are panels
    pane = md_pane(Index)
End Property
Property Let pane(Index As Integer, ByVal paneVal As Double)
    md_pane(Index) = paneVal
End Property
```

Reservoir Class

```
Option Explicit
Option Base 1
Private ep As cls04Point, el As cls03Layer
Private md_1ci As Double, md_p() As Double, md_q As Double, md_integral()
As Double, mi_NotEqual() As Integer
Sub Class_Initialize()
    ReDim u(nx)
    ReDim md_integral(nx)
End Sub
```

```
Property Let oneci(oneciVal As Double)
    md_1ci = oneciVal
End Property
Sub Pressure()
Dim i As Integer, s As Double
    ReDim md_p(nx)
    For i = 1 To nx
        s = 0#
        For Each el In Layers
            s = s + el.pnew(i) * el.hgamma
        Next
        md_p(i) = s
    Next i
End Sub
Sub Deformation(jjj, ind)
Dim i As Integer, j As Integer, k As Integer, n As Integer, khi As
Integer, klo As Integer
Dim i1 As Integer, i2 As Integer, jj As Integer
Dim x1 As Double, x2 As Double, f1 As Double, f2 As Double, f As Double,
ff As Double, s As Double, up As Double
    ReDim u(nx)
    i = 0
    If jjj = 0 Then
        For Each ep In Points
            With ep
                i = i + 1
                s = 0#
                n = .number
                x1 = .xx(1)
                klo = 1
                khi = nx / 4
                Call fappar(klo, khi, x1, f)
                f1 = f * .yy(1)
                For j = 2 To n
                    x2 = .xx(j)
                    While x2 > rD(khi)
                        khi = khi + 1
                    Wend
                    While x2 < rD(klo)
                        klo = klo - 1
                    Wend
                    Call fappar(klo, khi, x2, f)
                    f2 = f * .yy(j)
                    ff = (f1 + f2) * Abs(x2 - x1) * 0.5
                    .pane(j) = ff
                    s = s + ff
                    x1 = x2
                    f1 = f2
                Next j
                md_integral(i) = s
                u(i) = (s + md_p(1) * .small - md_p(i)) / md_1ci
            End With
        Next
    Else
        If ind = 0 Then
            If jjj = 1 Then ReDim mi_NotEqual(nx, nx, 500)
            jj = Corresponds(jjj)
```

```
    For Each ep In Points
        With ep
            i = i + 1
            k = 0
            s = 0#
            n = .number
            x1 = .xx(1)
            klo = 1
            khi = nx / 4
            Call fappar(klo, khi, x1, f)
            f1 = f * .yy(1)
            For j = 2 To n
                x2 = .xx(j)
                While x2 > rD(khi)
                    khi = khi + 1
                Wend
                While x2 < rD(klo)
                    klo = klo - 1
                Wend
                Call fappar(klo, khi, x2, f)
                f2 = f * .yy(j)
                ff = (f1 + f2) * Abs(x2 - x1) * 0.5
                If ff <> .pane(j) Then
                    k = k + 1
                    mi_NotEqual(jj, i, k) = j
                End If
                s = s + ff
                x1 = x2
                f1 = f2
            Next j
            mi_NotEqual(jj, i, 500) = k
            u(i) = (s + md_p(1) * .small - md_p(i)) / md_1ci
        End With
    Next
Else
    jj = Corresponds(jjj)
    For Each ep In Points
        With ep
            i = i + 1
            s = md_integral(i)
            n = .number
            i1 = mi_NotEqual(jj, i, 1) - 1
            i2 = mi_NotEqual(jj, i, 500)
            x1 = .xx(i1)
            klo = 1
            khi = nx / 4
            Call fappar(klo, khi, x1, f)
            f1 = f * .yy(i1)
            For j = i1 + 1 To i2
                x2 = .xx(j)
                While x2 > rD(khi)
                    khi = khi + 1
                Wend
                While x2 < rD(klo)
                    klo = klo - 1
                Wend
                Call fappar(klo, khi, x2, f)
```

```
                        f2 = f * .yy(j)
                        ff = (f1 + f2) * Abs(x2 - x1) * 0.5
                        s = s - .pane(j) + ff
                        x1 = x2
                        f1 = f2
                    Next j
                    u(i) = (s + md_p(1) * .small - md_p(i)) / md_1ci
                End With
            Next
        End If
    End If
End Sub
Sub CalculateLayersPermeability()
    For Each el In Layers
        el.Permeability
    Next
End Sub
Function Corresponds(jj)
    Corresponds = jj - Application.WorksheetFunction.RoundDown(jj / nx, 0)
* nx
    If Corresponds = 0 Then Corresponds = nx
End Function
Sub SetLayersPressure(x)
Dim i As Integer, j As Integer, k As Integer
    j = 0
    For Each el In Layers
        j = j + 1
        k = 0
        For i = nx * (j - 1) + 1 To nx * j
            k = k + 1
            el.pnew(k) = x(i)
        Next i
    Next
End Sub
Sub UpdateLayersPressure()
Dim s As Double
    For Each el In Layers
        el.pqAndPwd
        s = s + el.q
    Next
    md_q = CD / tau * (Layers(1).pnew(1) - pwD) - s
End Sub
Sub CrossFlow()
Dim i As Integer, j As Integer, k As Integer, dp As Double
    If nl > 1 Then
        For j = 1 To nl Step 2
            For i = 1 To nx
                dp = Layer(j).pnew(i) - Layer(j + 1).pnew(i)
                Layer(j).pXflow(i) = -Layer(j).xflow * dp
                Layer(j + 1).pXflow(i) = Layer(j).xflow * dp
            Next i
        Next j
    End If
End Sub
Property Get q() As Double
    q = md_q
End Property
```

```
Private Sub fappar(klo, khi, z, zz)
Dim i As Integer, k As Integer, a As Double, b As Double, c As Double, f1
As Double, f2 As Double, f3 As Double
Dim x1 As Double, x2 As Double, x3 As Double
    If klo = 1 Then
        klo = 2
        If khi <> nx Then khi = khi + 1
    End If
    For i = klo To khi
        If z = rD(i) Then
            zz = md_p(i)
            GoTo 1
        End If
        If z > rD(i - 1) And z < rD(i) Then
            If i = 2 Then
                k = i - 1
            Else
                k = i - 2
            End If
            x1 = rD(k)
            x2 = rD(k + 1)
            x3 = rD(k + 2)
            f1 = md_p(k)
            f2 = md_p(k + 1)
            f3 = md_p(k + 2)
            b = ((f1 - f3) / (x1 * x1 - x3 * x3) - (f1 - f2) / (x1 * x1 -
x2 * x2)) * _
                (x1 + x3) * (x1 + x2) / (x2 - x3)
            a = ((f1 - f3) - b * (x1 - x3)) / (x1 * x1 - x3 * x3)
            c = f1 - a * x1 * x1 - b * x1
            zz = a * z * z + b * z + c
            GoTo 1
        End If
    Next i
1   klo = i - 1
    khi = i
End Sub
```

Exit Criteria

```
Option Explicit
Option Base 1
Private md_x() As Double
Sub Class_Initialize()
    bDone = False
    ReDim md_x(m)
End Sub
Sub Evaluate(x)
    If TotalTime / CD > MaxT Or pwD > MaxP Then bDone = True
End Sub
Function bConverged(x)
Dim i As Integer, razn0 As Double, razn As Double
    razn0 = -1000#
    razn = razn0
    bConverged = False
    For i = 1 To m
        If x(i) <> 0# Then razn = Application.WorksheetFunction.Max(razn,
Abs(1# - md_x(i) / x(i)) * 100#)
```

```
    Next i
    If razn < 0.00001 And razn <> razn0 Then
        bConverged = True
        ReDim md_x(m)
    Else
        md_x = x
    End If
End Function
```

Matrix Solution

```
Option Explicit
Option Base 1
Private Const itol As Integer = 1, tiny As Double = 1E-20
Private ija() As Double, indx() As Double
Sub SolveSparse(a, b)
Dim iter As Integer, err As Double, x() As Double
    ReDim x(m)
    Call sprsin(a, m)
    Call linbcg(m, b, x, itol, 1E-16, 2000, iter, err)
    b = x
End Sub
Private Sub sprsin(a, n)      'convert matrix to sparse format
Dim i As Integer, j As Integer, k As Integer, nmax As Integer, aij As
Double
    ReDim ija(n)
    ija(1) = n + 2
    k = n + 1
    For i = 1 To n
        For j = 1 To n
            aij = a(i, j)
            If Abs(aij) <> 0# Then
                If i <> j Then
                    k = k + 1
                    ReDim Preserve sa(k)
                    ReDim Preserve ija(k)
                    sa(k) = aij
                    ija(k) = j
                End If
            End If
        Next j
        ija(i + 1) = k + 1
    Next i
End Sub
Private Sub dsprsax(x, b, n)                    'product of sparse matrix
and vector
Dim i As Integer, k As Integer
    If ija(1) <> n + 2 Then MsgBox "mismatched vector and matrix in
sprsax"
    For i = 1 To n
        b(i) = sa(i) * x(i)
        For k = ija(i) To ija(i + 1) - 1
            b(i) = b(i) + sa(k) * x(ija(k))
        Next k
    Next i
End Sub
Private Sub dsprstx(x, b, n)                    'product of transpose
sparse matrix and vector
```

```
Dim i As Integer, j As Integer, k As Integer
    If ija(1) <> n + 2 Then MsgBox "mismatched vector and matrix in
sprstx"
    For i = 1 To n
        b(i) = sa(i) * x(i)
    Next i
    For i = 1 To n
        For k = ija(i) To ija(i + 1) - 1
            j = ija(k)
            b(j) = b(j) + sa(k) * x(i)
        Next k
    Next i
End Sub
Private Function snrm(n, sx, itol)                        'used by linbcg
for vector norm
Dim i As Integer, isamax As Integer
    If itol <= 3 Then
        snrm = 0#
        For i = 1 To n
            snrm = snrm + sx(i) ^ 2
        Next i
        snrm = Sqr(snrm)
    Else
        isamax = 1
        For i = 1 To n
            If Abs(sx(i)) > Abs(sx(isamax)) Then isamax = i
        Next i
        snrm = Abs(sx(isamax))
    End If
End Function
Private Sub atimes(n, x, r, itrnsp)                       'used by linbcg
for sparse multiplication
    If itrnsp = 0 Then
        Call dsprsax(x, r, n)
    Else
        Call dsprstx(x, r, n)
    End If
End Sub
Private Sub asolve(n, b, x, itrnsp)                       'used by linbcg
for preconditioner
Dim i As Integer
    For i = 1 To n
        x(i) = b(i) / sa(i)
    Next i
End Sub
Private Sub linbcg(n, b, x, itol, tol, ITMAX, iter, err)
Dim nmax As Integer, i As Integer, j As Integer
Dim eps As Double
Dim ak As Double, akden As Double, bk As Double, bkden As Double, bknum As
Double, bnrm As Double
Dim dxnrm As Double, xnrm As Double, zm1nrm As Double, znrm As Double, p()
As Double, pp() As Double
Dim r() As Double, rr() As Double, z() As Double, zz() As Double
    nmax = 1024
    eps = 0.00000000000001
    ReDim p(nmax):      ReDim pp(nmax):      ReDim r(nmax):      ReDim
rr(nmax):      ReDim z(nmax):    ReDim zz(nmax)
```

```
    iter = 0
    Call atimes(n, x, r, 0)
    For j = 1 To n
        r(j) = b(j) - r(j)
        rr(j) = r(j)
    Next j
    If itol = 1 Then
        bnrm = snrm(n, b, itol)
        Call asolve(n, r, z, 0)
    ElseIf itol = 2 Then
        Call asolve(n, b, z, 0)
        bnrm = snrm(n, z, itol)
        Call asolve(n, r, z, 0)
    ElseIf itol = 3 Or itol = 4 Then
        Call asolve(n, b, z, 0)
        bnrm = snrm(n, z, itol)
        Call asolve(n, r, z, 0)
        znrm = snrm(n, z, itol)
    Else
        MsgBox "illegal itol in linbcg'"
    End If
100 If iter <= ITMAX Then
        iter = iter + 1
        Call asolve(n, rr, zz, 1)
        bknum = 0#
        For j = 1 To n
            bknum = bknum + z(j) * rr(j)
        Next j
        If iter = 1 Then
            For j = 1 To n
                p(j) = z(j)
                pp(j) = zz(j)
            Next j
        Else
            bk = bknum / bkden
            For j = 1 To n
                p(j) = bk * p(j) + z(j)
                pp(j) = bk * pp(j) + zz(j)
            Next j
        End If
        bkden = bknum
        Call atimes(n, p, z, 0)
        akden = 0#
        For j = 1 To n
            akden = akden + z(j) * pp(j)
        Next j
        ak = bknum / akden
        Call atimes(n, pp, zz, 1)
        For j = 1 To n
            x(j) = x(j) + ak * p(j)
            r(j) = r(j) - ak * z(j)
            rr(j) = rr(j) - ak * zz(j)
        Next j
        Call asolve(n, r, z, 0)
        If itol = 1 Then
            err = snrm(n, r, itol) / bnrm
        ElseIf itol = 2 Then
```

```
            err = snrm(n, z, itol) / bnrm
        ElseIf itol = 3 Or itol = 4 Then
            zm1nrm = znrm
            znrm = snrm(n, z, itol)
            If Abs(zm1nrm - znrm) > eps * znrm Then
                dxnrm = Abs(ak) * snrm(n, p, itol)
                err = znrm / Abs(zm1nrm - znrm) * dxnrm
            Else
                err = znrm / bnrm
                GoTo 100
            End If
            xnrm = snrm(n, x, itol)
            If err <= 0.5 * xnrm Then
                err = err / xnrm
            Else
                err = znrm / bnrm
                GoTo 100
            End If
        End If
        If err > tol Then GoTo 100
    End If
End Sub
Sub SolveLUD(fjac, p)
Dim d As Double
    ReDim indx(m)
    Call ludcmp(fjac, d)
    Call lubksb(fjac, p)
End Sub
Private Sub ludcmp(a, d)
Dim i As Integer, imax As Integer, j As Integer, k As Integer
Dim aamax As Double, dum As Double, sum As Double, vv() As Double
    ReDim vv(m)
    d = 1
    For i = 1 To m
        aamax = 0#
        For j = 1 To m
            If Abs(a(i, j)) > aamax Then aamax = Abs(a(i, j))
        Next j
        If aamax = 0 Then MsgBox "singular matrix in ludcmp"
        vv(i) = 1# / aamax
    Next i
    For j = 1 To m
        For i = 1 To j - 1
            sum = a(i, j)
            For k = 1 To i - 1
                sum = sum - a(i, k) * a(k, j)
            Next k
            a(i, j) = sum
        Next i
        aamax = 0#
        For i = j To m
            sum = a(i, j)
            For k = 1 To j - 1
                sum = sum - a(i, k) * a(k, j)
            Next k
            a(i, j) = sum
            dum = vv(i) * Abs(sum)
```

```
            If dum >= aamax Then
                imax = i
                aamax = dum
            End If
        Next i
        If j <> imax Then
            For k = 1 To m
                dum = a(imax, k)
                a(imax, k) = a(j, k)
                a(j, k) = dum
            Next k
            d = -d
            vv(imax) = vv(j)
        End If
        indx(j) = imax
        If a(j, j) = 0# Then a(j, j) = tiny
        If j <> m Then
            dum = 1# / a(j, j)
            For i = j + 1 To m
                a(i, j) = a(i, j) * dum
            Next i
        End If
    Next j
End Sub
Private Sub lubksb(a, b)
Dim i As Integer, ii As Integer, j As Integer, ll As Integer
Dim sum As Double
    ii = 0
    For i = 1 To m
        ll = indx(i)
        sum = b(ll)
        b(ll) = b(i)
        If ii <> 0 Then
            For j = ii To i - 1
                sum = sum - a(i, j) * b(j)
            Next j
        ElseIf sum <> 0# Then
            ii = i
        End If
        b(i) = sum
    Next i
    For i = m To 1 Step -1
        sum = b(i)
        For j = i + 1 To m
            sum = sum - a(i, j) * b(j)
        Next j
        b(i) = sum / a(i, i)
    Next i
End Sub
```

Newton Method

```
Option Explicit
Option Base 1
Private fvec() As Double, mi_ind As Integer, sigma As Double
Private Const maxits As Integer = 500, tolf As Double = 0.00001, tolmin As
Double = 0.000001, tolx As Double = 0.0000001
```

```
Private Const stpmx As Double = 100#, alf As Double = 0.0001, eps As
Double = 0.0001
Sub Class_Initialize()
    mi_ind = 0
End Sub
Sub Run(x, check, niter)
Dim i As Integer, its As Integer, j As Integer
Dim d As Double, den As Double, f As Double, fold As Double, stpmax As
Double, sum As Double, temp As Double
Dim test As Double, fjac() As Double, g() As Double, p() As Double, xold()
As Double, fjac1() As Double
    ReDim indx(m):      ReDim fjac(m, m):       ReDim g(m):     ReDim
p(m):     ReDim xold(m)
    f = fmin(x)
    test = 0#
    For i = 1 To m
        If Abs(fvec(i)) > test Then test = Abs(fvec(i))
    Next i
    If test < 0.01 * tolf Then
        check = False
        Exit Sub
    End If
    sum = Application.WorksheetFunction.SumProduct(x, x)
    stpmax = stpmx * Application.WorksheetFunction.Max(Sqr(sum), CDbl(m))
    For its = 1 To maxits
        niter = its
        Call fdjac(x, fvec, fjac)
        For i = 1 To m
            sum = 0#
            For j = 1 To m
                sum = sum + fjac(j, i) * fvec(j)
            Next j
            g(i) = sum
        Next i
        xold = x
        fold = f
        For i = 1 To m
            p(i) = -fvec(i)
        Next i
        If bSparse Then
            Call Matrix.SolveSparse(fjac, p)
        Else
            Call Matrix.SolveLUD(fjac, p)
        End If
        Call lnsrch(xold, fold, g, p, x, f, stpmax, check)
        test = 0#
        For i = 1 To m
            If Abs(fvec(i)) > test Then test = Abs(fvec(i))
        Next i
        If test < tolf Then
            check = False
            Exit Sub
        End If
        If check Then
            test = 0#
            den = Application.WorksheetFunction.Max(f, 0.5 * m)
            For i = 1 To m
```

```
                temp = Abs(g(i)) *
Application.WorksheetFunction.Max(Abs(x(i)), 1#) / den
                If temp > test Then test = temp
            Next i
            If test < tolmin Then
                check = True
            Else
                check = False
            End If
            Exit Sub
        End If
        test = 0#
        For i = 1 To m
            temp = (Abs(x(i) - xold(i))) /
Application.WorksheetFunction.Max(Abs(x(i)), 1#)
            If temp > test Then test = temp
        Next i
        If test < tolx Then Exit Sub
    Next its
End Sub
Private Sub lnsrch(xold, fold, g, p, x, f, stpmax, check)
Dim i As Integer
Dim temp As Double, test As Double, tmplam As Double
Dim a As Double, alam As Double, alam2 As Double, alamin As Double, b As
Double, disc As Double
Dim f2 As Double, fold2 As Double, rhs1 As Double, rhs2 As Double, slope
As Double, sum As Double
    check = False
    sum = Sqr(Application.WorksheetFunction.SumProduct(p, p))
    If sum > stpmax Then
        For i = 1 To m
            p(i) = p(i) * stpmax / sum
        Next i
    End If
    slope = Application.WorksheetFunction.SumProduct(g, p)
    test = 0#
    For i = 1 To m
        temp = Abs(p(i)) / Application.WorksheetFunction.Max(Abs(xold(i)),
1#)
        If temp > test Then test = temp
    Next i
    alamin = tolx / test
    alam = 1#
1   For i = 1 To m
        x(i) = xold(i) + alam * p(i)
    Next i
    f = fmin(x)
    If alam < alamin Then
        x = xold
        check = True
        Exit Sub
    ElseIf f <= fold + alf * alam * slope Then
        Exit Sub
    Else
        If alam = 1# Then
            tmplam = -slope / (2# * (f - fold - slope))
        Else
```

```
            rhs1 = f - fold - alam * slope
            rhs2 = f2 - fold2 - alam2 * slope
            a = (rhs1 / alam ^ 2 - rhs2 / alam2 ^ 2) / (alam - alam2)
            b = (-alam2 * rhs1 / alam ^ 2 + alam * rhs2 / alam2 ^ 2) /
(alam - alam2)
            If a = 0# Then
                tmplam = -slope / (2# * b)
            Else
                disc = b * b - 3# * a * slope
                If disc < 0# Then MsgBox "roundoff problem in lnsrch"
                tmplam = (-b + Sqr(disc)) / (3# * a)
            End If
            If tmplam > 0.5 * alam Then tmplam = 0.5 * alam
        End If
    End If
    alam2 = alam
    f2 = f
    fold2 = fold
    alam = Application.WorksheetFunction.Max(tmplam, 0.1 * alam)
    GoTo 1
End Sub
Private Function fdjac(x, fvec, df)
Dim i As Integer, j As Integer, h As Double, temp As Double, f() As
Double, dfij As Double, nonzerocount As Long
    ReDim f(m)
    nonzerocount = 0
    ReDim sa(m)
    For j = 1 To m
        temp = x(j)
        h = eps * Abs(temp)
        If h = 0# Then h = eps
        x(j) = temp + h
        h = x(j) - temp
        Call funcv(x, f, j)
        x(j) = temp
        For i = 1 To m
            dfij = (f(i) - fvec(i)) / h
            If dfij <> 0# Then nonzerocount = nonzerocount + 1
            If i = j Then sa(j) = dfij
            df(i, j) = dfij
        Next i
    Next j
    mi_ind = 1
    bSparse = False
    If nonzerocount / m / m < 0.5 Then bSparse = True
End Function
Private Function fmin(x)
    Call funcv(x, fvec, 0)
    fmin = 0.5 * Application.WorksheetFunction.SumProduct(fvec, fvec)
End Function
Private Sub funcv(x, ffvec, j)
    Call Reservoir.SetLayersPressure(x)
    Reservoir.Pressure
    Call Reservoir.Deformation(j, mi_ind)
    Reservoir.CalculateLayersPermeability
    Call Vector.Generate(ffvec)
End Sub
```

Output

```
Option Explicit
Option Base 1
Private Const md_min As Double = 1E-16
Private mv_rDtD() As Variant, elem As Variant, el As cls03Layer, md_xs()
As Variant, md_xxs() As Double, mb_BU As Boolean
Private md_p() As Double, md_k() As Double, md_u() As Double, mi_row As
Integer, mi_col As Integer, mi_start As Integer
Sub Class_Initialize()
Dim i As Integer
    mv_rDtD = Array("P", "K", "U")
    If bBoth Then CleanUp
    ReDim md_xxs(nx)
    Sheets("tD").Activate
    Cells(1, 20).Select
    For i = 1 To nx
        md_xxs(i) = reD ^ rD(i)
        ActiveCell.Offset(i - 1, 0) = md_xxs(i)
        ActiveCell.Offset(i - 1, 6) = md_xxs(i)
    Next i
    ReDim md_xs(1)
    For i = 1 To nl
        Call ConcatenateTwoArrays(md_xs, md_xxs)
    Next i
    For Each elem In mv_rDtD
        Sheets(elem).Activate
        Cells(2, 1).Select
        For i = 1 To m
            ActiveCell.Offset(i - 1, 0) = md_xs(i)
        Next i
    Next elem
    Sheets("uu").Activate
    Cells(2, 1).Select
    For i = 1 To nx
        ActiveCell.Offset(i - 1, 0) = md_xxs(i)
    Next i
    mi_row = 1
    mi_col = 2
    mb_BU = True
End Sub
Sub Intermediate()
Dim a1() As Double, a2() As Double, a3() As Double, q As Double, rangeX As
Range, rangeY1 As Range, rangeY2 As Range
Dim i1 As Integer, i2 As Integer
    Application.ScreenUpdating = False
    If bBuildUp Then
        mi_start = 9
        mi_row = m + 4
        If mb_BU Then
            mi_col = 2
            mb_BU = False
        End If
    Else
        mi_start = 1
        mi_row = 2
    End If
```

```
    If bConstantQ Then
        i1 = mi_start + 2
        i2 = mi_start + 3
    Else
        i1 = mi_start + 3
        i2 = mi_start + 2
    End If
    ReDim a1(nx):       ReDim a2(nx):       ReDim a3(nx):       ReDim
md_p(1):      ReDim md_k(1):      ReDim md_u(1)
    q = Reservoir.q
    Sheets("tD").Select
    Cells(ntau, mi_start) = TotalTime / CD
    Cells(ntau, mi_start + 1) = Log(TotalTime / CD)
    If Abs(pwDinit - pwD) <> 0# Then
        Cells(ntau, i1) = Abs(pwDinit - pwD)
    Else
        Cells(ntau, i1) = md_min
    End If
    If q <> 0# Then
        Cells(ntau, i2) = 1# / q
    Else
        Cells(ntau, i2) = md_min
    End If
    If ntau > 2 Then
        Set rangeX = Range(Cells(ntau - 2, mi_start + 1), Cells(ntau,
mi_start + 1))
        Set rangeY1 = Range(Cells(ntau - 2, mi_start + 2), Cells(ntau,
mi_start + 2))
        Set rangeY2 = Range(Cells(ntau - 2, mi_start + 3), Cells(ntau,
mi_start + 3))
        Cells(ntau - 1, mi_start + 4) = _
            Application.WorksheetFunction.Max(md_min,
Application.WorksheetFunction.slope(rangeY1, rangeX))
        Cells(ntau - 1, mi_start + 5) = _
            Application.WorksheetFunction.Max(md_min,
Application.WorksheetFunction.slope(rangeY2, rangeX))
    End If
    If TotalTime <> 0# Then Cells(ntau, mi_start + 6) = Abs(1# - Abs(pwD -
pwDinit) / VEH.Stehfest(TotalTime, 1#)) * 100#
    Cells(1, 21).Select
    i1 = 0
    For Each el In Layers
        i1 = i1 + 1
        Call el.RetrievePKU(a1, a2, a3)
        For i2 = 1 To nx
            ActiveCell.Offset(i2 - 1, i1 - 1) = a1(i2)
            ActiveCell.Offset(i2 - 1, i1 - 1 + 6) = a2(i2)
        Next i2
        If ntau Mod PrintFrequency = 0 Then
            Call ConcatenateTwoArrays(md_p, a1)
            Call ConcatenateTwoArrays(md_k, a2)
            Call ConcatenateTwoArrays(md_u, a3)
        End If
    Next el
    If ntau Mod PrintFrequency = 0 Then
        For Each elem In mv_rDtD
            Sheets(elem).Activate
```

```
            Cells(mi_row, mi_col).Select
            ActiveCell.Offset(-1, 0) = TotalTime / CD
            Select Case elem
            Case Is = "P"
                For i1 = 1 To m
                    ActiveCell.Offset(i1 - 1, 0) = md_p(i1)
                Next i1
            Case Is = "K"
                For i1 = 1 To m
                    ActiveCell.Offset(i1 - 1, 0) = md_k(i1)
                Next i1
            Case Is = "U"
                For i1 = 1 To m
                    ActiveCell.Offset(i1 - 1, 0) = md_u(i1)
                Next i1
            Case Else
            End Select
        Next elem
        Sheets("uu").Activate
        Cells(mi_row, mi_col).Select
        ActiveCell.Offset(-1, 0) = TotalTime / CD
        For i1 = 1 To nx
            ActiveCell.Offset(i1 - 1, 0) = u(i1)
        Next i1
        mi_col = mi_col + 1
    End If
    Sheets("Results").Activate
    ActiveSheet.TextBoxes("Progress").Text = "Time = " & Format(TotalTime
/ CD, "0.00E+00") & Chr(10) & _
        "Error = " & Format(2#, "0.00E+00")
    If ntau Mod 10 = 0 Then Application.ScreenUpdating = True
End Sub
Private Sub ConcatenateTwoArrays(arr1, arr2)
Dim i As Integer, n1 As Integer, N2 As Integer
    n1 = UBound(arr1)
    If n1 = 1 Then n1 = 0
    N2 = UBound(arr2)
    ReDim Preserve arr1(n1 + N2)
    For i = 1 To N2
        arr1(i + n1) = arr2(i)
    Next i
End Sub
Private Sub CleanUp()
    Application.ScreenUpdating = False
    For Each elem In mv_rDtD
        Sheets(elem).Activate
        Cells.ClearContents
    Next elem
    Sheets("tD").Activate
    Cells.ClearContents
    Sheets("Input").Activate
    Cells(30, 2).ClearContents
End Sub
Sub Store(x)
Dim i As Integer
    Application.ScreenUpdating = False
    Sheets("All").Select
```

```
    Cells(2, 1).Select
    ActiveCell.Offset(-1, 0) = TotalTime / CD
    For i = 1 To m
        ActiveCell.Offset(i - 1, 0) = x(i)
    Next i
End Sub
Sub Retrieve(x)
Dim i As Integer
    Application.ScreenUpdating = False
    Sheets("All").Select
    Cells(2, 1).Select
    For i = 1 To m
        x(i) = ActiveCell.Offset(i - 1, 0)
    Next i
    pwD = x(1)
    Call Reservoir.SetLayersPressure(x)
    Reservoir.UpdateLayersPressure
End Sub
```

Vector-Function Calculation

```
Option Explicit
Option Base 1
Private el As cls03Layer
Private Sub ConcatenateTwoArrays(arr1, arr2)
Dim i As Integer, n1 As Integer, N2 As Integer
    n1 = UBound(arr1)
    If n1 = 1 Then n1 = 0
    N2 = UBound(arr2)
    ReDim Preserve arr1(n1 + N2)
    For i = 1 To N2
        arr1(i + n1) = arr2(i)
    Next i
End Sub
Sub Generate(fvec)
Dim i As Integer, j As Integer, k As Integer, bi As Double, a() As Double,
b() As Double
    ReDim fvec(1)
    ReDim b(1)
    i = 0
    For Each el In Layers
        i = i + 1
        ReDim a(nx)
        el.CalculateArrays
        Call el.RetrieveArray(a, bi)
        ReDim Preserve b(i)
        b(i) = bi
        Call ConcatenateTwoArrays(fvec, a)
    Next
    k = 0
    For i = 1 To m Step nx
        k = k + 1
        For j = 1 To UBound(b)
            If k <> j Then fvec(i) = fvec(i) + b(j)
        Next j
        fvec(i) = fvec(i) + qq
    Next i
End Sub
```

```
Sub Progonka(x)
Dim i As Integer, a() As Double
    ReDim x(1)
    i = 0
    For Each el In Layers
        i = i + 1
        ReDim a(nx)
        el.CalculateArrays
        Call el.RetrievePnew(a)
        Call ConcatenateTwoArrays(x, a)
    Next
End Sub
```

Van Everdingen and Hurst Solution

```
Option Explicit
Option Base 1
Function Stehfest(td As Double, rD As Double) As Double
Dim pwDs As Double, dp_dlntd As Double, dp_dtd As Double, qwd As Double,
Cumd As Double, v(20) As Double
Dim v_init As Double, vsum As Double, top As Double, bottom As Double, t1
As Double, t2 As Double
Dim b1 As Double, b2 As Double, b3 As Double, b4 As Double, b5 As Double,
a As Double, s As Double, fs As Double
Dim k_start As Long, k_end As Long, n As Long, i As Long, k As Long
    n = 10
    With Application
    For i = 1 To n
        v_init = (-1#) ^ (n / 2 + i)
        k_start = Int((i + 1) / 2)
        k_end = .Min(i, n / 2)
        vsum = 0#
        For k = k_start To k_end
            t1 = k ^ (n / 2)
            t2 = .Fact(2 * k):      b1 = .Fact(n / 2 - k):      b2 =
.Fact(k)
            b3 = .Fact(k - 1):      b4 = .Fact(i - k):          b5 =
.Fact(2 * k - i)
            top = t1 * t2
            bottom = b1 * b2 * b3 * b4 * b5
            vsum = vsum + top / bottom
        Next k
        v(i) = v_init * vsum
    Next i
    End With
    a = Log(2#) / td
    pwDs = 0#
'    dp_dtd = 0#:        dp_dlntd = 0#:          qwd = 0#:           Cumd
= 0#
    For i = 1 To n
        s = a * i
        fs = Lpd(s, rD)
        pwDs = pwDs + v(i) * fs
'        dp_dtd = dp_dtd + v(i) * s * fs:    qwd = qwd + v(i) / (s * s *
fs):    Cumd = Cumd + v(i) / (s * s * s * fs)
    Next i
    pwDs = a * pwDs
```

```
'    dp_dtd = a * dp_dtd:    dp_dlntd = dp_dtd * td:     qwd = a * qwd:
Cumd = a * Cumd
    Stehfest = pwDs
End Function
Private Function Lpd(s As Double, rD As Double) As Double
Dim bb As Double
    bb = BesselK0(Sqr(s))
'    Lpd = (BesselK0(rd * sqr(s))) / (s ^ (3 / 2) * BesselK1(sqr(s)))
'    Lpd = (BesselK0(rd * Sqr(s))) / s / (1# + CD * s * BesselK0(Sqr(s)))
    Lpd = bb / s / (1# + CD * s * bb)
End Function
Private Function BesselK0(arg As Double) As Double
Dim y As Double, z As Double, i As Integer, n As Integer
    y = arg / 2#
    z = 1# / y
    If arg < 2# Then
        BesselK0 = -Log(y) * BesselI0(arg) - 0.57721566 + 0.4227842 * (y ^
2) _
                                    + 0.23069756 * (y ^ 4) + 0.0348859 *
(y ^ 6) _
                                    + 0.00262698 * (y ^ 8) + 0.0001075 *
(y ^ 10) _
                                    + 0.0000074 * (y ^ 12)
    Else
        BesselK0 = 1.25331414 - 0.07832358 * z + 0.02189568 * (z ^ 2) _
                        - 0.01062446 * (z ^ 3) + 0.00587872 * (z ^ 4) _
                        - 0.0025154 * (z ^ 5) + 0.00053208 * (z ^ 6)
        If arg > 700# Then
            n = Application.WorksheetFunction.RoundDown(arg / 700#, 0)
            BesselK0 = BesselK0 / (arg ^ 0.5) / Exp(arg - 700# * n)
            For i = 1 To n
                BesselK0 = BesselK0 / Exp(arg / 700#)
                If BesselK0 < 1E-50 Then Exit Function
            Next i
        Else
            BesselK0 = BesselK0 / (arg ^ 0.5) / Exp(arg)
        End If
    End If
End Function
Private Function BesselK1(arg As Double) As Double
Dim y As Double, z As Double
    y = arg / 2#
    z = 1# / y
    If arg < 2# Then
        BesselK1 = arg * Log(y) * BesselI1(arg) + 1 + 0.15443144 * (y ^ 2)
- 0.67278579 * (y ^ 4) - 0.18156897 * (y ^ 6) _
                    - 0.01919402 * (y ^ 8) - 0.00110404 * (y ^ 10) -
0.00004686 * (y ^ 12)
        BesselK1 = BesselK1 / arg
    Else
        BesselK1 = 1.25331414 + 0.23498619 * (z) - 0.0365562 * (z ^ 2) +
0.01504268 * (z ^ 3) - 0.00780353 * (z ^ 4) _
                    + 0.00325614 * (z ^ 5) - 0.00068245 * (z ^ 6)
        BesselK1 = BesselK1 / Exp(arg) / Sqr(arg)
    End If
End Function
Private Function Ei(arg As Double) As Double
```

```
Dim t1 As Double, t2 As Double, t3 As Double, t4 As Double, t5 As Double
Dim b1 As Double, b2 As Double, b3 As Double, b4 As Double, b5 As Double
    If arg < 1# Then
        t1 = -0.57721566 + 0.99999193 * arg
        t2 = -0.24991055 * (arg * arg) + 0.05519968 * (arg * arg * arg)
        t3 = -0.00976004 * (arg * arg * arg * arg) + 0.00107857 * (arg *
arg * arg * arg * arg)
        t4 = -Log(arg)
        Ei = t1 + t2 + t3 + t4
    ElseIf arg >= 1# And arg <= 50# Then
        t1 = 1 * (arg * arg * arg * arg)
        t2 = 8.5733287401 * (arg * arg * arg)
        t3 = 18.059016973 * (arg * arg)
        t4 = 8.6347608925 * (arg)
        t5 = 0.2677737343
        b1 = 1# * (arg * arg * arg * arg)
        b2 = 9.5733223454 * (arg * arg * arg)
        b3 = 25.6329561486 * (arg * arg)
        b4 = 21.0996530827 * (arg)
        b5 = 3.9584969228
        Ei = (1# / (arg * Exp(arg))) * ((t1 + t2 + t3 + t4 + t5) / (b1 +
b2 + b3 + b4 + b5))
    Else
        Ei = 0#
    End If
End Function
Private Function BesselI1(arg As Double) As Double
Dim T As Double
    T = arg / 3.75
    If arg < 3.75 Then
        BesselI1 = 0.5 + 0.87890594 * (T ^ 2) + 0.51498869 * (T ^ 4) +
0.15084934 * (T ^ 6) + 0.02658733 * (T ^ 8) _
                  + 0.00301532 * (T ^ 10) + 0.00032411 * (T ^ 12)
        BesselI1 = arg * BesselI1
    Else
        BesselI1 = 0.39894228 - 0.03988024 / T - 0.00362018 / (T ^ 2) +
0.00163801 / (T ^ 3) - 0.01031555 / (T ^ 4) _
                   + 0.02282967 / (T ^ 5) - 0.02895312 / (T ^ 6) +
0.01787654 / (T ^ 7) - 0.00420059 / (T ^ 8)
        BesselI1 = BesselI1 * Exp(arg) / Sqr(arg)
    End If
End Function
Private Function BesselI0(arg As Double) As Double
Dim T As Double
    T = arg / 3.75
    If arg < 3.75 Then
        BesselI0 = 1# + 3.5156229 * (T ^ 2) + 3.0899424 * (T ^ 4) +
1.2067492 * (T ^ 6) + 0.2659732 * (T ^ 8) _
               + 0.0360768 * (T ^ 10) + 0.0045813 * (T ^ 12)
    Else
        BesselI0 = 0.39894228 + 0.01328592 / T + 0.00225319 / (T ^ 2) -
0.00157565 / (T ^ 3) + 0.00916281 / (T ^ 4) _
               - 0.02057706 / (T ^ 5) + 0.02635537 / (T ^ 6) - 0.01647633
/ (T ^ 7) + 0.00392377 / (T ^ 8)
        BesselI0 = BesselI0 * Exp(arg) / Sqr(arg)
    End If
End Function
```

VITA

Ildar Diyashev

Diploma, Mechanics and Applied Mathematics, Kazan State University, 1991

Candidate of Science, Mechanics of Liquid, Gas, and Plasma, Kazan State University, 1995

Master of Engineering, Petroleum Engineering, Texas A&M University, 1998

Doctor of Philisophy, Petroleum Engineering, Texas A&M University, 2005

Schlumberger – NExT (Network of Excellence in Training)

The University of Tulsa

539 South Gary Place

Tulsa, OK 74104-3189